STUDIA UNIVERSITATIS
BABEŞ-BOLYAI

UNIVERSITATEA BABEŞ-BOLYAI
BABEŞ-BOLYAI TUDOMÁNYEGYETEM
BABEŞ-BOLYAI UNIVERSITÄT
BABEŞ-BOLYAI UNIVERSITY
TRADITIO ET EXCELLENTIA

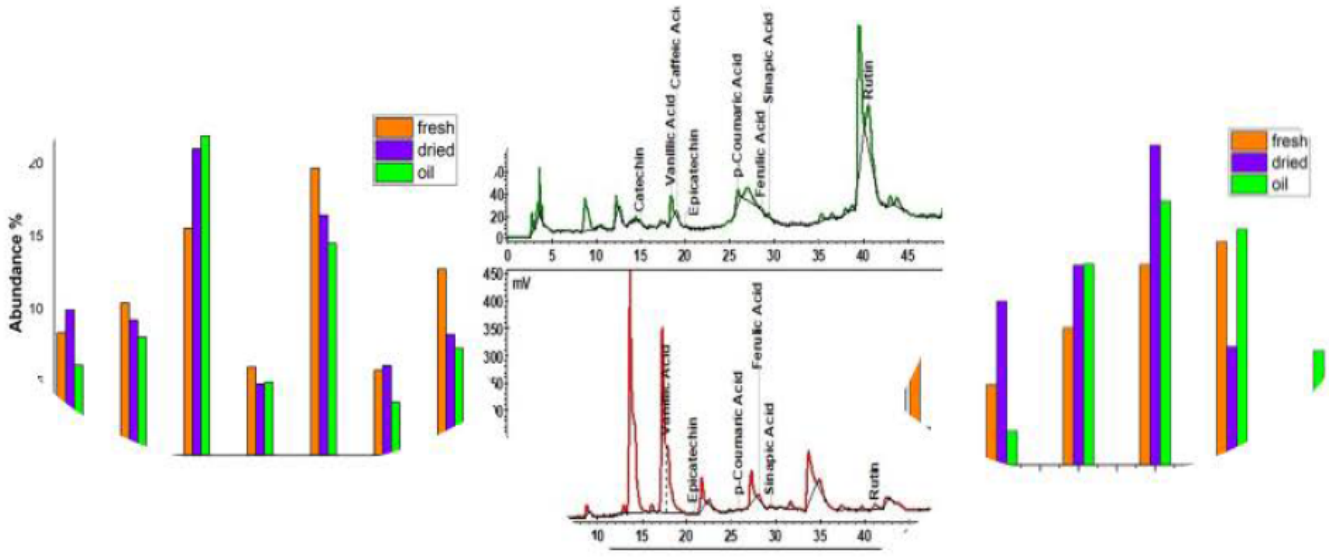

CHEMIA

1/2024

STUDIA UNIVERSITATIS BABEŞ-BOLYAI CHEMIA

1/2024

ISSN (print): 1224-7154;
ISSN (online): 2065-9520; ISSN-L: 2065-9520

Published by Babeş-Bolyai University

http://chem.ubbcluj.ro/~studiachemia/;
http://www.studia.ubbcluj.ro/serii/chemia/index_en.html

YEAR **Volume 69 (LXIX) 2024**
MONTH **MARCH**
ISSUE **1**

PUBLISHED ONLINE: 2024-03-30
PUBLISHED PRINT: 2024-03-30
ISSUE DOI: 10.24193/subbchem.2024.1

S T U D I A
UNIVERSITATIS BABEŞ–BOLYAI
CHEMIA

1

CONTENT/ SOMMAIRE/ INHALT/ CUPRINS

Studia Universitatis Babes-Bolyai Chemia has been selected for coverage in Thomson Reuters products and custom information services. Beginning with V. 53 (1) 2008, this publication is indexed and abstracted in the following:

- Science Citation Index Expanded (also known as SciSearch®)
- Chemistry Citation Index®
- Journal Citation Reports/Science Edition

STUDIA UBB CHEMIA, LXIX, 1, 2024 (p. 7-16)
(RECOMMENDED CITATION)
DOI:10.24193/subbchem.2024.1.01

DESULFURIZATION OF CRUMB RUBBER BY MODIFIED NATURAL ZEOLITIC CATALYSTS

Dorin BOMBOȘ[a,b,*], Mihaela BOMBOȘ[a], Emilian ZAHARIA[a], Andreea-Luiza MIRȚ[c], Gabriel VASILIEVICI[c]

ABSTRACT. The high elastomer content of the crumb rubber powder obtained from the processing of used tires increases the interest for its valorization when modifying road bitumen in order to improve its elastic characteristics. Sulfur cross-linking of elastomer chains reduces the dispersion of the crumb rubber in the road bitumen during the modification process. A novel approach was explored, involving the partial desulfurization of rubber powder using a natural zeolitic catalyst, clinoptilolite, modified in its acid form. The catalytic desulfurization of the powder was carried out in a batch system at a temperature of 280°C for 6 hours in the presence of high aromaticity solvents. The catalysts' high acidity facilitated the conversion of rubber powder effectively, reaching a more suitable form to use in improving road bitumen.

Keywords: *natural zeolite, desulfurization, crumb rubber*

INTRODUCTION

The utilization of crumb tire rubber resulted from the grinding of end-of-life tires as a bitumen modifier in road pavement has emerged as a viable solution for waste management challenges [1, 2].

[a] *ATICA Chemicals SRL, 202 Căzănești str., Râmnicu Vâlcea, 240414, Vâlcea, Romania*
[b] *PETROLEUM-GAS UNIVERSITY OF PLOIEŞTI, The Faculty of Petroleum Refining and Petrochemistry, Bucharest Boulevard, no. 39, Ploiesti, Prahova, RO 100680*
[c] *National Institute for Research Development for Chemistry and Petrochemistry-ICECHIM-București, 202 Spl. Independenței, 060021, Bucharest, Romania*
** Corresponding author: bombos.dorin@gmail.com*

In contrast, the conventional methods of waste tire disposal, such as dumping or stacking, not only waste substantial land resources but also pose a risk of fire hazard. Historical approaches like land filling and incineration, once prevalent, have been largely abandoned. Incineration, though not environmentally friendly, releases pollutants like CO, CO_2, dioxins, dioxin-like compounds and volatile organic compounds (VOC) [3].

To address these challenges, pyrolysis emerges as an alternative for waste tire treatment [4,5]. This method not only minimizes waste but also produces valuable by-products such as syngas, fuel oil and char. The gaseous fraction contains C1-C4 hydrocarbons and hydrogen, the oil product is easily storable and can be further upgraded as fuel oil, and the residual char finds applications in diverse fields, including battery electrodes, super-capacitor materials and sorbents [6].

There are different kinds of zeolite structures, each with unique shapes and can be used for many processes [7]. Beyond their conventional role as adsorbents, zeolites exhibit versatility as catalysts, separation media, catalyst supports and even in animal feeding applications. The specific utilization of zeolites depends on the position of active centers, as well as the dimensions and geometric attributes of the internal cavities within the zeolite structure [8, 9]. Zeolites special catalytic abilities are being used in new applications. This is happening because environmental rules are getting stricter, requiring the use of catalysis to meet high standards. Natural zeolites stand out due to their widespread availability, cost-effectiveness and robust mechanical strength. However, their applications in adsorption studies are seldom explored, possibly due to the challenge posed by purifying them from various impurity phases present in their main structure [10,11]. The augmentation of its industrial applicability can be achieved through thermal and chemical treatments, inducing alterations in composition, structure and properties. While zeolite catalysts, in general, share essential features such as optimal acid strength, pore size and pore structure, there exists a noticeable gap in research concerning the catalytic potential of zeolite [12, 13].

Desulfurization of crumb rubber with modified natural zeolites offers numerous benefits, such as: improved mechanical properties of rubber products, reduced environmental pollution, increased reusability and recyclability of crumb rubber and sustainable and cost-effective desulfurization method [14]. The crumb rubber obtained, combined with bitumen can find application in various fields, such as road paving materials, playground surfaces, thermal insulation materials [15, 16].

This paper introduces a sustainable approach in the desulfurization process of crumb rubber, by utilizing natural zeolites, like volcano tuff, found abundantly in Romania. Incorporating modified natural zeolitic catalysts in the

desulfurization of crumb rubber not only addresses environmental and industrial challenges related to sulfur-containing compounds, but also offers a cost-effective and environmentally friendly solution. By harnessing the catalytic properties of modified zeolites, particularly in the context of road pavement applications, this process aims to enhance the performance of crumb rubber while minimizing the environmental footprint of sulfur emissions.

RESULTS AND DISCUSSION

During the experimental program, volcanic tuff sourced from Mirsid, located in the county of Mirsid, Romania, was utilized. The volcanic tuff had a grain size ranging from 0.5 to 1.5 mm and consisted of 60 to 70% clinoptilolite content. [17].

To modify the initial tuff, coded *Tuf 0*, 250 g of tuff were weighed and mixed with 2 litres of aqueous solution containing 10% ammonium nitrate and 5% nitric acid in a glass reactor while stirring at 95 °C for 3 hours. After centrifugation the ammonium form of the zeolite was washed with 8 litres of distilled water and the suspension obtained was again centrifuged. The resulting zeolite was dried at 120 °C for 12 hours, then calcined at 450 °C at a heating rate of 5° C/min for 6 hours. After grinding in a planetary ball mill it was passed through a 0.63 mm sieve, the resulting sample was coded *Tuf 1*. For obtaining the zeolite sample coded *Tuf 2* the same procedure was followed, except that the reaction time with ammonium nitrate and nitric acid solution was increased to 6 hours.

Absorption isotherms and BJH desorption curves of volcanic tuff before and after modification are shown in Figures 1-3.

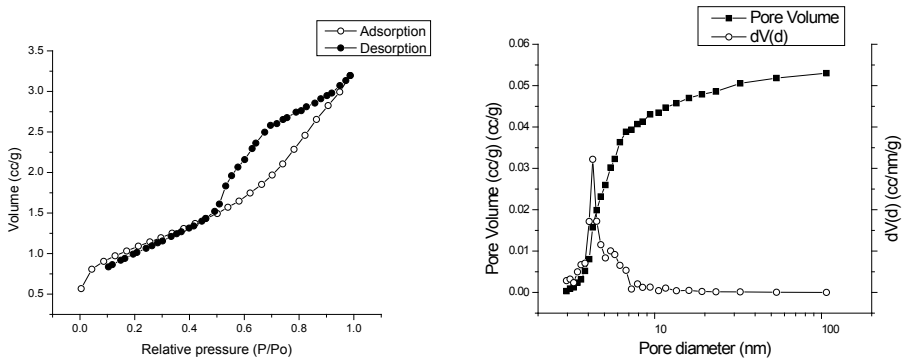

(a) (b)

Figure 1. Isotherm (a) and BJH desorption (b) of zeolite Tuf 0

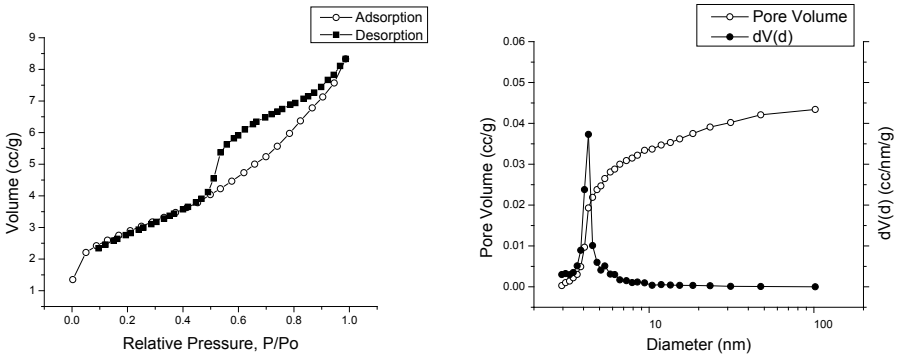

(a) (b)

Figure 2. Isotherm (a) and BJH desorption (b) of zeolite Tuf 1

Based on the conventional classification of adsorption-desorption all measured isotherms can be considered as type IV isotherms, a typical characteristic of mesoporous materials with multilayer adsorption. A type H3 hysteresis according to the IUPAC classification can be observed in all the samples, the materials analyzed being mesoporous with an average pore diameter of 4.2 nm. In this case, there is no limitation of absorption at high P/P_0 values with aggregates of plate-like particles giving rise to slit-shaped pores.

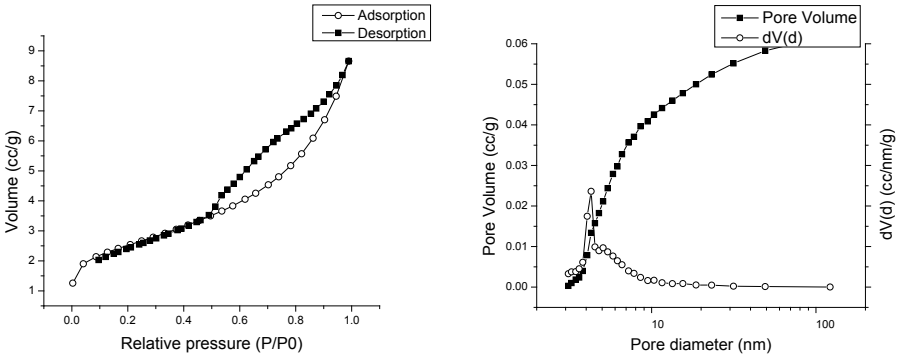

(a) (b)

Figure 3. Isotherm (a) and BJH desorption (b) of zeolite Tuf 2

Table 1 presents the main textural characteristics of the tuff before and after modification, determined by nitrogen porosimetry.

Table 1. Porosimetry data of tuff before and after modification

Sample	Specific surface area (m^2/g)	Total pore volume (cm^3/g)	Average pore diameter (nm)
Tuf 0	38.41	0.043	4.254
Tuf 1	43.62	0.056	4.282
Tuf 2	46.16	0.062	4.288

The results of particle size determinations and particle size distribution of zeolites by dynamic light scattering (DLS) are shown in Figures 4 and 5 and Table 2. The Tuf 1 and Tuf 2 samples show a bimodal distribution, showing two particle populations.

Table 2. DLS analysis of modified zeolite particles

Sample	Average diameter (nm)	Peak (Intensity) (nm)
Tuf1	726	P_1 = 655; P_2 = 151
Tuf2	1611	P_1 = 715; P_2 = 170

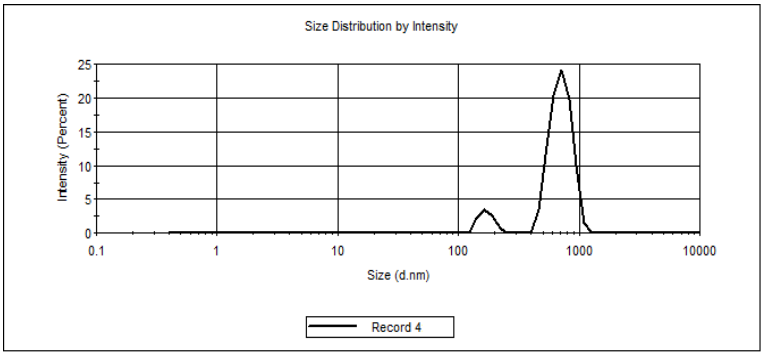

Figure 4. DLS distribution of particle sizes of Tuf 1

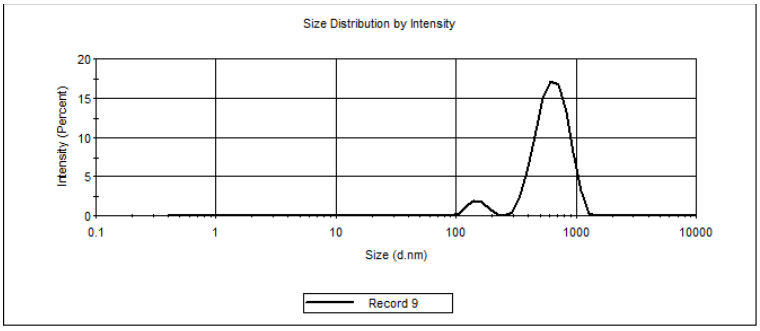

Figure 5. DLS distribution of particle sizes of Tuf 2

It can be observed that the particles of the Tuf 2 sample are relatively larger and more polydisperse than those of the Tuf 1 sample. For both samples the presence of large aggregates/particles is observed. Table 3 shows the results of acid strength determination grouped by weak, medium and strong centers obtained by diethylamine thermodesorption. A higher acid strength is observed over the whole range for the zeolite Tuf 2, with a significant increase for the medium acid centers.

Table 3. Results of acid strength determination of modified zeolites.

Sample	**Acid strength** mEq/ g sample		
	weak	**medium**	**strong**
Tuf 1	0.0899	0.0466	0.3065
Tuf 2	0.1005	0.1081	0.3107

The XRF analysis (Table 4) shows that the volcanic tuff has an initial Si/Al ratio of 11.8, and the modification of the tuff increases the Si/Al ratio for samples Tuf 1 and Tuf 2 to 14.23 and 16.09 respectively.

Table 4. Main elements as determined by the XRF method.

Element	**Conc., %**		
	Tuf 0	**Tuf 1**	**Tuf 2**
Al	2.020	1.670	1.51
Si	23.840	23.76	24.31
K	1.806	1.790	1.735
Fe	1.059	1.039	1.026

Crumb rubber powder devulcanization experiments were carried out in the presence of zeolite catalysts dispersed in xylene aromatic solvent and catalytic cracking oil (CCS) at 280ºC for 6 hours. It is observed that on the Tuf 2 zeolite catalyst, 4.0% higher conversions are obtained in the presence of xylene and 2.8% in the presence of CCS, values due to the higher acidity of the Tuf 2 catalyst (Table 5).

Table 5. Performance of the zeolite on the crumb rubber devulcanization process

Catalyst	**Tuf 1**		**Tuf 2**	
Solvent	xylene	CCS	xylene	CCS
Conversion, %	50.5	45.2	52.4	46.6

CONCLUSIONS

The desulfurization of crumb rubber was achieved using a modified clinoptilolite natural zeolitic catalyst, obtained through ion exchange with ammonium ions, the catalyst being dispersed in two types of solvents. Superior results were observed with a more acidic type of zeolite Tuf 2, due to its enhanced catalytic activity, which facilitated the desulfurization process by promoting stronger interactions between the catalyst and sulfur-containing compounds in the crumb rubber. The modification of the natural zeolite was achieved by ion exchange of alkali ions with ammonium ion followed by calcination to proton form. The modification resulted in nanostructured catalysts with an acidity distribution favorable to hydrogenolysis processes and a high concentration of strong acid centers. Total acidity also increased with the duration of the ion exchange step. The textural characteristics and size distribution of the zeolite particles changed following ion exchange.

Catalytic desulfurization of rubber powder dispersion in catalytic cracking oil and xylene in batch system at 280ºC for 6 h in the presence of modified zeolite catalysts proceeded at conversion values of application interest, being favored by higher acidity catalyst and solvent aromaticity. The applicability of this research lies in its ability to offer a sustainable solution for the desulfurization of crumb rubber using readily available natural zeolites, therefore addressing environmental concerns and enhancing the performance of road pavement materials.

EXPERIMENTAL SECTION

Materials

In the experimental program a natural zeolite was used, specifically volcanic tuff from the Mirsid area, Salaj county, Romania, with a grain size of 0.5...1.5 mm, with a clinoptilolite content of 60-70% [11]. Crumb rubber powder 30Mesh from waste tires with average particle size 0.595 mm, density 459 kg/m3, with a sulfur content of 2.16% (Grote combustion method) was used.

Catalytic cracking oil, coded *CCS* (Rompetrol) and a mixture of o,m,p-xylene, referred to as xylene (Chimreactiv SRL), was used for catalyst dispersion. Chemical reagents of analytical purity ammonium nitrate, nitric acid 55% (Chimopar SRL) were used to modify the natural zeolite.

Characterization Methods

Textural characteristics of catalysts - specific surface area, pore volume and pore size distribution were determined by nitrogen porosimetry with a NOVA 2200e apparatus (Quantachrome). From the nitrogen adsorption/ desorption isotherm recorded at 77.35 K in the relative pressure range p/po 0.005-1.0 the porosimetry data were obtained and processed with a NovaWin software. Samples were degassed for 4 h at 180°C in vacuum before adsorption measurements were performed. The specific surface area was determined from the standard BET (Brunauer-Emmett-Teller) equation, and the total pore volume was estimated from the adsorbed volume at relative pressure P/P_0 close to unity. By applying the Barrett-Joyner-Halenda (BJH) model from the desorption branch of the isotherm, the mesopore volume and pore size distribution were calculated.

The particle sizes and particle size distribution of the zeolite catalysts were determined by dynamic light scattering (DLS) with a NanoZS Zetasizer, Malvern Instruments UK. For the determinations the samples were dispersed in water, approximately 0.005g zeolite in 25 mL distilled water, prior to each determination the samples were ultrasonicated in an ultrasonic bath.

The acid strength and acid strength distribution of the modified zeolites was carried out with a DuPont Instruments apparatus by diethylamine thermodesorption [18]. Samples were maintained in a vacuum oven for 12 hours at 120ºC prior to analysis for moisture removal.

The elemental composition of samples of zeolites was determined by X-ray fluorescence spectrometry (XRF) using a portable Olympus Vanta C XRF Analyzer in GeoChem mode, an X-ray tube with rhodium anode at 40 kV and a silicon drift detector.

Modification of zeolites

For the modification of the tuff, the following procedure was used: the zeolite in powder form was mixed with an aqueous solution of nitric acid and ammonium nitrate in a glass stirred reactor with a thermostated heating jacket. A laboratory centrifuge Rotina 420R was used for separation. After centrifugation the resulting zeolite was washed with distilled water and the obtained suspension was centrifuged again. The resulting zeolite was dried in an air circulation oven and then calcined in a temperature programmed furnace. After grinding in a Fritch Pulverisette planetary ball mill, it was passed through a 0.63 mm sieve.

Desulfurization experiments

The devulcanization experiments were carried out in a stainless steel autoclave, with stirring at a speed of 180 rpm, at a temperature of 280ºC at a mass ratio of crumb rubber to aromatic solvent of 1/2 for 6 hours in an inert gas atmosphere (nitrogen). The solvents used for the experimental tests were aromatic catalytic cracking oil (CCS) and xylene. The desulfurization conversion of rubber powder in the presence of modified zeolites was calculated with equation (1), based on the total sulfur content of rubber powder before and after the experiments.

$$Conversion, \% = \frac{TSCi - TSCf}{TSCi} \cdot 100 \quad (1)$$

TSCi = initial total sulfur content of the crumb rubber sample;

TSCf = final total sulfur content of the crumb rubber sample after the desulfurization with zeolites.

ACKNOWLEDGMENTS

This work was supported by a grant of the Ministry of Research, Innovation and Digitization, CCCDI - UEFISCDI, project number PN-III-P2-2.1-PTE-2021-0552, within PNCDI III.

REFERENCES

1. R. Dong; M. Zhao; W. Xia; X. Yi; P. Dai; N. Tang; *Waste Manag.,* **2018**, *79*, 516-525.
2. J. Bian; Q. Zhang; X. Min; S. Zhang; L. Feng; C. Li; *Proc. Safety and Environ. Prot.*, **2016**, *101*, 117-123.
3. M. Labaki; M. Jeguirim; *Environ. Sci. Pollut. Res. Int.,* **2017**, *24,* 9962-9992.
4. M. Arabiourrutia; G. Lopez; M. Artetxe; J. Alvarez Bilbao; M. Olazar, *Renew. Sustain. Energy Rev*., **2020**, *129*, 109-932.
5. J. Liang, Z. Liang, R. Zou and Y. Zhao, *Adv. Mater*., **2017**, *29*,1–21.
6. K. Wang; Y. Xu; P. Duan; F. Wang; Z.-X. Xu; *J. Waste Manag.,* **2019**, *86*, 1–12.
7. B. Qu; A. Li; Y. Qu; T. Wang; Y. Zhang; X. Wang; Y. Gao; W. Fu; G. Ji; *J. Analyt. Appl. Pyrol.*, **2020**, 152.
8. R. Dehghan; M. Anbia; *Fuel Process. Techn.,* **2017**, *167*, 99-116.
9. J.R. Kima; Y.A. Kima; J.H. Yoona; D.W. Parka; H.C. Woo; *Polym. Degrad. Stab.*, **2002**, *75*, 287–294.

10. Z. Honggang; Z. Yangpeng; C. Jie; L. Wenchang; W. Wenshen; *Polymers,* **2022**, *14*, 13-65.
11. S.A. Ganiyu; S.A. Lateef; *Fuel,* **2021**, *29*, 120-273.
12. P. Xu; J. Gao; J. Pei; Z. Chen; J. Zhang; R. Li; *Constr. Build. Mater*., **2021**, 282.
13. S.-Y. Lee; J.-H. Yoon; J.-R. Kim; D.-W. Park; *J. Analyt. Appl. Pyrol.,* **2001**, *64*, 71-83.
14. M. Myhre; S.Saiwari; W. Dierkes; J. Noordermeer; *Rubber Chem. Technol,* **2012**, *85(3)*, 408–449.
15. K. Yamamoto; US Patent 4,357,377, Thermal insulating and bituminous waterproofing board and application process thereof, **1982**.
16. J. Pavlovic; M. Popova; R.M. Mihalyi; M. Mazaj; G. Mali; J. Kovač, H. Lazarova, N. Rajic, *Micropor. Mesopor. Mater*., **2019**, *279*, 10-18.
17. E. Popovici; G. Burtica; R. Pode; I. Bedelean; I. Calb; Romanian Volcanic Tuffs Exploitation in Environmental Protection. In *Natural Microporous Materials in Environmental Technology. NATO Science Series,* P. Misaelides, F. Macášek, T.J. Pinnavaia, C. Colella Eds., Springer, Dordrecht**. 1999**, vol 362, pp. 345-352.
18. D. Ion, M. Bombos, G. Vasilievici, A. Radu, P. Rosca, *Rev.Chim*. *(Bucharest)*, **2019**, *70*, 4266-4274.

STUDIA UBB CHEMIA, LXIX, 1, 2024 (p. 17-34)
(RECOMMENDED CITATION)
DOI:10.24193/subbchem.2024.1.02

HYDROTHERMAL CARBONIZATION OF DECIDUOUS WOODY BIOMASS: PATH TO ENERGY INTENSIFICATION AND FINE CHEMICALS

Mothil SENGOTTIAN[a,*], Chitra Devi VENKATACHALAM[b], Sathish Raam RAVICHANDRAN[a], Sarath SEKAR[b]

ABSTRACT. Four deciduous woody feedstocks (*Casuarina equisetifolia L., Eucalyptus globulus, Wrightia tinctoria*, and *Neolamarika cadamba*) were subjected to the Hydrothermal Carbonization (HTC) process inside a 50 mL stainless steel hydrothermal reactor at varying temperatures (180°C, 215°C, and 250°C), while keeping water-to-feedstock ratio (6:1 v/w%) and residence time (1.5 h) constant. The mass yield and energy yield of the resulting biomass were calculated as parameters for energy intensification. Characterization of the biomass, biochar, and bio-oil was conducted using elemental analysis, SEM, and GC–MS. Interestingly, the mass yield of biochar decreased with increasing temperature, but it significantly improved the energy densification ratio, with a minimum of 1.06 observed for *Neolamarika cadamba* biomass at 180°C and a maximum of 1.23 observed for *Eucalyptus globulus* biomass at 250°C. Moreover, detailed analysis of the bio-oil obtained at 250°C using GC-MS revealed the presence of a diverse range of fine chemicals, including benzyl, carboxylic acid, ester, methyl, phenol, pyrrole, nitro, and aliphatic hydrocarbons. These findings suggest that the HTC process can be optimized to tailor the production of specific value-added chemicals from lignocellulosic woody biomass.

Keywords: *Hydrothermal carbonization (HTC), Biomass, Bio-oil, Biochar, Fine chemicals*

[a] *Department of Chemical Engineering, Kongu Engineering College, Erode-638060, Tamil Nadu, India*
[b] *Department of Food Technology, Kongu Engineering College, Erode-638060, Tamil Nadu, India*
* *Corresponding author smothil666@gmail.com*

INTRODUCTION

Biomass refers to the organic matter derived from plants and animals including the wastes generated out of them [1]. Utilization of this effectively as a resource for energy, heat production, and value added products and chemicals are done through various energy production and intensification process. The search for effective, sustainable and non-polluting technology has never ended and each of them has its own merits and demerits. The main problem during this conversion is the non-uniformity in composition, availability of the resource in a continuous manner, pretreatment of the feedstock and purity of products obtained [2]. Some of the technologies that has been developed by the primitive humans and they are being fine-tuned ever since via both biochemical and thermochemical pathways. The biochemical methods include: extraction, hydrolysis followed by trans-esterification or fermentation resulting in bioethanol and other products [3]. The thermochemical methods include: combustion, gasification, pyrolysis, carbonization and hydrothermal treatment [4,5]. The hydrothermal treatment is the main concern in this study and the focus is given to especially hydrothermal carbonization of selective species of lignocellulosic woody biomass.

Hydrothermal Carbonization (HTC) involves thermal degradation of biomass under subcritical water environment at high temperatures (180 to 250°C) and pressures (2 to 10 MPa) for several hours [6]. This process mimics the natural coalification that takes several hundred years to form peat and million years to form coal, but it only takes a few hours to yield biochar with properties similar to brown coal [7]. HTC is an exothermic reaction and is characterized by the production of solid carbonaceous material called biochar or hydrochar, as well as special chemicals in the form of liquid or dissolved in the residual water through hydrolysis of the biomass. Some of the chemicals produced include organic acids, furfural, and furanoid derivatives [8]. HTC holds significant importance in the production of high-quality biochar with special properties used in pollution control, as adsorbents for removing heavy metals [8, 9] and dyes [10, 11], soil remediation [13], energy generation [14], storage [15] and many other applications.

This study was conducted to gain insights into the reaction mechanism and chemistry underlying the hydrothermal carbonization of lignocellulosic biomass. The primary constituents of plant cell walls are lignocellulose, consisting of layers of cellulose microfibrils, hemicellulose, pectin, and lignin arranged in a uniform structure [16]. Additionally, plant cell walls contain proteins, soluble extractives in smaller amounts, and non-structural materials, such as sugars, nitrogenous compounds, waxes, chlorophyll, and ash [17].

Lu X et al. investigated the hydrothermal carbonization of cellulose at temperatures ranging from 225°C to 275°C, with reaction times between 0.5 to 4 hours. They reported faster conversion at higher temperatures, leading to increased cellulose solubilization and lower wt% of solids with sp2 carbons (furanic and aromatic groups) and alkyl groups [18]. HTC of hemicellulose substitute (D-xylose) exhibited a high hydrochar yield of 50 wt% at 225°C, which slightly decreased at 265°C due to dehydration and decarboxylation, with the formation of furfural as an important intermediate [19]. *Kim D et al.* observed a modest increase in energy densification and high heating value (HHV), but temperatures between 250°C and 280°C favored faster decomposition of lignin, resulting in improved energy densification of 28% and fixed densification of 55% compared to feedstock composition [20].

The chemical composition of biomass can vary from one plant species to another, impacting the yield of HTC products. Although the chemical reactions of the three main model compounds: cellulose, hemicellulose, and lignin are well-defined, the interactions of intermediate reaction species of these individual compounds vary with each biomass, leading to a diverse range of products [21, 22]. Thus, this study aims to explore different woody species of biomass: *Casuarina equisetifolia L. (CE), Eucalyptus globulus (EG), Wrightia tinctoria (WT)*, and *Neolamarika cadamba* (NC) to establish relationships between their constituent ratios, yield, obtain optimized conditions for hydrothermal carbonization and identify the constituents present in the bio-oil obtained.

RESULTS AND DISCUSSION

The physical properties of woody species are listed in Table 1 which was obtained from: Research Wing, Tamil Nadu Forests Department, Chennai. The woody species were chosen based on the wide differences in their morphology, physical properties, and internal tissue structure, as shown in Figure 1.

Table 1. Physical Properties of raw biomass for four wood species

Deciduous Tree Species	Density kg/m^3	Modulus of elasticity kgf/cm^2	Modulus of Rupture kgf/cm^2	Hardness & Grain structure
CE	693	1,14,400	732	Hard to very hard with straight grains
EG	678	99,400	1312	Moderately hard with straight to slightly interlocked grains
ET	570	98,560	946.3	Moderately Hard with even grains
NC	463	95,200	884.1	Soft, Light and Even grained

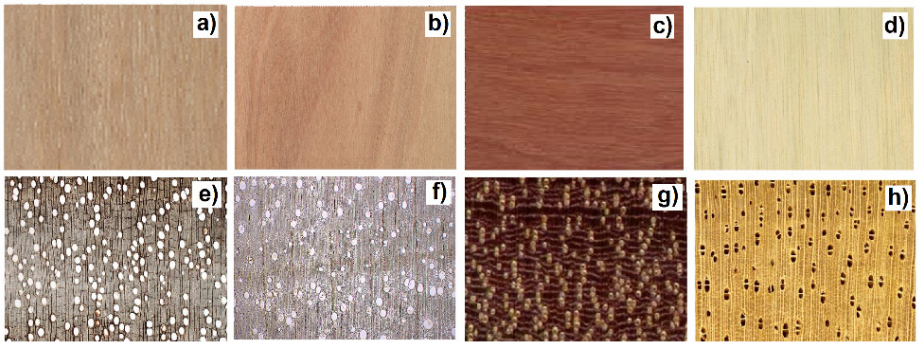

Figure 1. Wood Macroscopic Tangential Section (Polished) a) *CE* b) *EG* c) *WT* d) *NC, Wood Microscopic Transverse Section* - e) *CE* f) EG g) WT h) NC (Adopted from Richter, H.G., Gembruch, K., and Koch, G. 2014 onwards. CITESwoodID: descriptions, illustrations, identification, and information retrieval. In English, French, German, and Spanish. Version: 17th February 2019. delta-intkey.com)

The chemical constituents and the proximate analysis results are presented in Table 2. Although there is no direct relationship between these two sets of data, they were considered to aid in comprehending the hydrothermal carbonization of the four deciduous wood species. It's crucial to emphasize that the composition of chemical constituents in biomass can undergo significant variations influenced by several factors. These include the type of biomass, plant species, growth processes and conditions, plant age, doses of fertilizers and pesticides applied, harvest timing, collection methods, potential contamination, transportation, storage, processing, and other contributing factors [29]. However, in the context of this study, the findings were derived from tree cuttings (12 cm in diameter and 50 cm in length) sourced from the Forest College & Research Institute, Tamil Nadu Agricultural University, Mettupalayam.

Table 2. Chemical Constituents for four wood species

Species	Holo-cellulose (%)	Lignin (%)	Extractives (%)	Ash (%)	Moisture (%)	Fixed Carbon (%)	Volatile (%)
CE	68	39.5	7.5	0.3	10.8	16.4	72.5
EG	66.2	27.7	6.1	0.4	2.28	13.89	83.44
WT	70.1	22.1	7.8	0.65	1.1	17.8	80.45
NC	85.47	31.24	2.45	0.55	9.06	18.4	71.99

The structural characteristics of raw wood, as outlined in Table 1, evidently hinge on the chemical constituents present. Holocellulose, encompassing both cellulose and hemicellulose, in conjunction with lignin, assumes a crucial role in constituting the fundamental building blocks of the wood's cell wall. A higher lignin percentage contributes to denser wood with enhanced flexural properties. Meanwhile, cellulose, hemicellulose (xyloglucan), and pectin are essential for both inherent strength and the capacity to respond to cell expansion during growth. The interplay between hemicellulose and cellulose networks provides a harmonious blend of extensibility and strength, vital for primary cell walls, a balance unattainable with cellulose alone [30].

Table 2 distinctly illustrates notable differences in chemical constituents among various wood species, facilitating a comprehensive examination of their impact on hydrothermal carbonization. Fig 2 presents a comparative analysis of the chemical constituents of wood obtained through proximate analysis, juxtaposed with its pure chemical components and other energy-intensive products such as lignite and coal [20] [31].

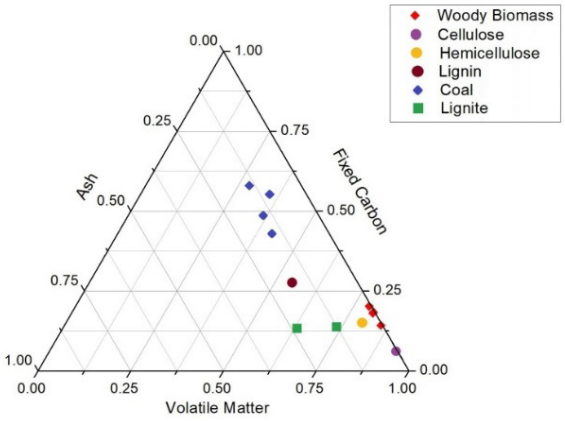

Figure 2. Proximate Analysis of Woody Biomass Feedstock: Comparing Constituents and Energy-Intensive Products.

Hydrothermal carbonization and Energy intensification

Figure 3 shows the biochar obtained during the HTC process. In Figure 4, the yields of hydrothermal carbonization (HTC) products, including biochar, bio-oil, and biogas, are depicted for four biomass species: *Casuarina equisetifolia L., Eucalyptus globulus, Wrightia tinctoria,* and *Neolamarika cadamba*. The experiments were conducted at various temperatures (180°C, 215°C, and 250°C), maintaining a consistent reaction time of 1.5 hours and a water-to-feedstock ratio of 6:1.

The hydrothermal carbonization (HTC) on the four biomass feedstocks revealed similar trends at 180°C and 215°C, whereas at 250°C, there was a decrease in biochar yield accompanied by an increase in biooil production. Casuarina equisetifolia L. and Eucalyptus globulus exhibited similarities to other coniferous trees like pine and spruce. In contrast, Wrightia tinctoria and Neolamarika cadamba displayed a notable increase in biooil yield, attributed to the higher content of crystalline hemicellulose in the softwood species. The important parameters for hydrothermal carbonization, such as mass yield, energy densification ratio, and energy yield, were calculated using equations (3, 4, and 5), with the results presented in Table 3.

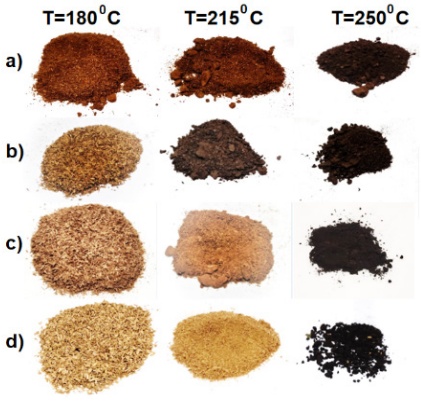

Figure 3. Biochar after HTC -*a) Casuarina equisetifolia L. b) Eucalyptus globulus c) Wrightia tinctoria d) Neolamarika cadamba*

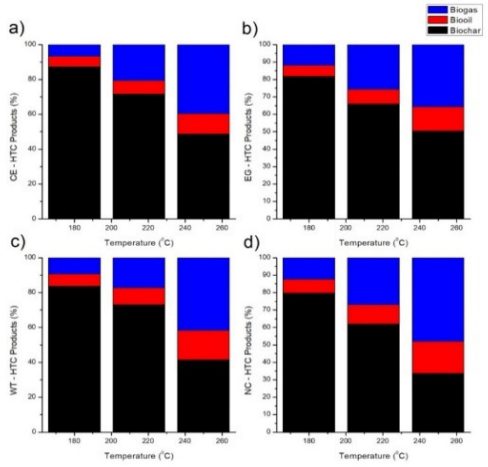

Figure 4. Effect of temperature and yield of HTC products -
a) *Casuarina equisetifolia L.* b) *Eucalyptus globulus* c) *Wrightia tinctoria* d) *Neolamarika cadamba*

Table 3. Energy intensification of HTC products

Species	Temperature (°C)	C (%)	H (%)	N (%)	O (%)	HHV $MJkg^{-1}$	MY (%)	EDR	EY (%)
CE	30	43.8	5.8	0.28	45.37	14.08			
	180	49.4	5.1	0.13	43.20	17.33	87.33	1.11	97.29
	215	52.5	4.2	0.10	39.22	17.64	71.67	1.13	81.24
	250	58.2	2.5	0.08	33.39	18.14	48.67	1.17	56.75
EG	30	42.4	6.1	0.12	51.37	13.91			
	180	48.3	5.4	0.10	46.20	17.19	81.67	1.12	91.66
	215	56.1	3.5	0.09	40.31	18.45	66.00	1.20	79.47
	250	59.7	2.5	0.09	37.71	18.86	50.33	1.23	61.97
WT	30	43.2	6.0	0.62	50.20	14.25			
	180	47.5	5.3	0.47	46.73	16.72	83.67	1.07	89.63
	215	53.4	4.1	0.43	42.07	17.98	73.00	1.15	84.06
	250	60.8	2.1	0.41	36.69	18.90	41.33	1.21	50.05
AC	30	44.5	6.4	0.31	48.80	15.46			
	180	49.9	5.2	0.32	44.58	17.72	79.67	1.06	84.60
	215	54.2	3.9	0.30	41.61	18.08	62.00	1.08	67.17
	250	62.5	1.8	0.28	35.42	19.31	33.67	1.16	38.95

Table 3 presents the fuel properties of HTC biochar, indicating a noticeable increase in the Higher Heating Value (HHV) with higher temperatures. Concurrently, as the temperature increased, the mass yield of biochar decreased while the energy densification demonstrated improvement. Specifically, Neolamarika cadamba biomass showed a minimum energy densification of 6% at 180°C, while Eucalyptus globulus biomass exhibited the highest energy densification of 23% at 250°C. Figure 5 depicts the Van Krevelen diagram, which enables a meaningful comparison of biomass feedstock, biochar at different temperatures, and energy intensified reference products like lignite, coal, and coke.

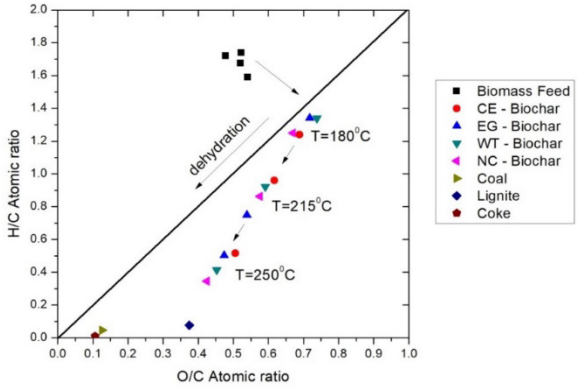

Figure 5. The Van Krevelen diagram of biomass at three HTC reaction temperatures in comparison with energy intensified reference products

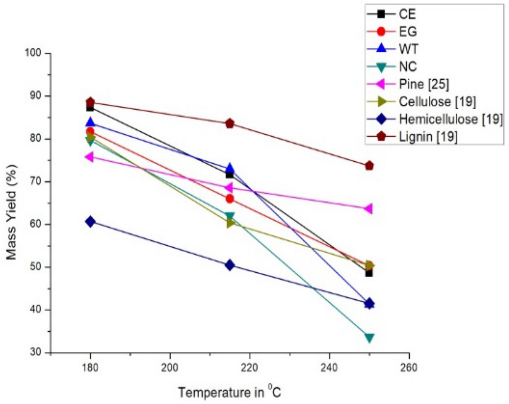

Figure 6. Mass yield in comparison with that of obtained from pure components

An intriguing observation is the significant dehydration effect during HTC compared to conventional coalification processes. In Figures 6 and 7, the mass yield and energy yield of the four deciduous biomass species are depicted at various reaction temperatures (180°C, 215°C, and 250°C). These results are compared with their pure components and simulated outcomes from correlations developed for coniferous pine species, as presented in Equations 6 and 7, respectively [20] [28].

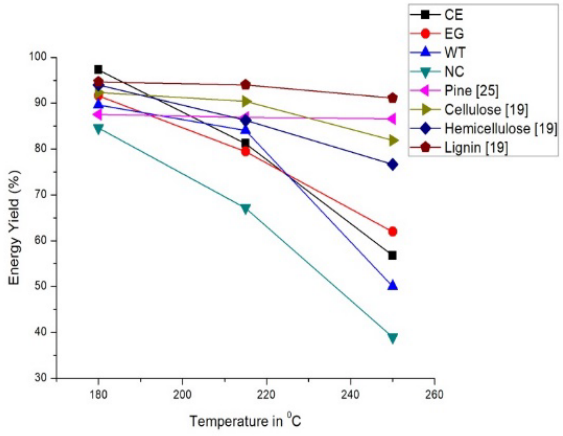

Figure 7. Energy yield in comparison with that of obtained from pure components

The SEM analysis was conducted on the selected biomass (Eucalyptus globulus) resulting from HTC at different temperatures (180°C, 215°C, and 250°C) under constant reaction time (1.5 hours) and a consistent water to feedstock ratio of 6:1. Figure 8 a) depicts the biochar obtained at 180°C at

x150 magnification, indicating the initiation of carbonization with the biomass beginning to flake on the surface. Similarly, Figure 8 b) illustrates the biochar at 215°C, where the biomass is further broken down into smaller particles (250 μm) compared to the previous condition. While in Figure 8 c), the biochar particles at 250°C show further intensification to a size of 50 μm.

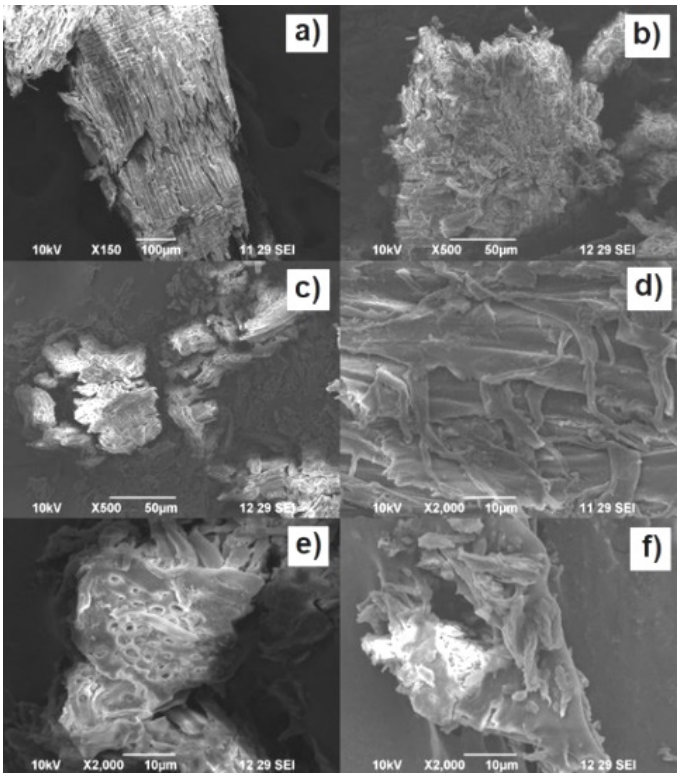

Figure 8. SEM Image of *Eucalyptus globulus* - HTC biochar a) 180°C at x150, b) 215°C at x500, c) 250°C at x500, d) 180°C at x2000, e) 215°C at x2000, f) 250°C at x2000

Figure 8 d), e) and f) shows thermally disintegrated biomass at higher magnification (x2000) at temperatures 180°C, 215 °C and 250 °C respectively. Figure 8 d) shows that the exterior fibres of the woody biomass are observed to be disintegrated. Figure 8 e) shows the transverse section of the biochar with enlarged vessels and this indicate that the reaction is not solely oriented inward but also outward from the vessels. Figure 8 f) reveals a completely modified surface with amorphous lumps.

Chemical characterization of bio-oil from HTC

The experimental results indicated that the highest biooil yield was observed at 250°C. The composition of the bio-oil obtained from the four deciduous feedstocks was analyzed using Gas Chromatography-Mass Spectrometer (GC-MS), and the detailed analysis results are presented in Table 4.

Table 4 Chemical constituents in HTC bio-oil

	Retention Time (min)	Area (%)	Molecular Formula	Average Mass (Da)	IUPAC Name
CE	7.17	1.510	$C_{20}H_{32}O_3$	320.46	Benzyl oxy tridecanoic acid
	13.25	1.578	$C_{20}H_{32}O_3$	320.46	Benzyl oxy tridecanoic acid
	25.76	62.07	$C_{24}H_{38}O_4$	390.55	1,2-Benzenedicarboxylic acid, diisooctyl ester
	31.79	2.077	$C_{25}H_{50}O_2$	370.67	Methyl 12-methyltetradecanoate
	31.86	7.693	$C_{25}H_{50}O_2$	370.67	Methyl 12-methyltetradecanoate
EG	7.9	3.138	$C_{11}H_{11}N$	157.21	Pyrrole, 2-methyl-5-phenyl-
	8.36	31.937	$C_8H_{10}O_3$	154.16	Phenol, 2,6-dimethoxy-
	13.67	5.391	$C_{11}H_{14}O_3$	194.23	Phenol, 2,6-dimethoxy-4-[2-propenyl]-
	14.58	11.608	$C_{11}H_{14}O_4$	210.23	2-Pentanone, 1-[2,4,6-trihydroxyphenyl]
	31.82	4.181	$C_{25}H_{50}O_2$	370.67	Methyl 12-methyltetradecanoate
WT	4.16	11.130	$C_{15}H_{14}O_2$	226.28	3-Benzyl-4-methoxybenzaldehyde
	4.5	10.153	C_8H_{14}	110.20	1-Methylcyclohex-1-ene
	8.39	33.838	$C_8H_{10}O_3$	154.16	Phenol, 2,6-dimethoxy-
	11	3.158	$C_9H_{13}NO_3$	183.2	Cyclohexanone, 2-[2-nitro-2-propenyl]-
	11.2	9.586	$C_{15}H_{14}O_2$	226.28	3-Benzyl-4-methoxybenzaldehyde
	14.59	13.261	$C_{11}H_{14}O_4$	210.23	2-Pentanone, 1-[2,4,6-trihydroxyphenyl]
	31.87	18.874	$C_{25}H_{50}O_2$	370.67	Methyl 12-methyltetradecanoate
NC	4.15	4.774	$C_{16}H_{24}$	216.37	3-Phenyldecane
	7.04	1.513	$C_{20}H_{38}O_2$	310.52	Methyl 9-octadecenoate
	13.42	1.716	$C_{13}H_{16}O$	188.27	1-Benzyloxy-2,4-dimethylbenzene
	17.02	1.988	$C_{34}H_{50}O$	474.76	2,3,5,6-Tetramethylphenol
	17.94	11.916	$C_{23}H_{30}O_4$	370.48	1,4-Benzenedicarboxylic acid, 2-(decyloxy)ethyl ester
	20.65	0.929	$C_{25}H_{48}O_2$	368.66	Methyl 9-octadecenoate
	25.76	68.694	$C_{24}H_{38}O_4$	390.55	1,2-Benzenedicarboxylic acid, diisooctyl ester
	31.85	6.207	$C_{23}H_{30}O_4$	370.48	1,4-Benzenedicarboxylic acid, 2-(decyloxy)ethyl ester

The biooil obtained from HTC of *Casuarina equisetifolia L*. biomass at 250°C was analyzed to have Benzyl oxy tridecanoic acid, 1,2-Benzenedicarboxylic acid, diisooctyl ester, and Methyl 12-methyltetradecanoate. The formation of these compounds was attributed to various chemical reactions that occur during the HTC process [32]. Benzyl oxy tridecanoic acid was identified as a product of lignin degradation, while 1,2-Benzene dicarboxylic acid, diisooctyl ester, likely resulted from reactions between aromatic compounds and aliphatic alcohols or carboxylic acids[33]. Furthermore, Methyl 12-methyltetradecanoate was found to be produced through the decarboxylation of fatty acids present in the biomass [34].

The biooil obtained from the HTC of *Eucalyptus globulus* at 250°C revealed the presence of several important constituents, including Pyrrole, 2-methyl-5-phenyl-, Phenol, 2,6-dimethoxy-, and Phenol, 2,6-dimethoxy-4-[2-propenyl]-, which were likely formed through the degradation and condensation of lignin and hemicellulose components [35]. The thermal decomposition of polyphenols present in the Eucalyptus biomass resulted in the formation of 2-Pentanone, 1-[2,4,6-trihydroxyphenyl]. Furthermore, Methyl 12-methyltetradecanoate was detected, indicating the presence of fatty acids and their derivatives in the biooil [34].

The biooil resulted from the HTC of *Wrightia tinctoria* at 250°C exhibited a diverse array of constituents, including 3-Benzyl-4-methoxybenzaldehyde, 1-Methylcyclohex-1-ene, Phenol, 2,6-dimethoxy-, and Cyclohexanone, 2-[2-nitro-2-propenyl]-. These compounds are likely formed through various chemical reactions involving the breakdown and rearrangement of lignin, cellulose, and hemicellulose present in the biomass [36][37]. The detection of 3-Benzyl-4-methoxybenzaldehyde suggests the involvement of benzyl groups in the degradation processes. Furthermore, the presence of 2-Pentanone, 1-[2,4,6-trihydroxyphenyl], and Methyl 12-methyltetradecanoate indicates the presence of polyphenolic compounds and fatty acids in the biooil [34].

The biooil resulted from the HTC of *Neolamarika cadamba* at 250°C exhibited a varied range of constituents, including 3-Phenyl decane, Methyl 9-octadecenoate, 1-Benzyloxy-2,4-dimethyl benzene, 2,3,5,6-Tetramethylphenol, 1,4-Benzene dicarboxylic acid, 2-(decyloxy)ethyl ester, and 1,2-Benzene dicarboxylic acid, diisooctyl ester. The presence of 3-Phenyldecane suggests the involvement of aromatic compounds and aliphatic alcohols in the biooil formation and aging of biooil on storage [38]. Methyl 9-octadecenoate indicates the presence of fatty acids and their derivatives in the biooil [34]. Furthermore, the identification of 1-Benzyloxy-2,4-dimethylbenzene and 2,3,5,6-Tetramethylphenol implies the possible involvement of lignin degradation and the formation of phenolic compounds during the HTC process. Additionally, the presence of 1,4-Benzenedicarboxylic acid, 2-(decyloxy)ethyl

ester, and 1,2-Benzenedicarboxylic acid, diisooctyl ester may be attributed to the interaction of aromatic compounds with aliphatic alcohols or carboxylic acids during the biomass conversion.

The biooils resulted from the hydrothermal carbonization (HTC) process of various biomass sources exhibited a variety of functional groups, including benzyl, carboxylic acid, ester, methyl, phenol, pyrrole, nitro, and aliphatic hydrocarbons. These functional groups are indicative of the chemical transformations that occur during the HTC process, involving lignin degradation, esterification, condensation reactions, and decarboxylation of fatty acids. The presence of these diverse functional groups highlights the complex nature of the biooil composition and its potential for various applications in renewable energy and value-added products.

CONCLUSIONS

The hydrothermal carbonization (HTC) process was successfully applied to four different biomass sources, namely *Casuarina equisetifolia L., Eucalyptus globulus, Wrightia tinctoria*, and *Neolamarika cadamba*, at varying reaction temperatures of 180°C, 215°C, and 250°C. The results showed that HTC can effectively convert woody biomass into biooil, biochar, and biogas products. It was observed that at 180°C maximum mass yield was obtained while maximum energy intensification was achieved at 250°C. The surface morphology study confirmed that HTC changes the uniform fibrous woody biomass structure to an amorphous biochar at higher temperatures. Higher biooil yield was observed at 250°C. The biooil obtained from the HTC process exhibited a complex composition with various functional groups, including benzyl, carboxylic acid, ester, methyl, phenol, pyrrole, nitro, and aliphatic hydrocarbons. These functional groups indicate the occurrence of diverse chemical reactions during the HTC process, involving lignin degradation, esterification, and fatty acid decarboxylation. The study demonstrated that the reaction temperature significantly influenced the biooil yield and composition, with higher temperatures favoring the formation of biooil and reducing the biochar yield. Moreover, specific biomasses exhibited unique compositions of biooil constituents, indicating that the HTC process can be tailored to optimize the production of desired products from different feedstocks. Overall, this study sheds light on the potential of HTC as a promising thermochemical conversion technology for the valorization of woody biomass into valuable bio-based products and renewable energy sources.

EXPERIMENTAL SECTION

Chemical constituent analysis and proximate analysis

A typical wood or plant material consists of four basic constituents: extractives, holo-cellulose (cellulose + hemicellulose), lignin, and ash. For this study, 4 grams of oven-dried wood of particle size 0.40 mm (40 mesh) was subjected to sequential extraction using 95% ethanol, pure benzene, 98% dichloromethane, 1:2 volume mixture of ethanol-benzene, and 99.5% acetone, each for 4-5 hours using a Soxhlet extraction setup. The percentage of extractives was determined using TAPPI (T 204 cm-97) after the evaporation of residual solvent and drying for 1 hour at 105 ± 3°C, followed by cooling in a desiccator and calculated using Equation (1) [23]. The percentage of holo-cellulose and lignin was determined from the extractives-free wood sample using standard methods provided by TAPPI T 203 and TAPPI T 222 om-21 respectively [24]. The wood was extracted consecutively with 17.5% and 9.45% sodium hydroxide solutions at 25°C. The soluble fraction, consisting of beta- and gamma-celluloses, is determined volumetrically by oxidation with potassium dichromate, and the alpha-cellulose, as an insoluble fraction, is derived by difference. The acid-soluble lignin was determined in a solution, after filtering off the insoluble lignin, by a spectrophotometric method based on absorption of ultraviolet radiation at wavelength 205 nm.

$$\text{Extractives (\%)} = [(W_e - W_b)/ W_p] \times 100 \quad (1)$$

where W_e is the dry weight of extract in g, W_b is the dry weight of blank residue in g and W_p is the dry weight of the wood in g.

The proximate analysis was performed as per ASTM standards to determine volatile matter, ash, moisture, and fixed carbon present in the solid samples. The volatile matter was determined by subjecting the sample to a temperature of 950 ± 20°C for 7 minutes in a covered crucible within a muffle furnace. Subsequently, the cooled sample was placed in a desiccator for further analysis as per ASTM-E872. To ascertain the percentage ash content (in accordance with ASTM-E1755), the desiccated solid samples underwent heating at 575 ± 25°C for a duration of 3 hours in a muffle furnace. Concurrently, the percentage moisture content was determined by exposing a measured sample quantity to an air oven set at 103°C for a period of 16 hours, following ASTM-E871-82. [25]. Equation (2) was utilized to estimate the Fixed Carbon Content (FCC) as given in ASTM D3172-13.

$$\text{FCC (\%)} = 100 - (\text{\% volatile matter} + \text{\% ash} + \text{\% moisture}) \quad (2)$$

Hydrothermal carbonization and Energy intensification

HTC of woody biomass was conducted in a 50 mL non-stirred hydrothermal reactor at varying reaction temperatures (180°C, 215°C, and 250°C), maintaining a consistent reaction time of 1.5 hours. The reactor was fitted with a k-type temperature transducer to measure the internal temperature. The setup was placed inside a muffle furnace, and the furnace temperature was controlled proportionally to the internal reactor temperature. A total of 3 grams of woody biomass feedstock with 18 mL of deionized water was added to maintain a water to feedstock ratio of 6:1 (on volume to mass ratio). The initial average moisture content of the woody biomass feedstock was measured using Thermo-gravimetry to be 7.85%. The reactor was heated at a rate of 40°C/min and held for the specified reaction duration. Subsequently, rapid cooling was achieved by immersing the reactor in cold water. Once the system reached room temperature, the pressure release valve was opened, and the evolved gaseous products were collected in a 1 L Tedlar bag. Separation of solid and liquid products was accomplished using a fine mesh nylon cloth with a maximum pore size of 0.15 mm. The liquid product obtained was subjected to cooling at 15°C, followed by centrifugation to separate residual water from the bio-oil. The solid component was washed with dichloromethane, filtered through paper with a pore size of 2.5 µm, and then subjected to evaporation to gather the bio-oil mixed with solid char. The solid char was subsequently dried overnight (for a minimum of 12 hours) in an oven set at 103°C. Figure 9 illustrates the schematic diagram of the HTC process employed in this study.

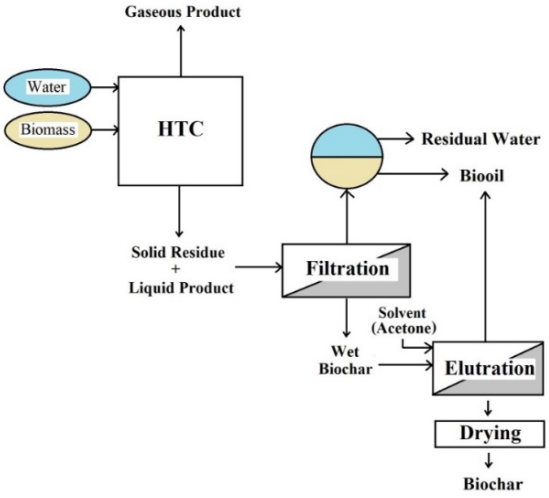

Figure 9. Schematic diagram for hydrothermal carbonization process.

The CHN Elemental analyzer (Thermo Finnigan, Italy) was employed to determine the elemental composition (C, H, and N) of both the feed and biochar samples. The oxygen content was derived by difference. The theoretical higher heating value (HHV) in MJ/kg was computed using an empirical correlation established by Channiwala and Parikh (2002) through Equation (3):

$$HHV=0.3491C+1.1783H+0.1005S-0.1034O-0.0015N-0.0211A \quad (3)$$

In this equation, C, H, S, O, N, and A denotes the weight percentages of carbon, hydrogen, sulfur, oxygen, nitrogen, and ash in solids, respectively [26].

Kambo, H. and Dutta, A. [27] pinpointed crucial parameters for hydrothermal carbonization, specifically mass yield, energy densification ratio, and energy yield. These parameters were computed using the following equations (4, 5, and 6)

$$\text{Mass yield (MY)} = M_{product} / M_{feed} \quad (4)$$

$$\text{Energy densification ratio (EDR)} = HHV_{char} / HHV_{feed} \quad (5)$$

$$\text{Energy yield (EY)} = MY / EDR \quad (6)$$

where M_product and M_feed are the mass of dried and moisture free char, oil or gas produced individually and mass of dried raw feedstock, while HHV_char and HHV_feed are the HHV of biochar (on dry basis) and HHV of raw feedstock (on dry basis).

The following correlation was used by Sermyagina, E et al. (2015) to describe the experimental results for mass yield and energy yield with satisfactory accuracy for temperature range between 180 and 250°C; calculating the constants by minimizing the RSS:

$$\text{Mass yield (MY\_Ser)} = (1-0.04079(T-150)^{0.337} t^{0.2142} r^{0.3055}) \quad (7)$$

$$\text{Energy yield (EY\_Ser)} = (1-0.05632(T-150)^{0.062} t^{0.2846} r^{0.4405}) \quad (8)$$

In the experimental study, the process temperature (T) was measured in °C, the residence time (t) was measured in hours, and the water to biomass ratio (r) was considered. The obtained experimental results from equations (3) and (4) were compared with the corresponding correlation curves obtained from equations (7) and (8). This comparison aimed to determine the similarity in the hydrothermal carbonization (HTC) of biomass that exhibited similar characteristics but with somewhat different rates [28].

To investigate the morphology of the selected biochars at different experimental temperatures (180°C, 215°C, 250°C) and magnifications (x150, x500, x2000), Scanning Electron Microscope (SEM) analysis was conducted using a Jeol JSM 6390 instrument. This analysis aimed to identify the morphological changes in the surfaces and structures of the biochar during the HTC process.

Chemical Characterization of bio-oil from HTC

To examine the liquid fraction known as bio-oil from HTC, Gas Chromatography-Mass Spectrometer (GC-MS) analysis was conducted employing Agilent 7890 with a Flame Ionization Detector (FID) and Jeol AccuTOF GCV to identify its chemical constituents. The GC-MS system included a glass column with a 0.53 mm internal diameter, 105 m length, and a film thickness of 0.25 µm. A 2 µL sample was introduced through the injector, utilizing helium as the carrier gas. The MS operated at 70 eV of ionization energy. Carrier gas column flow and purge flow were maintained at 1 mL/min and 5 mL/min, respectively, initiating with an oven temperature of 50°C, escalating to 280°C over 22 min, and held for 35 min. The mass range spanned from 45 to 300 amu, with a scan interval of 0.50 s, and the MS source temperature was set at 260 °C. The split ratio was 10:0, and the entire duration of the GC-MS analysis amounted to 65 min. The relative percentage of each component was expressed as a percentage with peak area normalization.

ACKNOWLEDGMENTS

The authors would like to extend their thanks to SAIF, IIT Bombay, the Center of Research in Nanotechnology at Karunya Institute of Technology and Sciences, Coimbatore, for their assistance in analysis and particle characterization, and Tamil Nadu Forests Department, Chennai and Mettupalayam for their guidance and support. Additionally, gratitude is expressed to the Department of Chemical Engineering, Kongu Engineering College, Perundurai, Erode, for providing the necessary infrastructure facilities and support for conducting the aforementioned research.

REFERENCES

1. J.J. Chew, V. Doshi, *Renew. Sustain. Energy Rev*., **2011**, *15*, 4212–4222.
2. B. Dou, H. Zhang, Y. Song, L. Zhao, B. Jiang, M. He, C. Ruan, H. Chen, Y. Xu, *Sustain. Energy Fuels*, **2019**, *3*, 314–342.
3. H. Chen, X. Fu, *Renew. Sustain. Energy Rev*., **2016**, *57*, 468–478.
4. B. Ercan, K. Alper, S. Ucar, S. Karagoz, *J. Energy Inst*., **2023**, *109*, 101298.

5. P. Basu, Biomass Gasification, Pyrolysis Torrefaction Pract. Des. Theory **2013**, 1–530.
6. S.S. Jamari, J.R. Howse, *Biomass Bioenerg*, **2012**, *47*, 82–90.
7. H.-G. Ramke, D. Blöhse, H.-J. Lehmann, J. Fettig, S.T. Höxter, Sardinia 2009 Twelfth Int. Waste Manag. Landfill Symp. **2009**.
8. A. Funke, F. Ziegler, *Biofuels, Bioprod. Biorefining*, **2010**, *4,* 160–177.
9. S.E. Elaigwu, V. Rocher, G. Kyriakou, G.M. Greenway, *J. Ind. Eng. Chem.*, **2014**, *20*, 3467–3473.
10. P. Regmi, J.L. Garcia Moscoso, S. Kumar, X. Cao, J. Mao, G. Schafran, *J. Environ. Manage.*, **2012**, *109*, 61–69.
11. M.A. Islam, A. Benhouria, M. Asif, B.H. Hameed, *J. Taiwan Inst. Chem. Eng.*, **2015**, *52*, 57–64.
12. H.H. Hammud, A. Shmait, N. Hourani, *RSC Adv.*, **2015**, *5*, 7909–7920.
13. S.M. Heilmann, J.S. Molde, J.G. Timler, B.M. Wood, A.L. Mikula, G. V. Vozhdayev, E.C. Colosky, K.A. Spokas, K.J. Valentas, *Environ. Sci. Technol.*, **2014**, *48*, 10323–10329.
14. N.D. Berge, L. Li, J.R.V. Flora, K.S. Ro, *Waste Manag.*, **2015**, *43*, 203–217.
15. Z. Gao, Y. Zhang, N. Song, X. Li, *Mater. Res. Lett.*, **2017**, *5*, 69–88.
16. S. van L. and J. Koppejan, ed., The Handbook of Biomass Combustion and Co-Firing, Routledge, **2012**, London.
17. M.B. Sticklen, *Nat. Rev. Genet.*, **2008**, *9*, 433–443.
18. X. Lu, P.J. Pellechia, J.R.V. Flora, N.D. Berge, *Bioresour. Technol.*, **2013**, *138*, 180–190.
19. S. Kang, X. Li, J. Fan, J. Chang, *Ind. Eng. Chem. Res.*, **2012**, *51*, 9023–9031.
20. D. Kim, K. Lee, K.Y. Park, *J. Ind. Eng. Chem.*, **2016**, *42*, 95–100.
21. S. Kamal, M.S. Hossain, I.H. Sadab, K.B. Kabir, K. Kirtania, *Fuel Commun.* **2023**, 100090.
22. M. Volpe, A. Messineo, M. Mäkelä, M.R. Barr, R. Volpe, C. Corrado, L. Fiori, *Fuel Process. Technol.*, **2020**, *206*, 106456.
23. TAPPI (*Technical Association of Pulp and Paper Industry*), T 204 C. **2007**.
24. T. Ona, T. Sonoda, M. Shibata, K. Fukazawa, *Tappi J.*, **1995**, 78,121–126.
25. P. Basu, Biomass Gasification, Pyrolysis and Torrefaction **2018**, 479–495.
26. S.A. Channiwala, P.P. Parikh, *Fuel*, **2002**, 1051–1063.
27. H.S. Kambo, A. Dutta, *Energy Convers. Manag.*, **2015**, *105*, 746–755.
28. E. Sermyagina, J. Saari, J. Kaikko, E. Vakkilainen, *J. Anal. Appl. Pyrolysis*, **2015**, *113*, 551–556.
29. S. V. Vassilev, C.G. Vassileva, V.S. Vassilev, *Fuel*, **2015**, *158*, 330–350.
30. S.E.C. Whitney, M.G.E. Gothard, J.T. Mitchell, M.J. Gidley, *Plant Physiol.*, **1999**,*121*, 657–663.
31. S. Bilgen, K. Kaygusuz, A. Sari, *Energy Sources*, **2004**, *26*, 1083–1094.
32. G. Ischia, L. Fiori, *Waste Biomass Valori.*, **2021**, *12*, 2797–2824.
33. L. Liu, Biomass-Derived Humins Form. Chem. Struct., Springer, **2023**, pp. 85–99.
34. M. do S.B. da Silva, J.G.L. de Araujo, J.C.C. V Bento, A.M. de Azevedo, C.R.O. Souto, A.S.D. dos Anjos, A.M.M. de Araújo, D.R. da Silva, F.G. Menezes, A.D. Gondim, L.N. Cavalcanti, *RSC Adv.*, **2022**, *12*, 27889–27894.

35. K. Werner, L. Pommer, M. Broström, *J. Anal. Appl. Pyrolysis*, **2014**, *110*, 130–137.
36. D. Chen, K. Cen, X. Zhuang, Z. Gan, J. Zhou, Y. Zhang, H. Zhang, *Combust. Flame*, **2022**, *242*, 112142.
37. C. Zhou, X. Xia, C. Lin, D. Tong, J. Beltramini, *Chem. Soc. Rev*., **2011**, *40*, 5588–617.
38. R. Wang, H. Ben, *Front. Energy Res*., **2020**, *8*, 1–12.

STUDIA UBB CHEMIA, LXIX, 1, 2024 (p. 35-50)
(RECOMMENDED CITATION)
DOI:10.24193/subbchem.2024.1.03

TUNGSTATE-BORATE IONIC LIQUIDS: STRUCTURE, ELECTROCHEMICAL BEHAVIOR AND ELECTRODEPOSITION OF TUNGSTEN COATINGS

Angelina GAB[a], Victor MALYSHEV[a], Dmytro SHAKHNIN[a], Ana-Maria POPESCU[b*], Virgil CONSTANTIN[b*]

ABSTRACT. This work was undertaken to study the electrodeposition of tungsten from the Na_2WO_4-B_2O_3 system in the molten state. The measurement of the EMF being made with platinum-oxygen indicator and tungsten relative electrodes versus platinum-oxygen.

Experiment due to dependencies of the platinum-oxygen potential and tungsten electrodes on the B_2O_3 concentration, are validate by the forming of ditungstate ions $W_2O_7^{2-}$ in the high temperature ionic liquids (HTILs).The electroreduction process of the active species, is controlled by the diffusion; the rate of formation of the active species does not limit the electrode process; Polarization, in galvanostatic and potentiodynamic mode, have highlighted the fact that charge transfer is reversible.

In the Na_2WO_4-B_2O_3 melt (acid-basic character), in a narrow potential range and at a controlled process potential, the electroreduction of tungsten from its dimeric form is possible due to the multielectronic processes that take place at the electrode surface. This study played an important role in the evolution tungsten coatings; the corrosion potentials of electrodes (copper, nickel, steel) plated with tungsten, were also measured.

In this study, the influence of some parameters (temperature, electrolysis time, cathodic current density, B_2O_3 concentration) on the cathodic structure and composition was quantified, determining the optimal conditions of the reverse electrodeposition.

Keywords: *Tungstate, Borate, Ionic liquid, Electrodeposition, Voltammetry*

[a] *International European University, 42 V Academician Glushkov Avenue, 03187, Kyiv, Ukraine*
[b] *Romanian Academy, "Ilie Murgulescu" Institute of Physical Chemistry, Laboratory of Electrochemistry and Corrosion, 202 Splaiul Independentei, 060021, Bucharest, Romania*
* *Corresponding authors: virgilconstantin@yahoo.com, popescuamj@yahoo.com*

INTRODUCTION

Increased interest in the development of new effective methods for obtaining refractory compounds such as carbides, borides, silicides, alloys, and intermetallic compounds of Groups IV–VIB of the periodic table is dictated by their use in modern technique. A comparative analysis of the synthesis of metal-like refractory compounds showed that high-temperature electrochemical synthesis (HTES) is one of the most promising but still poorly known methods and it is based on processes of the electrical separation of metals and nonmetals from ion melts [1–3]. These coatings are characterized by yet another important feature, that is, they are economically profitable because in some cases their use allows simplifying the technology and replacing expensive and rare metals by more abundant metals without any sacrifice in the operation of parts, structures, and aggregates.

Vast family of highly prospective and widely used ionic liquids encompasses, among all, high-temperature ionic liquids (HTILs) inorganic salts systems, in particular tungstate-borate (Na2WO4-B2O3) melts Acid-base properties of tungstate HTILs have substantial effect both on electrode processes and composition of cathodic products. Various acceptors of oxygen ions, such as cations Li^+, Ca^{2+}, Mg^{2+}, Zn^{2+}, Al^{3+} anions PO^{3-}, and neutral molecules WO_3, MoO_3, CO_2, were used to modify acidity of the melts [4-7]. The cations of alkali and alkaline-earth metals form cationized electrochemically active species while PO^{3-}, WO_3, MoO_3, CO_2 produce dimeric complexes. Earlier we studied peculiarities of molybdenum and tungsten different ionic forms in tungstate melt in the presence of strong-polarizing cations: Li^+, Ca^{2+}, Mg^{2+}, Zn^{2+}, Al^{3+}, neutral molecules WO_3, MoO_3, and CO_2, anions PO^{3-} [6-8]. Investigations showed that it is possible to realize multielectron equilibria and processes with the use of acid-base interactions in sodium tungstate melt. Depending on the acid-base properties of the melt, cathode products can be tungsten, its oxides, and/or tungsten bronzes. The possibility of electrodeposition of tungsten in the form of dispersed powders or coatings in the presence of a parallel process of electroreduction of a non-metal (C, Si, B) allows HTES of carbides, silicides, and borides of tungsten [7, 9].

In the present work, studies results of the boron oxide effect on platinum-oxygen and tungsten electrodes in sodium tungstate melt and of the electrochemical behavior of this melt were presented. The electrochemical behavior of (and electrodeposition from) Na2WO4-B2O3 melts, the electrodeposition of tungsten coatings from them, as well as their physicochemical and operational properties, were determined. The study of electrochemical behavior of platinum-oxygen and tungsten electrodes in the Na_2WO_4-B_2O_3 melts made it possible to confirm the capability of the melts model with the formation of ditungstate ions and the possibility of realization of

multi-electron equilibria with these ions participation. The interest to this work was determined by the following: (a) a significant influence of boron oxide is observed onto the structure of cathodic deposits obtained from molybdenum containing melts [10-14]; (b) on the base of peculiarities of tungstate melts nature and structure, one can expect the better solubility and less fugacity of boron oxide than was observed in halide melts [10]; (c) boron oxide forms oxo-acid particles able to influence the acid-base interactions in tungstate melts [6].

RESULTS AND DISCUSSION

In the present work the effect of boron oxide on platinum-oxygen and tungsten electrodes in sodium tungstate melt.

The variation in activity of the melt components is not only of theoretical but also of practical interest in tungsten electrodeposition and synthesis of tungsten borides. Potentiometry was employed for the study under equilibrium conditions. The electromotive force (emf) of the following cells was measured:

$$Pt, O_2 \mid (1\text{-}x)\ Na_2WO_4 - xB_2O_3 \mid Na_2WO_4 - 0.2\ WO_3 \mid O_2, Pt \quad (1)$$

$$W \mid (1\text{-}x)\ Na_2WO_4 - xB_2O_3 \mid Na_2WO_4 - 0.2\ WO_3 \mid O_2, Pt \quad (2)$$

where x is the mole fraction of B_2O_3 in the melt.

1. Electrochemical behavior of platinum-oxygen and tungsten electrodes in the Na_2WO_4-B_2O_3 melt

The emf of cells (1) and (2) was measured at 1173 K varying the concentration of B_2O_3 in the range of 0-10 mol.% (the corresponding samples of B_2O_3 added to molten Na_2WO_4). The equilibrium potentials were established within 2-3 h judging by constancy of their final value to within 0.005 V for 1 h.

The variation of the oxygen electrode potential in Na_2WO_4-B_2O_3 melts (Fig. 1) can be explained in terms of the model we proposed for ion composition of such systems.

The expression for oxygen-electrode steady potential is written as follows:

$$1/2\ O_2 + 2e^- \leftrightarrow O^{2-} \quad (3)$$

$$E_{O^{2-}/O_2} = E^0_{O^{2-}/O_2} + \frac{2.3RT}{2F}\log\frac{P_{O_2}^{1/2}}{\left[O^{2-}\right]} \quad (4)$$

or, taking into account the constant partial pressure of oxygen over the melt, as:

$$E_{O^{2-}/O_2} = E^*_{O^{2-}/O_2} + \frac{2.3RT}{2F}\log\left[O^{2-}\right]^{-1} \quad (5)$$

The difference in potentials of the oxygen electrodes in cell (1) is described by the ratio of activities of oxygen ions in the melts, i.e.:

$$E = \frac{2.3RT}{2F}\log\left(a' / a''\right) \tag{6}$$

where: a'=activity of O^{2-} and a''=activity of O_2

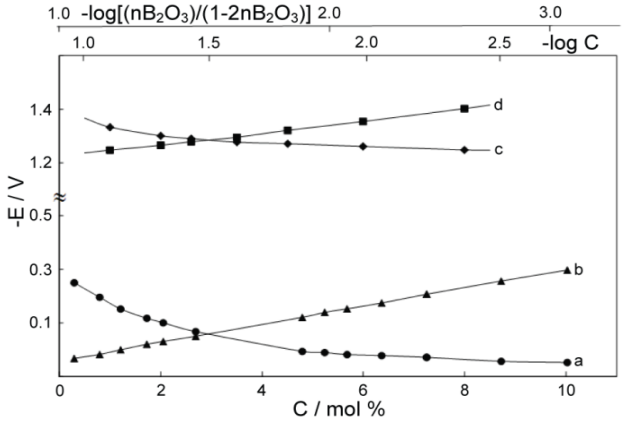

Figure 1. Dependence of potentials of platinum-oxygen (a) and tungsten (c); electrodes on B_2O_3 concentration and their analysis in the logarithmic coordinate system: (b) – platinum-oxygen electrode; (d) – tungsten electrode. (T = 1173 K).

In the neat tungstate melt there is the equilibrium:

$$(W_2O_7)^{2-} + O^{2-} = 2\,(WO_4)^{2-} \tag{7}$$

with the constant $K = \frac{[n(WO_4)^{2-}]^2}{[n(O)^{2-}][n(W_2O_7)^{2-}]}$ and n = the fraction of all species $[n(WO_4)^{2-}]$, $[n(W_2O_7)^{2-}]$, $[n(O)^{2-}]$ taking part in equilibrium (7). So the the tungsten ion balance can be written as follows:

$$n(WO4)^{2-} + 2n(W_2O_7)^{2-} = 1 \tag{8}$$

For stoichiometric sodium tungstate $[n(WO_4)^{2-}] \approx 1$, $[n(O)^{2-}] = [n(W_2O_7)^{2-}] << 1$, we have from eq.(7):

$$[n(O)^{2-}] = 1/K^{1/2} \tag{9}$$

In the presence of B_2O_3 acting as an acceptor of oxygen ions the following reactions can occur in the sodium tungstate melt:

$$2\,(WO_4)^{2-} + B_2O_3 \leftrightarrow (W_2O_7)^{2-} + 2\,(BO_2)^{-} \tag{10}$$

$$2\,(WO_4)^{2-} + 2\,B_2O_3 \leftrightarrow (W_2O_7)^{2-} + 2\,(B_4O_7)^{2-} \tag{11}$$

The mole fractions of tungstate and ditungstate ions, as determined from the ion balance, are:

$$n\ (WO_4)^{2-} = 1\text{-}2n\ (W_2O_7)^{2-} = 1\text{-}\ 2n\ B_2O_3 \quad (12)$$

$$n\ (W_2O_7)^{2-} = n\ B_2O_3 \quad (13)$$

for reaction (10) and

$$n\ (WO_4)^{2-} = 1\ -\ 2n\ (W_20_7)^{2-}\ = 1\ -\ 4n\ B_2O_3 \quad (14)$$

$$n\ (W_2O_7)^{2-} = 2n\ B_2O_3 \quad (15)$$

for reaction (11).

Inserting (12), (13), and (14), (15) in Eq. (7) we obtain equation for mole fractions of oxygen ions involved in reactions (10) and (11):

$$[\frac{1}{n(O)^{2-}}] = \frac{[K \cdot nB_2O_3]}{[1-2n \cdot B_2O_3]^2} \quad (16)$$

$$[\frac{1}{n(O)^{2-}}] = \frac{[2K \cdot nB_2O_3]}{[1-4n \cdot B_2O_3]^2} \quad (17)$$

After insertion of (16) and (17) in (5), the final equations relating the oxygen electrode potential and the concentration of B_2O_3 take the form:

$$E_{O^{2-}/O_2} = E^{*}_{O^{2-}/O_2} + \frac{2.3RT}{2F}\log\frac{\left(K \cdot nB_2O_3\right)}{\left(1-2nB_2O_3\right)^2} = E^{**}_{O^{2-}/O_2} + \frac{2.3RT}{2F}\log\frac{\left(nB_2O_3\right)}{\left(1-2nB_2O_3\right)^2} \quad (18)$$

$$E_{O^{2-}/O_2} = E^{*}_{O^{2-}/O_2} + \frac{2.3RT}{2F}\log\frac{\left(2K \cdot nB_2O_3\right)}{\left(1-4nB_2O_3\right)^2} = E^{**}_{O^{2-}/O_2} + \frac{2.3RT}{2F}\log\frac{\left(nB_2O_3\right)}{\left(1-4nB_2O_3\right)^2} \quad (19)$$

According to equations (18) and (19), the slopes of the curves $E_{O^{2-}/O_2} - \log[nB_2O_3/(1-2nB_2O_3)^2$ and $E_{O^{2-}/O_2} - \log[nB_2O_3/(1-4nB_2O_3)^2]$ at 1173 K should be 0.116 and 0.035 V, respectively. The experimentally determined slope for the first curve is 0.111-0.120 V (Fig. 1) whereas in the second semi-log coordinates the data points do not give a straight line. This suggests the occurrence of reaction (10) in the studied range of B_2O_3 concentration and the validity of the model used.

The constant K was estimated by solving eq. (18) with two values of the oxygen electrode potential, for stoichiometric sodium tungstate and the melt (Na_2WO_4-1 mol.% B_2O_3). The calculations give K = 108.6, $E^{*}_{O^{2-}/O_2} = -1.06$ V

and $nO^{2-} = 10^{-4.3}$. These values are in good agreement with the corresponding parameters found for Na_2WO_4 melts containing WO_3 and MoO_3 [3, 5].

The emf of cell (2) was measured, varying the concentration of B_2O_3 in the range of 0.5-10.0 mol.% with a small monocrystalline tungsten bar hung up by a platinum wire as an indicator electrode. The measurements were performed by the same procedure as for the oxygen electrode. At B_2O_3 concentration < 0.5 mol.% the chemically pure tungsten electrode undergoes corrosion because of which the measured emf values are nonreproducible. The corrosion is suppressed at $[B_2O_3] > 0.5$ mol.%.

The tungsten electrode potential is created by the reactions:

$$(WO_4)^{2-} + 6e^- = W + 4\ O^{2-} \quad (20)$$

$$4\ (W_2O_7)^{2-} + 6e^- = W + 7\ (WO_4)^{2-} \quad (21)$$

for tungsten in equilibrium with tungstate or ditungstate ions, respectively. The number of electrons per electroactive particle was estimated to be 1.5 from the slope of the $dE - d\log C_{B_2O_3}$ curve in the range of 0-5-10 mol.% B_2O_3 (Fig. 1). This value corresponds to reaction (21).

The possibility of reactions (10) and (11) is confirmed by the results of our thermodynamic calculations and of studies of the frozen $Na_2WO_4 – B_2O_3$ melts structure. The Gibbs free energy of reactions (10) and (11) at 1200 K is -112.67 kJ and -56.53 kJ, respectively. IR spectra of frozen melts confirm the ditungstate ions compounds presence.

2. Electroreduction of tungsten (VI) in Na_2WO_4-B_2O_3 melts

The reduction wave was observed at 1.1-1.3 V in stationary and nonstationary voltammograms of the tungstate melts containing B_2O_3 (Fig. 2). The limiting currents are proportional to the concentration of B_2O_3 rather than to the total concentration of tungsten in the melt. The major wave is preceed by an alloy-formation wave. To exclude the alloy formation we used a silver cathode which does not interact with tungsten. As the concentration of B_2O_3 is raised, the major wave becomes more intense and is displaced to positive potentials. At the same time it takes a sickle-shaped form. The reduction process proceeds in one step at any electrode polarization rate up to 10 V/s. The product of the potentiostatic electrolysis at the potential of –1.2 V is tungsten metal.

The plots of peak current versus B_2O_3 concentration at different polarization rates are linear (Fig. 3).

The values of $i_p/v^{1/2}$ are nearly constant over a wide range of polarization rates (0.05-2.0 V/s) (Fig. 4).

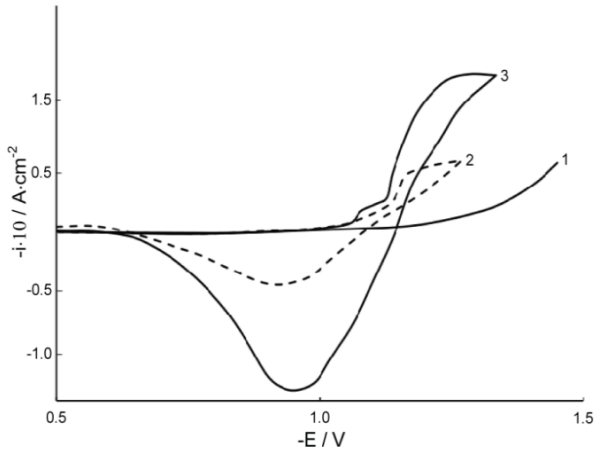

Figure 2. Voltammetric dependencies of Na_2WO_4 melt (1) when added sequentially B_2O_3: (2) – $1 \cdot 10^{-4}$ mol/cm^3; (3) – $8 \cdot 10^{-4}$ mol/cm^3;T = 1173 K, cathode – Pt, v = 0.1 V/s.

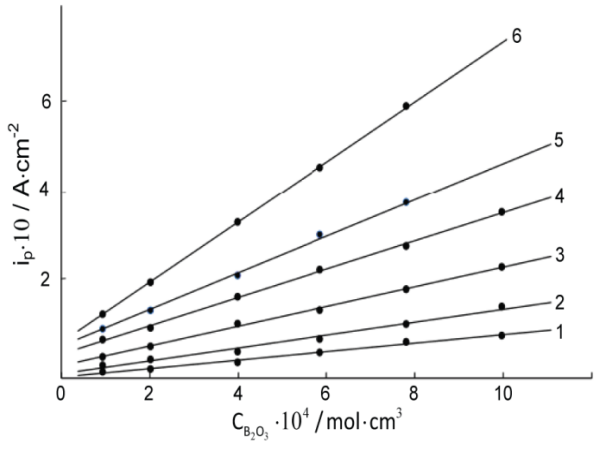

Figure 3. Dependence of the peak current on the B_2O_3 concentration at different polarization speeds: (1) – 0.02 V/s; (2) – 0.05 V/s; (3) – 0.1 V/s; (4) – 0.5 V/s; (5) – 1.0 V/s; (6) – 2.0 V/s ;T = 1173 K.

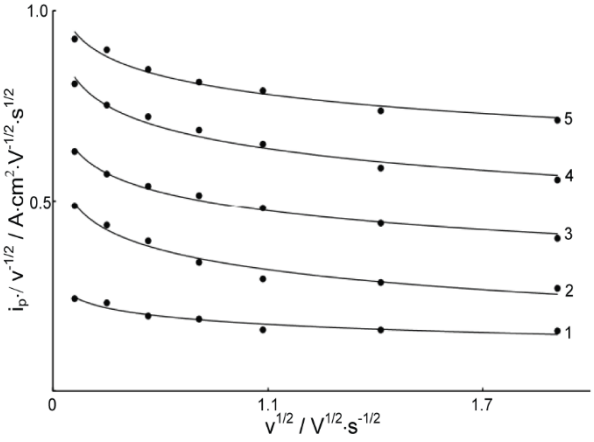

Figure 4. Dependence $i_p/v^{-1/2}$ – $v^{1/2}$ for the tungsten-containing ions electroreduction process at $C(B_2O_3)\cdot10^4$ mol/cm^3: (1) – 2 mol/cm^3; (2) – 6 mol/cm^3; (3) – 8 mol/cm^3; (4) – 10 mol/cm^3; (5) – 12 mol/cm^3; T = 1173 K.

The kinetic constant for stationary waves, $i_p/nFC = (0.7\text{-}1.0)\cdot10^{-4}$ cm/s, characterizing the transport of the reacting substances to the electrode surface is comparable to the values of χ for diffusion migration.

All these data suggest that the electrode process is limited by diffusion of electroactive species to the electrode, that is, under polarization conditions used, the rate of generation of the species is not the limiting factor.

The nature of the waves can be explained in terms of the acid-base interaction concept and the model we proposed earlier for the ionic composition of the melts in [6, 8]. The following equilibrium is established in the tungstate melt:

$$2\ (WO_4)^{2-} \leftrightarrow (W_2O_7)^{2-} + O^{2-} \tag{22}$$

with the equilibrium constant:

$$K = \frac{\left[WO_4^{2-}\right]^2}{\left[W_2O_7^{2-}\right]\left[O^{2-}\right]} \tag{23}$$

From the reported value of $K \approx 10^{10}\text{-}10^{12}$ [6, 8], the concentration of electroactive species $(W_2O_7)^{2-}$ was estimated to be in the range of $10^{-5}\text{-}10^{-4}$ mol % that is much lower than the voltammetry sensitivity limit. Because of this no waves were observed in the neat tungstate melt.

Boron oxide acting as an acceptor of oxygen ions displaces equilibrium (22) to the right increasing thereby the concentration of $(W_2O_7)^{2-}$ in the melt by eq.(10). The decrease in activity of oxygen ions in the presence of B_2O_3 added to the tungstate HTIL was studied on the platinum-oxygen electrode under equilibrium conditions. With boron oxide introduced in the HTIL, the concentration of $(W_2O_7)^{2-}$ increases and the system exhibits electrochemical activity at more positive potentials. The overall electrode process under these conditions can be presented by the equation (21). In order to elucidate the nature of the charge-transfer step (21) and to determine the number of electrons taking part in the electrode process, the stationary current-potential curves were presented in semilog coordinates log (i_d - i) - E (Fig. 5).

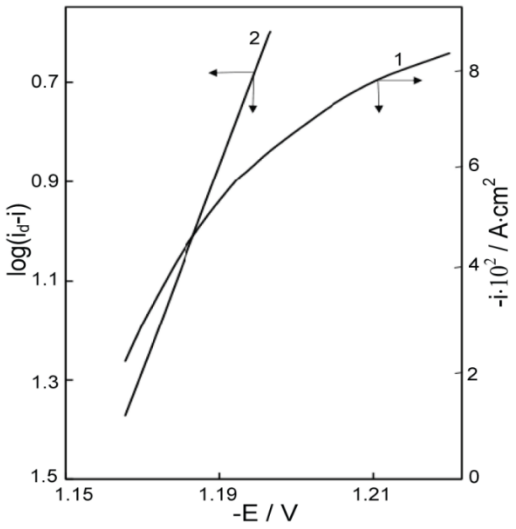

Figure 5. Cathodic polarization of tungsten electrode (1) and its analysis in the semi-logarithmic coordinate system (2);v = 0.02 V/s, T = 1173 K, $C(B_2O_3) = 6 \cdot 10^{-4}$ mol/cm^3.

In view of the sickle-shaped form of the stationary waves, the Kolthoff-Lingame equation was used. The slope of the log(i_d - i) - E curves at different B_2O_3 concentrations was found to be 37-44 mV and n = 5.3-6.2. The theoretical slope for a six-electron reversible reaction is 39 mV. A good agreement between the experimental and theoretical values testifies that the charge-transfer step (21) is reversible. This inference is confirmed by the following experimental facts: the deposition potential and the half-wave potential are independent of the polarization rate up to 0.2 V/s; the concentration dependence of the potential for equilibrium (21) is well described by the Nernst equation.

We determined the number of electrons involved in the electrode process also from the equation for nonstationary current-potential curves:

$$E_{p/2} - E_p = 2.2RT/nF \quad (24)$$

The result at different B_2O_3 concentrations and polarization rates (0.05-0.2 V/s) is n = 5.6-6.1.

At higher polarization rates (v > 0.5 V/s) the reversible process becomes quasi-reversible as shown by deviation of the $i_p /v^{1/2}$ relationship from linearity *vs.* $v^{1/2}$ and the dependence of E_p and $E_{p/2}$ on the polarization rate.

3. Electrodeposition of tungsten coatings, their physicochemical and operational properties.

3.1. Electrodeposition of tungsten coatings by electrolysis of tungsten-borate melts

For successful coating, it is important that the corrosion potential is higher than the deposition potential. Therefore, to assess the possibility of coating nickel, various steels, and titanium (usually, tungsten is not deposited on these metals from halide and halide-oxide melts), the stationary potentials of these metals relative to the $Na_2WO_4 – 0.2WO_3 \mid O_2$, Pt half-element (table 1) were measured. The deposition potential of tungsten is lower than the corrosion potentials of nickel, ST3, stainless steel, which opens up the possibility of good coatings. The stationary potential of titanium was not established for a long time and changed abruptly. Apparently, this is due to the formation of low-valence titanium oxides. Therefore, before the deposition of tungsten, titanium was nickel-plated or nitrided.

Table 1. Free corrosion potentials (E_{cor}) of nickel, ST3, stainless steel 12X18H10T and deposition potential (E_{dep}) of tungsten in tungstate-borate melts Na_2WO_4 – 5 mol% B_2O_3.

E_{cor}, V			E_{dep}, V
Ni	**ST3**	**Steel 12X18H10T**	
-1.17	-1.31	-1.30	-1.5
-1.22	-1.35	-1.3	-1.75

We have studied the effect of boron oxide concentration, temperature, cathode current density, and electrolysis duration on the composition and structure of cathodic deposits, optimal parameters of reverse deposition of tungsten from Na_2WO_4 - B_2O_3 melts were selected.

Tungsten precipitates if the concentration of boron oxide does not exceed 10 mol %, at a higher concentration, tungsten and bronze oxides are found on the diffractograms. Tungsten precipitates if the concentration of boron oxide does not exceed 10 mol %, at a higher concentration, tungsten bronze (M_xWO_3), where M denote monovalent cation and x is in the range 0 to 1 [15]. Solid coatings were obtained at 1073-1323 K and current densities up to 10 A/dm^2.

The higher the electrolysis temperature, the coarser the precipitate is. However, at a temperature of 1073 K, tungsten layers no thicker than 10 μm are obtained, which are not sufficiently adhered to the substrate. At temperatures below 1073 K and current density above 50 A/dm^2, a highly dispersed powder with a specific surface area up to 30 m^2/g will precipitate.

The effect of cathode density, electrolysis duration, and reverse mode parameters was studied in (Na_2WO_4 + 5 mol % B_2O_3). Well-adhered, uniform, continuous, absolutely pore-free coatings were obtained at a temperature of 1173 K and a current density of 1-10 A/dm^2. In the initial period of deposition, the size of deposit crystallites decreased with increasing current density. However, at a density above 10 A/dm^2, the grain became significantly coarser, the roughness amplitude increased from 1 to 2–3 μm, and the progressive growth of individual protrusions turned into dendrite formation, which prevented further thickening of the coating. Below 1 A/dm^2, the corrosion rate of the substrate exceeds the rate of tungsten deposition, causing poor adhesion of the coatings. The rate of tungsten deposition in the studied range of current densities is 15–40 μm/h, the current efficiency of tungsten is 85% (Fig. 6). As the duration of electrolysis increases, the current efficiency decreases (Fig. 7).

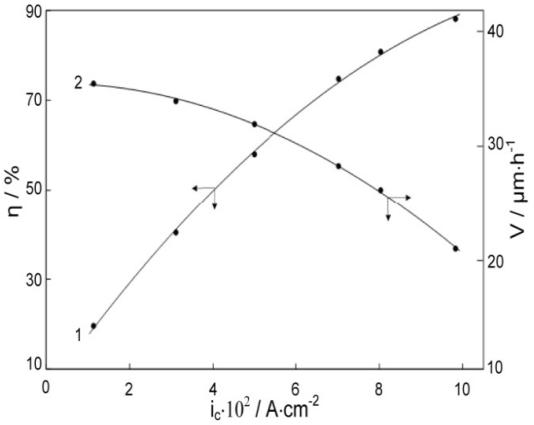

Figure 6. Dependence of the tungsten coating deposition rate (1) and the yield of tungsten by current (2) on steel samples from the cathodic current density; T = 1173 K.

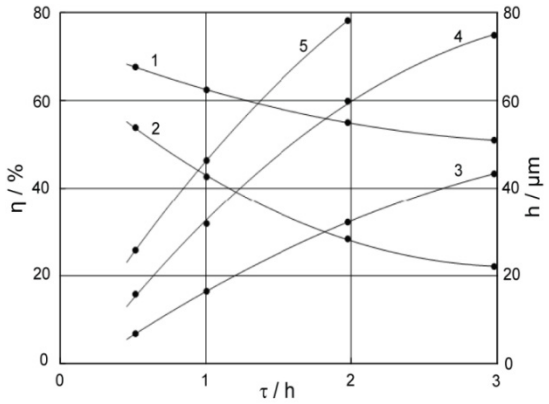

Figure 7. The dependence of the thickness of the tungsten coating (1-3) and the yield of tungsten according to the current (4) and (5) on steel samples from the duration of electrolysis at the current density: (1) and (4) – 4 A/dm^2; (2) and (5) – 6 A/dm^2; (3) – 8 A/dm^2;T = 1173 K.

With thickening of the coating, the structure of its surface changes from finely crystalline with a uniform grain to coarse-grained. The SEM images of the tungsten deposit on steel depending on electrodeposition time and the current density in Fig.8. As one can see the deposit change from homogenous low small grains to enough homogenous large-grained with deposition time and current density. To obtain a fine-grained structure, a reverse electrolysis mode was used. The ratio t_k:t_a was changed within 20 - 40, the duration of the anodic phase is 0.5-2.0 s, the anodic current density is 15 - 50 A/dm^2. To obtain a coating, the following electrolysis parameters are optimal: t_k = 20 s, t_a = 0.5-1.0 s, i_k = 8-10 A/dm^2, i_a = 15-30 A/dm^2. This way of doing electrolysis leads to reducing the roughness of the coatings by half, as well as increasing their thickness to 200 µm.

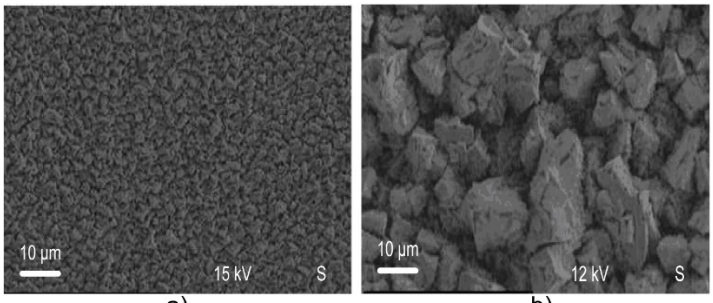

Figure 8. SEM image of tungsten coating deposited on steel substrate: a) 20 s; 8 A/dm^2; b) 60 s, 15 A/dm^2.

3.2. Physico-chemical and operational properties of tungsten coatings

Solid tungsten coatings on graphite, nickel, copper, molybdenum, tungsten, machine-building structural steels, heat-resistant and tool hard alloys, on nitrided and nickel-plated titanium have been obtained.

Under laboratory conditions, alundum containers, tungsten plates or rods were used as anodes, and chemically pure initial components. In the resulting tungsten coatings, X-ray microanalysis revealed impurities (Al, Cr, Mo, Ni) within only $2 \cdot 10^{-2}$ - $4 \cdot 10^{-4}$ wt. %. Such a content of impurities does not noticeably affect the structure of the coatings. An indirect criterion for the high adhesion strength of a coating to a substrate is the absence of its peeling during qualitative tests.

The porosity of the coating was determined by applying filter paper impregnated with a 10 g/l solution of $K_3Fe(CN)_6$ + 20 g/l NaCl on coated steel ST3 and 45. Test duration was 5 min. The average number of pores per 100 cm^2 of the surface was 5-6. According to the evaluation standards (ASTM B809), the pore area is 0.0–0.1%, which corresponds to practically pore-free coatings [16]. The microhardness of the coating is 4.3-4.5 GPa. The layers of the base adjacent to the coating are noticeably strengthened, which indicates the mutual diffusion of the elements of the coating and the base. A diffusion zone with a length of 10-15 μm is shown by X-ray microanalysis of a transverse section of ST3 coated with tungsten.

Wear resistance tests were carried out on an SMC-2 instrument at a specific load of 5 MPa in transformer oil in a wide range of sliding speeds. The counterbody is hardened steel 45. The coating increased wear resistance by 4-6 times.

For abrasive resistance, steel 45 samples with coatings were tested in the medium of a fraction of 150 μm of electrocorundum at a load of 44.1 + 0.25 N. Due to the coating, the wear resistance increased by a factor of 3-5 and was only slightly inferior to the resistance of samples borated from the gas phase.

Thus, we have studied the electrochemical behavior of tungstate-borate melts, mastered the electrodeposition of tungsten coatings and their properties.

CONCLUSIONS

The study of electrochemical behavior of platinum-oxygen and tungsten electrodes in the Na_2WO_4-B_2O_3 melts made it possible to confirm the capability of the HTILs model with the formation of ditungstate ions and the possibility of realization of multi-electron equilibrium with these ions participation.

According to the electrochemical measurements results, namely, due to the linear dependence of the peak current of ditungstate ion reduction waves

on the concentration of B_2O_3, to the constancy of the values of the ratio of the peak current to the square root of the polarization speed, as well as to the values of the kinetic constants, electrode process is limited by diffusion of electroactive species to the electrode. Under polarization conditions used, the particles species generation rate is not the limiting factor.

A good agreement between the experimental and theoretical numbers of electrons taking part in the electrode process testifies that the charge-transfer step of ditungstate-ion electroreduction is reversible. This inference is confirmed by the experimental facts that the deposition potential and the half-wave potential are independent of the polarization rate up to 0.2 V/s, and that the concentration dependence of the equilibrium potential of tungsten electrode within melt is well described by the Nernst equation.

The influence of boron oxide concentration, temperature, cathodic current density, and duration of electrolysis on the composition and structure of cathodic deposits was studied. The coatings were obtained in the temperature range of 1073-1323 K at a current densities up to 1-10 A/dm^2, if the concentration of B_2O_3 does not exceed 10 mol %. A reversible deposition mode was used to obtain a fine crystal structure.

Electrolysis of Na_2WO_4-B_2O_3 melts produced continuous nonporous tungsten coatings on graphite and metal materials. The speed of their deposition was up to 15-40 μm/h, the current yield was up to 85%, the thickness was up to 100 μm in the direct current mode of deposition and up to 200 μm in the reverse mode of deposition.

The microhardness of the coatings is 4.3-4.5 GPa. As a result of their deposition the wear resistance of steel materials increases by 4-6 times, and abrasive resistance by 3-5 times.

EXPERIMENTAL

The platinum-oxygen reference electrode was semi-dipped in the melt of constant composition, Na_2WO_4 - 20 mol % WO_3, separated from the main electrolyte with an alundum jacket 6-8 mm in diameter playing the role of a diaphragm. The open end of the jacket communicated with the atmosphere. Potentiometric measurements were carried out in air ($P_{O_2} = 21.3$ kPa). Such electrodes are widely used in oxide melts, specifically in tungstate systems [17, 18].

Investigations of Na_2WO_4-B_2O_3 melt electrochemical behavior were carried out in the three-electrode quartz electrochemical cell at 1173 K. Used methods of investigation – single and multi cycle voltammetry. Voltammetric curves were registered with the pulse potentiostat PI-50-1

As anode and at the same time as the melt container the platinum crucible was used. As indicator electrodes were used semi-dipped and full dipped needle platinum and silver and tungsten electrodes (wire diameter 0.5-1.0 mm, square of electrodes was 0.1-0.3 cm^2). As reference electrode a platinum-oxygen electrode 0.8 Na_2WO_4-0.2 WO_3/O_2,Pt was used [17]. Diagnostics and estimation of electrode processes kinetic parameters was carried out according to the theory of stationary and non-stationary electrode processes [19]. Systems for the tungsten coatings electrochemical deposition were based on Na_2WO_4-B_2O_3 melt. As anode a tungsten plates in alundum container or graphite crucibles was used and as cathodes – plates of metals for electrodeposition (10×20×1 mm).

The thickness and deposition rate of coatings at the surface of plane-parallel plates were assessed by gravimetric and metallographic methods, as well as using a VTO-25 micrometer and 2IGM detector [20,21].

REFERENCES

1. J. S. Wilkes; *Green Chem*., **2002**, *4*, 73-80.
2. A. Nishikata; H. Numata; T. Tsuru; *Mater. Sci. Eng*: *A*, **1991**, *146*, 15-31.
3. V. V. Malyshev; H. B. Kushkov; V. I. Shapoval; *J. Appl. Electrochem*., **2002**, *32*, 573-579.
4. V. L. Cherginets; *Russ. Chem. Rev*., **1997**, *66,* 597-611.
5. V. L. Cherginets; *Oxoacidity: Reactions of Oxo-compounds in Ionic Solvents*, N. J. B Green; Ed.; Netherland: Elsevier Science, **2005**. ISBN: 978-0-444-51782-1
6. V. A. Onischenko; V. V. Soloviev; L. A. Chernenko; V. V. Malyshev; S. N. Bondus; *Materialwiss. Werkst*., **2014**, *45*(11), 1030-1038.
7. V. V. Malyshev; V. V. Soloviev; L. A. Chernenko; V. N. Rozhko; *Materialwiss. Werkst*., **2015**, *46*(1), 5-9.
8. V. Malyshev; A. Gab; A. M. Popescu; V. Constantin; *Chem. Res. Chin. Univ*. **2013**, *29*, 771-775.
9. V. Malyshev; D. Shakhnin;A. Gab; I. Astrelin; L. Molotovska; V. Soare; C. Donath; E.I. Neacsu; V. Constantin; A.M. Popescu; *Rev. Chim. (Bucharest)*, **2016**, *67*(12), 2490-2500.
10. V. Danek; *Physico-chemical analysis of molten electrolytes*, Amsterdam: Elsevier Science, **2006**.
11. S. K. Ghosh; J. Varshney; A. Srivastava; Ch. Srivastava; *J. Electrochem. Soc*., **2021**, *168*(4), 046502.
12. W. Jin; Ch. Ge; Q. Kou; P. Jiang; S. Xiao; *Int. J. Electrochem. Sci*., **2021**, *16*(3), 210311.
13. V. Malyshev; A. Gab; D. Shakhnin; C. Donath; E. I. Neacsu; A. M. Popescu; V. Constantin; *Rev. Chim. (Bucharest)*, **2018**, *69*(9), 2411-2415.

14. V. Malyshev; A. Gab; D. Bruskova; T. Dmytrenko; M. Gaune-Escard; *Nano Studies*., **2019**, *19*, 77-86.
15. J. D. Guo; M. S. Whittingham; *IJMP B,* **1993**, *7,* 4145-4164.
16. ASTM B809, Standard test method for porosity in metallic coatings by humid sulfur vapor ("Flowers-of-Sulfur"), ASTM International, West Conshohocken, PA, **2016**, (2018).
17. G. Inzelt; A. Lewenstam; F. Scholz; *Handbook of Reference Electrodes*, Berlin, Heidelberg: Springer-Verlag, **2015**. ISBN: 978-3-642-44873-7.
18. A.I. Bhatt; G.A. Snook; *Reference electrodes for ionic liquids and molten salts*, in: G. Inzelt; A. Lewenstam; F. Scholz; (Eds). *Handbook of Reference Electrodes*. Berlin, Heidelberg: Springer-Verlag, **2013**, 189-227. ISBN: 978-3-642-36187-6.
19. C. G. Zoski; Ed., *Handbook of electrochemistry*, Amsterdam: Elsevier Science, **2006**. ISBN 978-0-444-51958-0.
20. V. Malyshev; D. Shakhnin; A. Gab; M. Gaune-Escard; I.M. Astrelin; Effect of electrolysis parameters on the coating composition and properties during electrodeposition of tungsten carbides and zirconium diborides, cap. 4.8, pag.295, in Molten Salts Chemistry and Technology, First ed., Marcelle Gaune-Escard; Geir Martin Haarberg; (Eds.). **2014,** John Wiley & Sons, Ltd.
21. V. Malyshev; N. Kushchevska; G. Bagliuk; D.Shakhnin; O. Paprotskaya; V. Kurovskyi; *Int. Sci. J. Mach. Tech. Mater*., **2018**, *12*(7), 302-304.

STUDIA UBB CHEMIA, LXIX, 1, 2024 (p. 51-68)
(RECOMMENDED CITATION)
DOI:10.24193/subbchem.2024.1.04

EFFECT OF THALLIUM (I) IONS ON THE ZINC ELECTROWINNING PROCESS

Ning YUAN[a], Xi CHEN[a], Xing LIU[a], Lin FU[a], Yan CUI[a,*], Shihong HUANG[b,*], Wenjia ZHAO[a]

ABSTRACT. The effects of thallium(Ⅰ) ions on the surface morphology, cathode current efficiency, cathode potential, polarization behavior, and electrochemical impedance spectroscopy of zinc electrowinning were studied by scanning electron microscopy and electrochemical measurements. The results showed that with increasing thallium(Ⅰ) ion concentration in the electrolyte, the hydrogen evolution reaction and the galvanic effect produced during zinc electrowinning increased. When the concentration of thallium(Ⅰ) ions in the electrolyte was 0.6 mg L^{-1}, the exchange current density of the zinc electrowinning process was maximum and the polarization was minimum. At this time, the R_{ct} of the equivalent circuit was minimum, the CPE value was minimum, and the charge transfer rate was maximum. The cathodic current efficiency decreased from 80% to 55% when the thallium(Ⅰ) ion concentration was 1.5 mg L^{-1}. The presence of thallium(Ⅰ) ions also affected the surface macro- and microstructure of the zinc deposits. This result confirmed that thallium(Ⅰ) ions have a significant negative influence on the electrowinning of zinc.

Keywords: *Zinc electrowinning; Thallium(Ⅰ) ions; Cathodic current efficiency; Cathodic polarization; Electrochemical impedance spectroscopy*

[a] *Kunming University, School of Chemistry and Chemical Engineering, No. 2 Puxin Road, Kunming Economic and Technological Development Zone, 650214, Kunming, China*
[b] *Kunming University, Office of Science and Technology, No. 2 Puxin Road, Kunming Economic and Technological Development Zone, 650214, Kunming, China*
* *Corresponding author victory_me@outlook.com, 65865070@qq.com*

INTRODUCTION

Following iron, aluminum, and copper, zinc is regarded as the fourth most widely used metal [1]. More than 80% of the world's zinc is produced by the roasting–leaching–purification–electrowinning method [2-4]. Among the four steps, electrowinning is particularly critical because it directly determines the power consumption and quality of zinc production; energy consumed during this step accounts for about 60% of the total energy consumption of the zinc hydrometallurgy process [5]. The presence of metallic impurities in the zinc electrolyte is a common problem in electrowinning. Ivan [6] has reported that due to the presence of higher concentrations of metal impurities such as Sb and Ge, the current efficiency was reduced and complete redissolution of the deposited metal occurred. Muresan et al. [7] have studied the influence of metal impurities such as Cd, Fe and Cu in zinc electrowinning and showed that zinc deposition was prevented when Cd and Cu were present in solution because they coprecipitated on the cathode. In addition, there are some metal impurities present that promote the hydrogen evolution reaction during the zinc electrowinning process and decrease the current efficiency. Zhu et al. [8] have discovered that the concentration of co-deposited iridium in the deposited zinc layer increased with increasing Ir(IV) ion concentration in the electrolyte. The iridium deposited on the cathode acted as an active site for hydrogen evolution. Furthermore, some electronegativity impurities, such as alkali metals Na, Mg, Ca, etc., can make the surface of the deposited zinc dim and porous, which can also promote the hydrogen evolution reaction [9]. There are also variable-valence impurities that perform cyclic redox reactions at the anode and cathode, respectively, leading to a decrease in current efficiency, such as Mn, Fe, etc.

Zinc sulfide concentrate, as the main raw material for zinc refining, is commonly accompanied by a certain amount of thallium, with a normal content of 5–20 g/t. However, the content of thallium in some lead-zinc deposits was particularly high [10]. Liu et al. [11] showed that the Pb-Zn ore materials were relatively enriched with Tl (15.1–87.7 mg kg^{-1}), while even higher accumulation existed in the electrostatic dust (3280–4050 mg kg^{-1}) and acidic waste (13300 mg kg^{-1}). Karbowska et al. [12] investigated the translocation of thallium from zinc–lead ores from the Cracow–Silesia Upland due to ore flotation processing and natural processes and the element's mobility in these samples as determined by sequential extraction in accordance with a modified BCR procedure. Liu et al. [13] investigated the capacity for adsorption of thallium(Ⅰ) by a common sulfide mineral (zinc sulfide) in aerobic and anaerobic environments, which revealed three mechanisms for adsorption on the ZnS surface (surface complexation, electrostatic action and oxidation promotion).

In 2005, the electrolytic zinc plant of Huludao Nonferrous Metals Group Co., Ltd. purchased tens of thousands of tons of soot and zinc raw materials with high thallium content due to the shortage of mineral resources. The thallium content of this zinc-mixed raw material was as high as 0.015%, and the neutral leaching solution contained thallium greater than 0.01 g/L, which directly affected the electrical efficiency [14]. Therefore, it is important to study the effect of thallium(Ⅰ) ions on conventional zinc hydrometallurgy systems. The characteristics of the electrodeposition of thallium powder from sulphate baths containing a relatively low Tl ion content (0.005–0.020 mol L^{-1}) were examined. The cathodic polarization curves for thallium electrodeposition were greatly affected by the bath composition and the pH. The percentage cathodic current efficiency was relatively low and increased with increasing concentration of Tl ions in the bath to a maximum of 17% [15]. In earlier studies, Clavilier et al. [16] perfomed the underpotential deposition (UPD) of Tl^+ on Pt(111) electrode, arguing that there is an equilibrium in the adsorption-desorption process. More recently, Rodriguez et al. [17] have studied extensively either the UPD and irreversible adsorption of Tl on Pt(111) and vicinal surfaces. They were able to ascribe the processes Tl/Tl^+ oxidation and anion adsorption on the Tl-modified surface. Additionally, the results obtained with stepped surfaces indicate that some of the features are clearly associated to the presence of Pt(111) surface domains (terraces). Mirghasem Hosseini et al. [18] have studied the effect of Tl(Ⅰ) on the hard gold alloy electrodeposition of Au–Co from acid baths. They found that with addition of thallium in the hard gold electroplating bath an enhancement and inhibition of the gold deposition were observed at low and high cathodic potentials, respectively. Addition of trace quantities of Tl^+ to gold plating baths have been found to yield bright gold electrodeposits of suitable morphology, purity and hardness with depolarization effect. It is proposed that Tl^+ through its depolarization effect decreases the electrode inhibition brought by adsorbed cyanide species and increases deposition rate of gold. However, in zinc hydrometallurgy, the presence of thallium(Ⅰ) ions will reduce the current efficiency of zinc electrowinning.

During the roasting process of zinc concentrate, 70–84% of the thallium in the raw material evaporated into the soot; only 16–30% of the thallium remained in the roasted sand. However, due to the large proportion of roasted soot, the percentage of thallium content in the soot was relatively low, which generally did not meet the requirements of thallium purification, and most of the soot was still mixed with roasted sand as leaching material. In the leaching process, thallium mostly entered the acidic leaching solution with zinc calcine. During the purification stage, when impurities such as copper and cadmium were removed from the leaching solution, approximately 70% of the thallium in the leaching material entered the copper-cadmium slag for

enrichment. The small amount of thallium remaining in the leaching residue mostly entered the volatile soot during the volatilization kiln treatment [19]. The standard electrode potential of thallium ($E^{o}_{Tl^{+}/Tl}$ = -0.336 V) is more positive than that of zinc ($E^{o}_{Zn^{2+}/Zn}$ = -0.762 V), Therefore, thallium(Ⅰ) ions in the electrolyte will prefer to deposit on the cathode surface and probably lead to increased hydrogen evolution. What's more, in zinc electrowinning, the presence of thallium(Ⅰ) ions causes a galvanic effect on the zinc plate during electrolysis, resulting in the re-dissolution of zinc, which reduces the current efficiency. More seriously, thallium can induce other impurities to make the zinc electrowinning process produce "plate-burning" phenomena, which adversely affect the product yield and technoeconomic indexes, leading to continuous fluctuations in production that cannot be carried out normally. As a result, the selective removal of thallium from the electrolyte is critical for the stability of electrolytic production. The main methods for removing thallium from solutions are precipitation [20], sulfidation, adsorption [21], electroflocculation, and substitution. In the conventional zinc hydrometallurgy system, thallium is removed by the oxidation-precipitation method in the leaching stage. In this process, it is usually necessary to ensure that the thallium content of the zinc sulfate solution sent to the purification process is less than 1.0 mg/L. Existing Tl extraction methods consume excessive Zn and often result in incomplete removal. Xiong introduced an optimized technique that incorporates lead(Ⅱ) (Pb(Ⅱ)) to form a Pb-Tl compound during Zn cementation [22]. In the purification stage, thallium is removed by the substitution method. By adding lead-zinc powder, the content of thallium in the new solution can be theoretically controlled within 0.1 mg/L [14, 23]. However, few studies on this topic have been reported so far.

In this context, the purpose of this work was to study the influence of thallium(Ⅰ) ions on long term electrowinning of zinc from sulfate electrolytes by analyzing current efficiency, cathodic potential, cathodic polarization behavior, electrochemical impedance spectroscopy, and deposit morphology.

RESULTS AND DISCUSSION

Current efficiency

The effect of the presence of thallium(Ⅰ) ions on the current efficiency of zinc electrowinning is shown in Fig. 1. It can be seen that the current efficiency increased slightly between 0 and 0.6 mg L^{-1} thallium(Ⅰ) ions.

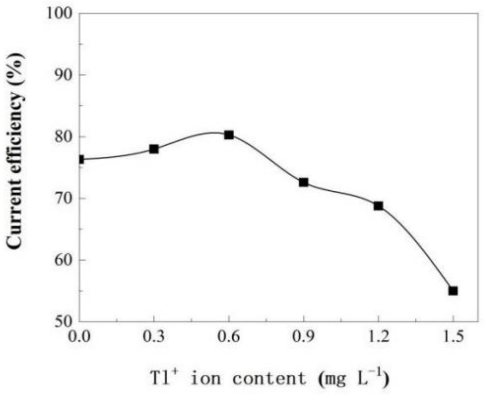

Figure 1. Effect of thallium(Ⅰ) ion content on the current efficiency of 24 h zinc deposition at a cathode current density of 518.86 A m^{-2}. Electrolyte: 35.46 g/L Zn^{2+} and 146.05 g/L H_2SO_4 electrolyte with varied Tl(Ⅰ) ions concentration (mg L^{-1}); temperature: 38 ± 1 ℃.

Since the standard electrode potential of thallium is more positive than that of zinc, thallium(Ⅰ) ions in the electrolyte will prefer to deposit on the cathode surface during zinc electrowinning. When thallium(Ⅰ) ions were present in the electrolyte, it probably led to increased hydrogen evolution, and the presence of thallium(Ⅰ) ions caused a galvanic effect on the zinc plate during electrolysis, resulting in the re-dissolution of the deposited zinc, which reduced the current efficiency [10]. The cathodic current efficiency decreased from 80% to 55% when 1.5 mg L^{-1} thallium(Ⅰ) ions were added to the electrolyte, as shown in Fig. 1. The above experiments confirmed that the presence of excess thallium(Ⅰ) ions in the electrolyte has a serious harmful effect on cathodic current efficiency. In actual production, considering that zinc electrowinning is a long-period continuous production method, if the content of thallium in the electrolyte was not controlled, thallium(Ⅰ) ions would gradually accumulate on the cathode surface via electrodeposition, thus probably increasing hydrogen evolution and causing a galvanic effect.

Deposit morphology

The concentration of thallium(Ⅰ) ions in the electrolyte was also found to greatly influence the morphology of the obtained zinc deposits. Deposited zinc was obtained by electrowinning in electrolytes with different thallium concentrations at a current density of 518.86 A m^{-2} for 24 h. The morphology of zinc deposition is shown in Figs. 2 and 3. Fig. 2 shows macroscopic photographs of the zinc plates, and Fig. 3 shows the corresponding SEM

micrographs. During the electrowinning process, a large number of circular holes were formed on the zinc plating surface regardless of the thallium(Ⅰ) ion concentration. However, there were significant differences in the size, roughness, and depth of the holes on different deposited zinc surfaces.

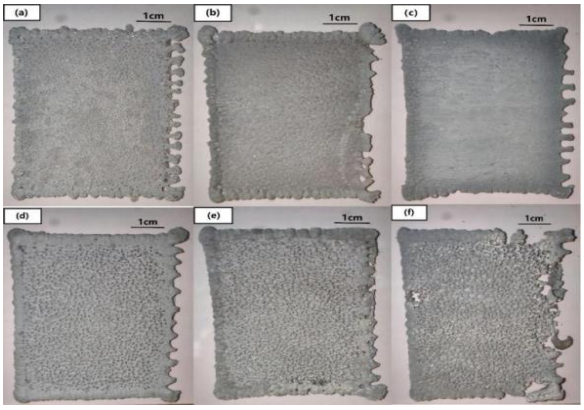

Figure 2. Photographs of zinc deposits showing the effect of various electrolyte thallium(Ⅰ) ion concentrations. (a) 0.0 mg L^{-1}, (b) 0.3 mg L^{-1}, (c) 0.6 mg L^{-1}, (d) 0.9 mg L^{-1}, (e) 1.2 mg L^{-1}, (f) 1.5 mg L^{-1}.

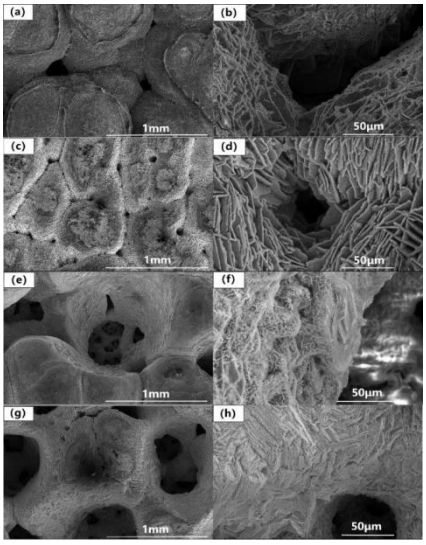

Figure 3. SEM micrographs showing the effect of electrolyte thallium(Ⅰ) ion concentrations on the morphology of deposits after electrowinning at 518.86 A m^{-2} for 24 h. (a) (b) 0.0 mg L^{-1}, (c) (d) 0.6 mg L^{-1}, (e) (f) 0.9 mg L^{-1}, (g) (h) 1.5 mg L^{-1} at different magnifications.

Zinc deposits obtained from impurity metal ion-free electrolytes usually consist of layers of flat platelets of dozens of micrometers in size. The SEM images of zinc deposited from the electrolyte containing 0.6 mg L^{-1} thallium(Ⅰ) ions showed that, similar to the zinc obtained from the impurity-free electrolyte, there were some obvious holes that may have caused gas evolution (Fig. 3(c) and (d)). When the thallium(Ⅰ) ion concentration increased from 0 mg L^{-1} to 0.6 mg L^{-1}, the surface of the deposited zinc was relatively flat, the holes were small, and the flaky deposition layers were stacked and relatively dense (Fig. 2(c) and Fig. 3(c), (d)). Further increase in the concentration of thallium(Ⅰ) ions in the electrolyte led to further changes in morphology. For example, when the thallium(Ⅰ) ion concentration increased from 0.6 mg L^{-1} to 1.5 mg L^{-1}, the surface of the deposited zinc was relatively rough and loose, and some deep holes appeared. These holes were large and embedded with small holes, and needle-like dendrites appeared on the flaky deposition layers (Fig. 2(f) and Fig. 3(g), (h)). It may be because the presence of thallium(Ⅰ) ions led to increased hydrogen evolution, resulting in the formation of a rough surface and some deep holes. Meanwhile, these morphologies could lead to further hydrogen evolution, during which small bubbles with a tendency to stick to the cathode surface could be formed. In addition, the deposited thallium and zinc formed microcells in the zinc electrowinning system. Where zinc, especially in the area connected to thallium, would redissolve and thallium would fall off from the cathode surface into the electrolyte. These led to the destruction of the cathode surface morphology.

Cathodic potential

The chronopotentiometric curves of the electrolytes with different thallium(Ⅰ) ion concentrations at 518.86 A m^{-2} cathode current density are shown in Fig. 4. The deposition potentials of zinc electrowinning under different thallium(Ⅰ) ion concentrations were obtained from Fig. 4. The effect of thallium(Ⅰ) ions on the cathodic potential of zinc electrowinning is shown in Fig. 5.

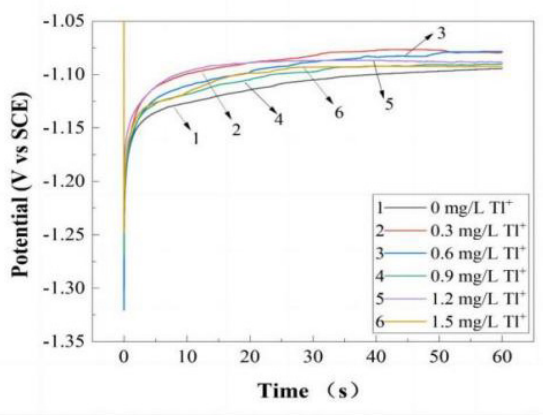

Figure 4. Chronopotentiometric curves measured in electrolytes with different thallium(Ⅰ) ion concentrations at 518.86 A m^{-2} cathode current density. Electrolyte: 35.46 g/L Zn^{2+} and 146.05 g/L H_2SO_4 electrolyte with varied Tl(Ⅰ) ions concentration (mg L^{-1}); temperature: 38 ± 1 ℃.

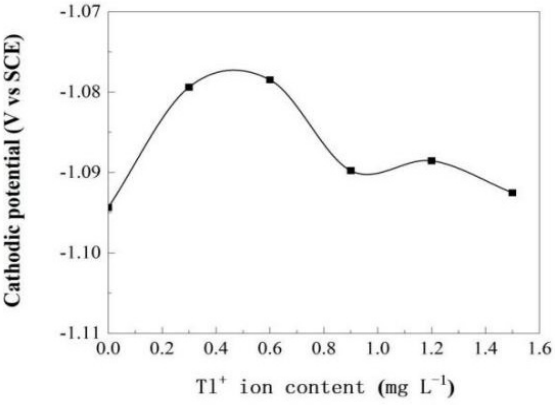

Figure 5. Effect of thallium(Ⅰ) ion concentration on cathodic potential curves for zinc deposition at a cathodic current density of 518.86 A m^{-2}. Electrolyte: 35.46 g/L Zn^{2+} and 146.05 g/L H_2SO_4 electrolyte with varied Tl(Ⅰ) ions concentration (mg L^{-1}); temperature: 38 ± 1 ℃.

As shown in Fig. 5, when the thallium(Ⅰ) ion concentration increased from 0 mg L^{-1} to 0.6 mg L^{-1}, the increase in cathode potential (becoming more positive) was caused by the increasing amount of current going to the hydrogen evolution reaction (HER) due to the depolarization of small amounts of thallium(Ⅰ) ions in zinc electrowinning. When the thallium(Ⅰ) ion concentration in the electrolyte increased from 0.6 mg L^{-1} to 1.5 mg L^{-1}, the

cathode potential decreased from -1.08 V to -1.09 V vs SCE (became more negative). The increase in the overpotential for zinc deposition was because, with increasing thallium(Ⅰ) ion concentration in the electrolyte, more thallium metal was deposited on the cathode surface and formed microcells with zinc. At the same time, bubbles produced by the hydrogen evolution reaction covered the cathode and thus decreased the effective cathodic area, resulting in a higher current density at the cathode. It resulted in an increase in the cathodic potential for zinc deposition. When the thallium(Ⅰ) ion concentration was less than 0.6 mg L^{-1}, the galvanic cell formed by deposited thallium and zinc had little influence on the zinc electrowinning process. Therefore, as shown in Fig. 1, the current efficiency changed little over this range.

Polarization behaviors

Fig. 6 shows the cathodic polarization curves measured in electrolytes with different thallium(Ⅰ) ion concentrations. When the overpotential was very low, we fitted the linear part of the cathodic polarization curves to obtain the slope, and then calculated the exchange current density according to formula (1). Fig. 7 shows the corrosion potential and corrosion current density of the zinc electrowinning process under different thallium(Ⅰ) ion concentrations using the slope extrapolation method. The above results are shown in Table 1.

$$\eta = -\frac{RTi}{nFi_0} \tag{1}$$

Where η is the overpotential at low overpotential, R is the gas constant, T is the absolute temperature, i is the polarization current density, n is the number of electrons involved in the electrode reaction, F is the Faraday constant, and i_0 is the exchange current density.

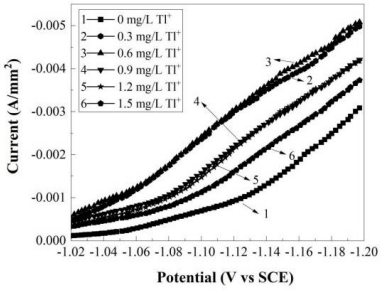

Figure 6. Cathodic polarization curves measured in electrolytes with different thallium(Ⅰ) ion concentrations at a scan rate of 10 mV s^{-1}. Electrolyte: 35.46 g/L Zn^{2+} and 146.05 g/L H_2SO_4 electrolyte with varied Tl(Ⅰ) ions concentration (mg L^{-1}); temperature: 38 ± 1 ℃.

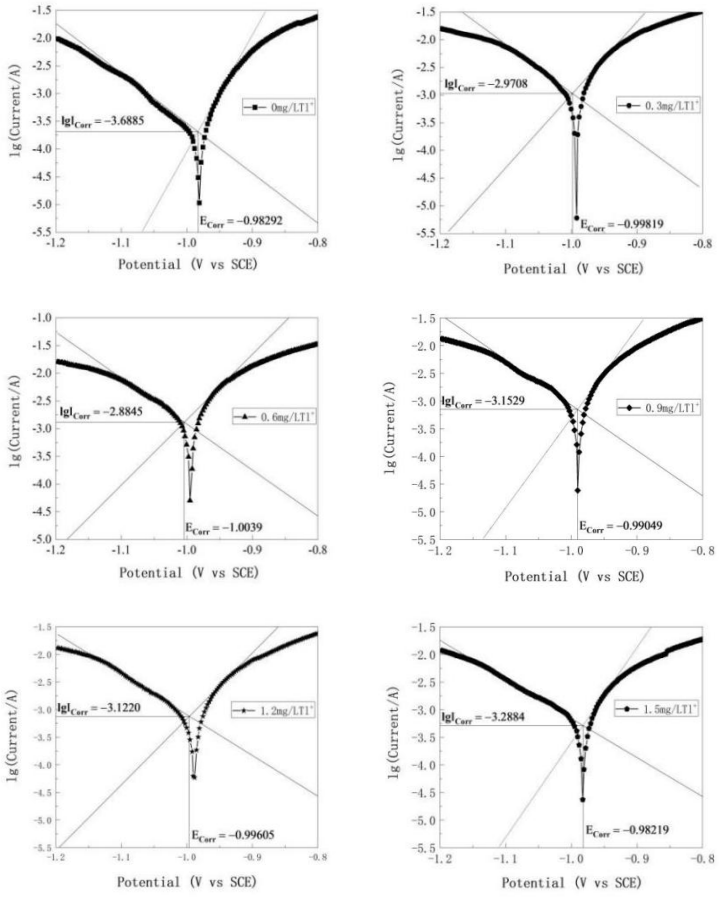

Figure 7. Corrosion potential and corrosion current density obtained by the slope extrapolation method at a scan rate of 10 mV s^{-1}. Electrolyte: 35.46 g/L Zn^{2+} and 146.05 g/L H_2SO_4 electrolyte with varied Tl(Ⅰ) ions concentration (mg L^{-1}); temperature: 38 ± 1 ℃.

Table 1. Corrosion potentials and exchange current densities obtained from cathodic polarization curves, Tafel curves and formula (1).

Tl^+ concentration (mg/L)	0	0.3	0.6	0.9	1.2	1.5
Peak potential (V vs SCE)	-0.98	-0.99	-1.00	-0.99	-0.99	-0.98
Corrosion potential (V vs SCE)	-0.983	-0.998	-1.004	-0.991	-0.996	-0.982
Exchange current density (A/mm^2)	6.9460×10^{-5}	5.6076×10^{-4}	7.5447×10^{-4}	4.0721×10^{-4}	3.1324×10^{-4}	2.4675×10^{-4}

The polarization current density (I_p) in Fig. 6 includes three parts: the first part is the zinc deposition current, the second part is the hydrogen evolution current, and the third part is the current resulting from the galvanic effect. The polarization current density was found to first increase and then decrease with increasing thallium(Ⅰ) ion concentration, with a maximum at the thallium(Ⅰ) ion concentration of 0.6 mg L^{-1}. This indicates that a small amount of thallium(Ⅰ) ions may have a depolarizing effect (promoting hydrogen evolution) during zinc electrowinning. As shown in Table 1, when the concentration of thallium(Ⅰ) ions in the electrolyte was 0.6 mg L^{-1}, the exchange current density of the zinc electrowinning process was maximum and the polarization was minimum. Therefore, when the thallium(Ⅰ) ion concentration increased from 0 mg L^{-1} to 0.6 mg L^{-1}, the hydrogen evolution current increased because a small amount of thallium(Ⅰ) ions may have a depolarization effect during the zinc deposition process. When the thallium(Ⅰ) ion concentration increased from 0.6mg L^{-1} to 1.5mg L^{-1}, with increasing thallium(Ⅰ) ion concentration in the electrolyte, more and more thallium co-deposited with zinc on the cathode, resulting in the galvanic effect. This increased the current produced by the microcells composed of thallium and zinc, decreasing the zinc deposition current and thus the current efficiency. In the microcells, the re-dissolution of zinc would cause thallium to fall off from the cathode surface, so that thallium(Ⅰ) ions would discharge and deposit on the cathode surface again. This cyclic change endangered the zinc electrowinning process. Therefore, when the thallium(Ⅰ) ion concentration was greater than 0.6 mg L^{-1}, a dramatic decrease in current efficiency occurred.

Electrochemical impedance spectroscopy

EIS technique has been employed in electrodeposition of zinc in acidic and alkaline media as well. A correlation between the impedance parameters and film morphology and corrosion resistance has been established in many research papers [24, 25]. After linear polarization experiments, EIS tests were carried out at -1 V, -1.05 V and -1.1 V, respectively, from frequency of 100 kHz to 0.01 Hz, with an amplitude of 10 mV. The Nyquist plots were found to consist of a large capacitive loop at high frequencies, as shown in Figs. 8, 9 and 10.

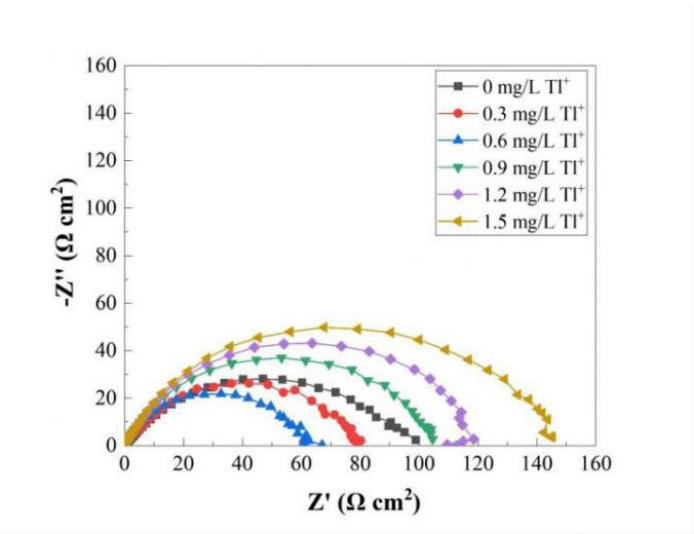

Figure 8. Nyquist plots measured in electrolytes with different thallium(Ⅰ) ion concentrations at a voltage of -1 V. Electrolyte: 35.46 g/L Zn^{2+} and 146.05 g/L H_2SO_4 electrolyte with varied Tl(Ⅰ) ion concentration; temperature: 38 ± 1 ℃.

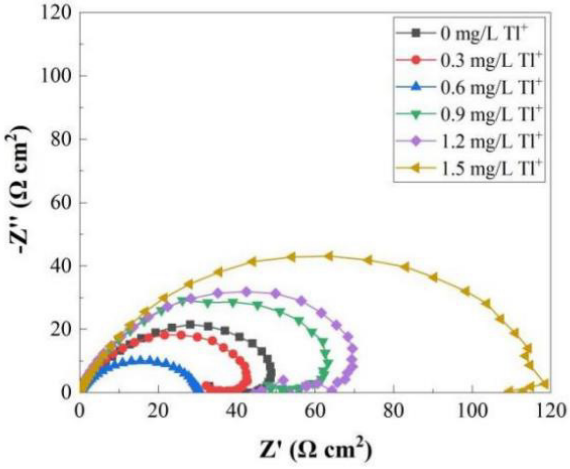

Figure 9. Nyquist plots measured in electrolytes with different thallium(Ⅰ) ion concentrations at a voltage of -1.05 V. Electrolyte: 35.46 g/L Zn^{2+} and 146.05 g/L H_2SO_4 electrolyte with varied Tl(Ⅰ) ion concentration; temperature: 38 ± 1 ℃.

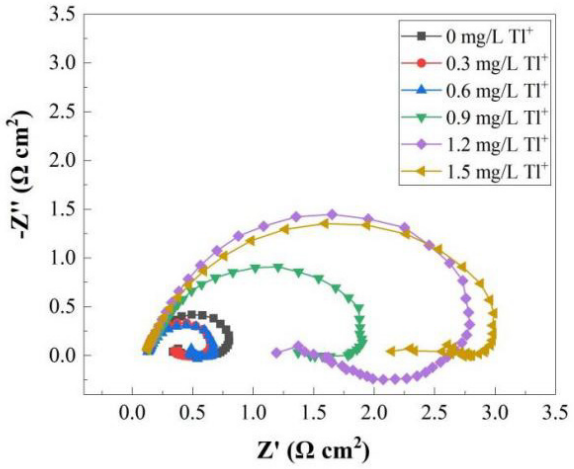

Figure 10. Nyquist plots measured in electrolytes with different thallium(Ⅰ) ion concentrations at a voltage of -1.1 V. Electrolyte: 35.46 g/L Zn^{2+} and 146.05 g/L H_2SO_4 electrolyte with varied Tl(Ⅰ) ion concentration; temperature: 38 ± 1 ℃.

The high frequency capacitive loop is usually attributed to the charge transfer resistance across the double layer. The electrochemical impedance data measured at a voltage of -1 V (Fig. 8) were modelled using the equivalent circuit presented in Fig. 11. This model consists of a solution resistance term (R_s), charge transfer resistance (R_{ct}) in the electrode reaction, and a constant phase element (CPE), which was used to model a double layer capacitance of the electrode/electrolyte interface. The impedance of CPE is defined by two parameters: CPE-T and CPE-P. Generally, when there is a dispersion effect on the electrode surface, the CPE-P value is always between 0.5 and 1. The corrosion current density is usually a parameter that characterizes the degree of corrosion of an electrode or material in an electrochemical environment. During the electrodeposition process, the corrosion of the electrode surface may occur simultaneously with the electrodeposition reaction. Appropriate corrosion current density can adjust the current efficiency to a certain extent. By understanding the relationship between the corrosion current density and the electrolysis conditions, the electrolyte composition, current density, temperature, and other parameters were adjusted to maximize the electrowinning efficiency and product quality. The corrosion current was calculated using impedance parameters employing the following equation (formula (2)):

$$i_{corr} = \frac{b_a \times b_c}{b_a + b_c} \times \frac{1}{R_{ct}} \quad (2)$$

where, b_a and b_c are the slopes of the anode and cathode Tafel, respectively. R_{ct} is the charge transfer resistance obtained from the EIS measurements.

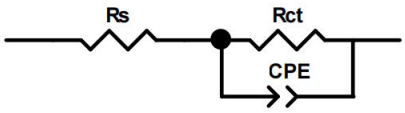

Figure 11. Equivalent circuit used to model the EIS data at a voltage of -1 V.

The degree of fitting between the measured EIS data and calculated results is evaluated by minimizing the chi-square statistic (χ^2). It is generally believed that it is acceptable when the chi-square value is less than or equal to 10^{-3} (order of magnitude). All measured impedance parameters were listed in Table 2. The chi-square values between calculated results and measured data were within 10^{-4} (order of magnitude), which depicted the best fitting agreement of the equivalent circuit model. The results revealed that, When the thallium(Ⅰ) ion concentration increased from 0 mg L^{-1} to 0.6 mg L^{-1}, the R_{ct} decreased from 97.94 Ω cm^2 to 60.19 Ω cm^2; when the thallium(Ⅰ) ion concentration increased from 0.6 mg L^{-1} to 1.5 mg L^{-1}, the R_{ct} increased from 60.19 Ω cm^2 to 142.27 Ω cm^2, indicating that a small amount of thallium(Ⅰ) ions accelerated the electrode reaction which reached the fastest at 0.6 mg L^{-1}. CPE is commonly used to describe the behavior of non-ideal double-layer capacitance. This non-ideal pure capacitance characteristic of CPE is usually caused by electrode surface non-uniformity, roughness, electrode porosity, and the uneven distribution of current and potential related to electrode geometry. When the thallium(Ⅰ) ion concentration was 0.6 mg L^{-1}, the CPE value was minimum, the charge transfer rate was maximum, and the electrode reaction was fastest, showing the maximum corrosion current density.

Table 2. Electrochemical parameters of the zinc sulfate system with different thallium(Ⅰ) ion concentrations at a voltage of -1 V fitted by EIS and corrosion current densities calculated by formula (2).

Tl^+ conc (mg/L)	R_s (Ω cm^2)	R_{ct} (Ω cm^2)	CPE (F cm^{-2})	CPE-P (n)	Chi-Squared (χ^2)	I_{corr} (A/mm^2)
0	0.07636	97.94	8.771×10^{-4}	0.678	5.829×10^{-4}	0.001782
0.3	0.06245	79.66	4.121×10^{-4}	0.724	6.590×10^{-4}	0.001975
0.6	0.08123	60.19	2.990×10^{-4}	0.837	9.270×10^{-4}	0.002773
0.9	0.07925	102.18	3.312×10^{-4}	0.810	9.349×10^{-4}	0.001806
1.2	0.08136	116.15	3.414×10^{-4}	0.807	9.493×10^{-4}	0.001722
1.5	0.08101	142.27	3.621×10^{-4}	0.797	7.184×10^{-4}	0.000928

In Fig. 9 and even more prominently in Fig. 10, a low-frequency inductive loop was present. Therefore, the electrochemical impedance data measured at a voltage of -1.1 V (Fig. 10) were modelled using the equivalent circuit presented in Fig. 12. In the low-frequency region, the induction loop was related to the adsorption of intermediate products on the electrode surface, represented by a resistance (R_L) and inductance (L_1). All measured impedance parameters were listed in Table 3. When the intermediate product appeared in the electrode reaction, the intermediate product adsorbed and produced a surface adsorption complex on the surface of the metal electrode. The surface complex was produced in the first step of the electrode reaction and consumed in the second step. Therefore, an inductive arc appeared in the low-frequency part of the impedance diagram. The deposition of zinc in zinc electrowinning was mainly carried out in two steps. First, Zn^{2+} obtained an electron to form an adsorbed zinc monovalent ion, and then another electron was obtained to form an active zinc molecule. From Table 3, it can be seen that at -1.1 V potential, with the increase in Tl^+ concentration, the R_{ct} of zinc electrowinning decreased first and then increased, and the CPE-P was all less than 1, indicating that the electrode surface was relatively rough. When the concentration of Tl^+ was 0.6 mg L^{-1}, the R_{ct} and CPE of zinc electrowinning were minimum. When the concentration of Tl^+ increased from 0 mg L^{-1} to 0.6 mg L^{-1}, the adsorption resistance R_L did not change much, and the inductance L_1 caused by the surface diffusion of adsorbed atoms decreased. When the concentration of Tl^+ increased from 0.6 mg L^{-1} to 1.5 mg L^{-1}, the adsorption resistance R_L and the inductance L_1 caused by surface diffusion of adsorbed atoms increased significantly. This may be because the zinc monovalent ions generated in the first step of zinc electrowinning were adsorbed on the electrode surface. As the concentration of Tl^+ increased to 1.5 mg L^{-1}, the adsorption of zinc monovalent ions was more difficult and the adsorption behavior was more complex, resulting in an increase in R_{ct}, R_L and L_1.

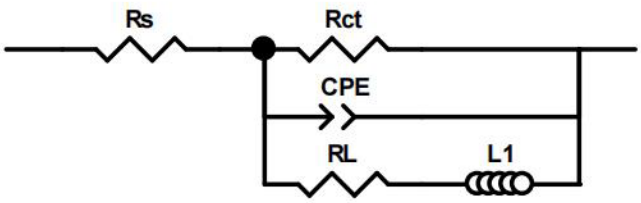

Figure 12. Equivalent circuit used to model the EIS data at a voltage of -1.1 V.

Table 3. Electrochemical parameters of the zinc sulfate system with different thallium(Ⅰ) ion concentrations at a voltage of -1.1 V fitted by EIS.

Tl^+ conc (mg/L)	R_s (Ω cm^2)	R_{ct} (Ω cm^2)	CPE (F cm^{-2})	CPE-P (n)	R_L (Ω cm^2)	L_1 (H cm^2)	Chi-Squared (χ^2)
0	0.1197	1.4262	3.841×10^{-3}	0.899	0.7370	1.90×10^{-3}	4.328×10^{-4}
0.3	0.1086	1.0246	4.818×10^{-3}	0.898	0.7084	1.92×10^{-3}	7.569×10^{-4}
0.6	0.0996	0.8280	5.796×10^{-4}	0.923	0.8051	8.00×10^{-4}	8.964×10^{-4}
0.9	0.1053	3.2713	6.787×10^{-4}	0.706	2.9346	8.64×10^{-4}	9.584×10^{-4}
1.2	0.1082	4.2789	6.019×10^{-3}	0.828	3.6273	9.46×10^{-2}	9.527×10^{-4}
1.5	0.1103	4.3429	6.248×10^{-3}	0.845	3.6857	9.34×10^{-2}	8.193×10^{-4}

CONCLUSIONS

Concerning the effect of thallium(Ⅰ) ions on the electrowinning of zinc from acidic sulfuric acid electrolytes, the following conclusions were obtained:

(1) With increasing thallium(Ⅰ) ion concentration in the electrolyte, the hydrogen evolution reaction and the galvanic effect produced during zinc electrowinning increased. This led to the re-dissolution of cathode zinc, which influenced the morphology of the obtained zinc deposits and severely reduced the current efficiency.

(2) A small amount of thallium(Ⅰ) ions in the electrolyte had a depolarization effect during zinc deposition, which increased the hydrogen evolution current. When the concentration of thallium(Ⅰ) ions in the electrolyte was 0.6 mg L^{-1}, the exchange current density of the zinc electrowinning process was maximum and the polarization was minimum. When the thallium(Ⅰ) ion concentration increased from 0.6 mg L^{-1} to 1.5 mg L^{-1}, with increasing thallium(Ⅰ) ion concentration in the electrolyte, more and more thallium co-deposited with zinc on the cathode, resulting in the galvanic effect.

(3) When the concentration of thallium(Ⅰ) ions was 0.6 mg L^{-1}, the R_{ct} of the equivalent circuit was minimum, the CPE value was minimum, the charge transfer rate was maximum, and the electrode reaction was fastest, showing the maximum corrosion current density. When EIS tests were carried out at -1.1 V, a low-frequency inductive loop was present. At this time, when the concentration of Tl^+ increased from 0 mg L^{-1} to 0.6 mg L^{-1}, the adsorption resistance R_L did not change much, and the inductance L_1 caused by the surface diffusion of adsorbed atoms decreased. When the concentration of Tl^+ increased from 0.6 mg L^{-1} to 1.5 mg L^{-1}, the adsorption resistance R_L and the inductance L_1 caused by surface diffusion of adsorbed atoms increased significantly.

EXPERIMENTAL SECTION

The electrolyte used in this study was prepared with distilled water, 0.1 g/L terpenic oil, 35.46 g/L Zn^{2+}, and 146.05 g/L H_2SO_4 as the base electrolyte for different concentrations of thallium(Ⅰ) ions. All electrochemical measurements were carried out using the Autolab PGSTAT 302N electrochemical workstation. The three-electrode system was used in the experiment. The saturated calomel electrode was used as the reference electrode. The auxiliary electrode was a square platinum electrode of 1 cm × 1 cm. The working electrode was a circular glassy carbon electrode with a diameter of 2 mm. The working electrode was polished, then soaked in alcohol for 5 minutes, and finally cleaned with distilled water before use. This cathode pretreatment procedure was essential to obtaining reproducible results. A Luggin capillary was used to reduce the ohmic drop from the solution. In all electrochemical measurements, the anode to cathode surface area ratio was greater than 50. This ensured that the anodic process had a negligible influence on the cathodic process because the anodic current density of polarization and anodic polarization potential were less than the cathodic current density and polarization potential. The cathodic polarization curves were measured at a scan rate of 10 mV s^{-1}.

During all the electrodeposition experiments, the cathode current density was maintained at 518.86 A m^{-2}, and the electrolysis time was 24 h. The temperature of the electrolytic cell was maintained at 38 ± 1 ℃ in a constant temperature bath. The current efficiency (η) was obtained from the following equation:

$$\eta = \frac{2mF}{MIt} \times 100\% \quad (3)$$

where m is the mass of Zn deposited on the cathode, M is the molar mass of zinc (M = 65.39 g mol^{-1}), I is the cathodic current, t is the electrowinning time, and F is the Faraday constant (F = 96485 C mol^{-1}).

The deposited morphology was examined by a scanning electron microscope (SEM).

ACKNOWLEDGMENTS

The authors acknowledge the funding support from the Applied Basic Research Project of Yunnan (No. 202001BA070001-135) and the Scientific Research Foundation of Education Department of Yunnan Province of China (No. 2022Y751).

REFERENCES

1. F. Porter; *Zinc Handbook,* Faulkener, New York, **1991**, ISBN: 9780824783402.
2. S. Gürmen; M. Emre; *Miner. Eng.,* **2003**, *16,* 559-562.
3. A. E. Saba; A. E. Elsherief; *Hydrometallurgy,* **2000**, *54,* 91-106.
4. H. Zhang; Y. Li; J. Wang; X. Hong; *Hydrometallurgy,* **2009**, *99,* 127-130.
5. F. Parada T; E. Asselin; *JOM,* **2009**, *61,* 54-58.
6. I. Ivan; St. Rashkov; *Stud. Univ. Babes-Bolyai Chem.,* **1996**, *2,* 122-137.
7. L. Muresan; G. Maurin; L. Oniciu; *Hydrometallurgy,* **1996**, *43,* 345-354.
8. J. Q. Zhu; Y. M. Wu; J. Zuo; D. F. Khan; C. H. Jiang; *Hydrometallurgy,* **2017**, *174,* 248-252.
9. M. Saloma; H. Holtan Jr; *Acta Chem. Scand.,* **1974**, *28a,* 86-92.
10. J. Wu; P. Zeng; Q. Feng; Z. M. Liu; W. J. Qiu; S. B. Zhang; Q. S. Yang; Y. Jiang; *China Nonferrous Metallurgy,* **2021**, *50,* 34-38 (in Chinese).
11. J. Liu; J. Wang; Y. H. Chen; X. F. Xie; J. Y. Qi; H. Lippold; D. G. Luo; C. L. Wang; L. X. Su; L. C. He; Q. W. Wu; *Environ. Pollut.*, **2016**, *212*, 77-89.
12. B. Karbowska; W. Zembrzuski; M. Jakubowska; T. Wojtkowiak; A. Pasieczna; Z. Lukaszewski; *J. Geochem. Explor.*, **2014**, *143*, 127-135.
13. Y. Liu; W. P. Chen; Y. H. Huang; Z. H. Li; C. S. Li; H. X. Liu; X. L. Huangfu; *J. Hazard. Mater.*, **2024**, *462*, 132745.
14. F. G. Zhao; *Non-Ferrous Mining and Metallurgy,* **2008**, *24,* 24-26 (in Chinese).
15. A. M. Abd El-Halim; R. M. Khalil; *Surf. Technol.*, **1984**, *23*, 215-223.
16. J. Clavilier; J. P. Ganon; M. Petit; *J. Electroanal. Chem.,* **1989**, *265,* 231-245.
17. P. Rodriguez; N. García-Aráez; E. Herrero; J. M. Feliu; *Electrochim. Acta,* **2015**, *151,* 319-325.
18. M. Hosseini; S. Ebrahimi; *J. Electroanal Chem.,* **2010**, *645,* 109-114.
19. H. J. Wang; X. Wang; Z. Jin; *China Nonferrous Metallurgy,* **2022**, *51,* 105-111 (in Chinese).
20. Y. J. Zou; H. J. Cheng; H. N. Wang; R. X. Huang; Y. H. Xu; J. Jiang; Q. He; C. H. Liu; J. C. Liu; J. M. Xiong; J. N. Yao; X. L. Huangfu; J. Ma; *Environ. Sci. Technol.,* **2020**, *54,* 7205-7216.
21. Z. M. Senol; U. Ulusoy; *Chem. Eng. J.,* **2010**, *162,* 97-105.
22. B.G. Xiong; S. F. Liu; Y. Wang; Z. M. Xia; L. G. Ye; *J. Clean. Prod.*, **2023**, *430*, 139695.
23. T. J. Yang; J. H. Kong; J. Tao; B. Xu; G. F. Dong; H. F. Shang; *China Nonferrous Metallurgy,* **2019**, *48,* 29-32 (in Chinese).
24. D. Desai; X. Wei; D. A. Steingart; S. Banerjee; *J. Power Sources,* **2014**, *256,* 145-152.
25. X. Wei; D. Desai; G. G. Yadav; D. E. Turney; A. Couzis; S. Banerjee; *Electrochim. Acta,* **2016**, *212,* 603-613.

STUDIA UBB CHEMIA, LXIX, 1, 2024 (p. 69-83)
(RECOMMENDED CITATION)
DOI:10.24193/subbchem.2024.1.05

PHYTOCHEMICAL COMPOSITION, ANTIOXIDANT, ENZYME INHIBITORY AND CYTOTOXIC ACTIVITIES OF FLOWERS AND LEAVES OF *MALVA SYLVESTRIS* L.

Selen İLGÜN[a,*], Derya ÇİÇEK POLAT[b], Gökçe ŞEKER KARATOPRAK[c]

ABSTRACT. The objective of the study was to assess the biological functions and chemical composition of *Malva sylvestris* L. from Ida Mountain of Turkiye, a medicinal plant used for a variety of therapeutic applications. The antioxidant (DPPH, ABTS, Iron (II) chelate activity), enzyme inhibition (acetylcholinesterase), and cytotoxic properties of methanol extracts prepared from leaves and flowers were investigated. The chemical composition of the extracts was evaluated in terms of spectrophotometric (total phenol and total flavonoid) and chromatographic (HPLC) techniques. IC50 value of the DPPH radical scavenging effect of the flower extract, with the highest total phenol and flavonoid content, was found to be 0.5 mg/mL. The ABTS radical scavenging effect was 2.56 mmol/ L Trolox. While the extracts' chelating activity was not as great as that of EDTA, the enzyme inhibition of the flower extract was determined to be 37.67%. Flower extract was shown to have the most cytotoxic activity in both Hela and Hep G2 cell lines. In HPLC analysis; amounts of the detected phenolic compounds were determined, and method validation was performed. This research has given us a better understanding of the traditional use of the *M. sylvestris* plant from Turkiye, which stands out for its therapeutic properties.

Keywords: *M. sylvestris; Malvaceae; antioxidant; anticholinesterase activity; cytotoxic activity*

[a] *Erciyes University, Faculty of Pharmacy, Department of Pharmaceutical Botany, 38039, Kayseri, Türkiye*
[b] *Ankara University, Faculty of Pharmacy, Department of Pharmaceutical Botany, 06560, Ankara, Türkiye*
[c] *Erciyes University, Faculty of Pharmacy, Department of Pharmacognosy, 38039, Kayseri, Türkiye*
* *Corresponding author: serturk@erciyes.edu.tr*

INTRODUCTION

Humans have been using medicinal plants to heal ailments for centuries. Nowadays, there is a growth in the usage of medicinal plants across the world as a result of their demonstrated efficiency in treating specific ailments and assertions that their usage is safe. Medicinal plants, with the knowledge they have accumulated over time, also contribute to the production of medicines today [1]. Active compounds produced during secondary plant metabolism are generally responsible for the biological properties of medicinal plants. Studies on the chemical structures of plants and the mechanisms behind their biological processes are increasing day by day [2].

Malva sylvestris L. from the Malvaceae family is known as “ebegümeci” in Turkiye. The biennial-perennial herbaceous plant. *M. sylvestris* is often found in North Africa, Europe, and Southwest Asia [3,4]. The leaves are heart-shaped and have 5 to 7 lobes, and the flowers are a bright pink color with purple streaks [5]. This medicinal plant has historically been used to cure a variety of illnesses and disorders, including colds, burns, coughs, tonsillitis, bronchitis, digestive issues, dermatitis, and cut wounds [6]. The most often utilized components of *M. sylvestris*, the leaves, and flowers, contain a variety of bioactive substances, including, mucilages, phenol derivatives, flavonoids, tannins, coumarins, sterols, terpenoids, saponins, alkaloids. Many researches have demonstrated the antibacterial, anti-inflammatory, hepatoprotective, and antioxidant benefits of this plant given its rich composition [6-10].

Even though *M. sylvestris* is a plant with extensive traditional usage and has been the focus of several studies, there are still issues that require further investigation. Above all, it appears that this species’s effectiveness in several cancer cell lines has not been established. Determining the toxicity of both flower and leaf extracts to Hela and Hep G2 cell lines, as well as if there is a relationship with their antioxidant capabilities, is the primary objective of our investigation. It was also aimed to determine the chemical composition of the extracts with HPLC and to evaluate their activities on acetylcholinesterase enzyme. To the best of our knowledge, this study represents the first comprehensive investigation, encompassing not only the exploration of the anticancer effects of the plant on specified cells but also concurrent phytochemical analyses, alongside the examination of other biological activities. This research holds significance in the context of comparative analyses with previous studies conducted to date, as it pioneers the simultaneous examination of phytochemical profiles along with specific biological activities, particularly focusing on the anticancer potential of the plant in question.

RESULTS AND DISCUSSION

Chemical composition

The highest total phenol content was found in a flower extract with a value of 172.77±14.08 $mg_{GAE}/g_{extract.}$ In total flavonoid content, flower extract has the highest content with a value of 73.72±3.34 $mg_{CA}/g_{extract}$ also. The results are given in Table 1. The total phenol content of *M. sylvestris,* which was collected in Pakistan and made using methanol extract from the aerial parts, was 59.91±0.08 $mg_{GAE}/g_{extract}$. In contrast, the total flavonoid content was 61.12±0.117 $mg_{RE}/g_{extract}$ [11]. As compared to our findings, we may conclude that the species collected from the outskirts of Ida Mountain in Turkiye have higher phenol and flavonoid contents.

Table 1. Total phenol/flavonoid amount of extracts of *M. sylvestris* and contents of caffeic acid, chlorogenic acid, coumaric acid, ferulic acid, rutin, rosmarinic acid, and tannic acid in extracts (n=3)

	Flower extracts	**Leaves extracts**
Caffeic acid (%±SD*)	0.261±0.003	0.248±0.005
Chlorogenic acid (%±SD*)	0.164±0.008	0.199±0.003
Coumaric acid (%±SD*)	0.144±0.001	0.130±0.001
Ferulic acid (%±SD*)	0.061±0.004	0.056±0.008
Rutin (%±SD*)	0.304±0.003	ND*
Rosmarinic acid (%±SD*)	0.105±0.009	ND*
Tannic acid (%±SD*)	2.784±0.433	ND*
Total Phenol [mg_{GAE}/g_{extact}]	172.77±14.08	148.86±4.94
Total Flavonoid [$mg_{CA}/g_{extract}$]	73.72±3.34	40.19±1.37

ND*: Not determined

The levels of caffeic acid, chlorogenic acid, coumaric acid, ferulic acid, rutin, rosmarinic acid, and tannic acid in the plant extracts were calculated using HPLC analysis (Figure 1), and the results are shown in Table 1. In HPLC analysis performed; caffeic acid, chlorogenic acid, coumaric acid, ferulic acid, rutin, rosmarinic acid, and tannic acid were detected in the flower extract, while only caffeic acid, chlorogenic acid, coumaric acid, and ferulic acid were detected in the leaves extract. The amounts of the detected phenolic compounds were

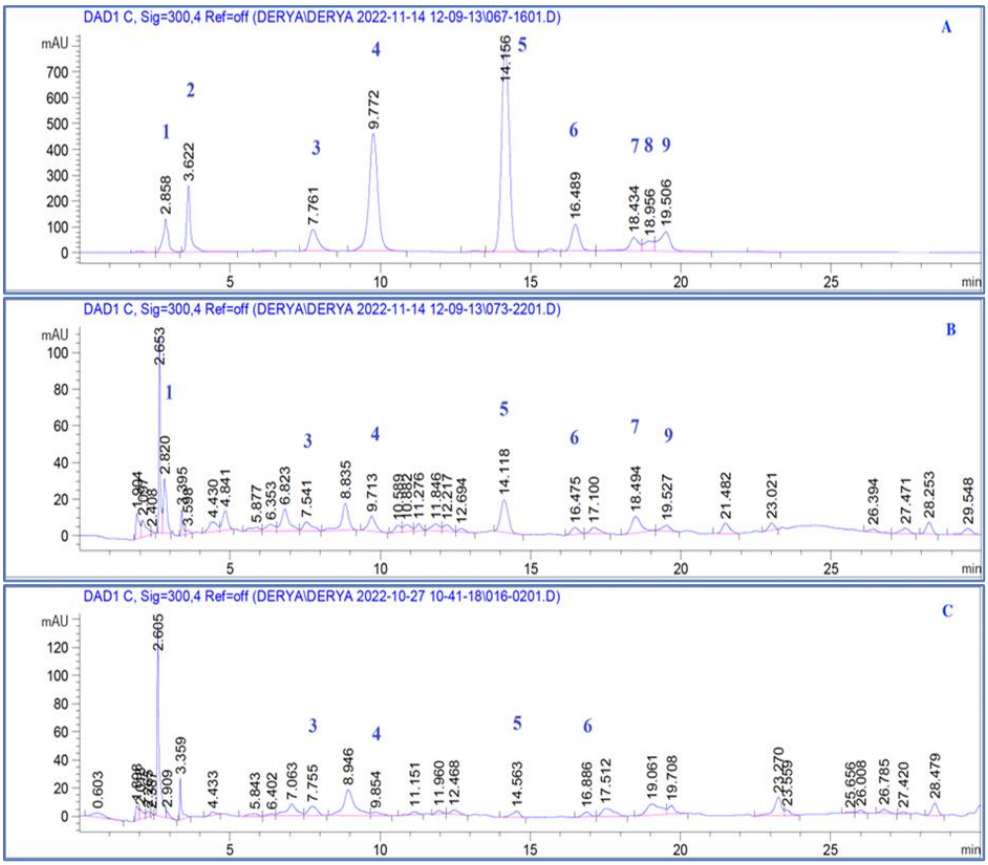

Figure 1. HPLC chromatograms. A. Standards: (1) Tannic acid, (2) Gallic acid, (3) Chlorogenic acid, (4) Caffeic acid, (5) Coumaric acid, (6) Ferulic acid, (7) Rutin, (8) Hyperoside, and (9) Rosmarinic acid; B. Flower extract; C. Leaf extract

determined, and method validation was performed. Calibration values, precision data, and statistical information from the recovery assays are included in Tables 2 and 3. The amounts of tannic acid (2.784±0.433 %) and rutin (0.304±0.003 %) in the flower extract were found to be higher than those of the other compounds. Likewise, caffeic acid content was found to be higher (0.248±0.005 %) in the leaf extract. Rutin, rosmarinic acid, and tannic acid were not detected in the leaf extract. In the study of Terninko et al. (2014), the presence of rutin and rosmarinic acid was also determined in flower extracts [12]. DellaGreca et al. (2009) isolated 4-hydroxybenzoic acid, 4-methoxybenzoic acid, 4-hydroxy-3-methoxybenzoic acid, 4-hydroxycinnamic acid, ferulic acid, methyl 2-hydroxydihydrocinnamate, scopoletin, N-trans-feruloyl

tyramine, and a sesquiterpene, (3R,7E)-3-hydroxy-5,7-megastigmadien-9-one from *M. sylvestris* leaf water extract [8]. In different studies, the presence of oxalic, malonic, fumaric, benzoic, malic, vanillic, ferulic, salicylic, and p-coumaric acids was detected in the leaves [13,14]. Luteolin, kaempferol, myricetin, apigenin, genistein, quercetin, kaempferol-3-*O*-rutinoside and quercetin-3-*O*-rutinoside and caffeoylquinic acid were detected in flowers [15]. In *M. neglecta* and *M. sherardiana* species, *p*-coumaric acid, caffeic acid, and rutin were found to be similar to our study [16].

Table 2. Calibration values for standards and precision data of the method

						Intra-day precision (RSD*%)			**Inter-day precision (RSD*%)**		
						Amount					
	Calibration range (µg/mL)	**Linear Equation**	**Correlation factor (r^2±SD*)**	**LOD µg/mL**	**LOQ µg/mL**	**50 µg/mL**	**100 µg/mL**	**200 µg/mL**	**50 µg/mL**	**100 µg/mL**	**200 µg/mL**
Caffeic acid	10-200	y=110424x-1591.6	0.9805±0.006	0.078	0.260	0.937	0.634	1.797	1.419	2.380	2.303
Chlorogenic acid	10-200	y=23710x-144.8	0.984±0.001	0.212	0.709	1.763	2.196	0.715	2.049	2.514	1.539
Coumaric acid	10-200	y=259913x-1950.2	0.997±0.008	0.014	0.047	1.445	0.395	1.244	3.835	3.423	0.948
Ferulic acid	10-200	y=24109x-27.692	0.999±0.003	0.067	0.225	0.583	0.869	0.558	1.118	3.253	1.127
Rutin	10-200	y=15370x-87.448	0.997±0.006	0.126	0.420	0.790	0.458	0.413	1.839	0.512	2.532
Rosmarinic acid	10-200	y=45771x-218.14	0.998±0.001	0.077	0.257	1.581	1.131	0.841	2.427	1.691	0.696
Tannic acid	10-200	y=1002.9x+43.687	0.990±0.002	0.418	1.394	2.625	2.993	1.243	3.846	1.544	0.741

Table 3. Recovery assay's statistical data of the method (n=3)

Standards	Concentration in sample (mg/mL)	Amount spiked (mg/mL)	Mean amount found in mixture (mg/mL)	Mean recovery (%±SD*)	RSD (%)
Caffeic acid	0.02	0.01	0.015	96.490±0.062	0.065
		0.02	0.02	96.259±0.282	0.293
		0.04	0.03	100.744±1.078	1.070
Chlorogenic acid	0.01	0.005	0.008	104.559±0.324	0.310
		0.01	0.01	103.645±0.233	0.224
		0.02	0.015	103.971±0.872	0.839
Coumaric acid	0.01	0.005	0.008	100.119±0.024	0.024
		0.01	0.01	95.332±0.205	0.215
		0.02	0.015	99.905±1.952	1.954
Ferulic acid	0.004	0.002	0.003	99.601±1.884	1.891
		0.004	0.004	103.39±0.285	0.276
		0.008	0.006	95.196±1.192	1.252
Rutin	0.02	0.01	0.015	100.539±0.591	0.587
		0.02	0.02	97.433±0.447	0.459
		0.04	0.03	101.028±1.072	1.061
Rosmarinic acid	0.006	0.003	0.005	106.398±0.004	0.004
		0.006	0.006	103.773±0.621	0.599
		0.012	0.009	98.784±0.699	0.708
Tannic acid	0.2	0.1	0.15	103.773±1.01	0.978
		0.2	0.2	103.587±0.430	0.415
		0.4	0.3	99.706±2.532	2.539

Antioxidant Activity

The scavenging effect of the extracts on both DPPH (1,1-Diphenyl-2-picrylhydrazyl radical) and ABTS (2,2′-Azino-bis (3-ethylbenzothiazoline-6-sulfonic acid) diammonium salt) radicals was evaluated. Flower extract with high total phenol and flavonoid content showed a stronger effect against both radicals. While none of the extracts could scavenge DPPH radicals as strongly as standard BHT (Butylated hydroxytoluene), the flower extract had the same significance as BHT against ABTS radical at 2 mg/mL concentration ($p>0.05$). The results are presented in Table 4. In the study by Irfan et al. (2021), the IC50 value of the dichloromethane fraction of the aerial part extract against the DPPH radical was found to be 22.11 µg/mL, and the IC 50 value of standard ascorbic acid was 7 µg/mL [11]. When the activity of the extract and the standard is proportioned, it corresponds to 3.13, while the ratio of extract/standard BHT corresponds to 5 in our study. Although the experimental procedures are different, it is seen that the activity rates are close to each other. In a different investigation, the butanol

fraction of the aerial part water extract was shown to have an IC50 value of 78.14 µg/mL against the DPPH radical and an IC50 value of 12.55 µg/mL for Trolox. In comparison, the IC 50 value against the ABTS radical was 166.79 µg/mL and that for Trolox was 188.16 µg/mL [17]. In this study, the extract and standard substance activity rates were found to be compatible with our study. Interestingly, in the study of Beghdad et al. (2014), leaf extract was emphasized as a stronger antioxidant than flower extract [18]. Similar to our results Petkova et al. (2019) discovered that flower extracts were more antioxidant than leaves in DPPH and FRAP assay [19].

The measurement of the chelating activity of the extracts for Fe^{2+} ions was studied at concentrations in the range of 250-8000 µg/mL, and Na_2EDTA at concentrations in the range of 100-350 µg/mL. It was observed that the Fe^{2+} chelating activity of the extracts increased depending on the concentration, but it was determined that no extract showed as much activity as EDTA used as a standard (Figure 2). Reducing their concentration in the medium by binding transition metal ions and thus delaying Fe^{2+} catalyzed lipid peroxidation is an important mechanism for measuring antioxidant capacity. Flavonols with 3-hydroxy-4-keto or 5-hydroxy-4-keto groups exhibit substantial metal chelation activities and form stable complexes with metals, according to the literature [20]. In this experiment, the stronger chelating of flower extracts was associated with the presence of anthocyanins present in the flowers [21]. Only the chelating activity of leaves has been previously assessed, even though there is no study in the literature that documents the metal chelating activity of flowers. The methanolic extract of *M. sylvestris* was shown to have remarkable activity in terms of chelating iron ions, with an IC50 value of 52.7±1.8 µg/mL [10].

Table 4. Radical scavenging effects of the *M. sylvestris* extracts

Extracts	DPPH IC50 (mg/mL)	TEAC mmol/ L Trolox
Flower extract	0.50±0.02*	2.56±0.08^{a} (2 mg/mL) 2.152±0.15^{b} (1 mg/mL)
Leaf extract	0.84±0.14**	2.48±0.16^{a,b}(2 mg/mL) 1.93±0.19^{c}(1 mg/mL)
BHT	0.1±0.05***	2.79±0.01^{a}(2 mg/mL) 2.63±0.03^{a}(1 mg/mL)

Values expressed as mean±standard error (n = 3), statistical analyses by Tukey comparison test. Bars with the same lower-case letters (a–b,) superscripts (*–***), are not significantly ($p>0.05$) different.

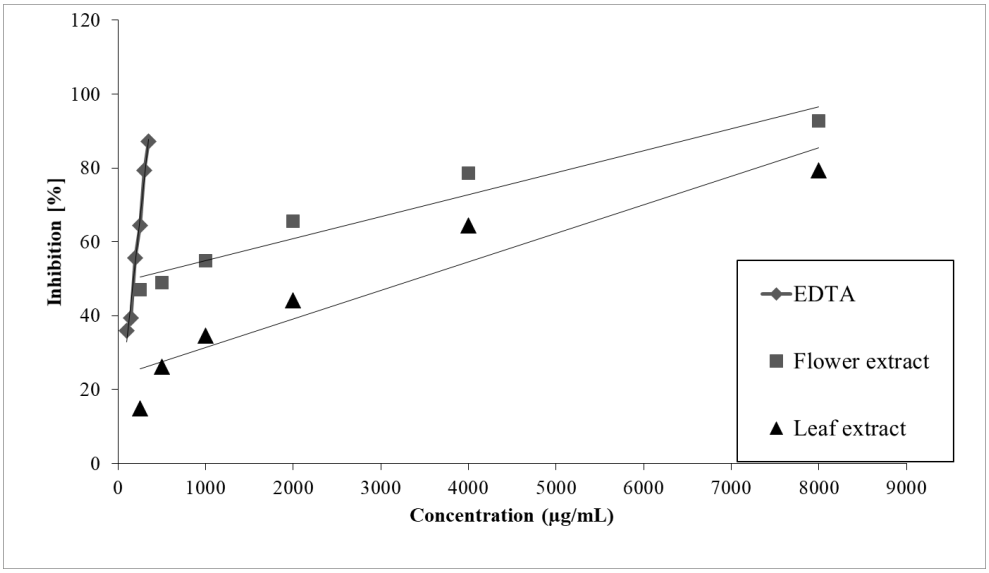

Figure 2. The chelating activity of extracts for Fe^{2+} ions

Acetylcholinesterase Enzyme Inhibition Activity

Acetylcholine is a neurotransmitter that is largely blocked by acetylcholinesterase (AChE) and is thought to have a role in the pathophysiology of Alzheimer's disease. Despite the fact that the cause of Alzheimer's disease is unknown, increasing acetylcholine levels through AChE enzyme inhibition is widely accepted as the most effective treatment strategy [22]. Table 5 provides a summary of the plant extracts' AChE inhibitory effects. Extracts were studied at a concentration of 8 mg/mL and standard galanthamine at a concentration of 1 mg/mL. Despite being at high concentrations, neither extract was statistically significant with galanthamine ($p>0.05$). While most acetylcholinesterase inhibitors contain nitrogen, the limited efficacy of these extracts might be attributed to a lack of alkaloid content [31]. Although there is little evidence of *M. sylvestris* AChE inhibition, the research found that a decoction of the aerial part decoction inhibited AChE by 25% at 5 mg/mL [7]. Results comparing enzyme inhibition of flower and leaf extracts are presented for the first time in this article.

Table 5. AChE inhibitory activities of the M. *sylvestris* extracts

	AChE Inhibition%
Flower extract (8 mg/mL)	37.67±2.15[a]
Leaf extract (8 mg/mL)	33.56±2.13[a]
Galanthamine(1 mg/mL)	63.43±1.64[b]

The values are exhibited as the mean ± standard error (SE, n = 3), and statistical comparisons were performed using the Tukey comparison test. Bars with the same lowercase letters (a–b) do not exhibit significant differences ($p > 0.05$).

Cytotoxic activity

Both flower and leaf extracts were more effective against the HeLa cell line. It was determined that flower extract inhibited viability significantly ($p<0.05$) even at 31.25 µg/mL concentration. The viability was found to be 25.57% at 1000 µg/mL in the group to which the flower extract was administered ($p<0.001$). Leaf extract showed a significant inhibition effect on viability in the concentration range of 62.5-1000 µg/mL. The viability was 38.47% in the leaf extract applied group at 1000 µg/mL ($p<0.001$). In the Hep G2 cell line, flower extract showed a significant inhibition effect on viability in the concentration range of 125-1000 µg/mL, while leaf extract showed significant inhibition only at 1000 µg/mL. Flower extract decreased the viability by 51.19% at 125 µg/mL ($p<0.01$). When all the results were examined, the flower extract was found to be more effective than the leaf extract in both cell lines. Results are given in Figure 3. Total phenol, flavonoid contents, as well as rutin, rosmarinic acid, and tannic acid, which are found in the flower extract different from the leaf extract, may be responsible for this effect. In a study with *M. sylvestris* leaf extract, it was reported that it showed a cytotoxic effect for B16 (murine melanoma) and A375 (human melanoma) cell lines. According to research, the extract had antiproliferative activity in B16 cells that was 61% and 97% higher than that of the control 1:200 and 1:40 dilutions, respectively. A 1:10 dilution resulted in a substantial 58% decrease in cell proliferation in A375 cells compared to the control [23]. To our knowledge, there is no study in the literature that determined the cytotoxic activity of flower and leaf extracts of *M. sylvestris* in HeLa and Hep G2 cell lines. *M. sylvestris* leaf hydro methanolic extract was studied in MCF-7 (human breast carcinoma), Hep G2 (human epiglottis cancer), and WEHI (mouse leukemia) cell lines in a study by Boutennoun et al. (2019), and its toxicity was found to be 45.20%, 62.62%, and 82.04%, respectively, at 125 µg/mL concentration [24]. More recently the cytotoxicity of Fe_3O_4 nanoparticles synthesized by *M. sylvestris* extract was analyzed by exposure to MCF-7 and Hep-G2 cancer cell lines, and the

IC50 value was reported as 100 µg/mL and 200 µg/mL, respectively [14]. Comparative toxicity of *M. sylvestris* leaf and flower extracts in HeLa and Hep G2 cell lines was elucidated for the first time in this study.

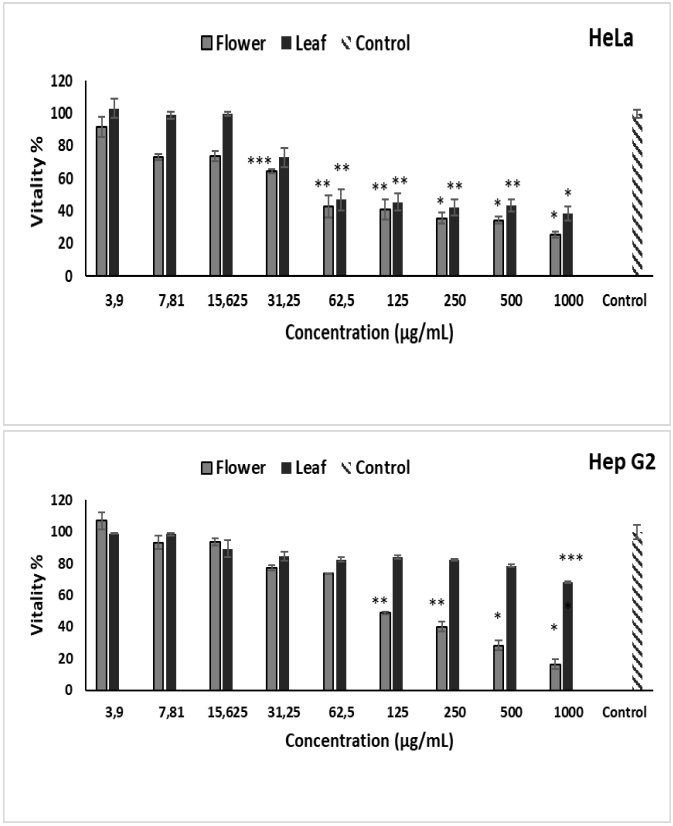

Figure 3. Cytotoxic activities of the extracts on HeLa and Hep G2 cell line. Values are given as mean ± sd (n = 3), statistical analyses by Dunnett's comparison test. *** p<0.05 ** p<0.01* p<0.001

CONCLUSION

We demonstrated, for the first time, the potential use of *M. sylvestris* flowers and leaves gathered from Ida Mountain of Turkiye as a functional food due to the presence of polyphenols and some biological activities exhibited *in vitro. M. sylvestris* flowers are a rich source of phenolic compounds. The extracts have demonstrated antioxidant and acetylcholinesterase-inhibiting

properties, as well as cytotoxic activity in cancer cell lines. This study supports the idea of using different parts (leaves and flowers) of traditionally used plants grown in different regions as edible, healthy ingredients with health-protective properties.

EXPERIMENTAL SECTION

Plant material and Extraction procedure

M. sylvestris were gathered in Altınoluk, Balıkesir. in May 2022. Dr. Derya Çiçek Polat authenticated the sample. *M. sylvestris* samples' flowers and leaves were separated and then dried individually. At room temperature, dry materials (each sample 100 g) were pulverized and extracted three times with methanol (24 h). An ultrasonic bath was used to complete the extraction (60 min.) After filtering, the extracts were concentrated to dryness in an evaporator. They were kept in the refrigerator throughout the study.

Total phenolic and flavonoid content

Total phenol and flavonoid levels were computed using gallic acid equivalents (GAE) and catechin equivalents (CA), respectively. The Folin-Ciocalteu method was employed to figure out the total quantity of phenolic substances in the extracts [25]. The total flavonoid level was measured using a colorimetric aluminum chloride assay [26].

High-performance liquid chromatography (HPLC) analysis

30 mg dry extracts were dissolved in 5 mL methanol (6 mg/mL) to make the sample solution. Vortex was used to homogenize the dissolution and ensure easy dissolution. Standards were prepared at a 500 µg/mL concentration for stock solution. A Waters Spherisorb C18 column (25 cm 4.6 mm, 5 m) was utilized for measurement. The gradient system delivered the mobile phase, which was 0.01% formic acid (A) and acetonitrile (B), at a 1 mL/min flow rate and maintained at 40 °C. The proportion of B was increased from 10% to 30% over 30 minutes, then returned to the initial conditions in 5 minutes. Measurements were carried out at a wavelength of 300 nm, because of obtained the best results in all samples.

Three injections of each of the five distinct standard concentrations (10, 25, 50, 100 and 200 mg/mL) were made. A calibration curve for quantification was created for each standard. Accuracy, precision, limit of detection (LOD), limit of quantitation (LOQ), and recovery values were computed for method validation [27,28]. It was determined using intra-day and inter-

day variance for precision assay. On the same day, triple injections of all standard solutions in three different concentrations were evaluated as precision of intra-day. The method used for intra-day precision was repeated on different days for inter-day precision, and differences were expressed by RSD. Ten injections of standards were done to analyze the LOD and LOQ values and the signal/noise ratio was determined. LOD, signal/noise value is 3:1, LOQ signal/ noise value is 10:1. Three different known concentrations of the standard were added to the sample for the recovery analysis, and the recovery percentage was computed.

For the robustness investigation, minor changes to the flow rate, column temperature, mobile phase, and wavelength were made and their effects were investigated.

Antioxidant Activity

DPPH• Radical Scavenging Activity

The method described by Hatano et al. (1989) was adapted and used to determine the extracts' DPPH radical scavenging properties [29]. In 96-well plates, 100 µL of extract solutions at various concentrations were dispersed, followed by 100 µL of DPPH (0.1 mM, in ethanol) solution. As a reference antioxidant, BHT (Butylated Hydroxytoluene) was utilized. The absorbance at 517 nm was recorded after 30 minutes in the dark at 37 °C to quantify the radical scavenging effect. The experiments were carried out three times. The percentage inhibition was calculated using Eq. 1. Non-linear regression curves were used to calculate IC50 values (Sigma Plot 2001 version 7.0, SPSS Inc., Chicago IL). (Sigma Plot 2001 version 7.0, SPSS Inc., Chicago IL).

$$\% \text{ Inhibition} = [(\text{Absorbance control} - \text{Absorbance sample}) / (\text{Absorbance control})] \times 100 \quad (1)$$

$ABTS^{\bullet+}$ Radical Scavenging Activity

By maintaining an aqueous solution of ABTS (7 mM) and potassium persulfate ($K_2S_2O_8$) (2.45 mM, final concentration) in the dark for 12-16 hours, an $ABTS^+$ radical was generated, and its absorbance at 734 nm was adjusted to be 0.700 (±0.020). Extracts were made in two concentrations (1 and 2 mg/mL). As a control antioxidant, BHT was utilized. The produced radical solution and extract were combined in an amount of 990 µL and 10 µL respectively. The reaction kinetics were measured at 734 nm once every minute for 30 minutes [30]. The percentages of inhibition examined versus concentration were found to be equal to Trolox (TEAC).

Iron (II) Chelate Activity

The extract solution was combined with 100 µL of 2.0 mM aqueous $FeCl_2$ and 900 µL of methanol in a volume of 200 µL. After five minutes, the reaction was accelerated by 400 µL of 5.0 mM ferrozine solution, and the absorbance at 562 nm was measured after ten minutes. Na_2EDTA was utilized as a control and the percentage inhibition of extracts was analyzed. The percentage inhibition was calculated using Eq. 1. Non-linear regression curves were used to calculate EC50 values (Sigma Plot 2001 version 7.0, SPSS Inc., Chicago IL). (Sigma Plot 2001 version 7.0, SPSS Inc., Chicago IL). The average of three parallel experiments was used to calculate the results [31].

Acetylcholinesterase Enzyme Inhibition Activity

With minor modifications, Ellman's method was employed to examine the extracts' ability to inhibit acetylcholinesterase (AChE) [32]. The 96-well plates were loaded with a sample (25µL), buffer (50 µL), and AChE solution (25 µL at 0.22 U/mL). The plates were then incubated for 15 minutes at 25 °C. Following that, 25 µL of ATCI substrate and 125 µL of DTNB (3.0 mM, 5,5-dithiol-bis-(2-nitrobenzoic acid)) were added. A microplate reader was used to read the mixture at 412 nm after it had been kept at 25 °C for 15 minutes. As a positive control, galantamine solution was prepared at a concentration of 1 mg/mL. A blank control was also created by blending the sample solution with all of the other solutions.

Cytotoxic Activity

The American Type Culture Collection provided the HeLa (CCL-2TM cervical cancer) and Hep G2 (HB-8065TM hepatocellular carcinoma) cell lines. The cells were cultured in RPMI and DMEM, respectively, with 1% combined antibiotics (penicillin and streptomycin) and 10% fetal bovine serum at 37 ºC and 5% CO_2.

HeLa and Hep G2 cells were sown at a density of $1x10^4$ cells/mL 100 (100 µL each well) in a 96-well plate and separated into three groups: blank, control, and extracts (3.9; 7.81; 15.6; 31.25; 62.5; 125; 250; 500, and 1000 µg/L). After 24 hours of incubation, cells were treated with 100 µL of vehicle or samples for 24 hours. The MTT 1-(4,5-Dimethylthiazol-2-yl)-3,5-diphenyl formazan) reagent (stock: 5 mg/mL in PBS) was then applied to each well and incubated for 4 hours at 37 °C. Each well received 100 µL of DMSO to dissolve the formazan crystals produced by MTT. After 10 minutes, each well was examined using a microplate reader with a 540 nm wavelength [33].

Statistical Analysis

For pairwise comparison tests, the Dunnett and Tukey tests were used at the p <0.05 level using the SPSS Version 11.0 statistic software package.

REFERENCES

1. J. Michel; N.Z. Abd Rani; K. Husain; *Front. Pharmacol.,* **2020**, *5(11)*, 852.
2. N.C.C. Silva; A. Fernandes Júnior; *J. Venom. Anim. Toxins Incl. Trop. Dis*., **2010**, *16*, 402-413.
3. F. Alizadeh; A. Khodavandi; F.S. Faraji; *J. Herb. Med. Pharmacol.,* **2017**, *6(2),* 62-68.
4. L. Barros; A.M. Carvalho; I.C.Ferreira; *Food Chem. Toxicol.,* **2010**, *48(6)*, 1466-1472.
5. G.E.S. Batiha; S.T. Tene; J.O. Teibo; H. M. Shaheen; O.S. Oluwatoba; T.K.A. Teibo; M. Papadakis; *Arch. Pharmacol.,* **2023**, *396(3)*, 421-440.
6. A.G. Pirbalouti; S. Azizi; A. Koohpayeh; B. Hamedi; *Acta Pol Pharm.,* **2010**, *67(5)*, 511-516.
7. A. Ferreira; C. Proença; M.L.M. Serralheiro; M.E.M. Araujo; *J. Ethnopharmacol.* **2006**, *108(1)*, 31-37.
8. M. Dellagreca; F. Cutillo; B.D. Abrosc; A. Fiorentino; S. Pacifico; A. Zarrelli; *Nat. Prod. Commun.,* **2009**, *4(7)*, 893-896.
9. H. Najafi; Z. Mohamadi Yarijani; S. Changizi-Ashtiyani; K. Mansouri; M. Modarresi; S.H. Madani; B. Bastani; *Plos One,* **2017**, *12(11)*, E0188270.
10. K. A. Shadid; A.K. Shakya; R.R. Naik; N. Jaradat; H.S. Farah; N. Shalan; G.A. Oriquat; *J. Chem.,* **2021**, *2021*, 1-10.
11. A. Irfan; M. Imran; M. Khalid; M.S. Ullah; N. Khalid; M.A. Assiri; M. Shahzad; *J. Saudi Chem. Soc.,* **2021**, *25(8)*, 101277.
12. L.I. Terninko, U.E. Onishchenko; A. Frolova; *J. Pharm. Innov.* **2014**, *3(4)*, 46-50.
13. M. Fathi; M. Ghane; L. Pishkar; *J. Nat. Pharm. Prod.,* **2022**, *17(1)*, e114164.
14. S. M. Mousavi; S.A. Hashemi; G. Behbudi, S. Mazraedoost; N. Omidifar; A. Gholami; N. Pynadathu Rumjit; *J Evid Based Complementary Altern Med.,* **2021**, *2021*,1-13.
15. Committee On Herbal Medicinal Products (Hmpc) Assessment Report On Malva Sylvestris L. And/Or Malva Neglecta Wallr., Folium And Malva Sylvestris L., Flos, **2018**, Ema/Hmpc/749518/2016
16. N. Hasimi; A. Ertaş; E.V. Oral; H. Alkan; M. Boğa; M. A. Yilmaz; U. Kolak; Marmara *Pharm. J.,* **2017**, *21(3)*, 471-484.
17. G.M.S.Tomala; Y.I.G. Gaitén; R.D. Hernández; Z.D.C. Burbano; P.A. Gómez; N. D.J. Sarmiento; L.A.V. Prias; *J. Pharm. Pharmacogn. Res.,* **2022**, *10(3)*, 551-561.
18. M.C. Beghdad; C. Benammar; F. Bensalah; F. Z. Sabri; M. Belarbi; F. Chemat; *Afr. J. Biotechnol.,* **2014**, *13(3)*, 486-491.

19. N. Petkova; A. Popova; I. Alexieva; *J. Med. Plants*., **2019**, *7(1)*, 96-99.
20. F. Shahidi; (Ed.). Natural Antioxidants: Chemistry, Health Effects, And Applications. **1997**, The American Oil Chemists Society.
21. H. Pourrat; O. Texier; C. Barthomeuf; *Pharm. Acta Helv.* **1990**, *65(3)*, 93-96.
22. I. Orhan; B. Şener; M. I. Choudhary; A. Khalid; *J. Ethnopharmacol.,* **2004**, *91(1)*, 57-60.
23. A. Daniela; E. Pichichero; L. Canuti; R. Cicconi; D. Karou; G. D'arcangelo; A. Canini; *Caryologia,* **2007**, *60(1-2)*, 90-95.
24. H. M. Boutennoun; L. Boussoufe; M. Kebieche; K. Al-Qaoud; K. Madani; *Eur. J. Biol. Res.* **2019**, *9(1)*,10-19.
25. V. l. Singleton; R. Orthofer; R. M. Lamuela-Raventós; *Meth Enzymol.,* **1999**, *299*,152-178.
26. Z, Jia; M. Tang; J. Wu; *Food Chem*., **1999**, *64(4)*, 555-559.
27. Ich Expert Working Group Ich Guideline Q2(R1) Validation of Analytical Procedures: Text and Methodology. *BMJ* (Clinical Research Ed.), **2005**, 333 (7574).
28. D.Ç. Polat; M. Coskun; *Nat. Prod. Commun.* **2016**, *11*, 1665-1666.
29. T. Hatano; R. Edamatsu; M. Hiramatsu; A. Mori; Y. Fujita; T. Yasuhara; T. Okuda; *Chem. Pharm. Bull.,* **1989**, *37(8)*, 2016-2021.
30. R. Re; N. Pellegrini; A. Proteggente; A. Pannala; M. Yang; C. Rice-Evans; *Free Radic. Biol. Med.* **1999**, *26(9-10)*, 1231-1237.
31. G. Şeker Karatoprak; F. Göger; M.B. Yerer; *M. Pharm. Biol.,* **2017**, *55(1)*,1608-1618.
32. G.L. Ellman; K.D. Courtney; V. Andres Jr; R.M. Feather-Stone; *Biochem Pharmacol.,* **1961**, *7*, 88-95.
33. G. Ş. Karatoprak; Ç. Yücel; F. Göger; E. Sobarzo-Sánchez; E. Küpeli Akkol; *Antioxidants*, **2020**, *9*, 293.

STUDIA UBB CHEMIA, LXIX, 1, 2024 (p.85-105)
(RECOMMENDED CITATION)
DOI:10.24193/subbchem.2024.1.06

NOVEL TETRAZOLE AND 1,3,4-OXADIAZOLE DERIVATIVES SYNTHESIS, MOLECULAR DOCKING, ADME, POTENTIAL ACTIVATOR FOR RABBIT MUSCLE PYRUVATE KINASE

Mustafa Oğuzhan KAYA[a,*], Tuna DEMİRCİ[b], Selman KARİPÇİN[c], Oğuzhan ÖZDEMİR[d], Yeşim KAYA[a], Mustafa ARSLAN[c]

ABSTRACT. The activation of muscle pyruvate kinase (PK) increases the conversion of phosphoenolpyruvate (PEP) to pyruvate, which results in the production of ATP. This is critical for supplying the energy needed for muscle contraction. In this study, we synthesized 1,4-dihydropyridine/pyridine compounds bearing tetrazole and 1,3,4-oxadiazole groups by using Hantzsch method and characterized by FT-IR spectroscopy, elemental analysis, and ^{1}H and ^{13}C NMR and studied PK activation, ADME, and molecular docking. The studies revealed that all original synthesized compounds activated PK and AC_{50} (half-maximal activating concentration) values of the compounds were extremely effective (1.30 μM to 14.65 μM).

Keywords: *Rabbit Muscle Pyruvate Kinase, Tetrazole, 1,3,4-oxadiazole*

INTRODUCTION

Pyruvate kinase (PK, EC: 2.7.1.40) is recognised as a crucial mechanism in the metabolic pathway that generates energy for cells. There are four major PK isozymes of pyruvate kinase in mammals, and these are generally

[a] *Kocaeli University, Faculty of Arts and Science, Chemistry Department, Umuttepe Campus, Kocaeli, Turkey*
[b] *Duzce University, Scientific and Technological Research Laboratory, Konuralp Campus, Duzce, Turkey*
[c] *Sakarya University, Faculty of Science, Chemistry Department, Esentepe Campus, Serdivan, Sakarya, Turkey*
[d] *Batman University, Technical Sciences Vocational School, Veterinary Science Department, Raman Campus, Batman, Turkey*
* *Corresponding author: oguzhan.kaya@kocaeli.edu.tr*

associated with type M1, which is related to muscle, heart and brain, type L, which is related to liver, type R, which is related to red cells and type M2, which is related to early fetal tissues as well as most cancer cells. The PKM1 isoform is expressed in tissues of adults and eliminates the M2 isoform following birth. In comparison with M2, this isoform has powerful pyruvate kinase activity on its own as well. As is, action occurs without allosteric activation with D-fructose-1,6-bisphosphate (FBP). PK is known to generate ATP, the primary source of energy within the cell [1,2]. Accordingly, PK activation is known to be influenced (regulated) by several factors, including the availability of ATP, hormones, and metabolic intermediates. This contributes to balancing the energy demand in the body and when a high energy demand is needed, the PK enzyme is activated to meet this demand [3]. The activity of PK is generally known to be responsible for regulating the energy status of cells so that they can fulfil their functions and maintain cellular energy homeostasis [4]. From a health perspective, PK deficiency is a hereditary disorder caused by mutations in the gene encoding the enzyme. One of the best examples of this is hemolytic anaemia. Anaemia is known to cause a serious decrease in PK activity as it causes metabolic abnormalities [5]. It may induce symptoms that include weariness, jaundice, and muscle weakness, as well as muscle cramps, pain, and an increased risk of injury [6]. Furthermore, to how it functions in PK deficit, the drop-in PK activity with aging has been related with sarcopenia, a natural loss of muscular mass and strength [7]. Furthermore, some types of cancer may have altered PK activity which can affect their energy metabolism and contribute to their growth and survival. Finally, it is known to be affected in heart diseases such as heart failure, which can affect energy production in heart cells and contribute to disease progression [8]. Given these total conditions, changes in PK activity can have important effects on energy metabolism and contribute to the development and arrest of various diseases and conditions [9-11].

Tetrazoles are five-membered heterocyclic compounds containing four nitrogen atoms and one carbon atom in the ring structure and oxadiazoles are known as five-membered heterocyclic compounds containing one nitrogen atom, two oxygen atoms and two carbon atoms in the ring structure [12, 13]. Nitration of hydrazine [14-16], cyclisation of nitriles [17-19] and azidation of nitriles [19-22] are the most well-known methods used for the synthesis of tetrazoles. Oxadiazoles are synthesized by the reaction of nitriles with diazonium salt or isocyanate, reaction of carboxylic acids with hydrazine or hydrazides or reaction of amides/nitriles with isocyanate or diazonium salt [23-25]. Tetrazoles are known for their stability and high explosive potential and used in military applications [26]. They are also used in pharmaceuticals as active ingredients in some drugs [27], including anti-ulcer [28], anti-fungal [29]

and anti-tumour [30,31] drugs. Oxadiazoles are used in various applications in medicinal chemistry, including anti-proliferative [32], anti-tumour [33, 34], anti-thrombotic [35] and anti-microbial agents [36, 37], as well as the active ingredient in some herbicides [38] and in the synthesis of composite materials due to their high thermal stabilities and electrical conductivities [39].

Tetrazole and oxadiazole chemical compounds have been found to have a variety of effects on pyruvate kinase. Tetrazole was discovered to mobilize the enzyme under pressure, and the presence of K^+, Mg^{2+}, and ADP offered additional protection [40]. Oxadiazole, on the other hand, has been demonstrated to have a twofold impact on liver and erythrocyte pyruvate kinases, serving as an allosteric activator in the absence of fructose 1,6 bisphosphate and a competitive inhibitor in its presence [41]. These findings indicate that both substances may regulate pyruvate kinase activity, potentially influencing its role in glycolysis and other metabolic processes. In addition, investigations have revealed that tetrazole and oxadiazole can alter pyruvate kinase activity by binding to particular locations on the enzyme [42]. This highlights the possibility for tetrazole and oxadiazole to be used as key drugs in the research of the pyruvate kinase enzyme mechanism, modulating enzyme activity and regulation.

This study was designed on the basis of the good results of our previously synthesized ureido phenyl substituted 1,4-dihydropyridines on pyruvate kinase [43]. The 1,4-dihydropyridine/pyridine compounds with tetrazole and 1,3,4-oxadiazole groups were produced and described. *In vitro* studies demonstrated that these compounds have activatory effects on PK. The chemical features of the produced compounds were examined in computational molecular modeling. Additionally, drug-likeness score, bio-based RO5, docking of molecular structures with PK, and frontier molecular orbitals (ΔE, LUMO-HOMO gap) were calculated. The goal is to detect possible new medication substances that are active for the therapy of cancer and muscle-related sickness by activating the PK with synthetically produced substances.

RESULTS AND DISCUSSION

4-cyanophenyl-1,4-dihydropyridine compound was synthesized in a high yield by the Hantzsch method using 4-cyano benzaldehyde, ethyl acetoacetate, ammonium acetate and L-proline as a catalyst. Firstly, the tetrazole compounds were obtained with NaN_3-NH_4Cl in DMF at 140°C for overnight. Then, Oxadiazole substituted-1,4-dihydropyridine and 2,6- dimethylpyridine derivatives were successfully synthesized with reacting acid chlorides and tetrazole compounds by heating and shown in scheme 1.

In the ^{1}H NMR spectrum of the 4-cyanophenyl-1,4-dihydropyridine compound, the hydrogen atom attached to the nitrogen atom at the position 1 resonances as a singlet around 6.0 ppm due to the electronegativity of nitrogen, while the hydrogen atom at the position 4 resonances around 5.0 ppm. The protons of the aromatic ring containing nitrile group at the fourth position are seen as doublet at 7.4 and 7.6 ppm. In the IR spectra, nitrile stretching is observed in the 2230 cm^{-1}. The peak of the carbon atom of the nitrile was observed at 119 ppm in the ^{13}C NMR.

While obtaining tetrazole compound from 4-cyanophenyl-1,4-dihydropyridine compound, azide−nitrile 1,3-dipolar cycloaddition reaction was carried out. In the tetrazole compound, while the hydrogen atom attached to the nitrogen atom at the position 1 was seen as a singlet around 6.0 ppm in the ^{1}H NMR, nitrile stretching peak was disappeared in the 2230 cm^{-1} in IR and the peak of carbon atom of the nitrile was not seen any more at 119 ppm in the ^{13}C NMR. Hydrogen atom of the tetrazole ring was not observed in ^{1}H NMR due to its acidity. However, the chemical shifts of the doublets of the aromatic ring attached to the tetrazole ring shifted to the downfield due to the tetrazole ring and resonance as two doublets between 7.40 and 8.00 ppm. In addition, the specific stretching peak of the tetrazole ring in IR was observed between 2600-3000 cm^{-1}.

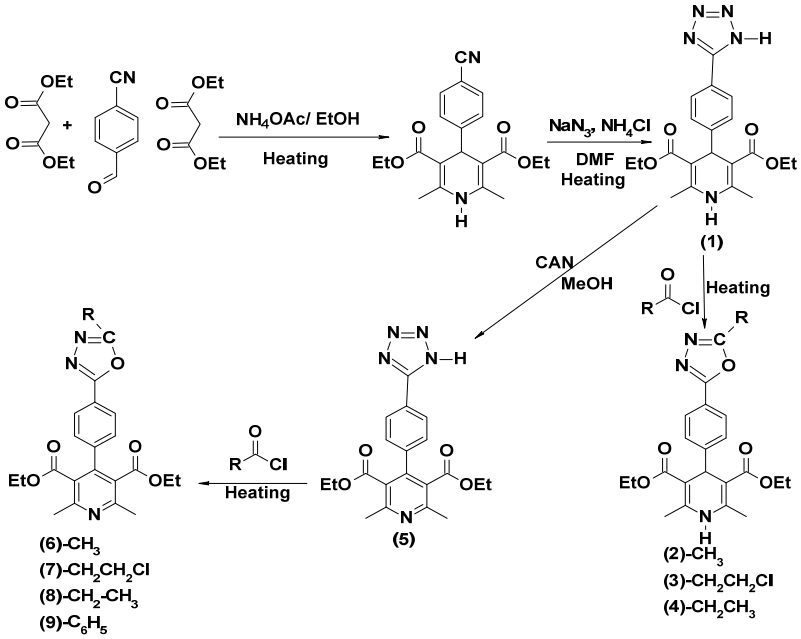

Scheme 1. Synthesis of tetrazole and 1,3,4-oxadiazole substituted 1,4-dihydropyridine

The compound (1) was oxidized with cerium (IV) ammonium nitrate (CAN) in methanol at room temperature to obtain an aromatized pyridine compound containing tetrazole. When the ^{1}H NMR values of the compound (5) was examined, the hydrogen atom attached to the nitrogen atom at the position 1 and hydrogen atoms at the position 4 were not seen any more due to aromatization of the 1,4-dihydropyridine ring. For the 1, 3, 4-oxadiazole compounds for example the compound (6), two different carbon peaks were observed in ^{13}C NMR. One is for the oxadiazole ring at around 165 ppm and the other is methyl at around 25 ppm.

Activation effect on rabbit muscle PK is demonstrated *in vitro*. The study was carried out on nine organic substances containing 1,4-dihydropyridine/pyridine compounds including tetrazole and oxadiazole, with AC_{50} values between 1.30 μM and 14.65 μM. The AC_{50} values for tetrazole and oxadiazole compounds containing 1,4-dihydropyridine/pyridine is given in Table 1.

Table 1. AC_{50} result of tetrazole and 1,3,4-oxadiazole compounds

Structure	AC_{50} (μM)	Structure	AC_{50} (μM)	Structure	AC_{50} (μM)
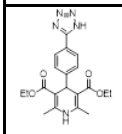 **1**	2.01	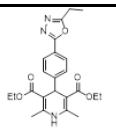 **4**	3.73	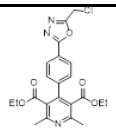 **7**	1.79
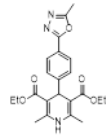 **2**	1.62	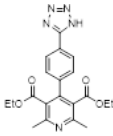 **5**	10.31	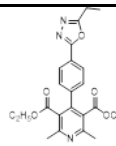 **8**	6.05
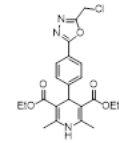 **3**	1.30	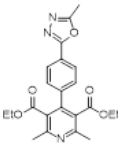 **6**	14.65	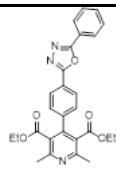 **9**	9.76

According to the results shown in Table 1, the activators used in this study exhibited the values in the range of 1.30 μM - 14.65 μM and were shown to exhibit better activation than N-(4-Chloro-3-fluorophenyl)-7-fluoro-2-oxo-1,2,3,4-tetrahydroquinoline-6-sulfonamide (90 μM) [44], DASA-10 (10 μM), TEPP-46 (79.5 μM) [45], which are the best-known activators in the literature.

However, although it was observed that 1,4 dihydropyridine derivatives containing 1, 3, 4-oxadiazole showed higher activation than 1,4-dihydropyrimidine, both types of compounds have good activation when the chlorine group is bound on the 1,3,4- oxadiazole structure ((7) = 1.79 μM and (3) = 1.30 μM). But, 1,3,4-oxadiazole with an ethyl group on it was 3,73 μM for (4) and 6,05 μM for compound (8), indicating that 1,4 dihydropyridine was almost twice active in the activation value. While the methyl (6) and benzyl (9) groups bearing 2,6-dimethylpyridine structure exhibited AC_{50} values of 14.65 μM and 9.76 μM respectively, the results in the form methyl (2) groups of 1, 4 dihydropyridine structures were 1.62 μM, approximately nine times lower AC_{50} values. All results are supported by the recent use in the literature of activators such as AMPK (α1β1γ1) [46], Nrf2 activator [47] and Caspase-3 [48] with oxadiazole compounds.

Pharmacokinetic properties prediction

ADME (Absorption, Distribution, Metabolism and Excretion) plays an important role in the evaluation of whether organic molecules can be active pharmaceutical ingredients. Because thanks to the results evaluated as a result of ADME studies, many organic molecules are eliminated before *in vitro* and *in vitro* studies. The tetrazole and oxadiazole compounds designed and synthesised by us were evaluated mutually via SwissADME, Molsoft and Molinspiration. These results were shown in Table 2. The evaluation was based on water solubility (MolLogS), octanol water partition (MolLogP), hydrogen bond acceptors (HBA), hydrogen bond donors (HBD), total surface area (TPSA), the blood-brain barrier (BBB) and drug-likeness score. All results are presented in Table 2. The molecular weight of tetrazole and 1,3,4-oxadiazole compounds were found to be 395.41 g/mol and 473.52 g/mol, which fulfils the RO5 rule of molecular weight less than 500. The solubility of the molecules in water was found to be between 2.46 and 5.18 moderate to poor. Drug similarity scores ranged from -0.14 to 0.34, indicating potential drug active ingredient. The BBB Score is computed utilizing statistical assessments of the number of aromatic rings, MWHBN (a combination of molecular weight, hydrogen bond donor, and hydrogen bond acceptor), heavy atoms, topological polar surface area, and pKa. The scores for each of the nine molecules varied between 1.58 to 2.61, signifying a medium value (6-High, 0-Low). [49].

The synthesized two-tetrazole and seven-oxadiazole compounds fulfilled all the pharmacokinetic properties required by the Lipinski rule [50]. Again, all molecules fulfil the requirements of Veber's rule, HBA number should be less than 10, polar surface area should be <140 and molecular weight should be <500 [51]. By fulfilling $1 \geq \log P \leq 6$ and $0 \geq tPSA \leq 132$ Å2,

all compounds satisfied the Egan rule. Drug similarity regulates for the Ghose rule should be demonstrated to be between 20 and 70 total atomic numbers, molecular weight 160 to 480, log P -0.4 to 5.6, and molar refraction 40 to 130. Complete the rule and compare it to all compounds [52, 53]. Furthermore, the Muegge rule was looked into, and it became apparent that all created ligands entirely fulfilled the rule. A comparison of all compounds is provided in Table 2.

Table 2. ADME result of synthesized compounds

Ligands	**1**	**2**	**3**	**4**	**5**	**6**	**7**	**8**	**9**
No. HBA	7	7	7	7	8	8	7	7	7
No. HBD	2	1	1	1	1	0	1	2	1
Num. rotatable bonds	8	8	9	9	8	8	9	8	9
MolLogP (mg/L)	2.46	2.78	3.38	3.56	3.03	3.35	3.96	2.46	5.18
MolLogS (mg/L)	-2.77	-3.11	-3.40	-3.52	-3.39	-3.56	-4.49	-2.77	-5.30
Molar Refractivity	108.4	113.5	118.3	118.3	104.9	110.0	118.3	108.4	118.3
TPSA(Å^2)	103.55	103.55	103.55	103.55	103.55	104.41	103.55	103.55	103.55
Mol. Vol. (A3)	418	445	456	462	384	411	422	418	463
Drug Likeness Score	0.23	0.25	0.17	0.28	-0.11	-0.13	-0.14	0.23	0.01
Synthetic accessibility	4.19	4.39	4.41	4.55	3.19	3.47	4.56	4.19	4.56
BBB Score	2.36	2.61	2.56	2.56	2.06	2.31	2.26	2.36	1.58
pKa of most Basic/Acidic group	-1.24 / 3.51	-1.24 / 4.97	-1.24 / 4.97	-1.24 / 4.98	-0.48 / 3.70	-0.48 / 24.80	-0.48 / 22.71	-1.24 / 3.51	-0.48 / 24.80

HOMO-LUMO levels

In molecular orbital theory, The HOMO-LUMO (Highest Occupied Molecular Orbital - Lowest Occupied Molecular Orbital) computation analyzes the electronic structure and reactivity of molecules. Table 3 illustrates the results of theoretical DFT calculations for nine novel compounds. Based on the research, a small HOMO-LUMO gap increases the molecule's susceptibility to chemical processes because transporting an electron from HOMO to LUMO needs less energy [54–57]. The larger the gap, the more energy needs to be transferred to move an electron to the LUMO, making the molecule less reactive. Compound (1) has the highest activity (E=4.01 Ev), whereas compound (5) has the lowest activity (E=5.13 Ev).

Examination of Table 3 reveals that the molecular LUMO-HOMO range (AE) is between 4.01 eV and 5.13 eV. Therefore, although the results seem to be very close to each other, the highest reactivity was observed in compound (1) and compound (9), while the lowest reaction reactivity was observed in compound (5). Furthermore, from the boundary orbital representation in Table 3, the molecules exhibited electrophilic attacks on atoms with HOMO orbitals (positive charges or atoms) and nucleophilic attacks on atoms with LUMO orbitals (negative charges or electrons).

Table 3. HOMO. LUMO. IP. EA and ΔE (LUMO-HOMO gap) data for synthesized compounds

Compound	HOMO eV	LUMO eV	ΔE (LUMO-HOMO gap)	Ionization potential (IP) eV	Electron affinity (EA) eV
1	-5.46	-1.45	4.01	-5.46	-1.45
2	-5.45	-1.25	4.20	-5.45	-1.25
3	-6.45	-2.00	4.46	-6.45	-2.00
4	-6.85	-2.01	4.84	-6.85	-2.01
5	-7.07	-1.94	5.13	-7.07	-1.94
6	-5.43	-1.23	4.20	-5.43	-1.23
7	-5.50	-1.29	4.21	-5.50	-1.29
8	-6.65	-1.82	4.83	-6.65	-1.82
9	-5.46	-1.43	4.04	-5.46	-1.43

Table 3 is also researched. The theoretical ionization potential (IP) using negative HOMO energies and possible electron affinity (EA) values using negative LUMO energies have been estimated (Koopman's theorem) [58].

Molecular docking and structure activity relationship (SAR) study

This molecular docking evaluation was performed on the PK (PDB:1PKN) via the Swiss Dock docking server [59, 60]. The evaluation of the docking results and the selection of the structure with the best value were performed via UCSF chimera [61]. Various insertion parameters such as fullfitness (FF), van der Waals energy (ΔGvdw), ΔGligsolvpol and Gibbs free energy (ΔG) were examined. The determined binding constants are in agreement with the experimental AC_{50} values, indicating a significant correlation between computational predictions and tetrazole, and 1,3,4-oxadiazole compounds experimental observations of the interaction, especially for the direct calculation of the AC_{50} for pyruvate kinase enzyme (Table 4).

Table 4. Molecular docking results of synthesized compounds

Compound	AC_{50} (μM)	ΔG (kcal/Mol)	Fullfitness (FF)	ΔGvdw (kcal/Mol)	ΔGligsolvpol (kcal/Mol)
1	2.01	-7.75	-3023.03	-41.55	-9.62
2	1.62	-7.45	-3000.90	-36.85	-9.77
3	1.30	-7.82	-2987.46	-59.89	-10.26
4	3.73	-7.27	-2950.90	-33.99	-8.65
5	10.31	-7.85	-2966.07	-60.19	-9.04
6	14.65	-7.26	-2950.90	-33.99	-10,43
7	1.79	-7.97	-2943.40	-53.07	-9.04
8	6.05	-7.88	-2951.21	-39.44	-9.62
9	9.76	-7.88	-2928.07	-39.81	-9.77

Details of the SAR study are given in Table 5, vdW (Van Der Waals) bonds are a critical step in the formation of a stable protein-ligand most active compound. Because vdW interactions are the most effective type of interaction in determining the shape and orientation of organic compounds within the active binding site of the protein [62]. This is the attractive factor that can attract organic substances towards the proteins and allow them to form a more stable complex [63]. In this study, we found that when tetrazole/1,3,4

oxadiazole molecules were near the active site of the PK (1PKN), the electron clouds of the two molecules (acceptor and donor) interacted to form partially positively and negatively charged regions. This formation occurred with a combination of tetrazole/1,3,4-oxadiazole molecules and a variety of residues such as methionine, arginine, proline, tyrosine, glycine and glutamic acid.

Conventional hydrogen bonds are established at molecular docking due to the difference in electronegativity between the nitrogen or oxygen atoms in the tetrazole/1,3,4 oxadiazole and the hydrogen atom of the amino acid residues [64]. These kinds of bonds generally have interaction weaker than covalent bonds, even though they are more powerful than vdW interactions [65]. In the context of protein-ligand interactions, conventional hydrogen bonding was occurred between the PK and the residues Glu A:383 and Glu A:331 for tetrazoles (two molecules) and Arg A:341 and Arg A:338 for oxadiazoles in the seven new molecules.

π-Alkyl and alkyl interactions appear in molecular docking through the attraction between π-electrons on aromatic groups in the structure of organic compounds and alkyl groups in the opposite structure. π-Alkyl and alkyl interactions are much weaker than both traditional hydrogen bonds and vdW interactions, but they are important for stabilization in protein-ligand interactions [66]. The interactions between PK and tetrazoles were observed between Arg A:341, Ala A:348, Pro A:339, Ile A:380, Leu A:379 and Leu A:179 residues, whereas for 1,3, 4-oxadiazoles, it was realized through various residues of the amino acids such as arginine, alanine, proline, isoleucine, leucine and tyrosine.

Amide-π stack interactions are based on the interaction between the π-electrons of tetrazole or 1,3,4-oxadiazole rings and the carbonyl group of amino acid residues [67]. In the current study, the π-donor hydrogen bond interaction between the compound (5) and PK was observed through the Glu A:331 residue, whereas for the compound (2) it was observed through the Arg A:341 residue. The π-donor hydrogen bond interaction between the compound (5) and (4) with PK was mediated by an aliphatic or aromatic CH in the structure of the novel molecule, with the Gln A:328 and Asn A:74 residues acting as hydrogen bond donors.

π-Sigma interactions result in molecular docking via the C-H-π or C=C-π interaction when the π-electron cloud of an aromatic ring interacts with the sigma bond of a nearby atom [68]. It is found between the Ser A:345 residue and the compound (6), the Gly A:344 residue and the compound (2), the (8) with Met A:376 residue of muscle PK.

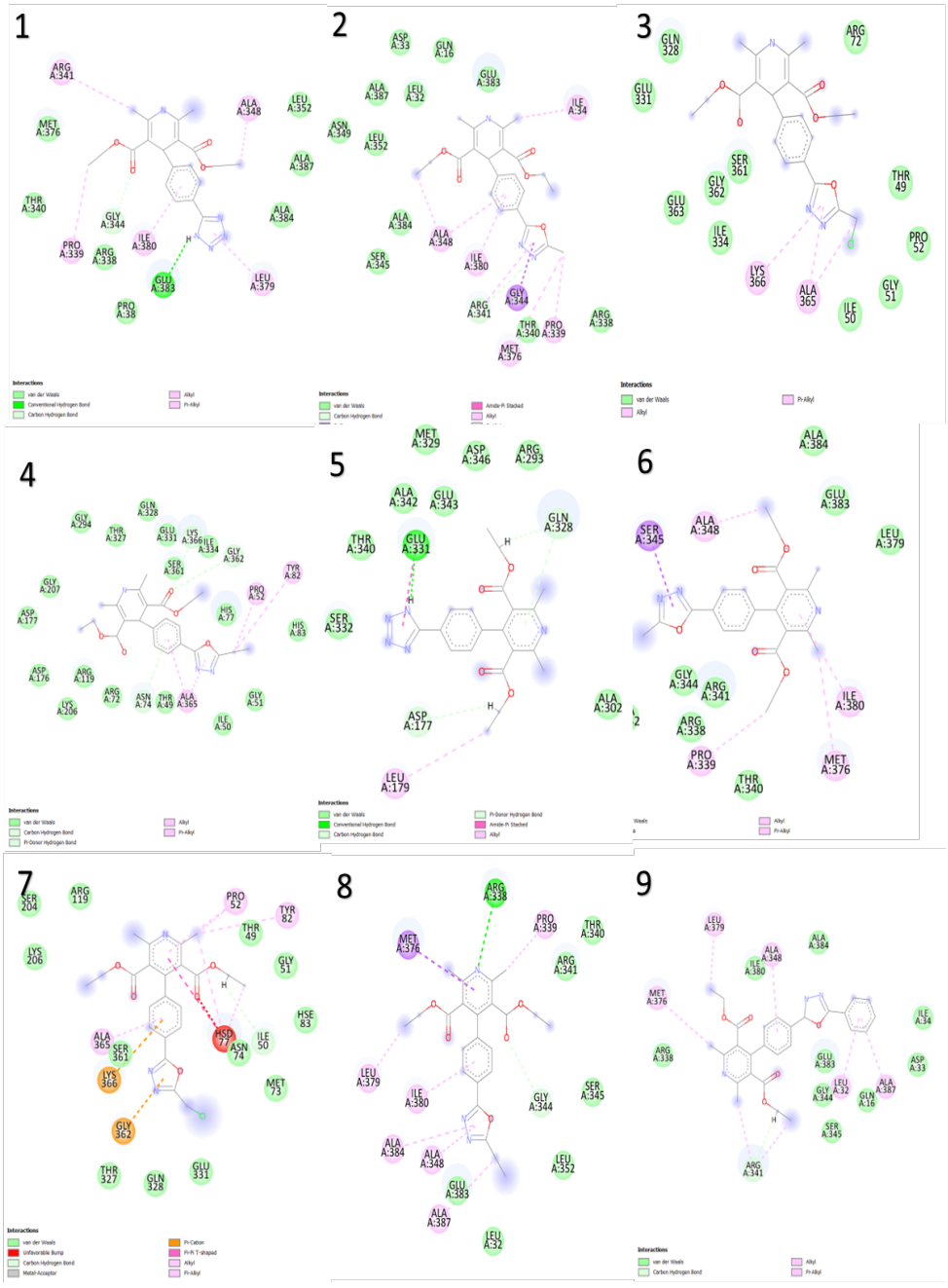

Figure 1. 2D interaction of compounds.

Table 5. Interaction results of synthesized compounds

	1	**2**	**3**	**4**	**5**	**6**	**7**	**8**	**9**
Van Der Waals	Met A:376, Thr A:340, Arg A:338, Pro A:38, Ala A:384, Ala A:387, Leu A:352	Ser A:345, Leu A:352, Asn A:349, Ala A:387, Leu A:32, Asp A:33,i Gln A:16, Glu A:383, Arg A:338	Gln A:328, Glu A:331, Ser A:361, Gly A:362, Glu A:363, İle A:334, Ile A:50, Gly A:51, Pra A:52, Thr A:49, Arg A:72	Asp A:176, Asp A:177, Gly A:207, Gly A:294, Thr A:327, Gln A:328, Glu A:331, Ile A:334, Ser A:361, His A:77, His A:83, Gly A:51, Ile A:50, Thr A:49,	Ser A:332, Thr A:340, Ala A:342, Met A:329, Glu A:343, Asp A:346, Arg A:293, Ala A:302	Ala A:342, Gly A:344, Arg A:341, Arg A:338, Ala A:384, Glu A:383, Leu A:379	Ser A:204, Arg A:119, Lys A:206, Thr A:327, Gln A:328, Ser A:361, Asn A:74, Met A:73, Hsd A:83, Gly A:51, Thr A:49	Glu A:383, Leu A:32, Leu A:352, Ser A: 345, Arg A:341, Thr A:340	Arg A:338, Ile A:380, Ala A:384, Ile A:34, Asp A:33, Glu A:383, Gly A:344, Gln A:16, Asp A:33, Ser A:345
Conven-tional Hydrogen band	Glu A:383	Arg A:341	-	-	Glu A:331	-	-	Arg A:338	-
π -Alkyl and Alkyl	Arg A:341, Ala A:348, Pro A:339, Ile A:380, Leu A:379	Ala A:348, Ile A:380, Pro A:339, Met A:376, Ile A:34	Lys A:366, Ala A:365	Ala A:365, Pro A:352, Tyr A:82	Leu A: 179	Ile A:380, Met A:376, Ala A:348,Pro A:339	Tyr A:82, Pro A:52, Ala A:365	Leu A:379, Ile A:380, Ala A:384, Ala A:387, Pro A:339	Ala A:387, Leu A:332, Ala A:348, Leu A:379, Met A:376
Amide -π stacked	-	Arg A:341	-	-	Glu A:331	-	-	-	-
π-Donor hydrogen	-	-	-	Asn A:74	Gln A:328	-	-	-	-
π-Sigma	-	Gly A:344	-	-	-	Ser A:345	-	Met A:376	-
Carbon Hydrogen	Gly A:344	-	-	Lys A:366, Gly A:362	Gln A:328	-	Ile A:50	Gly A:334	Arg A:341
π-Cation	-	-	-	-	-	-	Lys A:366, Gly A:362	-	-
π- π T Shaped	-	-	-	-	-	-	Hsd A: 77	-	-

CONCLUSIONS

This work was carried out to discuss the synthesis, characterization, computational analysis and *in vitro* activation study of novel nine compounds. The highest effect of the tetrazole and 1,3,4-oxadiazole substituted 1,4-dihydropyridine compounds were found to be 1.30 μM for the compound (3), while the compound (7) containing another chlorine functional group substituted 2,6-dimethylpyridine showed a very good result with 1.79 μM. Again, considering the whole study, it was observed that the AC50 values of 1,4- dihydropyridines were much higher than 2,6-dimethylpyridine. However, it was shown that all of the newly synthesized derivatives (1-9) have a very good activation potential against PK (1.30 μM-14.65 μM).

The molecular docking results of the nine new compounds synthesized for PK activation showed that the predicted ΔG values were close to each other (-7.27 and -7.97) and the ΔGvdw value was in the range of -39.33 to -60.19. The software Orca 5.0.2 was used to determine the HOMO-LUMO values, ionization potential, electron affinity and the most stable conformation of the compound using molecular mechanics and the B3LYP technique. The most reactive molecule was found to be compound (1) (ΔE=4.01eV).

The specific isoform of PK expressed in muscle tissue and is a key enzyme involved in the final step of glycolysis to generate energy in the form of ATP. So, it will be a pioneering result for many studies that muscle PK may also be involved in other cellular processes such as gene expression and cell proliferation.

EXPERIMENTAL SECTION

FT-IR spectra were collected using a SHIMADZU Prestige-21 (200 VCE) spectrometer via an ATR. The ^{1}H and ^{13}C NMR spectra were acquired with spectrometers set to 300 and 75 Hz on the VARIAN Infinity Plus, correspondingly. The chemical shifts ^{1}H and ^{13}C are referring to the internal deuterated solvent. A Thermo Scientific Flash 2000 instrument was used for the elemental analysis. Sigma Chem. Co. provided the materials used, which included ethyl acetoacetate, 4-cyanobenzaldehyde, ammonium acetate, and protein assay reagents. All of the chemicals used were of the analytical grade.

1,4-Dihydropyridine Synthesis; 4-Cyanobenzaldehyde (5.0 mmol), ethyl acetoacetate (10.0 mmol), ammonium acetate (5.0 mmol) and L-proline as a catalyst were dissolved in methanol (5 mL) and stirred for 6 hours at

80°C in a flask. At the end of the reaction, the reaction mixture was allowed to cool to room temperature and poured into 100.0 mL of ice-cold water and stirred. The precipitate was filtered off and dried. The product was purified by crystallisation from ethanol. The structural analysis of the product was confirmed by ^{1}H, ^{13}C NMR and FTIR spectra.

Tetrazole Synthesis: To the solution of nitrile compound (5.0 mmol) in Dimethylformamide (DMF, 5 mL), sodium azide (20.0 mmol) and ammonium chloride (20.0 mmol) were added and heated overnight at 140 °C in a flask. At the end of the reaction, the reaction mixture was allowed to cool to room temperature and poured into 100.0 mL of ice-cold water and stirred. HCl was used to adjust the pH of solution to 1. The precipitate was filtered off and dried. The product was purified by crystallisation from acetone/hexane. The structural analysis of the product was confirmed by ^{1}H, ^{13}C NMR and FTIR spectra.

Aromatization of 1,4-Dihydropyridine compounds: 1,4-dihydropyridine derivative (1 mmol) in 5.0 mL of water was dissolved. MeOH and NH_4SCN (1.20 mmol) were added to the solution and then stirred. Solution of 2.0 mmol CAN in MeOH (10 mL) was added to the reaction mixture by dropwise over 30 minutes using the dropping funnel and the mixture was stirred for two hours at room temperature. The reaction mixture was then poured into 100.0 mL of water and extracted with dichloromethane. The organic phase was washed three times with water and dried with sodium sulphate. Dichloromethane was removed using a rotary evaporator. The product was purified by crystallisation from acetone/hexane. The structural analysis of the product was confirmed by ^{1}H, ^{13}C NMR and FTIR spectra.

Oxadiazole Synthesis: Tetrazole derivatives (1.0 mmol) were dissolved in 2.0 mL of acyl chloride and heated overnight at 100°C under an inert atmosphere. The reaction mixture was then poured into 100 mL of water and extracted with dichloromethane. The organic phase was washed three times with water and dried with sodium sulphate. Dichloromethane was removed using a rotary evaporator. The product was purified by crystallisation from acetone/hexane. The structural analysis of the product was confirmed by ^{1}H, ^{13}C NMR and FTIR spectra.

Diethyl 4-(4-(1H-tetrazol-5-yl)phenyl)-2,6-dimethyl-1,4-dihydropyridine-3,5-dicarboxylate (1): M.p.100.8°C, ^{1}H NMR (300 MHz, CDCl3): 8.18 (2H, d, Ar-H), 7.62 (2H, d, Ar-H), 6.66 (1H, s NH), 4.99 (1H, s, CH), 4.00 (2x2H, q, CH_2), 2.39 (2x3H, s, CH_3), 1.47 (2x3H, t, CH_3). ^{13} CNMR (75 MHz): 166.7, 164.2, 164.4, 145.8, 139.0, 129.5, 128.5, 127.6, 121.6, 62.6, 22.7, 19.0. 11.74. FT-IR v (cm^{-1}): 3024.89 (Ar-H), 2939.52 (Aliphatic-H), 1722.43(C=O),

1656.77(C=O), 1500.62 (N=N). Chemical Formula: $C_{20}H_{23}N_5O_4$, Elemental Analysis (Calculated): C, 60.44; H, 5.83; N, 17.62; O, 16.10, (Found): C, 60.21; H, 5.94; N, 17.50.

Diethyl-2,6-dimethyl-4-(4-(5-methyl-1,3,4-oxadiazol-2-yl)phenyl)-1,4-dihydropyridine-3,5-dicarboxylate (2): M.p. 126.8°C, 1H NMR (300 MHz, $CDCl_3$): 7.81 (2H, d, Ar-H), 7.47 (2H, d, Ar-H), 6.82 (1H, s NH) , 5.09 (1H, s, CH), 4,05 (2x2H, q, CH_2), 2.75 (3H, s, CH_3), 2.61 (2x3H, s, CH_3), 1.33 (2x3H, t, CH_3), 13C NMR (75 MHz, $CDCl_3$): 167.7, 165.4, 163.7, 152.5, 145.3, 145.3, 129.2, 126.5, 121.5, 103.3, 60.0, 40.3, 19.4, 14.5, 11.3. FT-IR v (cm^{-1}): 3275,13 (N-H), 3097.89 (Ar-H), 2983.88 (Aliphatic-H), 1691.57 (C=O), 1651.07 (C=O), 1498.69 (N-N). Chemical Formula: $C_{22}H_{25}N_3O_5$. Elemental Analysis (Calculated): C, 64.22; H, 6.12; N, 10.21; O, 19.44, (Found): C, 64.56; H, 6.21; N, 10.04.

Diethyl-4-(4-(5-(chloromethyl)-1,3,4-oxadiazol-2-yl)phenyl)-2,6-dimethyl-1,4-dihydropy ridine-3,5-dicarboksilate (3): M.p. 87,8°C, ^{1}H NMR (300 MHz, $CDCl_3$): 7.92 (2H, d, Ar-H), 7.48 (2H, d, Ar-H), 6.02 (1H, s NH), 5.03 (1H, s, CH), 4.95 (2H, s, CH_2Cl), 4.06 (2x2H, q, CH2), 2.39 (2x3H, s, CH_3), 1.21 (2x3H, t, CH_3). ^{13}C NMR (75 MHz, $CDCl_3$): 167.5, 162.0, 152.5, 144.8, 139., 129.1, 127.5, 121.4, 103.6, 60.1, 46.1, 19.8, 14.5. FT-IR v (cm^{-1}): 3307,92 (N-H), 2980.09 (Aliphatic-H), 1691.15 (C=O), 1678.07 (C=O), 1485.19 (N-N), 1205.51 (C-O-C). Chemical Formula: $C_{22}H_{24}ClN_3O_5$, Elemental Analysis (Calculated): C, 59.26; H, 5.43; Cl, 7.95; N, 9.42; O, 17.94, (Found): C, 59.42; H, 5.51; N, 9.66.

Diethyl-4-(4-(5-ethyl-1,3,4-oxadiazol-2-yl)phenyl)-2,6-dimethyl-1,4-dihydropyridine-3,5-dicarboxylate (4): M.p. 99.6°C, ^{1}H NMR (300 MHz,$CDCl_3$): 9.22 (NH, s) , 7.89 (2H, d, Ar-H), 7.40 (2H, d, Ar-H), 6.02 (1H, s NH), 5.15 (1H, s, CH), 4.08 (2x2H, q, CH_2), 2.93 (2H, q, CH_2), 2.39 (2x3H, s, CH_3), 1.48 (3H, t, CH_3), 1.20 (6H, t, CH_3), ^{13}C NMR (75 MHz, $CDCl_3$): 167.8, 165.2, 152.4, 145.36, 129.0, 128.5, 121.6, 103.3, 60.6, 40.2, 21.2, 19.3, 14.9, 11.0. FT-IR v (cm^{-1}): 3304,05 (N-H), 2980.08 (Aliphatic-H), 1678.02 (C=O), 1651.07 (C=O), 1487.12 (N-N). Chemical Formula: $C_{23}H_{27}N_3O_5$, Elemental Analysis (Calculated): C, 64.93; H, 6.40; N, 9.88; O, 18.80, (Found): C, 65.02; H, 6.56; N, 9.69.

Diethyl-4-(4-(1H-tetrazol-5-yl)phenyl)-2,6-dimethylpyridine-3,5-dicarboxylate (5): M.p. 141.3°C, ^{1}H NMR (300 MHz, CDCl3): 8.21 (2H, d, Ar-H), 7.42 (2H, d, Ar-H), 4.05 (4H, q, CH_2), 2.69 (2x3H, s, CH_3), 0.90 (2x3H, t, CH_3), ^{13}C NMR(75 MHz, $CDCl_3$): 167.6, 158.0, 155.9, 145.9, 139.3, 129.3, 127.3, 125.4, 62.1, 22.7, 13.8. FT-IR v (cm^{-1}): 3096.78 (Ar-H), 2989.66 (Aliphatic-H), 2868.75, 1722.43 (C=O), 1556.20, Chemical Formula: $C_{20}H_{21}N_5O_4$, Elemental

Analysis (Calculated): C, 60.75; H, 5.35; N, 17.71; O, 16.19, (Found): C, 60.24; H, 5.41; N, 17.88.

Diethyl-2,6-dimethyl-4-(4-(5-methyl-1,3,4-oxadiazol-2-yl)phenyl) pyridine-3,5-dicarboxylate (6): M.p. 90.2°C, ^{1}H NMR (300 MHz, $CDCl_3$): 8.15 (2H, d, Ar-H), 7.52 (2H, d, Ar-H), 4.00 (4H, q, CH2), 2.69 (2x3H, s, CH_3), 2.65 (3H, s, CH_3), 0.90 (2x3H, t, CH_3), ^{13}C NMR(75 MHz, $CDCl_3$): 167.6, 164.5, 164.2, 155.9, 145.1, 140.1, 129.1, 127.1, 126.8, 124.9, 61.7, 23.0, 13.83, 11.29. FT-IR v (cm^{-1}): 3064.89 (Ar-H), 2980.66 (Aliphatic-H), 1720.22 (C=O), 1682.77 (C=O), 1556.55. Chemical Formula: $C_{22}H_{23}N_3O_5$, Elemental Analysis (Calculated): C, 64.54; H, 5.66; N, 10.26; O, 19.54, (Found): C, 64.25; H, 5.71; N, 10.42.

Diethyl-4-(4-(5-(chloromethyl)-1,3,4-oxadiazol-2-yl)phenyl)-2,6-dimethylpyridine-3,5-dicarboxylate (7): M.p. 81.5°C, ^{1}H NMR (300 MHz, $CDCl_3$): 8.11 (2H, d, Ar-H), 7.57 (2H, d, Ar-H), 4.89 (2H, s, CH_2), 4.01 (2x2H, q, CH_2), 2.59 (2x3H, s, CH_3), 1.00 (2x3H, t, CH_3). ^{13}C NMR (75 MHz, $CDCl_3$): 167.6, 165.6, 162.6, 156.0, 145.0, 140.0, 129.3, 127.5, 126.9, 126.7, 123.5, 61.7, 33.1, 23.1, 13.9. FT-IR v (cm-1): 3064.89 (Ar-H), 2980.66 (Aliphatic-H), 1720.52 (C=O), 1697.37 (C=O), 1556.66 (N-N). Chemical Formula: $C_{22}H_{22}ClN_3O_5$, Elemental Analysis (Calculated): C, 59.53; H, 5.00; Cl, 7.99; N, 9.47; O, 18.02, (Found): C, 59.88; H, 5.20; N, 9.65.

Diethyl-4-(4-(5-ethyl-1,3,4-oxadiazol-2-yl)phenyl)-2,6-dimethyl pyridine-3,5-dicarboxylate (8): M.p. 100.8°C, ^{1}H NMR (300 MHz, $CDCl_3$): 8.18 (2H, d, Ar-H), 7.62 (2H, d, Ar-H), 4.00 (2x2H, q, CH_2), 2.99 (2H, q, CH2), 2.39 (2x3H, s, CH_3), 1.47 (3H, t, CH_3), 1.24 (2x3H, t, CH3). ^{13}C NMR (75 MHz, $CDCl_3$): 166.7, 164.2, 164.4, 145.8, 139.0, 129.5, 128.5, 127.6, 121.6, 62.6, 22.7, 19.0, 11.7. FT-IR v (cm^{-1}): 3024.89 (N-H), 2939.52 (Aliphatic-H), 1722.43 (C=O), 1656.77 (C=O), 1500.62 (N-N). Chemical Formula: $C_{23}H_{25}N_3O_5$, Elemental Analysis (Calculated): C, 65.24; H, 5.95; N, 9.92; O, 18.89, (Found): C, 65.56; H, 6.11; N, 10.08.

Diethyl-2,6-dimethyl-4-(4-(5-phenyl-1,3,4-oxadiazol-2-yl)phenyl) pyridine-3,5-dicarboxylate (9): M.p. 130.9°C, ^{1}H NMR (300 MHz, $CDCl_3$): 8.11 (2H, d, Ar-H), 7.48 (2H, d, Ar-H), 7.32 (2H, d, Ar-H), 7.30 (2H, d, Ar-H), 7.25 (H, t, Ar-H), 4.05 (2x2H, q, CH_2), 2.39 (2x3H, s, CH_3), 1.37 (2x3H, t, CH_3). ^{13}C NMR (75 MHz, $CDCl_3$): 167.9, 165.0,164.4, 148.6, 139.6, 129.7, 129.1, 128.6, 128.1, 127.6, 127.3, 125.9, 119.5, 60.7, 19.3, 14.39, FT-IR v (cm^{-1}): 3038.89 (Ar-H), 2980.02 (Aliphatic-H), 1722.43 (C=O), 1548.84, 1487.12 (N-N). Chemical Formula: $C_{27}H_{25}N_3O_5$, Elemental Analysis (Calculated): C, 68.78; H, 5.34; N, 8.91; O, 16.97, (Found): C, 68.52; H, 5.18; N, 9.06.

HOMO-LUMO levels

The theoretical computations and geometrical optimization for the examined junctions were carried out using the open source DFT code, ORCA package version 5.0.2 [69], on an overclocked Intel®core i5-6400 CPU (2.71 GHz) with 8 GB RAM. Density functional theory B3LYP [70-73] is used as D3 zero [74] with dispersion correction and a damping function proposed by Becke and Johnson with a basis set (def-2-SVP) [75, 76]. Because there are no imaginary frequencies, the equilibrium geometry has a real minimum on the potential energy surface (PES).

PK Activity Assay

PK activity was assessed by measuring pyruvate subsequent generations, which was later measured by oxidization of NADH in the absence of excessive lactate dehydrogenase [2, 77]. The following reaction components (final concentrations) were added to a spectrophotometric cuvette (1 mL): 50 mM Tris-HCl buffer, pH 7.4; 100 mM KCl; 10 mM $MgCl_2$; 2 mM ADP; 1 mM PEP; 0.2 mM NAD-H; 8 un/mL LDH. The addition of PK preparation started the reaction (0.02–0.04 units). A decrease in optical density was registered at 340 nm on a spectrophotometer. Thermo Scientific Evolution 201 UV-Visible Spectrophotometer (Driesch, Germany). Activation effects of the novel compounds on enzyme activities were tested under *in vitro* conditions.

In vitro activation studies

Several amounts of these substances were added to the enzyme reaction mixture for the activation tests of nine compounds. Without a solution containing produced chemicals, PK activity was assumed to be 100%. Regression analysis was used in conjunction with the Microsoft Office Excel program to determine the activity percentage values of PK for various concentrations of each tetrazole and 1,3,4 oxadiazole. Table 1 contains the AC_{50} values that were determined from Lineweaver-Burk [78] graphs.

Molecular preparation of the structures

The 2D structures of the ligands were drawn using ACD chemsketch software. Iterative runs of Avogadro 1.9.0. through a shell script provided the primary 3D generation of the structures as mol2 format [79]. The shell script was provided by means of batch scripting in the Windows operating system. The 3D crystal structures for four PK isozymes, 1PKN, were retrieved from RCSB protein data bank [80]. Water molecules and the co-crystal ligands

were thereafter excluded from the structures and the PDBs were corrected in terms of missing atom types and application program interface (Discovery studio 2020 Client) was applied for generation and running of 2D interaction [81].

Pharmacokinetic properties prediction

Pharmacokinetic characteristics in computer-assisted drug design (CADD) are a significant component of drug discovery since they assist determine if a drug candidate should be tested in a biological system. PK characteristics aid in and explain the integrity & efficacy of compounds throughout the early phases of drug development. Therefore, the Swiss ADME, Molsoft and Molinspiration were used in the study to analyse the pharmacokinetic properties of the novel nine compounds [82-84].

ACKNOWLEDGMENTS

This work was supported by a SCIENTIFIC AND TECHNOLOGICAL RESEARCH INSTITUTION OF TURKEY (TUBİTAK) 2209 Project “Synthesis of Penta Substituted Pyridine Compounds Containing Alkyl/Aryl and Amino Oxadiazole in the 5-Position”.

REFERENCES

1. V. Gupta; R.N.K. Bamezai; *Protein Sci.,* **2010**, *19*, 2031-2044.
2. S. Strumilo; A. Tylicki; *Zh. Evol. Biokhim. Fiziol.,* **2015**, *51*,103-7.
3. M. Alquraishi; D.L. Puckett; D.S. Alani; A.S. Humidat; V.D. Frankel; D.R. Donohoe; J. Whelan; A. Bettaieb; *Free Radic. Biol. Med.,* **2019**, *143*,176-192.
4. D. Prasanta; J.Y. Son; A. Kundu; K. S. Kim; Y. Lee; K. Yoon; S. Yoon; B.M. Lee; K.T. Nam; and H.S. Kim. N. Kim; *Int. J. Mol. Sci.*, **2019**, *20*, 5622.
5. P. Bianchi; E. Fermo; B. Glader; Am. J. Hematol., **2019**, *94*,149-161.
6. S. Deane; B. E. Phillips; C. R. G. Willis; D.J. Wilkinson; K. Smith; N. Higashitani; J. P. Williams; N. J. Szewczyk; P.J. Atherton; A. Higashitani; T. Etheridge; *GeroScience*, **2023**, *45*, 1271-1287.
7. J. Y. Jan; D.Kim; N. D. Kim; *Biomedicines*; **2023**, *11* (6), 1635.
8. G.D. Lopaschuk; Q.G. Karwi; R. Tian; A.R. Wende; E.D. Abel; *Circ. Res.,* **2021**, *128*,1487-1513.
9. W.J. Israelsen; M.G.V. Heiden; *Semin. Cell. Dev. Biol.,* **2015**, *43*, 43-51.
10. J. Burns; G. Manda; *Int. J. Mol. Sci.,* **2017**, *18*, 2755-2783.
11. K. Zahra; T. Dey; Ashish, S.P. Mishra; U. Pandey; *Front. Oncol*., **2020**, *10*, 159.
12. C.X. Wei; M. Bian; G.H. Gong; *Molecules*, **2015**, *20*, 5528-5553.
13. C.G. Neochoritis; T. Zhao; A. Dömling; *Chem. Rev.*, **2019**, *119*, 1970-2042.
14. M. Benz; T.M. Klapötke; T. Lenz; J. Stierstorfer; *Chem. A Eur. J. l,* **2022**, *28*, 10.

15. M. Benz; T.M. Klapötke; J. Stierstorfer; M. Voggenreiter; *ACS Appl. Eng. Mat*., **2023**, *1*, 3-6.
16. M. Benz; T.M. Klapötke; J. Stierstorfer; *Chempluschem*., **2022**, *87*, 9.
17. R.Z. Zhang; R.X. Zhang; S. Wang; C. Xu; W. Guan; M. Wang; *Angew. Chem Int. Ed*., **2022**, *61*, 1.
18. D.R. Mishra; B.S. Panda; M.A. Ahemad; S. Nayak; S. Mohapatra; *ChemistrySelect*, **2022**, *7*, 46.
19. F. Celik; M. Arslan; M.O. Kaya; E. Yavuz; N. Gencer; O. Arslan; *Artif Cells Nanomed B.,* **2014**, *42*, 58-62.
20. S.J. Wittenberger, B.G. Donner; *J. Org. Chem.,* **1993**, *58*, 4139-4141.
21. S. L. Ramos; O.J. Cardoso; *Curr. Org. Chem.,* **2021**, *25*, 388-403.
22. M.A.E.A.A.A. El-Remaily; O.M. Elhady; *Appl Organomet Chem*., **2019**, *33*, 8.
23. M. Luczynski; A. Kudelko; *Appl. Sci*., **2022**, *12*, 3756.
24. J.J. Wang; W. Sun; W.D. Jia; M. Bian; L.J. Yu; *J. Enzyme. Inhib. Med. Chem.,* **2022**, *37*, 2304-2319.
25. K.D. Patel; S.M. Prajapati; S.N. Panchal; H.D. Patel; *Synth. Commun*., **2014**, *44*, 1859-1875.
26. D. Fischer; T.M. Klapötke; J. Stierstorfer; *Angew. Chem. Int. Edit.,* **2015**, *54*, 10299-10302.
27. K. Ferydoon; M. M. Seyed; B.D. Samaneh; A. Z. Mohammad; *Medicon Pharm. Sci*., **2022**, *2*, 04-10.
28. L. L. De Lócio; A. P. S. Do Nascimento; M.B. Santos; J. N.NS. Gomes; Y.M.S. De Medeiros; S.L. Albino; V.L. Dos Santos; R.O. De Moura; *Curr Pharm Des.,* **2022**, *28*, 1373-1388.
29. T. Ni; X. Chi; F. Xie; L. Li; H. Wu; Y. Hao; X. Wang; D. Zhang; Y. Jiang; *Eur. J. Med. Chem*., **2023**, *246*,115007.
30. S. DAS; A. Ghosh; P. Upadhyay; S. Sarker; M. Bhattacharjee;P. Gupta; A. Adhikary; *bioRxiv*, **2022**, 1-10.
31. T. Al-Warhi; A. A. Al-Karmalawy; A. A.; Elmaaty, M. A. Alshubramy; M. Abdel-Motaal; T.A. Majrashi; M. Asem; A. Nabil, W. M.Eldehna, M. Sharaky; *Enzyme. Inhib. Med. Chem*., **2023**, *38*,176-191.
32. B. Yadagiri; S. Gurrala; R. Bantu; L. Nagarapu; S. Polepalli; G. Srujana; N Jain; *Bioorg. Med. Chem. Lett*., **2015**, *25*, 2220-2224.
33. S. Bajaj; V. Asati; J. Singh; P.P. Roy; Eur. *J. Med. Chem*., **2015**, *97*, 124-141.
34. D. Kumar; S. Sundaree; E.O. Johnson; K. Shah; *Bioorg. Med. Chem. Lett*., **2009**, *19*, 4492-4494.
35. B. Vishwanathan; B.M. Gurupadayya; K. S. Venkata; *Bangladesh* J. *Pharmacol.,* **2016**, *11*, 67-74.
36. M. Bhatt; *Int. J. of Pharm. Sci. and Res*., **2010**, *1*, 172-179.
37. K. Rajeev; R. Meenakshi; M. S. Y. Prabodh; *Int. J. of Pharm. Innov.,* **2011**, *37*-55.
38. İ.H. Ciğerci; Pak. *J. Agric. Sci*., **2022**, *59*, 207-211.
39. M. G. Mohamed; M. M. Samy; T.H. Mansoure; S.U. Sharma; M.S. Tsai; J. H. Chen; J. T. Lee; S. W. Kuo; *ACS Appl. Energy Mater.,* **2022**, *5*, 3677-3688.
40. F. G. De Felice; V. C. Soares; S. T. Ferreira; *J. Biochem.,***1999**, *260*,163-169.

41. H. Buc; F. Demaugre; J.P. Leroux; *BBRC*, **1978**, *85*, 2, 774-779.
42. A. Veith; B. Moorthy; *Curr Opin Toxicol*., **2018**, *7*, 44-51.
43. M.O. Kaya; T. Demirci; Ü. Çalışır; O. Özdemir; Y. Kaya; M. Arslan. *Res Chem Intermed;* **2024**, *50*, 437-463.
44. M.J. Walsh; K.R. Brimacombe; H. Veith; J.M. Bougie; T. Daniel; W. Leister; L.C: Cantley; W.J. Israelsen; M.G. Vander Heiden; M. Shen; D.S. Auld; C.J. Thomas; M.B. Boxer. *Bioorg. Med. Chem. Lett.,* **2011**, *21*, 6322-6327.
45. D. Anastasiou; Y. Yu; W.J. Israelsen; J.K. Jiang; M.B. Boxer; B.S. Hong; W. Tempel; S. Dimov; M. Shen; A. Jha; H. Yang; K.R. Mattaini; C.M. Metallo; B.P. Fiske, K.D. Courtney; S. Malstrom; T.M. Khan; C. Kung; A.P. Skoumbourdis; H. Veith; Southall N; M.J Walsh; K.R. Brimacombe; W. Leister; S.Y. Lunt; Z.R. Johnson; K.E. Yen; K. Kunii; S.M. Davidson; H.R. Christofk; C.P. Austin; J. Inglese; M.H. Harris; J.M. Asara; G. Stephanopoulos; F.G: Salituro; S. Jin; L. Dang; D.S. Auld, H.W. Park, L.C. Cantley; C.J. Thomas; M.G. Vander Heiden. *Nat. Chem. Biol*., **2012**, *8*, 839-847.
46. Z. Xiao; Y. Peng; B. Zheng; Q. Chang; Y. Guo; Z. Chen; Q. Li; G. Hu; *Arch. Pharm.* (Weinheim), **2021**, *354*, 2000458.
47. L.L. Xu; Y.F. Wu; F. Yan; C.C. Li; Z. Dai; Q. D. You; Z. Y. Jiang; B. Di; *Free Radic. Biol. Med.,* **2019**, *134*, 288-303.
48. S. K. Kashaw; S. Agarwal; M. Mishra; S. Sau; A.K. Iyer; *Curr. Comput. Aided Drug Des.,* **2018**, *15*, 55-66.
49. M. Gupta; H. J. Lee; C. J. Barden; D. F. Weaver; *J. Med. Chem*., **2019**, *62*, 9824-9836.
50. C.A. Lipinski; F. Lombardo; B. W. Dominy; P.J. Feeney; *Adv. Drug. Deliv. Rev*., **2001**, *46*, 3-26.
51. D. F. Veber; S. R. Johnson; H.Y. Cheng; B. R. Smith; K. W. Ward;K. D. Kopple; *J. Med. Chem*., **2022**, *45*, 2615-2623.
52. A. K. Ghose; V. N. Viswanadhan; J. J. Wendoloski; *J. Comb. Chem*., **1999**, *1*, 55-68.
53. A. K. Ghose; T. Herbertz; R. L. Hudkins; B. D. Dorsey; J. P. Mallamo; *ACS Chem. Neurosci.,* **2012**, *3*, 50-68.
54. P. Y. Ayala; G. E. Scuseria; *J. Chem. Phys*., **1999**, *110*, 3660-3671.
55. A. Kumer; M. N. Sarker; S. Paul; *Int. J. of Chem. and Tech*., **2019**, *3*, 26-37.
56. S.Muthu; J. U. Maheswari; *Spectrochim*. *Acta A. Mol. Biomol. Spectrosc*., **2012**, *92*, 154-163.
57. L. Li; T. Cai; Z. Wang; Z. Zhou; Y. Geng; T. Sun; *Spectrochim. Acta A. Mol. Biomol. Spectrosc*., **2014**, *120*, 106-118.
58. T. Koopmans; *Physica*, **1934**, *1*, 104-113.
59. A. Grosdidier; V. Zoete; O. Michielin; *Nucleic Acids Res*., **2011**, *39*, 270-277.
60. A. Grosdidier; V. Zoete; O. Michielin; *J. Comput. Chem*., **2011**, *32*, 2149-2159.
61. E. F. Pettersen; T. D. Goddard; C. C. Huang; G. S. Couch; D. M. Greenblatt; E. C. Meng; T.E. Ferrin; *J. Comput. Chem.,* **2004**, *25*, 1605-1612.
62. S. Y. Huang; X. Zou; *Int. J. Mol. Sci*., **2010**, *11*, 3016-3034.
63. P. L. Kastritis; A. M. J. J. Bonvin; J. *R. Soc. Interface*, **2013**,*10*, 20120835.

64. X. Du; Y. Li; Y. L. Xia; S. M. Ai; J. Liang; P. Sang; X. L. Ji; S.Q. Liu; *Int. J. Mol. Sci.,* **2016**, *17*, 144.
65. L. Marchetti; D. Porciani; S. Mitola; C. Giacomelli; *Front. Mol. Biosci*., **2022**, 921677.
66. O.S. Wolfbeis; *Methods. Appl. Fluoresc*., **2021**, *9*, 042001.
67. M. Rahman; Z. Muhseen; M. Junaid; H. Zhang; *Curr. Protein. Pept. Sci.,* **2015**, *16*, 502-512.
68. D.A. Dougherty; *Science*, **1996**, *271*, 163-168.
69. F. Neese; Software update: The ORCA program system—Version 5.0, *WIREs Comp. Mol. Sci.,* **2022**, 12.
70. A.D. Becke; *J. Chem. Phys*., **1993**, *98*,1372-1377.
71. C. Lee; W. Yang; R.G. Parr; *Phys. Rev. B.,* **1988**, *37*, 785-789.
72. S.H. Vosko; L. Wilk; M. Nusair, *Can. J. Phys*., **1980**, *58*, 1200-1211.
73. P.J. Stephens; F.J. Devlin; C.F. Chabalowski; M.J. Frisch; *J. Phys Chem.,* **1994**, *98,* 11623-11627.
74. S. Grimme; J. Antony; S. Ehrlich; H. Krieg; *J. Chem. Phys*., **2010**, *132*, 154104.
75. S. Grimme; S. Ehrlich; L. Goerigk; *J. Comput. Chem*. **2011**, *32*, 1456-1465.
76. F. Weigend; R. Ahlrichs; *Phy. Chem*., **2005**, *7*, 3297.
77. H. R. Christofk; M. G. V. Heiden; N. Wu; J. M. Asara; L. C. Cantley; *Nature*, **2008**, *452*, 181-186.
78. H. Lineweaver; D. Burk; *J. Am. Chem. Soc*., **1934**, *56*, 658-666.
79. N. M. O'Boyle; M. Banck; C.A. James; C. Morley; T. Vandermeersch; G. R. Hutchison; *J. Cheminform.,* **2011**, *3*, 33.
80. T.M. Larsen; L.T. Laughlin; H.M. Holden; I. Rayment; G.H. Reed; *Biochemistry*, **1994**, *33*: 6301-6309
81. Dassault Systèmes BIOVIA, **2020** Discovery studio 2020 Client.
82. A. Daina; O. Michielin; V. Zoete; *Sci. Rep.,* **2017**, *7*, 42717.
83. M. Lobell; M. Hendrix; B. Hinzen; J. Keldenich; H. Meier; C. Schmeck; R. Schohe-Loop; T. Wunberg; A. Hillisch; *ChemMedChem.* **2006**, *1*, 1229-1236.
84. A. Daina; O. Michielin; V. Zoete; *J. Chem. Inf. Model*. **2014**, *54*, 3284-3

STUDIA UBB CHEMIA, LXIX, 1, 2024 (p. 107-120)
(RECOMMENDED CITATION)
DOI:10.24193/subbchem.2024.1.07

EVALUATION OF SOME BIOACTIVE NUTRACEUTICAL COMPOUNDS IN AGRO-INDUSTRIAL WASTE USED AS ANIMAL FEED ADDITIVES[1]

Mihaela VLASSA[a], Miuța FILIP[a,*], Ionelia ȚĂRANU[b], Daniela MARIN[b], Cătălin DRAGOMIR[b]

ABSTRACT. Some parts of agro-wastes (pomace meal) are used for animal food containing variability in composition (proteins, dietary fibres, carbohydrates, polyphenols, minerals). Paper aim was to evaluate some nutraceutical bioactive compounds from pomace meal for use as animal feed additives. Studied meals are pomace obtained from solid remains of grapes and sea buckthorn after juice pressing, as well as flaxseed and rapeseed after oil pressing. HPLC methods were used to determine some carbohydrates (glucose, fructose, sucrose, maltose), organic acids (oxalic, citric, tartaric, malic), flavonoids (catechin, epicatechin, rutin, quercetin, luteolin) and phenolic acids (gallic, vanillic, caffeic, *p*-coumaric, ferulic). The content of total polyphenolic compounds and the antioxidant activity (DPPH and ABTS assays) of the pomace meals were evaluated by spectrophotometry. The results obtained show that the carbohydrates quantities (mg/100 g) in pomace meals were between 2943.31 (grapeseed) and 3210.11 (rapeseed). Sea buckthorn contains the most important amount of total organic acids of 8078.89 mg/100 g. Also, the highest quantities (mg/100 g) of total polyphenolic compounds were found in grapeseed (10789) and flaxseed (8537), respectively. These findings indicate a good source of carbohydrates, organic acids and polyphenols (phenolic acids and flavonoids) therefore these meals can be used as animal feed additives.

Keywords: *bioactive compounds, animal feed additives, HPLC, total phenolic compounds, antioxidant activity*

---

[1] *Presented at "The 27th International Symposium on Separation Sciences", 24-27 September 2023, Cluj-Napoca, Romania (ISSS 2023)*

[a] *Babeș-Bolyai University, Raluca Ripan Institute for Research in Chemistry, 30 Fântânele Street, 400294 Cluj-Napoca, Romania*

[b] *National Institute for Research and Development for Biology and Animal Nutrition, 1 Calea București Street, Baloteşti, Ilfov 077015, Romania*

* *Corresponding author: miuta.filip@ubbcluj.ro*

INTRODUCTION

Fruit wastes cause a huge economic impact to environmental and the reduction and recycling of these waste need urgent attention since it would enhance food security, reduce the environmental footprint of food production chain, decrease waste management costs and open opportunities for production of novel products including animal feed [1].

To meet the high demand for animal feed, the efficient use of available feed resources, the enlargement of the feed resource base, and the search for new animal feed resources, particularly those not competing with human food, are pivotal for sustainable development of the livestock sector [2].

Some fruit wastes (apple, apricot, banana, citrus and raspberry) and by-products were used as animal feed and were evaluated by the nutritional value, conservation methods, feeding management and guidance on the levels at which these unconventional feed resources can be used in the diets of farm animal species [3]. Grape pomace contains up to 15% sugars, 0.9% phenolics and pigments (red grape pomace), 5.0–7.5% tartrates, 30–40% fibres, 9–12% crude proteins. The feed efficiency and growth rate of pigs declined with the increase in the level of dried, ground winery pomace, 10–15% level of incorporation in the diet [3, 4].

Sea buckthorn pomace as a coproduct of juice processing from the fleshy tissue of berries, contains many valuable vitamins, tocopherols, flavonoids, special fatty acids, and abundant amino acids [5, 6]. Sea-buckthorn flavonoids are beneficial for growth performance, rumen fermentation, and serum antioxidant activity in lambs and could be used as a natural feed additive in lamb production [7].

After extraction of oil from flaxseed, the by-product obtained, the flaxseed meal, still has good nutritional value. Flaxseed meal is rich in proteins, α-linolenic acid, dietary fibres, flaxseed gum, and other bioactive substances. Like many other feed ingredients, flaxseed meal has many excellent functions and can be used as a high-quality non-conventional protein feed for livestock and poultry [8–10].

Rapeseed meal was generated as a side stream of rapeseed oil production. It is commonly used as feed due to its high nutritional value. Rapeseed meal contains approximately 40% of proteins with balanced amino acid composition, phenolic compounds, fibres and minerals such as calcium, magnesium, zinc, and copper, a number of vitamins, tocopherols, B vitamins, and choline [11]. The effects of fermentation on individual polyphenolic compounds, carbohydrates, organic acids, fatty acids and minerals were evaluated on the fermented rapeseed meal [12]. Rapeseed meal could be supplemented up to 9% in growing-finishing pig diets without any detrimental effect on growth performance [13]. At the same time, the fermentation of rapeseed meal is an

effective way to reduce anti-nutrients [12,14] and to increase the level of lactic acid in the diet. It also stimulates the immune system, which improves piglet health, reducing the severity of diarrhoea and mortality [15].

Therefore, the aim of this study was to assess some nutraceutical bioactive compounds in pomace meal for use as additives in animal feed. Four types of pomaces such as grape seeds, sea buckthorn, flaxseed and rapeseed were evaluated regarding the content of some individual carbohydrates, organic acids, flavonoids and phenolic acids, as well as the total polyphenolic compounds (polyphenols). The antioxidant activity was also investigated.

RESULTS AND DISCUSSION

The use of natural products as food supplements has received increasing attention in recent years [1, 12, 16] due to their rich content in bioactive nutraceutical compounds.

HPLC of carbohydrates in pomace meals

The residual carbohydrates that remain in the pomace after the disintegration and pressing of grapes, are mainly water soluble. The content of the carbohydrates (glucose, fructose, sucrose and maltose) in pomace meals is shown in Figure 1.

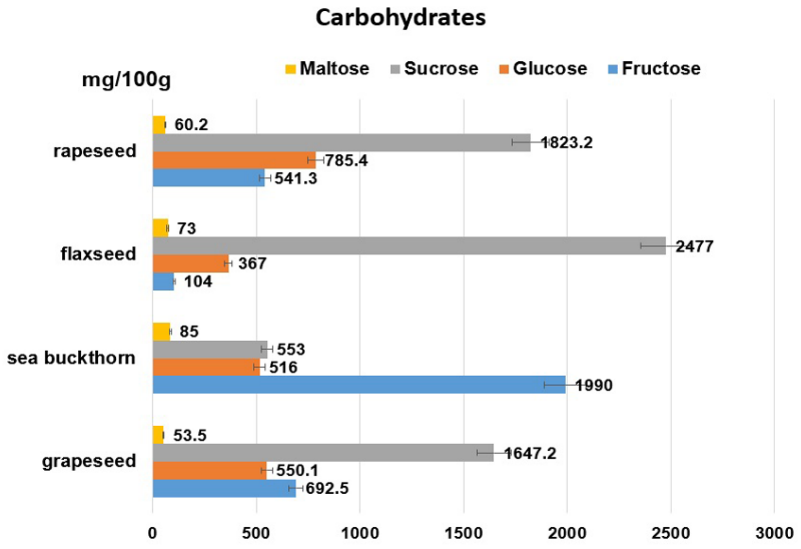

Figure 1. Concentrations of soluble carbohydrates (Mean ± SD) in the studied pomace meals

Thus, sucrose was found in the highest amount (mg/100 g meal) in 3 of the studied pomace meals: flaxseed (2477), rapeseed (1823.2) and grape seed (1647.2). The most important glucose amount of 785.4 mg/100 g was found in rapeseed meal while that of fructose of 1990 mg/100 g in sea buckthorn. In all studied pomace meals, maltose was found in the smallest amounts between 53.5 and 85 mg/100 g.

The total amount of carbohydrates in the studied meal samples (mg/100 g) were of 3210.1 for rapeseed meal, 3144 for sea buckthorn meal, 3021 for flaxseed meal, and 2943 for grapeseed meal, respectively.

Our results are in agreement with those reported in the references [12, 17, 18] for different pomace samples.

HPLC of organic acids in pomace meals

Figure 2 shows the content of organic acids found in the studied meals.

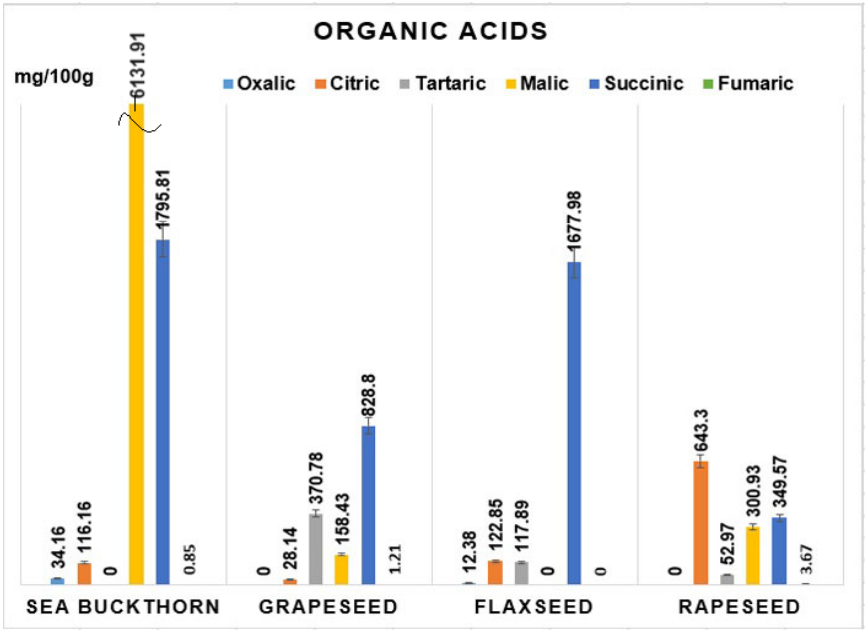

Figure 2. Concentrations of organic acids (Mean ± SD) in the studied pomace meals

The obtained results show that the largest content of organic acids was present in sea buckthorn meal, that also contains a highest amount of malic and succinic acids of 6131.91 and 1795.81 mg/100 g, respectively.

Also, the important amounts (mg/100 g) of succinic acid were found in grapeseed (828.8) and flaxseed (1677.98) meals, respectively.

Thus, the amount of total organic acids (mg/100 g) found in meal samples were as follows: 8078.89 in sea buckthorn, 1387.36 in grapeseed, 1931.1 in flaxseed, and 1350.44 in rapeseed, respectively.

Organic acids and their salts have been established as potential alternatives to prophylactic use of in-feed antibiotics in order to improve the performance of weaned piglets, fattening pigs and reproductive sows. Organic acids may also influence gut morphology, increasing the absorption capacity of proteins, energy and/or mineral [19].

HPLC of flavonoids and phenolic acids in pomace meals

The amounts of some individual flavonoids and phenolic acids present in studied pomace meals, namely grapeseed, sea buckthorn, and flaxseed and rapeseed are shown in Figure 3.

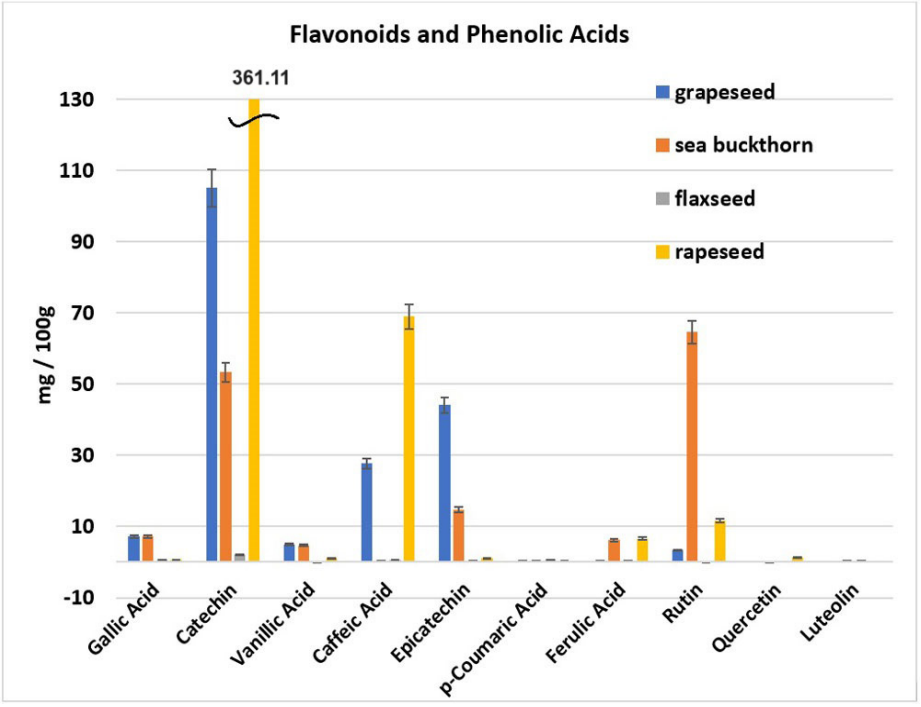

Figure 3. Concentrations (Mean ± SD) of individual phenolic compounds (flavonoids and phenolic acids) in the studied pomace meals (grapeseed, sea buckthorn, flaxseed and rapeseed.

In Figure 3 it can be observed that the pomace meals with the highest amount of catechin (mg/100 g) were rapeseed (361.11 mg), grapeseed (105.06 mg), and sea buckthorn (53.27 mg). Also, significant amounts of caffeic acid (mg/100 g) were found in grapeseed (27.67 mg) and rapeseed (68.01 mg) meals, as well as epicatechin in grapeseed (44.15 mg) and sea buckthorn (14.74 mg) meals. Moreover, the highest content of rutin was present in sea buckthorn meal (64.56 mg).

The total of individual phenolic compounds in the studied meals (mg/100 g meal) were 192.96 mg for grapeseed, 151.91 mg for sea buckthorn, 4.82 mg for flaxseed and 453.03 mg for rapeseed, respectively.

For comparison, similar results on the concentrations of caffeic, ferulic, and *p*-coumaric acids in different rapeseed varieties were reported by other authors [4, 20]. Grapeseed is also appreciated due to their content of phenolic compounds such as gallic acid, catechin and epicatechin, and a wide variety of procyanidins (mainly condensed tannin) [16] and resveratrol [21].

In Figure 4, the concentration of some individual phenolic compounds (flavonoids and phenolic acids) was studied for the grapeseed and sea buckthorn mixture prepared under different ratios (from 3 to 27 parts from each of them) to see the influence of the mixture composition over the concentration of each phenolic compound.

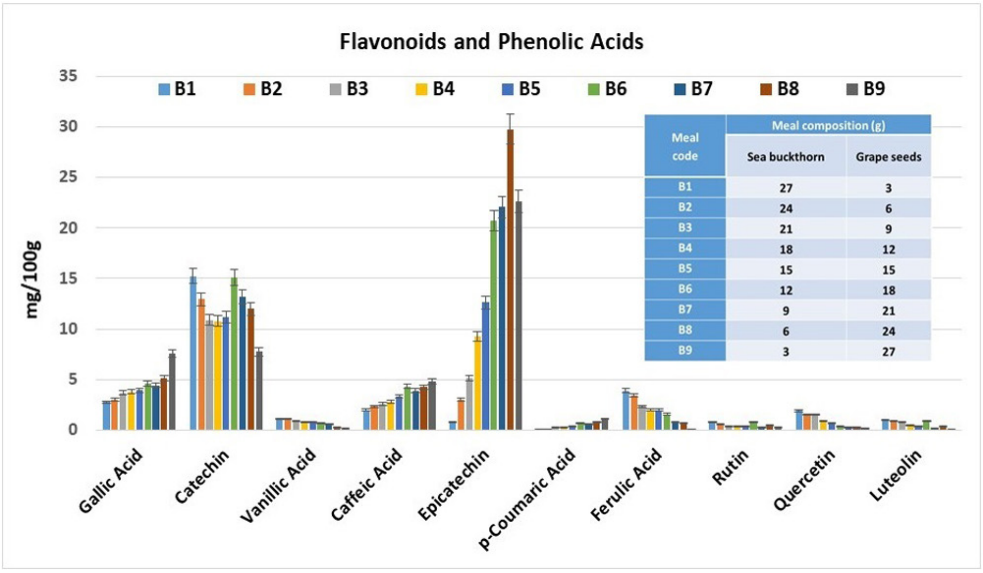

Figure 4. Concentrations (Mean ± SD) of individual phenolic compounds (flavonoids and phenolic acids) in meal samples containing mixtures of grapeseed and sea buckthorn in different ratios.

In Figure 4 it can be observed that with the increase in the amount of grapeseed in the studied meal samples, the amounts of some polyphenols increase as follows: gallic acid, caffeic acid, epicatechin, and p-coumaric acid. The B8 sample containing 6 parts of sea buckthorn and 24 parts of grapeseed represents the meal sample with the highest amount of epicatechin. It can be also seen that the majority polyphenols are represented by the flavonoids catechin and epicatechin. Catechin occurs in 8 meal samples (B1–B8) in amounts greater than 10 mg/100g, while epicatechin occurs in 5 meal samples (B5–B9) in amounts greater than 10 mg/100g, and in 4 meal samples (B6–B9) in amounts greater than 20 mg/100g. As for phenolic acids, they are represented by gallic and caffeic acids with amounts in all meal samples close to 5 mg/100g, except for sample B9 which presents gallic acid around 7 mg/100g.

Sea-buckthorn pulp and flaxseed residues are rich in phenolic fractions and aroma substances, thus providing high antioxidant and antimicrobial activity [22]. Sea buckthorn pomace contains dietary fibres that are bioactive and health promoting, but due to the lack of suitable handling and/or processing facilities, this pomace is often either used as animal feed or discarded [6]. Grapes from the common grapevine (*Vitis vinifera L.*) are grown worldwide and are common food sources of phenolic compounds, particularly flavonoids [23].

Literature data showed that by including 5% grapeseed cake in the diet of fattening-finishing pigs, a modulatory effect on antioxidative status was observed, as well as anti-inflammatory and hypocholesterolic properties without effect on pig performance [24].

Grape seed, whether whole, ground or after oil extraction, has been used in livestock feeds, mainly for rabbit, ruminants and piglets with a content of up to10% grapeseed meal in the feed [25, 26].

Total phenolic compounds and antioxidant activity

Total phenolic compound **(TPC)** and antioxidant activity of the studied pomace meals determined with DPPH and ABTS assays is shown in Table 1. TPC was determined spectrophotometrically at 760 nm with Folin-Ciocâlteu method and the results were expressed as mg GAE (gallic acid equivalent) / g dry weight (meal).

It is well known that polyphenolics can act as antioxidants due to their hydrogen atom and single electron donating capabilities. Velioglu et al. [27] reported in their study of several fruits and vegetables that there was a significant correlation among the total polyphenolic content and the antioxidant activity [27, 28].

TPC (mg GAE / g) was found in the studied pomace meals of 47.12 in sea buckthorn, 97.89 in grapeseed, 16.44 in flaxseed and 85.37 in rapeseed, respectively. Similar values of TPC were obtained by some authors [4, 18, 20].

The results of the antioxidant properties determined using DPPH and ABTS assays are expressed as mg TE (Trolox equivalent) / 100 g dry weight (meal).

Table 1. Total phenolic compounds and antioxidant activity (Mean ± SD) of pomace meals determined with DPPH and ABTS assays

Meal	**TPC*** mg GAE/ g	**DPPH****	**ABTS****
		mg TE/ 100 g	
sea buckthorn	47.12 ± 1.23	3925 ± 26.85	3018 ± 19.46
grapeseed	97.89 ± 6.89	7938 ± 21.21	8272 ± 26.70
flaxseed	16.44 ± 1.02	1887 ± 20.39	1872 ± 18.91
rapeseed	85.37 ± 3.85	5641 ± 18.97	6319 ± 29.20

*TPC – expressed by mg GAE (gallic acid equivalent) / g dry weight;
**DPPH and ABTS – expressed by mg TE (Trolox equivalent) / 100 g dry weight

The DPPH• radical scavenging activity ranged from 1887 to 7938 mg TE / 100 g. By using ABTS•+ assay, the antioxidant activity values were calculated between 1872 and 8272 mg TE / 100g. By both assays, the highest values of antioxidant activity were found for grapeseed and rapeseed meals.

The results of this investigation were, however, in agreement with other researches concerning the content of total phenolic compounds and antioxidant activity that were found in the studied pomace meals [4, 12, 18, 20, 29–31].

CONCLUSIONS

This study presents a modern approach regarding the evaluation of some bioactive nutraceutical compounds from pomace meals for use as additives in animal feed. Thus, pomace meals such as grapeseed and sea buckthorn, flaxseed and rapeseed were investigated to determine their content in carbohydrates, organic acids, individual polyphenolic compounds and total polyphenolic compounds, as well as to evaluate the antioxidant activity (DPPH and ABTS tests).

Thus, the studied pomace meals possess an important amount of carbohydrates with values between 2943.3 mg/100 g for grapeseed and 3210.1 mg/100 g for rapeseed. The organic acids (mg/100g) were present in the highest amount in sea buckthorn (8078.89) and in smaller amounts in rapeseed (1350.44), in grapeseed of 1387.36 and in flaxseed of 1931.1, respectively. Also, the highest quantities of TPC (mg GAE / g) were found in grapeseed of 97.89 and in rapeseed of 85.37, respectively. The antioxidant activity is correlated with TPC content and shows important values for grapeseed and rapeseed meals.

In conclusion, these pomace meals are a good and promising source of nutritionally bioactive compounds and can be used as additives in animal feed.

EXPERIMENTAL SECTION

Chemicals and materials

Acetonitrile and methanol with of HPLC-grade, sulphuric acid p.a., formic acid p.a., and standards of organic acids (tartaric, citric, malic, succinic and oxalic) were purchased from Merck (Darmstadt, Germany). The standards of flavonoids (catechin, epicatechin, rutin, quercetin and luteolin), phenolic acids (gallic, vanillic, caffeic, p-coumaric, ferulic), and carbohydrates (glucose, fructose, sucrose, maltose) were purchased from Sigma-Aldrich Co. (St. Louis, MO, USA). Folin-Ciocâlteu reagent, 2,2′-diphenyl-1-picrylhydrazyl radical (DPPH, 95%) and 2,2'-azino-bis-(3-ethylbenzothiazoline-6-sulfonic acid) diammonium salt (ABTS, 98%) were purchased from Alpha Aesar – Thermo Fisher Scientific, Lab Chemicals (Kandel, Germany). 6-hydroxy-2,5,7,8-tetramethylchroman-2-carboxylic acid (Trolox, 98%) was purchased from TCI America (Portland, OR, USA).

Pomace meals samples

Pomace by-products: grapeseed, sea buckthorn, flaxseed and rapeseed from local producers were dried in an industrial automated forced hot air dryer (Blue Spark Systems SRL, Bucharest, Romania) at 60ºC. Then, the dried pomaces were finely ground (1 mm mesh) using an IKA M 20 Universal Mill (7.5 kW) (IKA-Werke GmbH & Co. KG, Staufen, Germany).

Extraction procedure

Extraction of flavonoids and phenolic compounds from the studied samples was performed in 80% methanol solution, while carbohydrates and

organic acids were extracted in ultrapure water (18.2 MΩ cm ionic purity at 25ºC) produced in the laboratory by means of a Simplicity system (Millipore; Bedford, MA, USA).

A quantity of 1 g sample with 10 mL of extraction solvent was well stirred, sonicated for 60 minutes at ultrasonic power 100% and 80 KHz ultrasonic frequency (Ultrasonic bath Sonorex, Bandelin, Germany), centrifuged at 4500 rpm for 20 minutes, and then the supernatant was filtered through a 0.45 µm PTFE syringe filter (Chromafil Xtra PTFE, 25 mm, 0.45 µm; Macherey-Nagel, Düren, Germany) and injected into HPLC equipment.

Equipment and method

The analyses were performed by high-performance liquid chromatography (HPLC) on a Jasco Chromatograph (Jasco Corporation, Tokyo, Japan) equipped with an ultraviolet-visible (UV/Vis) detector and a refractive index (RI) detector, and an injection valve with a 20 µL sample loop (Rheodyne, Thermo Scientific). The ChromPass software (Varian Jasco, Tokio, Japan) was used to control the HPLC system and to collect and process data.

Total phenolic compounds and antioxidant activity was determined spectrophotometrically using an UV-Vis Spectrophotometer Specord 205 (Analytik Jena, GMbH, Germany).

HPLC methods

HPLC-RI analysis of carbohydrates was adapted from [32]. Separation was carried out on a Kromasil-NH_2 column (5 µm; 250 × 4.6 mm) (Nouryon AB, Göteborg, Sweden), set at 25ºC and eluted with the acetonitrile–water (70:30, v/v) mobile phase at a flow rate of 1 mL/min.

HPLC quantification of organic acids was carried out by the method described in [33]. Separation was done on a CarboSep Coregel 87H3 column (300 × 7.8 mm) (Phenomenex, Aschaffenburg, Germany) at a column temperature of 35ºC, with a 0.005 M sulfuric acid solution as the mobile phase at a flow rate of 1 mL/min. UV detection was at 214 nm.

HPLC analysis of flavonoids and phenolic compounds was carried out by the HPLC method described in [34] using a Lichrosorb RP-C18 column (5 µm; 250 × 4.6 mm) (Merck, Darmstadt, Germany) at 22ºC column temperature, a flow rate of 1 mL/min and UV detection at 270 nm. Elution was done by gradient using as mobile phase methanol (A, HPLC-grade) and 0.1% formic acid solution according to the method: 0–10 min, linear gradient 10–25% A; 10–25 min, linear gradient 25–30% A; 25–50 min, linear gradient 35–50% A; 50–70 min, isocratic 50% A.

Also, the all HPLC determinations were made by triplicate.

Total Phenolic Compounds (TPC)

TPC was determined spectrophotometrically using the Folin-Ciocâlteu method, according to our previous adapted procedure [12]. Briefly, 0.4 mL of methanolic meal extract and 2 mL of Folin-Ciocâlteu reagent (dilution 1:1) were shaken for 3 min and then 1.6 mL of sodium carbonate solution (7.5%) was added and brought to 10 mL, using water. After 10 minutes at 50ºC, the solutions were cooled, and the absorbance was measured at 760 nm against a reagent blank (0.4 mL water + 2 mL of Folin-Ciocâlteu reagent + 1.6 mL sodium carbonate solution). The absorbance of standard samples of gallic acid (GAE) were recorded. The TPC of each meal extract was quantified as mg gallic acid equivalent per 1 g dry weight (meal) (mg GAE/g). All determinations were performed in triplicates.

Determination of Antioxidant Activity

To evaluate the antioxidant activity of the studied samples, two different chemical methods were applied, namely the DPPH (2,2′-diphenyl-1-picrylhydrazyl radical) and ABTS (2,2'-azinobis-(3-ethylbenzothiazoline-6-sulfonate) assays. All determinations were performed in triplicate.

DPPH• radical scavenging assay. Our adapted DPPH method [12] was used for the spectrophotometrically determination (517 nm) against methanol, as the blank of the antioxidant capacity of the studied samples. The free radical scavenging activity of the extracts was measured by absorbance (Abs) with respect to the effect of standard solutions of methanolic Trolox (0.02–0.1 µmol/mL) or pomace meal extracts. An aliquot of 0.5 mL of each Trolox solution (or extract) was added to 2 mL methanol and 0.5 mL DPPH solution. The control sample was prepared by mixing 2.5 mL methanol with 0.5 mL of DPPH solution. The effective concentrations (DPPH) were expressed in µmol Trolox/ 100 g dry weight. The scavenging activity of DPPH was calculated with Equation (1):

$$\text{DPPH scavenging activity } (\%) = \frac{(\text{Abs control} - \text{Abs sample})}{\text{Abs control}} * 100 \qquad (1)$$

where: Abs control is the absorbance of DPPH• radical in methanol; Abs sample is the absorbance of DPPH• radical solution mixed with sample extract/ standard.

ABTS•+ radical scavenging assay. The spectrophotometric determination of the antioxidant activity of meal samples by the ABTS method is based on the percentage inhibition of peroxidation of this radical. The reaction was carried out according to our previously adapted method [12]. The radical cation ABTS•+

was generated by the persulphate oxidation of ABTS. The working solution (ABTS solution of 7 mM and potassium persulphate solution of 2.45 mM, 1:1, v/v) were left to react for 17 hours at room temperature in the dark. This solution was then diluted with methanol to obtain an absorbance between 0.700 to 0.800 units at 734 nm. Pomace meal extracts (0.5 mL) were allowed to react with 2.5 mL of the fresh ABTS solution for 6 min. The ABTS scavenging activity of the extracts was measured taking into account the effect of the Trolox standard solutions (2.5–12.5 µg/mL), regarding the discolouring capacity of the blue-green colour of the ABTS solution. The percentage inhibition was calculated using Equation (2):

$$\text{ABTS} \bullet + \text{radical scavenging activity } (\%) = \frac{(\text{Abs control} - \text{Abs sample})}{\text{Abs control}} * 100 \quad (2)$$

where: Abs control is the absorbance of ABTS• + radical in methanol; Abs sample is the absorbance of ABTS• + radical solution mixed with sample extract/standard.

ACKNOWLEDGMENTS

This work was supported by the Romanian Ministry of Research and Innovation, CCCDI-UEFISCDI, project number PN-III-P1-1.2-PCCDI-2017-0473/, within the PNCDI III.

REFERENCES

1. S. Hussain; I. Jõudu; R. Bhat; *Sustain.* **2020**, *12*, doi:10.3390/su12135401.
2. B. Martínez-Inda; I. Esparza; J. A. Moler; N. Jiménez-Moreno; C.Ancín-Azpilicueta; *J. Environ. Manage.* **2023**, *325*, 116460.
3. M. Wadhwa; M. P. S. Bakshi; H. P. S. Makkar; *CAB Rev. Perspect. Agric. Vet. Sci. Nutr. Nat. Resour.* **2015**, *10*, 031.
4. K. Vojáčkova; J. Mlček; S. Škrovankova; A. Adamkova; M. Adamek; J. Orsavova; M. Bučkova; V. Fic; L. Kouřimska; M. Buran; *Potravin. Slovak J. Food Sci.* **2020**, *14*, 854-861.
5. V. Nour; T. D. Panaite; A. R. Corbu; M. Ropota; R. P. Turcu; *Erwerbs-Obstbau* **2021**, *63*, 91–98.
6. I. Stanciu; E. L. Ungureanu; E. E. Popa; M. Geicu-Cristea; M. Draghici; A. C. Mitelut; G. Mustatea; M. E. Popa; *Appl. Sci.* **2023**, *13*, 6513.
7. X. Hao; X. Zhang; D. Yang; Y. Xie; C. Mu; J. Zhang; *Anim. Feed Sci. Technol.* **2023**, *305*, 115783.

8. L. Xu; Z. Wei; B. Guo; R. Bai; J. Liu; Y. Li; W. Sun; X. Jiang; X. Li; Y. Pi; A Review. *Agric.* **2022**, *12*, 1–16.
9. S. P. Ndou; E. Kiarie; M. C. Walsh; C. M. Nyachoti; *Anim. Feed Sci. Technol*. **2018**, *238*, 123–129.
10. P. Leterme; L. Eastwood; J. Patience, *Proceedings of the Western Nutrition Conference*, Saskatoon, SK, **2007**, Sept. 25-27, pp 241-252.
11. S. G. M. Sharaf eldin; H. M. S. Ziena; S. T. M. Khair; M. A. Rozan, *Alexandria Sci. Exch. J.* **2018**, *39*, 615–619.
12. M. Vlassa; M. Filip; I. Țăranu; D. Marin; A. E. Untea; M. Ropotă; C. Dragomir; M. Sărăcilă; *Foods* **2022**, *11*, 1–17.
13. H. B. Choi; J. H. Jeong; D. H. Kim; Y. Lee; H. Kwon; Y. Y. Kim; *Asian-Australasian J. Anim. Sci.* **2015**, *28*, 1345–1353.
14. C. Shi; J. He; J. Yu; B. Yu; Z. Huang; X. Mao; P. Zheng; D. Chen; *J. Anim. Sci. Biotechnol.* **2015**, *6*, 13.
15. E. R. Grela; A. Czech; M. Kiesz; Ł. Wlazło; B. Nowakowicz-Dębek; *Anim. Nutr.* **2019**, *5*, 373–379.
16. V. I. Popa, *Studia UBB Chemia* **2021**, *66*, 89–96.
17. D. D. Milinčić; A. Kostić; B. D. Špirović Trifunović; Ž. L. J. Tešić; T. B. Tosti; A. M. Dramićanin; M. B. Barać; M. B. Pešić; *J. Serbian Chem. Soc.* **2020**, *85*, 305-319.
18. I. Stanciu; R. Dima; E. E. Popa; M. E. Popa; *Sci. Pap. B-Horticulture* **2022**, *66*, 913-918.
19. K. H. Partanen; Z. Mroz; *Nutr. Res. Rev.* **1999**, *12*, 117-145.
20. A. Szydlowska-Czerniak; K. Trokowski; G. Karlovits; E. Szlyk; *J. Agric. Food Chem.* **2010**, *58*, 7502-7509.
21. S. Burcă; C. Indolean; *Studia UBB Chemia* **2022**, *67*, 45–60.
22. X. Guo; L. Shi; S. Yang; R. Yang; X. Dai; T. Zhang; R. Liu; M. Chang; Q. Jin; X. Wang; *Food Funct.* **2019**, *10*, 4220-4230.
23. R. Khiaosa-ard; M. Mahmood; E. Mickdam; C. Pacífico; J. Meixner; L. S. Traintinger; *J. Anim. Sci. Biotechnol.* **2023**, *14*, 1-15.
24. I. Taranu; M. Habeanu; M. A. Gras; G. C. Pistol; N. Lefter; M. Palade; M. Ropota; V. S. Chedea; D. E. Marin; *J. Anim. Physiol. Anim. Nutr. (Berl).* **2018**, *102*, e30–e42.
25. M. Ragni; A. Vicenti; L. Melodia; G. Marsico; *APCBEE Procedia* **2014**, *8*, 59-64.
26. M. M. Costa; C. M. Alfaia; P. A. Lopes; J. M. Pestana; J. A. M. Prates; *Animals* **2022**, *12*, 1-18.
27. Y. S. Velioglu; G. Mazza; L. Gao; B. D. Oomah; *J. Agric. Food Chem.* **1998**, *46*, 4113-4117.
28. A. Floegel; D. O. Kim; S. J. Chung; S. I. Koo; O. K. Chun, *J. Food Compos. Anal.* **2011**, *24*, 1043–1048.
29. A. Szydłowska-Czerniak; I. Bartkowiak-Broda; I. Karlović; G. Karlovits; E. Szłyk. *Food Chem.* **2011**, *127*, 556–563.
30. A. M. Alashi; C. L. Blanchard; R. J. Mailer; S. O. Agboola; A. J. Mawson; R. He; A. Girgih; R. E. Aluko; *Food Chem.* **2014**, *146*, 500–506.

31. A. Szydłowska-Czerniak; A. Tułodziecka; *JAOCS, J. Am. Oil Chem. Soc.* **2014**, *91*, 2011-2019.
32. M. Filip; M. Vlassa; V. Coman; A. Halmagyi; *Food Chem.* **2016**, *199*, 653-659.
33. M. Filip; M. Moldovan; M. Vlassa; C. Sarosi; I. Cojocaru. *Rev. Chim.* **2016**, *67*, 2440-2445.
34. M. Filip; L. Silaghi-Dumitrescu; D. Prodan; C. Sarosi; M. Moldovan; I. Cojocaru; *Key Eng. Mater.* **2017**, *752 KEM*, 24–28.

STUDIA UBB CHEMIA, LXIX, 1, 2024 (p. 121-145)
(RECOMMENDED CITATION)
DOI:10.24193/subbchem.2024.1.08

GC-MS AND HPLC CHROMATOGRAPHIC PROFILE OF MAJORITY VOLATILE AND PHENOLIC COMPOUNDS OF SOME MEDICINAL PLANTS FROM ROMANIA[1]

Irina CIOTLĂUȘ[a], Ana BALEA[a*], Maria POJAR-FENEȘAN[a], Miuța Rafila FILIP[a], Mihaela VLASSA[a]

ABSTRACT. This study reports the identification of volatile organic compounds (VOCs) and the phenolic composition for these medicinal plants: lemon balm (*Melissa officinalis*), lavender (*Lavandula angustifolia*), and elderflower (*Sambucus nigra*). The HS-SPME-GC-MS hyphenated technique was used to investigate the volatiles from the three plants in fresh and dried forms. The essential oils were obtained by hydrodistillation technique, followed by GC-MS analysis. Additionally, HPLC-UV/VIS detection was used to identify the phenolic compounds of these plants. The majority compounds identified in the fresh, dried and oil of lemon balm were *Z*-beta-ocimene, citronellal, citronellol, b-caryophyllene, (*E*)-citral, (*Z*)-citral and geraniol respectively. The aerial part of lavender contains mainly linalool, linalyl acetate, beta-myrcene, trans-beta-ocimene, lavandulyl acetate and caryophyllene. The most compounds identified in the fresh flowers of elderflower were linalool, cis-beta-ocimene, linalool oxide (II) pyran, cis-3-hexenyl isovalerate, while in the dry flowers the majority compounds were linalool oxide (II) pyran, cis-3-hexenyl isovalerate and hexenyl tiglate. The essential oil was rich in n-hexadecanoic acid, linoleic acid, and heneicosane. Majority phenolic compounds identified in the analysed species were vanillic, sinapic, ferulic, and p-coumaric acids, while the predominant flavonoids were rutin, quercetin and epicatechin. The profile of VOCs represents an indicator in the valorisation of medicinal plants.

Keywords: *medicinal plants, volatile organic compounds (VOCs), phenolic*

[1] *Presented at "The 27th International Symposium on Separation Sciences", 24-27 September 2023, Cluj-Napoca, Romania (ISSS 2023)*

[a] *Babeş-Bolyai University, "Raluca-Ripan" Institute for Research in Chemistry, 30 Fântânele str., RO- 400294, Cluj-Napoca, Romania*

** Corresponding author: ana.balea@ubbcluj.ro*

compounds, HS-SPME-GC-MS, HPLC-UV/VIS

INTRODUCTION

Aromatic and medicinal plants have been an important concern of man during the development of civilization, currently preparations of vegetable origin occupy an increasingly large place in the sphere of therapeutic applications [1]. Medicinal plants are of particular importance, due to their active principles, being successfully used in traditional medicine (volatiles, phenolic compounds), in the cosmetic industry (essential oil extracts, natural antioxidants) and the food industry (spices, nutritional supplements, teas) [2].

Melissa officinalis *L*., commonly known as lemon balm, is a well-known medicinal plant of the *Lamiaceae* family. Lemon balm is an herbaceous, melliferous plant native to southern Europe [3], in our country being spread spontaneously, but mostly cultivated in the western and southern regions of the country [4]. The lemon balm herb acts in different ways, such as antioxidant, sedative, antidepressant, anxiolytic, antispasmodic, antiseptic, cholagogue, choleretic, carminative, digestive, hypoglycemic and antimicrobial [5–8].

Monoterpenes and sesquiterpenes, responsible for the flavour and medicinal use of this plant, were the main classes of volatile constituents. The majority volatile compounds were geranial, neral, citronellal, geraniol, and caryophyllene, the citrus flavour of lemon balm oil being given by these compounds. Additionally, phytochemical investigations have revealed the presence of triterpenes (ursolic acid, oleanolic acid), phenolic compounds (chlorogenic, caffeic, ferulic and rosmarinic acid) and flavonoids (luteolin, quercetin, rutin, hesperidin) [9, 10].

Lavandula angustifolia, commonly known as lavender, is one of the most useful plants of aromatic and medicinal properties from the *Lavandula* species which are perennial and robust plants from the *Lamiaceae* family, being cultivated specially in Europe, China and USA [11]. Lavender has a great commercial value for cosmetic, perfumery, pharmaceutical, and food industries, and also for aromatherapy [12–14]. This plant is also used in traditional herbal medicine for its sedative, anxiolytic, carminative, antifungal, bactericidal, antiseptic, and anti-inflammatory effects [15]. The essential oil is used in salves, balms, cosmetics, perfumes, and topical skin preparation. Tea prepared from dried lavender flowers is beneficial for relieving mood, insomnia, and abdominal disorders [16–18]. The chemical composition of lavender oil has been studied extensively [19, 20]. Literature data on the activity of lavender oil show differences in the chemical profile between the various species of lavender [21]. The main compounds of lavender oil are the linalool and linalyl acetate, followed by lavandulyl acetate, terpinen-4-ol, lavandulol, beta-caryophenyllene, α-pinene, limonene, α-terpineol, nerol, geraniol, etc. [22–24].

The phenolic compounds and flavonoids are known as secondary metabolites of plants with important biological action. Lavender flowers contain phenolic compounds such as p-hydroxybenzoic acid, vanillic acid, gallic acid, rosmarinic acid, caffeic acid, p-coumaric acid, ferulic acid, chlorogenic acid, sinapic acid, cinnamic acid and flavonoids such as apigenin and luteolin glycosides, catechin, vanillin, etc. [25, 26].

Sambucus nigra, known as elder, is a flowering plant in the *Adoxaceae* family. From these species, elderflowers and elderberries have been used in folk medicine to treat fever, cold, flu, cough, nasal congestion, herpes, ear infections, or as products with anti-inflammatory, analgesic, antimicrobial and diuretic effect or with gentle astringent effect for the skin [27, 28].

The oil extracted from the elderberries contain volatile organic compounds with important bioactive action, namely linalool, terpineol, limonene, beta-caryophyllene, carane, beta-damascenone, cis-rose-oxide and alkane hydrocarbons [29]. The lipophilic fraction of elderflower aqueous extract is represented mainly by the saturated and unsaturated fatty acids, like palmitic, stearic, behenic, oleic, and lignoceric acids [30]. These flowers mainly contain flavonoids such as rutin, quercetin, iso-quercetin, astragalin, hyperoside, nicotiflorin, isorhamnetin and kaempherol, followed by phenolic acids such as caffeoylquinic, dicaffeoylquinic, p-coumaroylquinic, respectively caffeic, ferulic acids, etc. [31, 32].

Research on finding new biologically active compounds from plants involves their isolation and purification through various extraction methods and identification/quantification by different chromatographic techniques, and then performing tests to determine their biological action [33]. The conventional extractive techniques used are maceration, infusion, percolation, and Soxhlet extraction. Among the modern extraction techniques, it is mentioned accelerated solvent extraction, microwave-assisted extraction, ultrasound-assisted extraction, called also sonication extraction, and supercritical fluid extraction [33].

Hydrodistillation (HD) is another conventional method that uses water or steam to extract bioactive compounds, mainly essential oils. This technique is regularly carried out by means of a setup recognized as a Clevenger apparatus or simple steam distillation [34, 35].

For the identification of compounds, extraction techniques are used in combination with different analytical techniques, such as the chromatographic (GC, HPLC), spectroscopic (IR, UV-VIS, NMR) or spectrometric (MS) techniques [36–38].

Headspace solid-phase microextraction (HS-SPME) technique coupled to gas-chromatography with mass-spectrometry detection (GC-MS) is a hyphenated technique (HS-SPME-GC-MS) successfully used for sampling

and analysing the volatiles of a complex matrix from plants, animals or environmental samples, etc. [39]. Through this technique it is possible to easily establish the profile of volatiles and their variability in different stages of plant development, different anatomical parts of them (root, stem, leaves, flowers), different degrees of harvesting and processing (fresh, dried, oil) as well as the botanical and geographical origin of the plants [40,41].

In recent years, a re-evaluation of medicinal and aromatic plants is required, due to the modern concern developing new phytotherapeutic products based on nanotechnologies. Nano-formulations such as nano-emulsions, liposomes, micelles, hydrogels and nanoparticles are known as very good vehicles to obtain a high bioavailability of the active ingredients from plants [42–45].

The variation of the chemical profile of medicinal plants depending on the variety, the anatomical part of the plant, the stage of development, the types of products, the harvesting environment, requires a re-evaluation when it comes to their use in medicine, because the components can influence the pharmacological/therapeutic properties [41].

This study aimed to investigate by GC-MS the profile of the volatile organic compounds (VOCs) of three medicinal plants (lemon balm, lavender and elderflower) from Romania, Cluj County, each of them in three forms of presentation of the aerial part: fresh, dry, and essential oil. The VOC profile of the fresh and dried samples, respectively, was performed by HS-SPME-GC-MS while that of the essential oils, obtained by hydrodistillation of the dried aerial parts, by GC-MS. The content of some phenolic compounds and flavonoids in the alcoholic extracts of dried plants was performed by HPLC-UV/VIS analysis.

RESULTS AND DISCUSSION

In the present study, a comparative analysis on the abundance of volatile compounds in three forms of the plant, namely essential oil, fresh and dried plants, aims to trace their traceability. Phenolic and flavonoid compounds were also determined from the alcoholic extracts of the dried plants.

MELISSA OFFICINALIS – volatile profile

A total of 38 compounds were identified in all analysed samples. The GC-MS chemical composition of the HS-SPME extract of lemon balm from fresh and dried aerial part (leaves) includes mainly monoterpenes (55.19% and 72.95%) and sesquiterpenes (37.54% and 18.64%). The oxygenated

monoterpenes (50.85%) and the oxygenated sesquiterpenes (43.29%) are the main classes in lemon balm oil (Table 1). The fresh extract of lemon balm contains mainly: beta-caryophyllene (21.29%), *(E)*-citral (19.11%), (*Z)*-citral (13.07%), (*Z)*-beta-ocimene (11.12%), and citronellal (7.66%). The majority compounds identified in the dried extract were: (*E*)-citral (30.47%), (*Z*)-citral (19.03%), citronellal (15.61%) (*Z*)-beta-ocimene (3.59%), beta-caryophyllene (11.27%), while hydrodistilled essential oil was rich in (*E*)-citral (25.15%), beta-caryophyllene (22.47%), (*Z*)-citral (19.15%), germacrene-D (10.89%) and citronellal (3.26%).

Table 1. Volatile organic compounds identified in leaves (fresh, dried, and essential oil) of lemon balm

No.	**Compound**	**t_R (min)**	**LRIs**	**Lemon balm sample Normalised area (%)**		
				Fresh	Dried	Oil
1	***2***	***3***	***4***	***5***	***6***	***7***
1.	*E*-2-hexenal (OC)	9.776	835	nd	1.35	nd
2.	Benzaldehyde (OC)	13.107	955	nd	0.36	nd
3.	1-Octen-3-ol (OC)	13.533	971	1.03	nd	nd
4.	3-Octanone (OC)	13.694	976	nd	1.21	nd
5.	3-Heptanone, 5-methyl (OC)	13.715	977	3.36	nd	nd
6.	E,E-2,4-Heptadienal (OC)	14.534	1004	nd	0.17	nd
7.	E-beta-ocimene (MH)	15.209	1027	nd	0.14	nd
8.	Alpha-pinene (MH)	15.219	1028	0.75	nd	nd
9.	**Z-beta-ocimene (MH)**	**15.582**	**1040**	**11.12**	**3.59**	**1.60**
10.	(4E,6Z)-allo-ocimene (MH)	17.990	1123	0.50	0.15	nd
11.	1,5-Heptadiene-3,3-dimethyl (OC)	18.426	1139	0.26	0.56	nd
12.	**Citronellal (OM)**	**18.727**	**1149**	**7.66**	**15.61**	**3.26**
13.	Isoneral (OM)	18.945	1157	0.50	1.22	1.14
14.	Isogeranial (OM)	19.500	1177	0.70	1.23	1.50
15.	Methyl salicylate (OC)	20.003	1194	2.06	0.78	nd
16.	Nerol (OM)	20.849	1226	0.92	nd	nd
17.	**Z-citral (neral) (OM)**	**21.238**	**1240**	**13.07**	**19.03**	**19.15**
18.	Methyl citronellate (OM)	21.581	1253	0.35	4.92	0.65
19.	**E-citral (geranial) (OM)**	**22.058**	**1271**	**19.11**	**30.47**	**25.15**
20.	Methyl geranoate (OM)	23.303	1319	0.51	0.47	nd
21.	Alpha-cubenene (SH)	24.144	1352	0.62	0.33	nd
22.	Alpha-copaene (SH)	24.943	1384	1.34	0.79	0.77
23.	Beta-gurjunene (SH)	25.223	1395	1.08	0.46	1.28
24.	**Beta-caryophyllene (SH)**	**26.175**	**1434**	**21.29**	**11.27**	**22.47**

No.	Compound	t_R (min)	LRIs	Lemon balm sample Normalised area (%)		
				Fresh	Dried	Oil
1	*2*	*3*	*4*	*5*	*6*	*7*
25.	Trans-alpha-bergamotene (SH)	26.284	1439	1.51	0.65	nd
26.	Epi-bicyclosesquiphellandrene (SH)	26.338	1440	nd	nd	1.80
27.	Beta-farnasene (SH)	26.684	1456	nd	nd	0.23
28	Beta-copaene (SH)	26.865	1461	nd	nd	0.45
29.	Humulene (SH)	27.003	1467	1.35	0.64	1.31
30.	Gamma-muurolene (SH)	27.381	1485	1.83	0.83	nd
31.	Germacrene D (SH)	27.599	1494	3.30	1.68	10.89
32.	Alpha-farnesene (SH)	27.874	1505	1.81	0.80	1.44
33.	Gamma-cadinene (SH)	28.378	1522	2.35	0.95	1.67
34.	Trans-calamenene (SH)	28.487	1533	0.56	nd	nd
35.	Alpha-amorphene (SH)	28.829	1548	0.50	0.24	0.98
36.	Fenchone (OS)	29.829	1592	nd	nd	0.80
37.	Tau-cadinol (OS)	31.297	1660	nd	nd	1.31
38.	Alpha-cadinol (OS)	31.577	1673	nd	nd	2.08
	Monoterpene hydrocarbons (MH)			12.37	3.88	1.60
	Oxygenated monoterpenes (OM)			42.82	72.95	50.85
	Sesquiterpene hydrocarbons (SH)			37.54	18.64	43.29
	Oxygenated sesquiterpenes (OS)			0	0	4.19
	Other compounds (OC)			6.71	4.43	0
	Total %			**99.44**	**99.90**	**99.93**

t_R: retention time; LRIs: linear retention index (on HP-5ms column); nd: not detected;
The majority volatile organic compounds are written in bold.

In the case of this plant, fewer compounds were identified because its profile of volatiles is uniform, in the three samples (fresh, dried and essential oil) analysed. The main common compounds (6) of the three samples were: (*Z*)-beta-ocimene, citronellal, (*Z)*-citral, (*E)*-citral, beta-caryophylene, germacrene D in variable proportions (Figure 1). Other compounds common to the three samples were in smaller quantities: beta-gurjunene, humulene, alpha-farnasene, gamma cadinene, and S-citronellic methyl ester. A notable variability among the three samples would be the presence of (*Z*)-beta-ocimene in the fresh sample in a proportion of, 11.12%, compared to 3.59% in dried sample and 1.60% in the essential oil. (*Z*)-beta ocimene is a common monoterpenoid found in almost all fresh green plants with the role of attracting pollinators [46]. The oil sample contains 43.29% sesquiterpene compounds compared to the other samples, where the proportion of sesquiterpenes was 37.54% for fresh sample and 18.64% for dried sample. Another important thing to mention would be that

the lemon balm oil sample contains Gemacrene-D in a percentage of 10.89%, compared to the other samples where the amount found was lower.

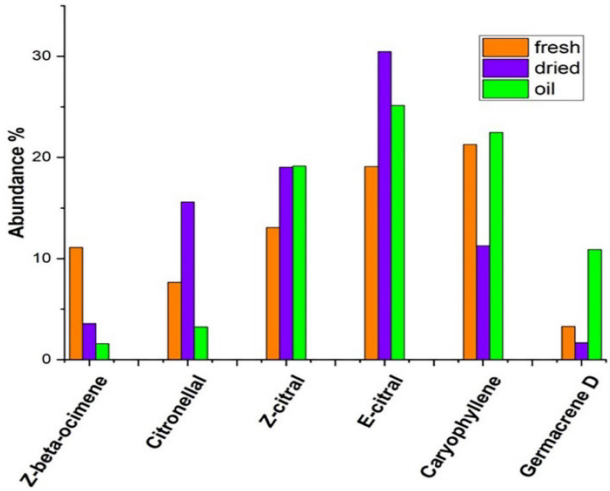

Figure 1. The six majority compounds found in lemon balm samples: fresh, dried and essential oil

In the literature, there are few data regarding the identification of volatiles from the leaves and oil of *Melissa officinalis* by the HS-SPME-GC-MS respecively HD-GC-MS techniques. A comparative study presents the collection of volatiles from fresh lemon balm leaves by the HS-SPME-GC-MS technique and from lemon balm oil obtained by hydrodistillation. The main compounds identified in both fresh leaves and essential oil were: citronellal (31.1% and 10.2%), (*E*)-citral (11.9% and 11.2%), (*Z*)-citral (9.6% and 19.6%), beta- caryophyllene (12.0% and 13.2 %) [47].

Ieri et al. [48] presents a study on HS-SPME-GC-MS analysis of the dried powdered foliar sample of *Melissa officinalis*. Terpenes were the most representative class of compounds monoterpenes (71.91%) beside the sesquiterpenes (19.01%). The most abundant compounds were citronellal (27.54%), α-citral, (25.00%), beta-caryophyllene (9.24%) and beta-citral (7.61%).

The chemical composition of lemon balm oil is mainly represented by compounds such as E/Z-citral, citronellal, caryophylene, in variable proportions [49, 50]. These compounds that give the smell and aroma of the plant [51]. Besides their use in perfumery, these compounds have antimicrobial, anxiolytic and antidiabetic action [52]. The other compounds found in the oil such as thymol [53], sesquiterpene alcohol (nerolidol) [54], are not specific to lemon balm oil. The volatile lemon balm oil from Romania was characterized [55] by a

higher content of monoterpenes (mainly *E* and *Z*-Citral, citronellal, ~32%) and by the presence in *Mellisa* of trans-anethole and estragole (26.44%) [55]. In this study trans-anethole and estragole were not found in the *Mellisa* samples.

LAVANDULA ANGUSTIFOLIA – volatile profile

A total of 41 compounds were identified in all the studied samples (fresh, dried and essential oil) of lavender aerial part (flowers). (**Table 2**) The bouquet of fresh and dried flowers of lavender contains mainly: linalyl acetate (19.70% and 16.48%), linalool (15.57% and 21.03%), caryophyllene (12.78% and 8.28%), trans-beta-ocimene (10.44%, and 9.28%), beta-myrcene (8.42% and 9.96%), lavandulyl acetate (5.81% and 6.15%) and allo-ocimene (6.05% and 4.88%). Extraction of essential oil from the dried lavender flowers was carried out by hydrodistillation, using a Clevenger-type apparatus. The majority components found were: linalool (21.91%), linalyl acetate (14.54%), E-beta-ocimene (8.11%), beta-caryophyllene (7.31%), and beta-myrcene (6.19%).

Table 2. Volatile compounds identified in the aerial part of *lavender*

No.	Compound	t_R (min)	LRIs	Lavender sample Normalised Area %		
				Fresh	Dried	Oil
1	***2***	***3***	***4***	***5***	***6***	***7***
1	Alpha-pinene (MH)	12.223	926	nd	nd	0.15
2	Camphene (MH)	12.770	944	nd	0.41	0.30
3	**Beta-myrcene (MH)**	**13.959**	**985**	**8.42**	**9.96**	**6.19**
4	Alpha-phellandrene (MH)	14.545	1005	0.56	0.60	0.65
5	**E-beta-ocimene (MH)**	**15.308**	**1031**	**10.44**	**9.28**	**8.11**
6	Z-beta-ocimene (MH)	15.697	1044	5.59	4.28	3.94
7	Gamma terpinene (MH)	16.038	1056	nd	0.20	nd
8	3-Carene (MH)	16.916	1078	0.41	nd	0.55
9	**Linalool (MH)**	**17.388**	**1100**	**15.57**	**21.03**	**21.91**
10	**Allo-ocimene (MH)**	**18.151**	**1129**	**6.05**	**4.88**	**5.00**
11	Camphor (OM)	18.442	1154	0.75	0.60	0.25
12	Borneol (OM)	19.147	1164	0.74	0.29	0.20
13	Lavandulol (OM)	19.292	1164	nd	0.98	nd
14	Terpinen-4-ol (OM)	19.884	1184	0.27	1.82	2.08
15	Cryptone (OM)	20.091	1196	nd	0.62	0.61
16	Alpha-terpineol (OM)	20.359	1207	nd	nd	6.12
17	**Linalyl acetate (OM)**	**21.513**	**1251**	**19.70**	**16.48**	**14.54**

No.	Compound	t_R (min)	LRIs	Lavender sample Normalised Area %		
				Fresh	Dried	Oil
1	*2*	*3*	*4*	*5*	*6*	*7*
18	Piperitone (OM)	22.157	1270	nd	0.21	nd
19	**Lavandulyl acetate (OM)**	**22.520**	**1289**	**5.81**	**6.15**	**3.64**
20	Bornyl acetate (OM)	22.707	1295	0.39	0.66	0.71
21	p-cymen-7-ol/cuminol (OM)	22.800	1299	nd	0.14	nd
22	Neryl acetate (OM)	24.357	1360	2.06	1.60	2.26
23	Geranyl acetate (OM)	24.912	1382	3.13	3.05	3.25
24	Alpha-cubenene (SH)	25.213	1388	0.20	nd	nd
25	**Beta-caryophyllene (SH)**	**26.245**	**1438**	**12.78**	**8.28**	**7.31**
26	Beta-farnasene (SH)	26.774	1458	4.14	3.83	2.12
27	Humulene (SH)	27.086	1471	0.58	0.46	0.33
28	Biciclosesquiphellandrene (SH)	27.193	1476	0.21	0.30	nd
29	Gamma-muurolene (SH)	27.470	1488	nd	nd	0.37
30	Germacrene D (SH)	27.646	1496	0.44	0.20	nd
31	Beta-bisabolene (SH)	28.094	1515	0.25	nd	nd
32	Gamma-muurolene (SH)	28.367	1527	1.21	2.11	0.98
33	Gamma-cadinene (SH)	28.476	1529	0.18	nd	nd
34	Caryophyllene oxide (OS)	30.007	1600	nd	0.12	0.79
35	Epicubenol (OS)	30.666	1630	nd	0.11	0.50
36	Tau-cadinol (OS)	31.288	1657	nd	1.17	4.14
37	Muurol-5-en-4-one (OS)	32.319	1708	nd	nd	0.22
38	Epicubenol (OS)	33.367	1723	nd	nd	0.15
39	2-Pentadecanone, 6,10,14-trimethyl (OC)	34.659	1802	nd	nd	0.29
40	Nonadecane (OC)	36.039	1900	nd	nd	1.27
41	Eicosane (OS)	36.325	2000	nd	nd	0.12
	Monoterpene hydrocarbons (MH)			31.47	29.61	24.89
	Oxygenated monoterpenes (OM)			48.42	53.63	55.57
	Sesquiterpene hydrocarbons (SH)			19.99	15.18	11.11
	Oxygenated sesquiterpenes (OS)			0	1.4	5.80
	Other compounds (OC)			0	0	1.68
	Total			**99.88**	**99.82**	**99.05**

t_R-retention time; LRIs: linear retention index (on HP-5ms column); nd: not detected;
The majority volatile organic compounds are written in bold.

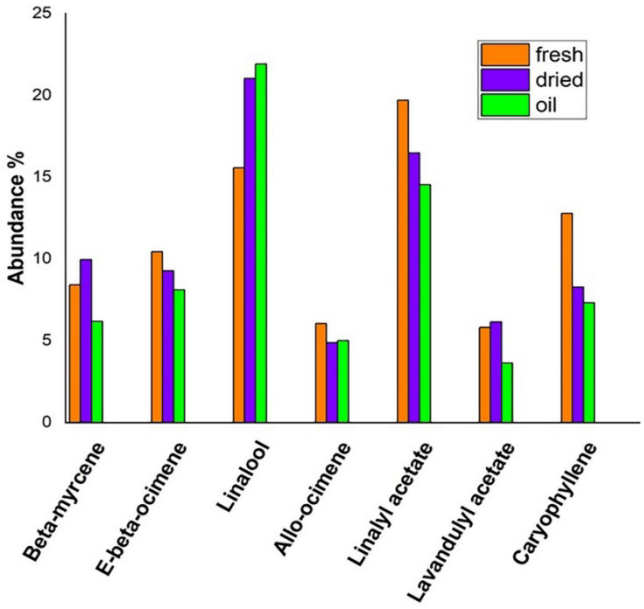

Figure 2. Majority compounds in lavender samples: fresh, dried and oil

There are numerous studies that have analysed the chemical composition of Lavender in all its forms (inflorescences, leaves, fresh, dried, oil) obtained through different extraction techniques and analysis methods [56–58].

The most characteristic and valuable constituents for lavender (*Lavandula angustifolia*) presented by Zagorcheva [59] and J. Fu [60] were linalool (20–35%), linalyl acetate (30–35%), and lavandulyl acetate (5–6%). Surprisingly, different studies also reported other main components such as eucalyptol (8.50% and 31.9%), borneol (15.21% and 24%) and camphor (2.00% and 16.1%), in the lavender aerial parts [61]. In our samples camphor and borneol were identified in traces, and eucalyptol is missing. Thus, a continuous evaluation of this plant with applications in medicine, cosmetic industry and aromatherapy is necessary, because it presents a great variability of biologically active compounds. These compositional variabilities can be dictated by environmental conditions, soil characteristics, harvesting time and drying/processing methods [62].

SAMBUCUS NIGRA – volatile profile

Through the GC-MS analysis of the aerial part (flowers) and the oil of elderflower, a total of 55 compounds were identified, grouped as follows: monoterpenes, sesquiterpenes, esters, acids, hydrocarbons and other compounds. In the case of this plant, in addition to the great variability of the main volatile compounds in the three samples, we also observe a great variability in the classes of compounds. In the flower samples monoterpenes predominate, they exist in a proportion of 83.05% in the fresh elderberry plant, 71.31% in the dry plant, while in the oil sample, monoterpenes represented only 9 .5%.

The esters were found in a proportion of 11.59% in the fresh sample, 22.85% in the dried sample and only 5.02% in the essential oil. Fatty acids were identified in a proportion of 59.84% and hydrocarbons 16.3% only in the essential oil sample (**Table 3**).

Table 3. Volatile constituents identified in aerial part of *elderflower:* fresh, dried, and essential oil

No.	Compound	t_R (min)	LRIs	Elderflower sample Normalised area %		
				Fresh	Dried	Oil
1	***2***	***3***	***4***	***5***	***6***	***7***
1.	3-Hexen-1-ol (OC)	9.818	838	1.29	nd	nd
2.	Hexenyl tiglate (E)	9.839	837	nd	**6.95**	nd
3.	1,5-Heptadiene-2,6-dimethyl (H)	10.574	865	nd	nd	1.03
4.	Pentanoic acid, 3 methyl-2-oxo, methyl ester (OC)	13.118	953	nd	1.16	nd
5.	Beta-myrcene (MT)	13.839	981	1.59	nd	nd
6.	*E*- β –ocimene (MT)	15.199	1027	1.24	nd	nd
7.	L-isoleucine, methyl ester (E)	15.341	1031	nd	2.34	nd
8.	***Z*- β-ocimene (MT)**	**15.551**	**1039**	**20.08**	**nd**	**nd**
9.	3-Carene (MT)	15.858	1051	0.37	nd	nd
10.	**Cis-Linalool oxide (MT)**	**16.366**	**1067**	**7.57**	**0.96**	**nd**
11.	Trans-Linalool oxide (MT)	16.833	1083	0.55	nd	nd
12.	**Linalool (MT)**	**17.165**	**1094**	**24.68**	**0.73**	**0.56**
13.	Hotrienol (MT)	17.258	1097	nd	2.73	nd
14.	Nonanal (OC)	17.378	1101	nd	nd	2.51
15.	Trans-rose oxide (MT)	17.489	1102	0.41	nd	**4.19**
16.	Phenylethyl alcohol (OC)	17.624	1110	nd	0.76	nd
17.	Trans-alloocimene (MT)	17.974	1123	0.90	nd	nd

No.	Compound	t_R (min)	LRIs	Elderflower sample Normalised area %		
				Fresh	Dried	Oil
1	*2*	*3*	*4*	*5*	*6*	*7*
18.	Cis-rose oxide (MT)	18.032	1134	nd	nd	2.01
19.	Cis-alloocimene (MT)	18.344	1136	1.00	nd	nd
20.	Citronellal (MT)	18.898	1148	0.52	nd	nd
21.	Nerol oxide (MT)	18.772	1151	nd	nd	0.44
22.	2,4-Dimethylfuran (OC)	18.903	1156	nd	3.57	nd
23.	**Linalool oxide (II) (pyran) (MT)**	**19.303**	**1170**	**14.18**	**63.56**	**0.65**
24.	Terpenediol (I) (MT)	19.682	1183	nd	0.53	nd
25.	**Citronellol (MT)**	**20.745**	**1222**	**8.89**	**1.60**	**0.65**
26.	**Cis-3-hexenyl isovalerate (E)**	**20.849**	**1226**	**9.88**	**9.06**	**nd**
27.	Butyl 2-methylbutenoate (E)	20.963	1230	nd	0.40	nd
28.	Geraniol (MT)	21.394	1246	1.10	nd	0.29
29.	Citral (MT)	21.913	1282	1.21	1.2	nd
30.	Dihydroedulan (OC)	22.855	1295	nd	nd	0.78
31.	(Z)-hexenyl angelate (E)	23.319	1319	1.71	2.94	1.73
32.	Beta-damascenone (OC)	24.938	1356	nd	nd	0.26
33.	Cis-jasmone (ST)	25.259	1396	0.72	nd	nd
34.	1,3,8-Menthatriene (MT)	25.285	1397	nd	nd	1.36
35.	Benzene-4-ethyl-1,2-dimethyl (H)	25.819	1421	nd	nd	0.43
36.	Beta - caryophyllene (MT)	26.095	1431	0.86	1.31	0.27
37.	Germacrene D (ST)	27.387	1485	0.20	nd	nd
38.	Trans-2-hexenyl isovalerate (E)	27.952	1490	nd	nd	0.86
39.	1,3-Benzenediol, 5-pentyl (OC)	28.324	1520	nd	nd	0.82
40.	3-Hexen-1-ol benzoate (E)	29.564	1580	nd	nd	1.21
41.	Benzoic acid, hexyl ester (E)	29.708	1581	nd	nd	0.14
42.	Tetradecanal (H)	30.370	1590	nd	nd	0.50
43.	Pentadecanal (H)	32.596	1725	nd	nd	0.26
44.	Tetradecanoic acid (OA)	33.572	1761	nd	nd	1.45
45.	Octadecanal (OC)	34.370	1800	nd	nd	0.74
46.	2-Pentadecanone-6,10,14-trimethyl (OC)	34.687	1852	nd	nd	1.72
47.	Nonadecane (H)	35.394	1900	nd	nd	**4.04**
48.	Citronellyl tiglate (E)	35.752	1934	nd	nd	1.08
49.	Geranyl vinyl ether (OC)	35.932	1942	nd	nd	1.46
50.	**n-Hexadecanoic acid (OA)**	**36.024**	**1964**	**nd**	**nd**	**45.13**
51.	9-Nonadecene (H)	37.593	1968	nd	nd	1.05

No.	Compound	t_R (min)	LRIs	Elderflower sample Normalised area %		
				Fresh	Dried	Oil
1	***2***	***3***	***4***	***5***	***6***	***7***
52.	Heneicosane (H)	37.974	2100	nd	nd	**6.62**
53.	**Linoleic acid (OA)**	**38.937**	**2140**	**nd**	**nd**	**9.33**
54.	Oleic acid (OA)	39.056	2147	nd	nd	**3.93**
55.	Docosane (H)	39.424	2200	nd	nd	2.37
	Monoterpenes (MT)			83.05	71.31	9.5
	Sesquiterpenes (ST)			1.78	1.31	0.53
	Esters (E)			11.59	22.85	5.02
	Organic Acids (OA)			0	0	59.84
	Hydrocarbons (H)			0	0	16.30
	Other compounds (OC)			2.53	4.33	8.68
	Total			**98.95**	**99.80**	**99.87**

t_R-retention time; LRIs: linear retention index (on HP-5ms column); nd: not detected; The majority volatile organic compounds are written in bold.

The main compounds from elderflower*,* fresh aerial part were found: cis- beta-ocimene (20,08%), linalool (24,68%), linalool oxide II (14,18%), cis-hexenyl-isovalerate (9,88%) and citronellol (8,89%). The main compounds from elderflower dried were identified: linalool oxide II (63,56%), cis-hexenyl-isovalerate (9,06%) and hexenyl tiglate (6,95%). The specific compounds in the elderflower oil were found: n-hexadecanoic acid (45,13%), heneicosane (6,62%), linoleic acid (9,33%), oleic acid (3,93%) and docosane (2,37%) (Figure 3).

Common compounds were identified in the three forms of *elderflower* thus: linalool, citronellol, linalool oxide pyran, citronellol, (*Z*)-hexenyl angelate and caryophyllene in different percentages.

Similar studies, which use the sampling of elder flowers, through the HS-SPME-GC-MS technique, have highlighted important compounds that give the characteristic aroma such as: linalool, hotrienol, linalool oxide, 2-hexanone, eugenol, 3-hexen-1-ol [63, 64]. Among the dominant compounds of the essential oil of elderflowers, hydrocarbons (nonadecane, tricosane, eicosane, pentacosane, heneicosane), followed by fatty acids such as n-hexadecanoic and linoleic acid are listed. Cis-linalool oxide, linalool, epoxy-linalool, rose oxide, carvacrol, and citronellol were the most prominent oxygenated monoterpenes found [65-67].

Other studies followed changes in the profile of volatiles before and after harvesting the flowers [68]. Drying for further use is an important preservation method for plant material, as it inhibits enzymatic degradation and limits microbial growth [69].

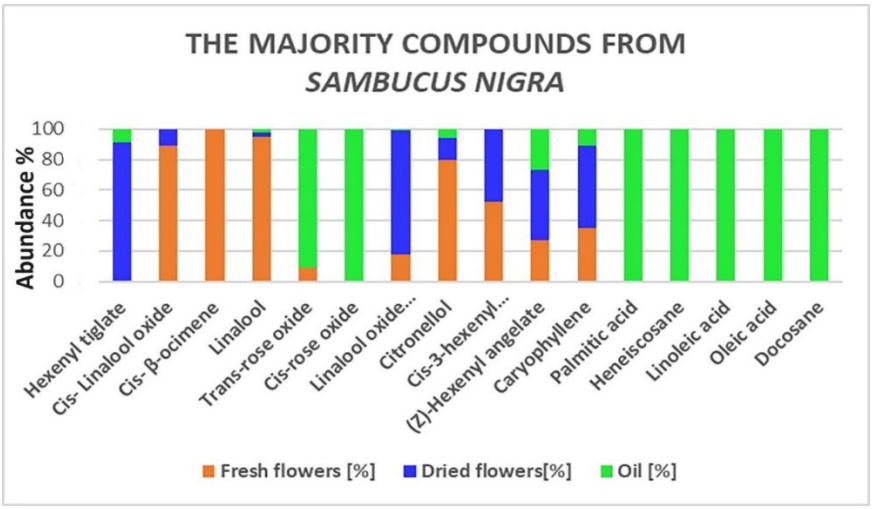

Figure 3. Majority compounds from aerial part (flowers) of elderflower: fresh, dried and essential oil

The studies regarding the use of this species in traditional medicine are focused more on the fruits and less on the effectiveness of the elder flowers.

The predominant compounds in the three samples, such as linalool, linalool oxide (II), pyran, citronellol and fatty acids show biological activity.

Linalool is a racemic mixture of both enantiomers, being present not only in the essential oil of plants but also in some fruits. The linalool has anti-inflammatory, anticancer, anti-hyperlipidemic, antimicrobial, antinociceptive, analgesic, anxiolytic, antidepressant and neuroprotective properties [70]. Using *in vitro* and *in vivo* models, linalool demonstrated to hold a broad spectrum of bioactive properties, that can be exploited by the pharmaceutical industry. Inhaled linalool showed anxiolytic properties in the light/dark test, increased social interaction and decreased aggressive behavior [71]. The antitumor activity of linalool has been studied *in vitro* and *in vivo* and its role as a modulator that increases the antitumor activity of some drugs and reduces the effect of cytotoxicity has been highlighted [72]. The linalool oxide can be used as natural flavoring and was tested by inhalation in case of animal model (mouse), without causing any motor deficit. These results suggest that inhaling of linalool oxide can be used against anxiety [73].

A systemaic review have highlighted the biological activities of citronellol, including antibiotic and antifungal effects *in vitro*, and pointed out various properties, including analgesic and anticonvulsant effects *in vivo*, in addition to showing low toxicity [74].

Fatty acids such as n-hexadecanoic acid, and linoleic acid have proven antibacterial activity against *Staphylococcus aureus, Bacillus subtilis, Escherichia coli,* and *Klebsiella pneumoniae*, *Mycobacteria*, *Helicobacter pylori*, etc. [75, 76] and also anti-inflammatory activity [77, 78].

PHENOLIC COMPOUNDS ANALYSIS

Phenolic compounds from plants of bioactive compounds with antioxidant activities. This study reports the content of phenolic acid and flavonoid contents of these three medicinal plants from Cluj County, Romania, including lemon balm (*Melissa officinalis*), lavender (*Lavandula angustifolia*) and elderflower (*Sambucus nigra*).

The majority compounds present in *lemon balm* extract were: rutin (364.05 µg/g), catechin (33.4 µg/g), sinapic acid (108.75 µg/g), vanillic acid (42.95 µg/g) and p-coumaric acid (36.95 µg/g).

Vanillic (2023.8 µg/g), sinapic (247.2 µg/g) and ferulic (171.55 µg/g) acids, epicatechin (341.45 µg/g) in *lavender* extract. Other compounds identified in low concentration were: p-coumaric (27.25 µg/g) and luteolin (142.95 µg/mg) and quercetin (82.7 µg/g).

For elderflower extract, the HPLC-UV/VIS technique revealed that the majority compounds were vanillic acid (444.1 µg/g), catechin (304 µg/g) and quercetin (77.3 µg/g), while the least abundant was gallic acid (2.1 µg/g) (Table 4).

Table 4. HPLC-UV/VIS determination of polyphenols from herbal materials: lemon balm, lavender, and elderflower

Polyphenols	Herbal materials		
	Lemon balm	Lavender	Elderflower
	Polyphenols (µg/g)		
Gallic acid*	0.00	0.00	2.1
Catechin**	33.4	0.00	304
Epicatechin**	16.8	341.45	0.00
Vanillic acid*	42.95	2023.8	444.1
Caffeic acid*	18.05	0.00	51.9
p-Coumaric acid*	36.95	27.25	5.5
Sinapic acid*	108.75	247.2	30.25
Ferulic acid*	9.2	171.55	0.00
Rutin**	364.05	20.1	24.35
Quercetin**	9.45	82.7	77.3
Luteolin**	0.00	142.95	0.00
SUM	**639.6**	**3057**	**939.5**

*Phenolic acid; **Flavonoid

The phenolic acids and flavonoids were identified by comparison with the standards followed by their quantification based on the HPLC-UV/VIS analysis (Figure 4).

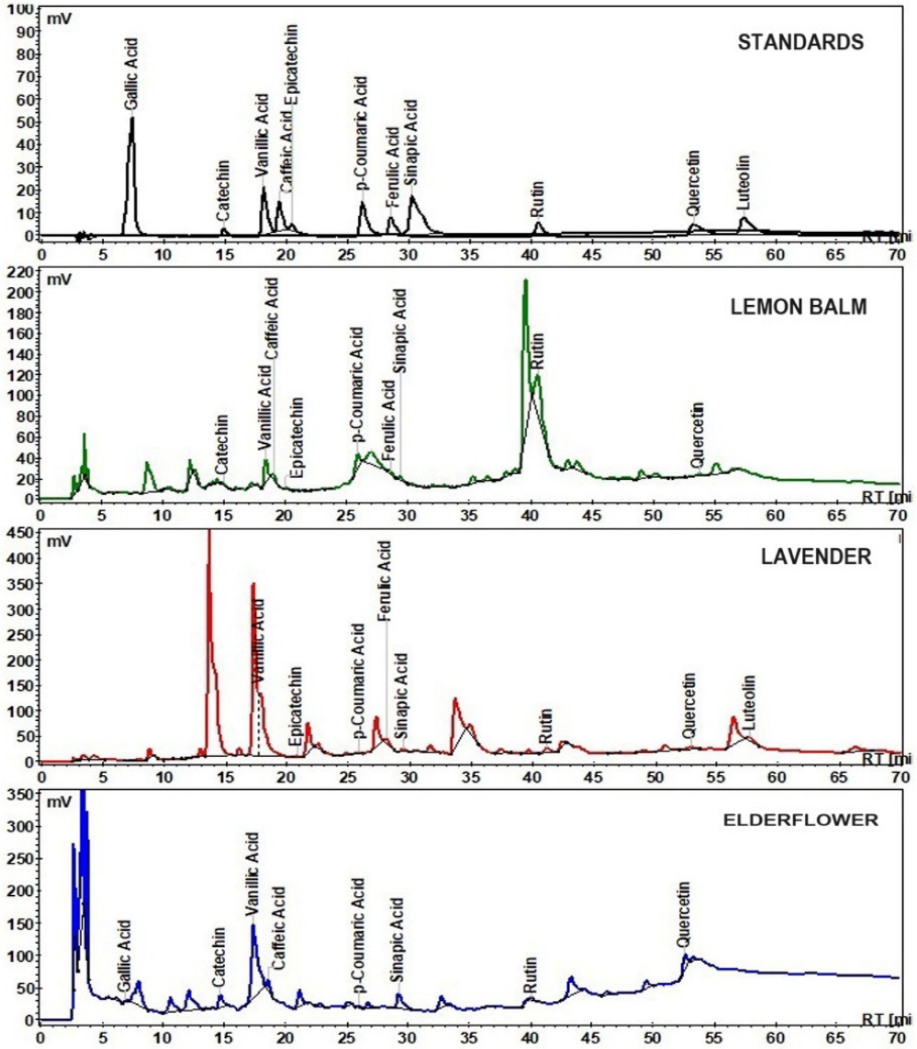

Figure 4. HPLC-UV-VIS chromatograms of polyphenols: standards and compounds found in the analysed samples (lemon balm, lavender, elderflower

HPLC parameters of the determination of polyphenols from the plant extracts are presented in Table 5.

Table 5. Validation parameters of HPLC method for determination of polyphenols from plant extracts

Compound	[a]t_R (min)	[b]Calibration curves	[c]Regression Coefficient R^2	[d]LOD (3 × S/N, µg/mL)	[e]LOQ (10 × S/N, µg/mL)
Gallic acid	7.40	A=0.023C+0.012	0.998	0.037	0.123
Catechin	14.88	A=0.122C+0.091	0.994	0.152	0.506
Vanillic acid	18.14	A=0.732C+0.887	0.997	0.081	0.270
Caffeic acid	19.41	A=0.354C-0.066	0.998	0.730	2.433
Epicatechin	20.47	A=0.064C-0.026	0.996	0.840	2.800
p-Coumaric Acid	26.19	A=0.174C-0.017	0.998	0.329	1.096
Ferulic acid	28.52	A=0.422C+0.357	0.997	0.103	0.343
Sinapic acid	30.27	A=0.521C+0.134	0.998	0.198	0.660
Rutin	40.56	A=0.309C+0.355	0.996	0.241	0.803
Quercetin	53.27	A=0.575C-0.032	0.998	0.321	1.070
Luteolin	57.38	A=0.586C+0.531	0.998	0.387	1.290

[a]t_R (min), Retention time; [b]Calibration curves; A, peak area; C, concentration of analyte (µg/mL); [c]Regression coefficient R^2; [d]LOD (3 × S/N, µg/mL), limit of detection; [e]LOQ (10 × S/N, µg/mL), limit of quantification; S/N, signal to noise ratio.

Our research was consistent with literature studies done on lemon balm. The polyphenols from lemon balm reported by Virchea et al. [79] were luteolin, quercetin, rhoocitrin, those reported by Miraj et al. [80] were rosmarinic, caffeic and protocatechuic acids, while those reported by Ordaz et al. [81] were astragalin and apigenin and vanillic, ferulic and caffeic acids.

The literature data [82–85] presents a multitude of HPLC methods for the analysis of ethanolic and aqueous extracts from fresh or dried flowers of *Lavandula angustifolia* using different detectors such as: UV-VIS, MS, DAD, UHPLC-DAD, UPLC-ESI-MS/MS. Thus, through these techniques, the polyphenolic markers of lavender flowers were identified the following phenolic acids such as rosmarinic, ferulic, caffeic, vanillic, chlorogenic, sinapic and p-coumaric acids and flavonoids such as apigenin, luteolin, catechin, naringenin, epicatechin and rutin.

Some of the phenolic compounds identified by us were also identified in different elderflower herb extract, but in different concentrations [86]. The difference in concentrations is due primarily to the way the samples were processed and secondly to the extraction method used.

Vanillic acid is a phenolic acid that has previously been attributed with antioxidant, anti-inflammatory, and neuroprotective features. It displays a variety of bioactivities that may be utilized to treat neurological, cardiovascular, and other chronic diseases [87].

Quercetin is considered beneficial against different types of cancers, including pancreatic cancer, osteosarcoma, breast cancer, cervical cancer, leukemia, colon cancer, gastrointestinal cancer, ovarian cancer, and oral cancer [88].

Using catechin and quercetin can reduce the amount of malondialdehyde which is the end product of lipid peroxidation during physical exercise and may create a protective effect against free radicals and increase the levels of antioxidant enzymes and strengthen the antioxidant defense systems of the cells and have a positive effect on exercise performance [89].

CONCLUSIONS

This study aimed to investigate the volatile chemical profile (VOC) from the aerial parts of three Romanian medicinal plants collected from Cluj county lemon balm (*Melissa officinalis*) (*Lavandula angustifolia*), and elderflower (*Sambucus nigra*). The studied plants were in fresh and dried form. The essential oils obtained by hydrodistillation from these plants were also studied.

HS-SPME is a simple and low-cost extraction technique which allows the obtaining of good results for the analysis of volatiles by GC-MS. In each plant we identified common compounds in varying proportions from the three samples (fresh, dry and essential oil) analysed.

For lemon balm and lavender, experimental data revealed the typical volatile constituent pattern for the *Lamiaceae* family: alpha-pinene, *Z*-beta-ocimene, *E*-beta-ocimene, beta-caryophyllene, beta-farnasene, humulene, etc.

In the elderflower plant, in the three samples, we observed a great variability for the classes of compounds obtained, such as monoterpenes, sesquiterpenes, esters, acids and hydrocarbons.

Specific markers for each type of plant indicate the originality/authenticity of floral. The profile of volatiles can be used as an indicator in the valorization of medicinal plants.

Majority phenolic compounds identified in the analysed samples were vanillic, sinapic, ferulic, and p-coumaric acids, while predominant flavonoids were rutin, quercetin and epicatechin.

The determination of volatile profile and polyphenol content from plant is important because it provides an assessment of their bioavailability according to their biological activity given by its majority compounds.

Regarding our three studied plants, under the three forms of presentation (fresh, dried and oil), the obtained results show that lemon balm is especially valued in dry form, lavender in all three forms, and elderberry in both fresh and dry form.

These researches will be useful for further studies in the formulation of new phytotherapeutic products, with applications in natural herb medicine.

EXPERIMENTAL SECTION

1. Plant material and chemicals

The fresh aerial part of *Melissa officinalis* (*Lamiaceae* family), *Lavandula angustifolia* (*Lamiaceae* family) and *Sambucus nigra* (*Adoxaceae* family) were collected during full flowering stage from Romanian flora (Cluj County), in June 2021. The aerial parts of these plants were submitted to research as follows: leaves for lemon balm, flowers and stems for lavender and flowers grouped in inflorescences for elderflower.

The analysis on fresh flowers was performed on the same day. The vegetal herbal material was air dried at room temperature in shade, in thin layers, in a well-ventilated place until they reached a constant weight (after 7 days). From 3.5 kg fresh plant 1 kg of dry matter was obtained.

GC-MS chemicals were purchased as follows: hexane 99% pure p.a from Chempur (Piekary Slaskie, Poland), methanol p.a from Penta (Prague, Czech Republic), alkane mixture containing C8-C20 alkanes (40 mg/mL in hexane) from Sigma Aldrich, St. Louis, MO, USA) and Helium 6.0 purity as carrier gas from Linde Gas (Romania).

HPLC chemicals: the standards of flavonoids (catechin, epicatechin, rutin, quercetin and luteolin), phenolic acids (gallic, vanillic, caffeic, p-coumaric, ferulic and sinapic) were purchased from Sigma-Aldrich Co. (St. Louis, MO, USA).

2. Profile analysis of volatile organic compounds

2.1 Headspace solid-phase microextraction (HS-SPME)

A 50/30 μm divinylbenzene-carboxen-polydimethylsiloxane (DVB/ CAR/PDMS) fibre purchased from Supelco (Bellefonte, PA, USA) was chosen to extract the volatile compounds from all samples. For each extraction, the

SPME fibre was preconditioned in the injection port of the Agilent 7890 gas chromatograph (Agilent Technologies, Inc., Palo Alto, CA, USA) at 220ºC for one hour.

Extraction of volatile organic compounds. In headspace vial, with a volume of 20 mL, 1 g of of aerial part of each plant (leaves for lemon balm, flowers and stems for lavender and flowers grouped in inflorescences for elderflower), fresh and dried and 8 mL distillated water together with 0.5 g of NaCl were placed. The sample bottle was preheated at 50ºC for 20 min. The fibre was then exposed to the sample headspace for 30 min prior to thermal desorption of the constituents at 240ºC into the splitless injection port of the GC-MS for 5 min.

2.2 Extraction of essential oil by hydrodistillation method (HD)

The aerial parts of the studied plants were dried in shadow at room temperature for one week, cut into pieces of size over the range 1–4 cm and grounded to a homogeneous powder. Extraction of es sential oils were carried out by hydrodistillation, using a Clevenger-type apparatus. Two distillations were carried out by boiling 100 g of dried material of each plant in 1 liter of distilled water during 3 hours. The yield of essential oils was determined in relation to the dry matter (1.1% w/w). The obtained essential oils were collected and dried over anhydrous $MgSO_4$, and stored in dark glass bottles at 4ºC prior to use.

2.3 GC-MS analysis

The quantification of volatile organic compounds was done using the GC-MS method presented in [90]. The volatile compounds were analysed using a GC-MS instrument, Model Agilent 7890 & 5975 Series MSD (Agilent Technologies, Inc., Palo Alto, CA, USA) equipped with a HP-5MS (5% phenyl)-methyl polysiloxane fused silica column Agilent (30 m $\times$ 0.25 mm $\times$ 0.25 µM) (Agilent Technologies, Inc., Palo Alto, CA, USA) Volatile compounds adsorbed on the SPME fibre were immediately thermally desorbed in the injector port of the GC and then separated on the GC column. Each essential oil sample (0.1 g) was diluted in n-hexane (1 mL) and a volume of 1 µl was injected into the GC instrument. GC-MS data were obtained in splitless mode under the following conditions: helium (He 6.0) as a carrier gas, flow rate of 1 mL/min, and injector temperature of 260ºC. The temperature programme was: oven temperature was set as 40ºC for 1 min with an increase of 5ºC/min up to 200ºC and from 200ºC to 240ºC the increase was with 20ºC /min and then it was maintained at 240ºC for 5 min. Mass spectra conditions: electron impact (EI+) mode, 70 eV, and ion source temperature of 230ºC. Mass spectra were

recorded over 50–500 a.m.u. range in scan mode. All analyses were carried out in triplicate. Data acquisition and processing were performed using MSD ChemStation software (Agilent Technologies,Inc., Palo Alto, CA, USA). NIST library (Agilent Technologies, Inc., Palo Alto, CA, USA) was used for identification/confirmation of the structure of compounds. In addition, an alkane standard solution C8–C20 (Sigma Aldrich, St. Louis, MO, USA) was used as analytical standard in the measurement of retention indices for the identification of alkanes co-existing in essential oils for GC-MS analysis. Based on this, the calculation of the linear retention indices (LRIs) was made, as well as the comparison of the experimental values with those reported in literature for similar chromatographic columns, in the same conditions. For the compounds with retention time $t_R < 5.690$ and $t_R > 29.978$, LRI_s was reported from Nist Library Spectra. The quantitative analysis was based on the percent area of each peak of the sample compounds.

3. Determination of polyphenolic compounds

HPLC analysis

The analysis of phenolic compounds (flavonoids and phenolic acids) was carried out by high-performance liquid chromatography (HPLC) on a Jasco Chromatograph (Jasco Corporation, Tokyo, Japan) equipped with UV/VIS detector and an injection valve equipped with a 20 µL sample loop (Rheodyne). The ChromPass software (Jasco Corporation, Tokyo, Japan) was used to control the HPLC system and to collect and process the chromatographic data.

Determination of the individual flavonoids and phenolic acids respectively was carried out using the HPLC gradient analysis method described by Filip et al. in [91]. The polyphenolic compounds were extracted in 80% methanolic solution. At 1 g of plant sample grinded was added 5 mL of extraction solution and was well stirred. Then, the mixture was sonicated for 60 minutes, centrifuged at 4500 rpm for 20 min and the supernatant was filtered through a 0.45 µm syringe filter and injected into HPLC. Separation of these compounds was carried out on the Lichrosorb RP-C18 column (25 × 0.46 cm) (Merck, Germany) at 22ºC column temperature and UV detection at 270 nm. The mobile phase was a mixture of methanol (A, HPLC grade) and 0.1% formic acid solution (Millipore ultrapure water). For the elution of compounds, the following gradient was applied: 0–10 min, linear gradient 10–25% A; 10–25 min, linear gradient 25–30% A; 25–50 min, linear gradient 35–50% A; 50–70 min, isocratic 50% A. The flow rate was 1 mL/min.

REFERENCES

1. A. K. Garg; M. Faheem; S. Singh; *Asian J. Plant Sci.,* **2021**, *11*, 19–21
2. Kavita; N. Singh; O. P. Sharma; *World J. Pharm. Res.,* **2022***, 8*, 197–199
3. S. Miraj; N. Azizi; S. Kiani; *Pharm. Lett.,* **2016***, 8,* 229–237
4. L. S. Muntean; M. Tămaş; S. Muntean; L. Muntean; M. M. Duda; D. I. Vârban, S. Florian; Tratat de plante medicinale cultivate şi spontane (Book with Cultivated and Spontaneous Medicinal Plants), 2nd edition, Risoprint Publishing House, Cluj-Napoca, ISBN 978-973-53-1873-4, **2016**, pp. 431
5. W. Zam; C. Quispe; J. Sharifi-Rad; M. D. López, M. Schoebitz, M. Martorell; F. Sharopov; P. V. T. Fokou; A. P. Mishra; D. Chandran; M. Kumar; J. T. Chen; R. Pezzani; *Front. Biosci. (Schol. Ed.)*, **2022**, *14*, 1–15
6. J. Ghazizadeh; S. Sadigh-Eteghad; W. Marx; A. Fakhari; S. Hamedeyazdan; M. Torbati; S. Taheri-Tarighi; M. Araj-Khodaei; M. Mirghafourvand; *Phytother. Res*., **2021**, *35*, 6690–6705
7. A. Sentkowska; M. Biesaga; K. Pyrzynska; *Int. J. Food Prop.,* **2015**, *18*, 2009–2014
8. Z Jalal; Y. El. Atki; B. Lyoussi; A. Abdellaoui; *Asian Pac. J. Trop. Biomed.*, **2015**, *5*, 458–461
9. G. Petrisor; L. Motelica; L. N. Craciun; O. C. Oprea; D. Ficai; A. Ficai; *Int. J. Mol. Sci*., **2022**, *23*, 3591, 1–25
10. A. Shakeri; A. Sahebkar; A. Abolfazl; B. Javadi; *J. Ethnopharmacol.,* **2016,** *188*, 204–228
11. A. S. Shawl; T. Kumar; S. Shabir; N. Chishti; Z. A. Kaloo; *Indian Perf*., **2005**, *49*, 235–238
12. T. Costea; A. M. Străinu; C. E. Gîrd; *Studia Univ. VG, SSV*, **2019**, *29*, 159–167
13. R. Prusinowska; K. B. Śmigielski; *Herba Pol.*, **2014**, *60*, 57–66
14. E. Kozuharova; V. Simeonov; D. Batovska; C. Stoycheva; H. Valchev; N. Benbassat; *Pharmacia*, **2023**, *70*, 395–403
15. M. Bogdan; S. Bungau; D. M. Tit; L. Copolovici; T. Behl; P. Otrisal; L. Aleya; G. Cioca; D. Berescu; D. Uivarosan; D. M. Copolovici; *Rev. Chim*. *(Bucharest)*, **2020**, *71*, 307–315
16. L. Hui; L. He; L. Huan; L. Xiaolan; Z. Aiguo; *Afr. J. Microbiol. Res.*, **2010**, *4*, 309
17. N. Dobros; K. D. Zawada; K. Paradowska; *Molecules*, **2023**, *28*, 256
18. C. Jianu; G. Pop; A. T. Gruia; F. G. Horhat; *Int. J. Agric. Biol*., **2013**, *15*, 772–776
19. P. Singh; H. Andola; M. S. M. Rawat; G. J. Pant; J. S. Jangwan; *J. Nat. Prod.*, **2015**, *5*, 268–272
20. A. C. Aprotosoaie; E. Gille; A. Trifan; V. S. Luca; A. Miron; *Phytochem. Rev*, **2017**, *16*, 761–799
21. E. Broșteanu; E. D. Hurjui; *J. Hortic. For. Biotech.*, **2017**, *21*, 62–67
22. M. Šoškić; D. Bojović; V. Tadic; *Studia UBB Chemia*, **2016**, *56*, 127–136

23. M. Popescu; D. Puiu; M. Mihalache; N. Bordei; A. D. Raiciu; I. Cristea; T. Galaon; L. F. Pascu, *International Symposium "The Environment and The Industry",* **2017***,* Proceedings Book, 206–212
24. E. Danila; D. A. Kaya; M. Patrascu; M. A. Kaya; S. Kumbakisaka; *Rev. Chim. (Bucharest),* **2018**, *69*; 2240–2244
25. N. Dobros; K. Zawada; K. Paradowska; *Antioxidants*, **2022**, *11*, 1–16
26. G. Stanciu; F. Aonofriesei; S. Lupsor; A. Popescu; R. Sirbu; *Rev. Chim. (Bucharest),* **2019**, *70*, 1800–1804
27. M. Mahboubi; *Adv. Tradit. Med.*, **2021**, *21*, 405–414
28. J. R. Santin; L. Benvenutti; M. F. Broering; R. Nunes; F. C. Goldoni; Y. B. K. Patel; J. A Souza; M. A. T. Kopp; P. Souza; R. Cassia; V. Silva; M. V. D. Pastor; A. B. Souza; L. D. Testoni; A. G. Couto; T. M. B. Bresolin; N. L. M. Quintao; *J. Ethnopharmacol.,* **2022**, *283*, 1–14
29. M. D. Vujanović; S. D. Đurović; M. M. Radojković; *Acta Period. Technol.*, **2021**, *52*, 229–237
30. P. Ferreira-Santos; H. Badim; Â. C. Salvador; A. J. D. Silvestre; S. A. O. Santos; S. M. Rocha; A. M. Sousa; M. O. Pereira; C. P. Wilson; C. M. R. Rocha; J. A. Teixeira; C. M. Botelho; *Biomolecules*, **2021**, *11*, 1–22
31. A. Laurutis; J. Liobikas; M. Stanciauskaite; M. Marksa; K. Ramanauskiene; D. Majiene; *Pharmaceutics*, **2022**, *14*, 1–15
32. A. Oniszczuk; M. Olech; T. Oniszczuk; K. Wojtunik-Kulesza; A. Wójtowicz; *Arab. J. Chem.*, **2019**, *12*, 4719–4730
33. C. Bitwell; S. S. Indra; C. Lukec; M. K. Kakoma; *Sci. African.*, **2023**, *19*, 1–20
34. R. Kant; A. Kumar; *Sustain. Chem. Pharm.,* **2022**, *30*, 1–20
35. A. A. Mohamed; B. M. Alotaibi; *J. Umm Al-Qura Univ. Appl. Sci.*, **2023**, *9*, 40–49
36. A. Iordache; M. Culea; C. Gherman; O. Cozar; *Nucl. Instrum. Methods Phys. Res*., **2009**, *267*, 338–342
37. J. D. Lozada-Ramírez; A. E. Ortega-Regules; L. R. Hernández; C. A. de Parrodi; *Appl. Sci.,* **2021**, *11*, 1–24
38. J. Zhao; M. Wang; S. G. Saroja; I. A. Khana; *J. Pharm. Biomed. Anal*., **2021**, *207*, 1–27
39. E. P. Siqueira; T M. A. Alves; C. L. Zani; *Rev. Bras. Farmacogn*., **2007**, *17*, 565–571
40. F. Belliardo; C. Bicchi; C. Cordero; E. Liberto; P. Rubiolo; B. Sgorbini; *J. Chromatogr. Sci.*, **2006**, *44*, 416–429
41. M. Ibrahim; M. Agarwal; G. Hardy; Y. Ren; *J. Biosci. Med*., **2017**, *5*, 13–31
42. L. M. Dascalu (Rusu); M. Moldovan; D. Prodan; I. Ciotlaus; R. Carpa; R. Ene; S. Sava; R. Chifor; M. E. Badea; *Studia UBB Chemia*, **2020**, *65*, 57–67
43. S. M. C. Mureșan; A. Dreanca; C. Repciuc; C. Dejescu; O. Rotar; R. A. Pop; S. Pantea; E. Pall; I. Ciotlaus; C. Sarosi; A. G. Mohan; M. Moldovan; L. Oana; *Appl. Sci*., **2023**, *13*, 1–20
44. H. Yu; C. Zhang; Y. Xie; J. Mei, J. Xie; *Membranes*, **2022**, *12*, 1–14
45. A. Wesołowska; P. Jadczak; D. Kulpa; W. Przewodowski; *Molecules*, **2019**, *24*, 1–13
46. G. Farré-Armengol; I. Filella; J. Llusià; J. Peñuelas; *Molecules*, **2017**, 22,1-9.

47. S.-U. Rehman; R. Latief; K. A. Bhat; M. A. Khuroo; A. S. Shawl; S. Chandra; *Arab. J. Chem.,* **2017**, *10*, S2 485–S2 490
48. F. Ieri; L. Cecchi; P. Vignolini; M. F. Belcaro; A. Romani*; Adv. Hort. Sci.*, **2017** *31*, 141–147
49. Ö. Çelebi; H. Fidan; I. Ilie; N. Petkova; I. Dincheva; V. Gandova; S. Stankov; A. Stoyanova; *Turk. J. Agric. For.,* **2023**, *47*, 67-78
50. F. Abdellatif; H. Boudjella; A. Zitouni; A. Hassani; *EXCLI J.*, **2014**, *13*, 772–781
51. A. A. Taherpour; H. Maroofi; Z. Rafiea; K. Larijani; *Nat. Prod. Res*., **2012**, *26*, 152–160
52. J. Sharifi-Rad; C. Quispe; J. Herrera-Bravo; M. Akram; W. Abbaass; P. Semwal; S. Painuli; D. A. Konovalov; M. A. Alfred; N. V. A. Kumar; M. Imran; M. Nadeem; B. Sawicka; P. Pszczółkowski; B. Bienia; P. Barbaś; S. Mahmud; A. Durazzo; M. Lucarini; A. Santini; M. Martorell; D. Calina; *Hindawi, Oxid. Med. Cell. Longev.,* **2021**, *2021*, 1–20
53. B. Cosge; A. Ipek; B. Gurbuz; *J. Appl. Biol. Sci.*, **2009**, *3*, 149–152
54. M. Kazemi; F. Esmaili; *J. Biol. Environ. Sci.*, **2014**, *8*, 111–113
55. M. Hanceanu; A. C. Aprostoaie; E. Gille; A. Poiata; C. Tuchilus; A. Spac; U. Stanescu; *Rev. Med. Chir. Soc. Med. Nat*., **2008**, *112*, 843-847
56. C. Da Porto; D. Decorti; *Planta Med.*, **2008**, *74*, 182–187
57. F. U. Afifi; R. Abu-Dahab; S. Beltran; B. B. Alcade; I. F. Abaza; *Arab. J. Med. Aromat. Plants.*, **2016**, *2*, 71–85
58. I. R. Suica-Bunghez; R. M. Senin; R. Stoica; *Biol. Life. Sci. Forum.*, **2022**, *20*, 1–15
59. T. Zagorcheva; S. D. Stanev; K. Rusanov; I. Atanassov; *J. Agri. Sci. Technol.*, **2013**, *5*, 459–462
60. J. Fu; J. Zhao; Y. Zhu; J. Tang; *Food Anal. Methods*, **2017**, *10*, 2373–2382
61. M. Torabbeigi; P. Aberoomand Azar; *Acta Chromatogr.*, **2013**, *3*, 571–579
62. G. E. S. Batiha; J. O. Teibo; L. Wasefet; H. M. Shaheen; A. P. Akomolafe; T. K. A. Teibo; M. Al-K. Hayder; A. I. Al-Garbeeb; A. Alexiou; M. Papadakis; *Naunyn-Schmiedeberg's Arch. Pharmacol.*, **2023**, *396*, 877–900
63. Â. C Salvador; A. J Silvestre; S. M. Rocha; *Food Chem*., **2017**, *229*, 276–285
64. K. R. Uhl; A. E. Mitchell; *ACS Food Sci. Technol.*, **2022,** *2*, 1535–1545
65. H. G. Ağalar; B. Demirci; F. Demirci; N. Kırımer; *Rec. Nat. Prod*., **2017**, *11*, 491–496
66. A. Hajdari; N. Kelmendi; G. Mustafa; B. Mustafa; D. Nebija; *Sci. World J.*, **2022**, *2022*, Article ID 2594195, 10 pages
67. M. Szymañski; M. Dudek-Makuch; E. Witkowska-Banaszczak; W. Bylka; A. Szymañski; *Pharm. Chem. J.,* **2020**, *54*, 496–503
68. T. Bajer; P. Bajerová; K. Ventura; *Nat. Prod. Commun.,* **2017**, 12, 1937–1942
69. N. Harbourne; E. Marete; J. C, Jacquier; D. O'Riordan; *'LWT Food Sci. Technol.,* **2009**, *42*, 1468–1473
70. I. Pereira; P. Severino; A. C. Santosa; A. M. Silva; E. B. Souto; *Colloids Surf. B: Biointerfaces*, **2018**, *171,* 566–578
71. V. M. Linck; A. L. da Silva; M. Figueiro; E. B. Caramao; P. R. H. Moreno; E. Elisabetsky; *Phytomedicine,* **2010**, *17*, 679–683

72. M. Miyashita; Y. Sadzuka; *Food Chem. Toxicol.,* **2013**, *53*, 174–179
73. F. N. Souto-Maior; F. L. de Carvalho; L. C. S. L. de Morais; S. M. Netto; D. P. de Sousa; R. N. de Almeida; *Pharmacol. Biochem. Behav.*, **2011**, *100*, 259–263
74. P. L. Santos; J. P. S. C. F. Matos; L. Picot; J. R. G. S. Almeida; J. S. S. Quintans; L. J. Quintans-Júnior; *Food Chem. Toxicol.,* **2019***, 123*, 459–469
75. T. Ganesan; M. Subban; L. D. B. C. Leslee; S. B. Kuppannan; P. Seedevi; *Biomass Convers. Biorefinery,* **2022**, 1–12
76. C. Ji Zheng; J.-S. Yooa; T.-G. Lee; H.-Y. Choc; Y.-H. Kimd; W.-G. Kima; *FEBS Letters*, **2005**, *579*, 5157–5162
77. V. Aparna; V. Dileep; P. K. Mandal; P. Karthe; C. Sadasivan; M. Haridas; *Chem. Biol. Drug Des.*, **2012**, *80*, 434–439
78. A. J. Eastman; R. E. Moore; S. D. Townsend; J. A. Gaddy; D. M. Aronoff; *Clin. Ther.,* **2021**, *43,* 265–278
79. L. I. Virchea; F. G. Gligor; A. Frum; M. Mironescu; N. I. Myachikova; C. Georgescu*; BIO Web of Conferences,* **2021,** *40*, 1–6
80. S. Miraj; Rafieian-Kopaei; S. Kiani; *J. Evid.-Based Complementary Altern. Med.*, **2017***, 22*, 385–394
81. J. Jaimez Ordaz; J. Martínez Hernánde; J. Ramírez-Godínez; A. Castañeda-Ovando; L. G. González-Olivares; E. Contreras-López; *Arch. Latinoam. Nutr.,* **2018**, *68*, 268–279
82. N. Dobros; K. Zawada; K. Paradowska; *Antioxidants (Basel)*, **2022**, *11*, 1–16
83. R. Tundis; F. Grande; M. A. Occhiuzzi; V. Sicari; M. R. Loizzo; A. R. Cappello; *J. Enzyme Inhib. Med. Chem.*, **2023**, *38*, 1–21
84. S. Özderin; *ACU J. For. Fac.*, **2022**, *23*, 96–101
85. G. I. Marovska; I. P. Hambarliyska; N. T. Petkova; I. G. Ivanov; I. N. Vasileva; A. M. Slavov; *Philipp J. Sci.,* **2023**, *152*, 861–870
86. A. Przybylska-Balcerek; T. Szablewski; L. Szwajkowska-Michałek; D. Swierk; R. Cegielska-Radziejewska; Z. Krejpcio; E. Suchowilska; L. Tomczyk, K. Stuper-Szablewska; *Molecules*, **2021**, *26*, 1–17
87. I. Osorio-Paz; X. Valle-Jiménez; R. Brunauer; S. Alavez*; J. Gerontol. Biol. Sci. Med. Sci.*, **2023**, *78*, 1100–1107
88. B. Salehi; L. Monzote; J. Sharifi-Rad; S. M. Ezzat; M. A. Salem; R. M. Merghany; N. M. El Mahdy; C. S. Kılıç; O. Sytar; M. Sharifi-Rad; F. Sharopov; N. Martins; M. Martorell; W. C. Cho; *ACS Omega*, **2020**, *5*, 11849–11872
89. E. Durukan; *Prog. Nutr.*, **2020**, *22*, 265–274
90. I. Ciotlaus; A. Balea; M. Pojar-Fenesan*; Rev. Chim. (Bucharest),* **2020**, *71*, 136–144
91. M. Filip; L. Silaghi-Dumitrescu; D. Prodan; C. Sarosi; M. Moldovan; I. Cojocaru; *Key Eng. Mater*. **2017**, *752*, 24–28

STUDIA UBB CHEMIA, LXIX, 1, 2024 (p. 147-161)
(RECOMMENDED CITATION)
DOI:10.24193/subbchem.2024.1.09

GC-MS COMPARATIVE CHEMICAL COMPOSITION OF ESSENTIAL OILS AND VOLATILE COMPOUNDS OF *ERYNGIUM PLANUM* L. USING CLASSICAL HYDRODISTILLATION, ULTRASOUND-ASSISTED HYDRODISTILLATION AND HEADSPACE SOLID-PHASE MICROEXTRACTION. ANTIMICROBIAL ACTIVITY[1]

Adriana-Maria ANDREICA[a,*], Ana BALEA[a], Maria POJAR-FENEȘAN[a], Rahela CARPA[b]

ABSTRACT. This study presents the extraction of essential oils and volatiles of *Eryngium planum* (*E. planum)* by classical hydrodistillation (HD), ultrasound-assisted hydrodistillation (UAHD) and headspace solid-phase microextraction (HS-SPME). The GC-MS analysis showed that the essential oil of *E. planum* obtained by UAHD contains the following majority compounds: β-copaene (11.97%), *cis*-chrysanthenyl acetate (10.14%), *(E)*-β-farnesene (6.79%), γ-gurjunene (6.53%), caryophyllene (5.73%), germacrene B (3.93%), (+)-*cis*-verbenol,2-methylpropionate (2.87%), β-selinene (2.73%). The GC-MS analysis showed that *E. planum* volatiles extracted by HS-SPME contains as majority compounds: *cis*-chrysanthenyl acetate (30.39%), *(E)*-β-farnesene (11.71%), γ-maaliene (7.69%), β-elemene (7.26%), caryophyllene (6.5%), β-selinene (4.72%), δ-cadinene (4.72%), β-copaene (4.61%), α-pinene (4.51%), γ-muurolene (2.98%). By using the UAHD method, the yield of *E. planum* oil was increased by 27.27% compared with the classical HD method. The essential oil of *E. planum* showed an excellent antimicrobial activity against *Escherichia coli* and *Staphylococcus aureus.*

Keywords: *Eryngium planum, essential oils, ultrasound-assisted hydrodistillation (UAHD), headspace solid-phase microextraction (HS-SPME), antimicrobial activity*

---

[1] *Presented at "The 27th International Symposium on Separation Sciences", 24-27 September 2023, Cluj-Napoca, Romania (ISSS 2023)*

[a] *Babeş-Bolyai University, "Raluca-Ripan" Institute for Research in Chemistry, 30 Fântânele str., RO-400294, Cluj-Napoca, Romania*

[b] *Babeş-Bolyai University, Faculty of Biology and Geology, Molecular Biology and Biotechnology Department, 1 Mihail Kogălniceanu str., RO-400084, Cluj-Napoca, Romania*

* *Corresponding author: adriana.andreica@ubbcluj.ro*

INTRODUCTION

The use of medicinal plants is becoming more popular in our society to prevent and treat many diseases [1–3].

Eryngium (E.) species that belong to the Apiaceae family are valuable for their use in traditional medicine due to their content in phenolic acids, saponins [4], flavonoids [5], coumarin derivatives [6, 7], essential oils [8] and acetylenes [9]. Some of these species such as *E. campestre* L., *E. caucasicum*, *E. creticum*, *E. foetidum* have been used in modern medicine for the treatment of several human diseases [10–13].

Eryngium planum L. (blue eryngo) is a perennial plant which in Romania was used in folk medicine in bronchitis, cough, wounds, urinary disorders, scars and burns as infusion [14]. It was also included in scientific studies for modern pharmaceuticals. The ethanolic extract of the aerial parts of *E. planum* was used for the treatment of active inflammatory periodontal disease in rats with potential therapeutic results [15]. The tincture from *E. planum* had dose-dependent anti-inflammatory properties in the rat paw-oedema test [16]. Ethanolic extracts from leaves and roots of three *Eryngium* species (*E. planum*, *E. campestre*, *E. maritimum*) showed a moderate antibacterial activity against *Staphylococcus aureus* and a significant antifungal activity [17]. The polyphenols and pectin from the aerial parts of the three mentioned *Eryngium* species were investigated, the results of their antimicrobial activity confirming that the tinctures obtained from these plants showed a high activity on *Pseudomonas aeruginosa,* a moderate activity against *Staphylococcus aureus* and *Staphylococcus epidermidis*, and no activity against *Escherichia coli* [18].

E. planum extracts are a source of biologically active compounds that have pharmaceutical and therapeutic potential applications. The bioactive compounds of *E. planum* were extracted with CO_2 under subcritical conditions using subterranean part of the plant [19], under supercritical conditions using aerial parts of the plant [20], by ultrasound-assisted alcoholic extraction using a sonication bath [21] or by methods such us percolation, maceration or microwave [22].

The composition of essential oils and the antimicrobial activity of some different *Eryngium* species such as *E. alpinum L., E. amethystinum L.* [23], *E. palmatum* [24], *E. campestre* [25], *E. maritimum L.* [26] were investigated by many researchers, but the essential oils from *Eryngium planum* were little investigated [27, 28]. These latter essential oils were obtained by classical hydrodistillation from different plant parts (inflorescences, stalk leaves, rosette leaves and root) and from *in vitro* shoot culture [28].

An improved hydrodistillation extraction was developed to isolate essential oil of fresh orange peel using a combination of hydrodistillation (HD) and ultrasound (UA) methods (Sono-Clevenger) [29]. Ultrasound-assisted hydrodistillation (UAHD) method was used to increase the extraction efficiency of essential oils from cinnamon barks [30]. Thus, the use of UAHD is a promising method for extracting essential oils from *E. planum*. Headspace solid-phase microextraction (HS-SPME) method was used for the isolation and determination of volatiles from plants [31, 32].

The aim of the present study was to investigate the composition of essential oils and volatile organic compounds from *Eryngium planum* aerial parts (stalk leaves, rosette leaves and inflorescences) extracted by the UAHD and HS-SPME methods and to compare these results with the chemical composition of the essential oil extracted by the classical hydrodistillation (HD). The antimicrobial activity of *E. planum* essential oil was tested against gram-negative and gram-positive strains. To our knowledge, the comparative chemical composition of essential oils and volatiles from *E. planum* using UAHD and HS-SPME extraction methods and their antimicrobial activity have not been previously reported.

RESULTS AND DISCUSSION

To improve this yield, before classical HD, an ultrasound treatment was done by an ultrasonic device (Hielscher UP200S). To obtain the essential oil by this UAHD method, we studied the influence of the amplitude size set at 20%, 40% and 60%, respectively, for a duty cycle of 0.5 for 60 minutes. The UAHD yields for the three amplitude sizes were as follows: 0.20% for 20% amplitude, 0.28% for 40% amplitude and 0.27% for 60% amplitude. Therefore, the best yield of 0.28% of the essential oil was obtained with UAHD method at the amplitude set at 40%. After the ultrasound treatment, the essential oil was extracted as in the classical HD. Therefore, by the UAHD method, the extraction process was improved with 27.27% compared to the classical HD method, as it is mentioned in literature for the yield of other essential oils [30, 33].

The chemical composition of the essential oils extracted by HD and UAHD methods and the volatiles extracted by HS-SPME method were analysed by gas chromatography-mass spectrometry (GC-MS). Identification and percentage area (normalisation) of compounds were based on NIST 20.L mass spectral library searching using the internal library search algorithm for the Agilent's ChemStation (GC-MS) and Agilent's MassHunter software. The identified groups of chemical compounds of *E. planum* oil obtained by UAHD

method were sesquiterpene hydrocarbons (50.46%), followed by oxygenated sesquiterpenes (21.33%), oxygenated monoterpenes (14.28%), monoterpenes hydrocarbons (1.22%) and other compounds (8.5%) (Table 1). The majority compounds of the oil were β-copaene (11.97%), *cis*-chrysanthenyl acetate (10.14%), *(E)*-β-farnesene (6.79%), γ-gurjunene (6.53%), caryophyllene (5.73%), germacrene B (3.93%), (+)-*cis*-verbenol,2-methylpropionate (2.87%), and β-selinene (2.73%). The chemical profile of the two types of essential oils obtained by UAHD and HD methods was comparable with some minor differences.

By both extraction methods were identified in *E. planum* plant 66 compounds (Table 1). In the essential oil obtained by UAHD method were identified 60 compounds (95.79%; not identified compounds from the positions 19, 37, 48, 61, 66; see Table 1) while in the essential oil obtained by classical HD method were identified 61 compounds (95.39%; not identified compounds from the positions 5, 12, 13, 24, 64; see Table 1). It can be mentioned that the nonidentified compounds by the two methods are complementary.

Thiem et al. [28] extracted by hydrodistillation for the first time the essential oils from different parts of *E. planum* plant and the chemical composition was analysed by GC-MS. The classes of compounds identified in oils obtained from stalk leaves, rosette leaves and inflorescences, respectively, were monoterpene hydrocarbons (42.0%, 28.4% and 12.9%, respectively), oxygenated monoterpenes (10.3%, 36.6% and 51.2%, respectively), sesquiterpene hydrocarbons (20.0%, 24.4% and 18%, respectively) and oxygenated sesquiterpenes (10%, 2.4%, and 7.7%, respectively). The majority classes of compounds identified in oil obtained from root were monoterpene hydrocarbons (4.0%), sesquiterpene hydrocarbons (3.1%) and polyacetylenes (64.4%).

Table 1. The chemical composition of the essential oils of *Eryngium planum* obtained by the UAHD and HD methods and analysed by GC-MS

No.	Compounds	Retention time (min)		Identification probability (%)		Normalised area (%)	
		UAHD*	HD**	UAHD	HD	UAHD	HD
1	***2***	***3***	***4***	***5***	***6***	***7***	***8***
1	Prenyl acetate (OC)	5.747	5.749	99.61	99.56	1.98	1.61
2	α-Pinene (MTH)	5.991	5.993	98.78	98.80	1.22	0.59
3	Oxalic acid, cyclohexyl pentyl ester (OC)	6.563	6.564	84.86	82.94	0.31	0.28
4	Octanal (OC)	7.229	7.231	98.87	99.32	0.38	0.34
5	*cis*-3-Hexenyl iso-butyrate (OC)	-	9.152	-	86.88	-	0.24
6	*cis*-Chrysanthenyl acetate (OMT)	12.070	12.075	97.73	97.63	**10.14**	**9.34*** **
7	Benzaldehyde, 2,4,6-trimethyl- (OC)	13.053	13.055	97.02	96.95	0.71	0.66
8	Benzaldehyde, 2,4,5-trimethyl- (OC)	13.742	13.744	98.73	98.67	1.37	1.22
9	Copaene (STH)	14.075	14.076	97.94	97.95	0.63	0.67

No.	Compounds	Retention time (min)		Identification probability (%)		Normalised area (%)	
		UAHD*	HD**	UAHD	HD	UAHD	HD
1	***2***	***3***	***4***	***5***	***6***	***7***	***8***
10	β-Elemene (STH)	14.319	14.322	97.45	97.46	2.29	2.73
11	Caryophyllene (STH)	14.828	14.834	99.35	99.22	**5.73**	**6.05**
12	(+)-*epi*-Bicyclosesquiphellandrene (STH)	-	14.962	-	83.55	-	0.41
13	Sesquithujene (STH)	-	14.993	-	77.71	-	0.24
14	Himachalol (OST)	15.073	15.074	75.94	86.56	0.73	0.74
15	Aromadendrene (STH)	-	15.135	-	77.59	-	0.28
16	*(E)*-β-Farnesene (STH)	15.274	15.283	96.25	96.10	**6.79**	**7.11**
17	Humulene (STH)	15.366	15.367	97.22	97.09	1.47	1.51
18	β-Cubebene (STH)	15.445	15.447	84.80	88.10	0.64	0.62
19	β-Ylangene (STH)	15.634	-	86.98	-	1.24	-
20	γ-Selinene (STH)	15.686	15.690	95.06	96.34	1.45	1.51
21	β-Copaene (STH)	15.803	15.810	95.16	95.16	**11.97**	**11.73**
22	β-Selinene (STH)	15.890	15.896	97.60	97.25	**2.73**	**2.82**
23	γ-Gurjunene (STH)	16.030	16.035	96.15	96.16	**6.53**	**6.87**
24	*trans*-Verbenyl isovalerate (OMT)	-	16.123	-	73.34	-	0.37
25	Guaia-10(14),11-diene (STH)	16.188	16.195	96.09	96.10	2.58	2.5
26	γ-Cadinene (STH)	16.278	16.280	91.94	92.51	0.34	0.35
27	δ-Cadinene (STH)	16.387	16.389	94.63	95.03	1.13	1.22
28	Elemol (OST)	16.778	16.781	91.43	92.24	0.33	0.36
29	14-Hydroxycaryophyllene (OST)	16.867	16.869	89.53	90.19	0.81	0.77
30	Germacrene B (STH)	16.973	16.977	98.93	98.77	**3.93**	**4.14**
31	Mint oxide (OST)	17.111	17.114	86.80	86.84	0.41	0.39
32	(+)-Spathulenol (OST)	17.262	17.264	98.83	98.90	2.05	1.84
33	Isoaromadendrene epoxide (OST)	17.361	17.363	95.09	94.52	1.71	1.54
34	2,2,4-Trimethyl-1,3-pentadienol diisobutyrate (OC)	17.424	17.426	76.41	74.04	0.66	0.58
35	Salvial-4(14)-en-1-one (OST)	17.515	17.517	91.99	90.56	1.04	0.95
36	Longipinocarveol, trans- (OST)	17.730	17.732	89.92	89.19	1.24	1.14
37	2,4a,8,8-Tetramethyldecahydro cyclopropa[d]naphthalene (STH)	17.880	-	74.56	-	0.37	-
38	tau-Cadinol (OST)	17.939	17.941	91.21	91.52	1.13	1.11
39	(+)-*cis*-Verbenol, 2-methylpropionate (OMT)	18.072	18.076	80.17	80.20	**2.87**	**3.19**
40	(-)-Spathulenol (OST)	18.114	18.113	83.20	70.47	0.31	0.3
41	α-Cadinol (OST)	18.166	18.167	71.64	72.08	0.24	0.24
42	γ-Costol (OST)	18.220	18.221	86.68	86.81	0.82	0.82
43	Megastigma-4,6(Z),8(Z)-triene (OC)	18.284	18.288	74.10	75.37	0.39	0.4
44	Muurola-4,10(14)-dien-1.beta.-ol (OST)	18.351	18.355	77.06	71.17	1.01	0.98
45	Neointermedeol (OST)	18.384	18.386	70.45	73.56	1.02	1.15
46	1-Isopropyl12-oxatetracyclo [5.2.1.1(2,6).1(9,11)]	18.536	18.538	72.66	74.36	0.54	0.52

No.	Compounds	Retention time (min)		Identification probability (%)		Normalised area (%)	
		UAHD*	HD**	UAHD	HD	UAHD	HD
1	***2***	***3***	***4***	***5***	***6***	***7***	***8***
	Dodecane (OC)						
47	Isospathulenol (OST)	18.585	18.587	87.04	86.36	1.17	1.21
48	α-Muurolene-14-hydroxy-(OST)	18.735	-	79.13	-	0.45	-
49	(1R,7S)-Germacra-4(15),5,10(14)-trien-1β-ol (OST)	18.806	18.809	94.81	94.56	1.65	1.65
50	Spiro[2.5]octane,3,3-dimethyl-2-(1-buten-3-on-1-yl)- (OC)	18.875	18.879	76.22	75.13	0.27	0.25
51	β-Costol (OST)	19.100	19.102	90.04	90.24	1.48	1.54
52	6-Isopropenyl-4,8a-dimethyl-1,2,3,4,5,6,7,8,8a-octahydronaphthalen-2-ol (OST)	19.212	19.213	89.28	90.53	0.43	0.43
53	α-Costol (OST)	19.258	19.262	86.82	86.48	0.69	0.77
54	Aristolene epoxide (OST)	19.303	19.306	89.55	91.28	1.22	1.32
55	Tricyclo[5.2.2.0(1,6)undecan-3-ol, 2-methylene-6,8,8-trimethyl- (OST)	19.347	19.350	89.59	90.52	0.28	0.3
56	α-Mintsulfide (STH)	19.583	19.586	77.73	77.63	0.36	0.35
57	β-Oplopenone (OST)	19.624	19.625	79.70	80.38	0.42	0.45
58	Ylangenol (OST)	19.728	19.729	69.69	73.74	0.31	0.34
59	7R,8R-8-Hydroxy-4-isopropylidene-7-methylbicyclo [5.3.1]undec-1-ene (OST)	19.901	19.903	83.17	87.40	0.35	0.37
60	Spiro[4.5]decan-7-one,1,8-dimethyl-8,9-epoxy-4-isopropyl- (OC)	19.935	19.937	75.20	82.40	0.38	0.44
61	Eremophilone (OST)	19.998	-	73.93	-	0.31	-
62	Neophytadiene (OC)	20.665	20.664	92.11	92.25	0.26	0.26
63	*cis*-Chrysanthenyl propionate (OMT)	20.803	20.804	82.55	82.40	1.27	1.54
64	n-Hexadecanoic acid (OC)	-	22.158	-	88.53	-	0.27
65	(+)-Falcarinol (OC)	23.060	23.063	96.93	97.75	0.97	1.47
66	1-Iodo-2-methylundecane (OC)	23.642	-	84.14	-	0.28	-
Total identified (TI)						**95.79**	**95.39**
Monoterpene hydrocarbons (MTH)						1.22	0.59
Oxygenated monoterpenes (OMT)						14.28	14.44
Sesquiterpene hydrocarbons (STH)						50.18	51.11
Oxygenated sesquiterpenes (OST)						21.61	20.71
Other compounds (OC)						8.50	8.54
Oil yield						**0.28**	**0.22**

*UAHD – ultrasound-assisted hydrodistillation; **HD – hydrodistillation;
***Majority compounds are written in bold.

By the HS-SPME method, 21 volatile organic compounds of *E. planum* were extracted.

The major groups of the identified compounds were sesquiterpene hydrocarbons and oxygenated monoterpenes (Table 2). The following majority compounds identified were: *cis*-chrysanthenyl acetate (30.39%), *(E)*-β-farnesene (11.71%), γ-maaliene (7.69%), β-elemene (7.26%), caryophyllene (6.5%), β-selinene (4.72%), δ-cadinene (4.72%), β-copaene (4.61%), α-pinene (4.51%), and γ-muurolene (2.98%). γ-Maaliene and γ-muurolene were not found in the essential oils extracted by UAHD and HD methods.

Table 2. Chemical composition of volatiles of *Eryngium planum* obtained by HS-SPME and analysed by GC-MS

No.	Compounds	Retention time (min)	Identification probability (%)	Normalised area (%)
1	***2***	***3***	***4***	***5***
1	α-Pinene (MTH)	5.445	98.54	**4.51***
2	*cis*-Chrysanthenyl acetate (OMT)	12.053	98.35	**30.39**
3	α-Cubebene (STH)	13.603	95.61	0.64
4	Copaene (STH)	14.069	96.85	1.34
5	β-Elemene (STH)	14.314	98.31	**7.26**
6	Caryophyllene (STH)	14.819	99.47	**6.5**
7	Isogermacrene D (STH)	14.968	94.33	1.29
8	Aromadendrene (STH)	15.128	94.76	0.99
9	*(E)*-β-Farnesene (STH)	15.264	97.15	**11.71**
10	Humulene (STH)	15.360	96.35	1.05
11	γ-Muurolene (STH)	15.680	97.09	**2.98**
12	β-Copaene (STH)	15.782	86.56	**4.61**
13	4a,8-Dimethyl-2-(prop-1-en-2-yl)-1,2,3,4,4a,5,6,7-octahydronaphthalene (STH)	15.821	84.99	1.11
14	β-Selinene (STH)	15.880	97.97	**4.72**
15	γ-Maaliene (STH)	16.009	97.06	**7.69**
16	(+)-Valencene (STH)	16.157	94.56	0.72
17	γ-Cadinene (STH)	16.272	98.74	2.03
18	δ-Cadinene (STH)	16.388	97.31	**4.72**
19	α-Cadinene (STH)	16.618	95.78	1.06
20	Germacrene B (STH)	16.962	98.17	0.99
21	1-Hexadecanol (OC)	23.502	92.88	0.81
Total identified (TI)				**97.12**
Monoterpene hydrocarbons (MTH)				4.51
Oxygenated monoterpenes (OMT)				30.39
Sesquiterpene hydrocarbons (STH)				61.41
Oxygenated sesquiterpenes (OST)				-
Other compounds (OC)				0.81

*Majority compounds are written in bold.

The main classes of compounds identified by GC-MS in the essential oils and volatiles obtained by the UAHD, HD and HS-SPME methods from the aerial parts of *E. planum* plant, are presented in Figure 1.

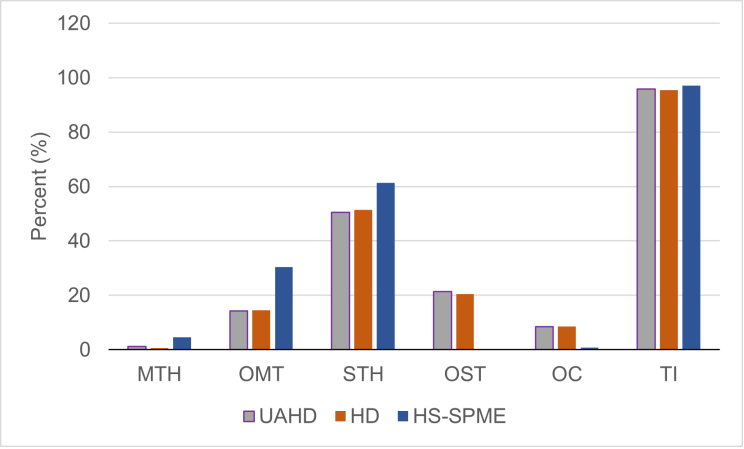

Figure 1. Main classes of compounds found by GC-MS in the essential oils and volatiles obtained by the UAHD, HD and HS-SPME extraction methods: MHT – Monoterpene hydrocarbons; OMT – Oxygenated monoterpenes; STH – Sesquiterpene hydrocarbons; OST – Oxygenated sesquiterpenes; OC – Other compounds; TI – Total identified.

In Figure 1, differences observed between the HS-SPME *versus* the UAHD and HD extraction methods consist in the absence of the oxygenated sesquiterpenes (OST) in the volatiles extracted by HS-SPME method, but also in the presence of the sesquiterpene hydrocarbons (STH) and oxygenated monoterpenes (OMT) after the extraction by all three methods, more increased in the first case. Regarding the total identified compounds by GC-MS after extraction by these three methods, it can state that the percentage values are very close.

The majority compounds identified by GC-MS in the essential oils and volatiles obtained by the UAHD, HD and HS-SPME methods from the aerial parts of *E. planum*, are presented in Figure 2. Differences observed between the UAHD and HD extraction methods were small but should be mentioned an increase in *cis*-chrysanthenyl acetate. Differences observed between the HS-SPME *versus* UAHD and HD extraction methods consist in the presence of γ-maaliene and γ-muurolene in the volatiles extracted by HS-SPME method. *Cis*-chrysanthenyl acetate followed by *(E)*-β-farnesene were the main compounds extracted by the HS-SPME method, while β-copaene

followed by *cis*-chrysanthenyl acetate were the main compounds extracted by both UAHD and HD methods. In the literature [28], the essential oils of *E. planum* were extracted by HD method from stalk leaves, rosette leaves, inflorescences and root. The majority compounds identified in stalk leaves and rosette leaves were α-pinene, β-pinene, β-phellandrene, limonene, camphene. The majority compounds identified in inflorescences and root were *cis*-chrysanthenyl acetate and *(Z)*-falcarinol. The chemical composition of the essential oil from aerial parts was quite different from that previously reported for essential oils from different parts of the plant. This variation in the chemical composition of essential oils can be attributed to the plant organ, soil composition, climate, etc. [34].

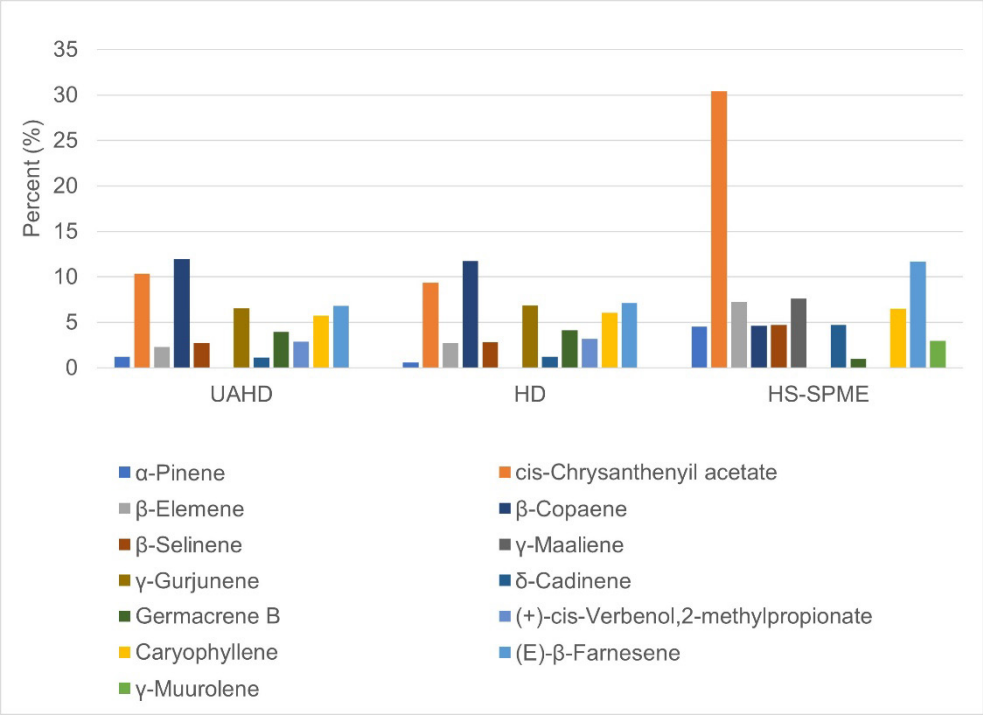

Figure 2. Majority compounds (%) found by GC-MS in the essential oils and volatiles obtained by the UAHD, HD and HS-SPME extraction methods

The essential oil of *E. planum* obtained by the UAHD method was chosen for antimicrobial evaluation because the UAHD extraction yield was

improved by 27.27%, the total identified compounds increased by 0.4%, and the highest increase for one of the main compounds was 0.8%, namely for *cis*-chrysanthenyl acetate.

Antimicrobial activity evaluation of UAHD E. planum essential oil

The antimicrobial activity of extracts was described for some *Eryngium* species in literature against gram-negative and gram-positive bacteria, some species of fungi, yeast and viruses [19, 35].

In this work, the antimicrobial activity of *E. planum* essential oil was tested against gram-negative and gram-positive bacteria using the agar-well diffusion method. After the end of the incubation period at 37ºC, the inhibition zones (mm) of the tested bacterial strains were determined. It was observed that in both bacterial strains, *E. planum* essential oil inhibited growth and the magnitude of the diameter of inhibition varied with the test strain. In the case of *Escherichia coli ATCC 25922*, the gram-negative bacterium strain indicated a very high inhibition reaching the inhibition diameter of 40 mm (Figure 3).

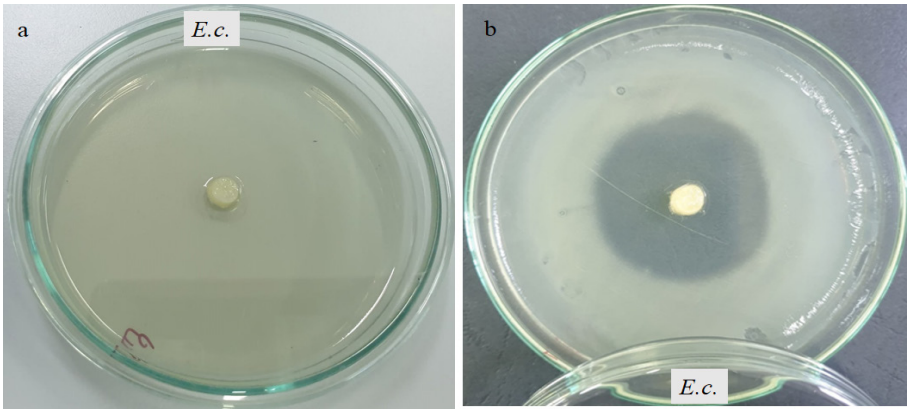

Figure 3. Effect of *Eryngium planum* essential oil on *Escherichia coli* (*E.c.*) ATCC 25922 (gram-negative bacterium strain): a) initial moment; b) after inhibition period

In the case of *Staphylococcus aureus ATCC 25923*, the gram-positive bacterium strain indicated a very high inhibition of the tested oil with an average diameter of 35 mm (Figure 4).

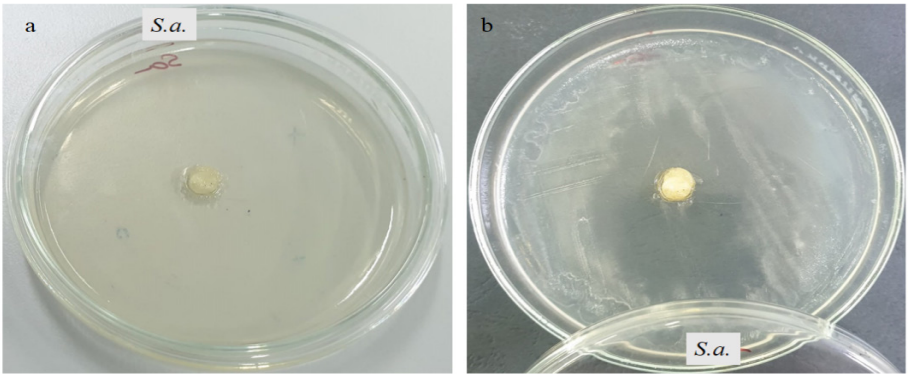

Figure 4. Effect of *Eryngium planum* essential oil on *Staphylococcus aureus* (*S.a.*) ATCC 25923 (gram-positive bacterium strain): a) initial moment; b) after inhibition period

Following these experiments, we can conclude that *E. planum* essential oil exhibits excellent antimicrobial activity against gram-negative and gram-positive bacterial strains.

CONCLUSIONS

The present study reports a comparative chemical composition of essential oils and volatile organic compounds extracted from *Eryngium planum* by different methods, as well as the antimicrobial activity capacity of the oil.

Methods such as classical hydrodistillation, ultrasound-assisted hydrodistillation, and headspace solid-phase microextraction were used to extract essential oils and volatiles from the aerial parts of *Eryngium planum*. The basic chemical composition of these essential oils extracted by the UAHD and HD methods was similar. Using the UAHD method, the oil yield from *E. planum* increased by 27.27% compared to the classical HD method, fact due to the optimisation of the extraction method by adding an ultrasound pretreatment.

The GC-MS analysis showed that β-copaene, a sesquiterpene hydrocarbon, was the majority compound of the *E. planum* oil obtained by both UAHD (11.97%) and HD (11.73%) methods. Within the *E. planum* volatiles extracted by HS-SPME method, *cis*-chrysanthenyl acetate (30.39%), an oxygenated monoterpene, was the majority compound.

The antimicrobial activity of *E. planum* essential oil extracted by UAHD was tested against gram-negative *(Escherichia coli)* and gram-positive *(Staphylococcus aureus)* bacterial strains using the agar-well diffusion method. The results obtained showed the capability of this essential oil to have excellent antimicrobial activity against both gram-negative and gram-positive bacterial strains.

The essential oil of *E. planum* due to its antimicrobial activity is promising for use and benefits in natural medicine, aromatherapy, cosmetics.

EXPERIMENTAL SECTION

Materials

The samples of *E. planum* plant were collected in July 2023 during the flowering period from Florești village, Cluj County, Romania. These plant materials were also identified at the "Alexandru Borza" Botanical Garden from Cluj-Napoca, and the voucher specimen (no. 673003) was deposited in the CL Herbarium, Babeș-Bolyai University, Cluj-Napoca. Aerial parts (stalk leaves, rosette leaves and inflorescences) of *E. planum* were shade-dried at room temperature and ground to powder before the extraction procedures.

Extraction of essential oil by classical HD

Essential oil of *E. planum* was extracted by hydrodistillation using a Clevenger-type apparatus. 100 g of dried aerial parts of *E. planum* were boiled in 1 L distilled water for 3 hours until no essential oil was released. The collected essential oil was dried over anhydrous $MgSO_4$ and stored in dark vials at 4ºC until use.

Extraction of essential oil by UAHD

Essential oil of *E. planum* was extracted by ultrasound-assisted hydrodistillation in two stages: (i) ultrasound treatment using a Hielscher UP200S (24 kHz, 200 W) ultrasonic device equipped with a titanium sonotrode of 14 mm (Hielscher Ultrasonics GmbH, Germany); (ii) hydrodistillation using a Clevenger-type apparatus. *E. planum* powder (50 g) was mixed with 0.5 L distilled water then the sonotrode was immersed in the sample at room temperature. The amplitude (power level of ultrasound) was set at 40%. The duty cycle was set at 0.5. After 60 minutes of ultrasound treatment, the sample was subjected to hydrodistillation for 3 hours. The collected essential oil followed the same procedure as in the case of classical HD extraction.

Extraction of volatiles by HS-SPME

A SPME fibre for manual use and a DVB/CAR/PDMS (50 µm DVB layer; 30 µm CAR/PDM layer) fibre (Supelco, USA) used. The collection of volatiles from the *E. planum* sample was done from the head-space on the SPME fibre: 1 g sample, 8 mL distilled water and 0.5 g NaCl were placed in a 20 mL vial at a temperature of 55ºC for 10 min, followed by adsorption of volatile organic compounds on the SPME fibre for 30 min. These compounds were immediately thermally desorbed in the injector port of GC-MS equipment for their separation on column and MS identification.

Gas chromatography-mass spectrometry (GC-MS) analysis

For GC-MS analysis of essential oils was used an Agilent 8890/ 5977B/2019 (Agilent Technologies, Santa Clara, California, USA) equipment. The analysis was performed in scan mode using a capillary column HP5-MS UI:2556856 (30 m × 250 µm × 0.25 µm) (Agilent Technologies, Santa Clara, California, USA) with Helium (grade 6.0) as carrier gas (Linde Gaz, Cluj-Napoca, Romania) at a flow rate of 1 mL/min. Temperature programme was: 40ºC hold 1 min, ramp to 220ºC with 8ºC/min rate, and then ramped up to 240ºC with 20ºC/min rate and hold at 240ºC for 5 min. The injection volume was 1µL. The GC/MS operated under the following temperature conditions: injector, 200ºC; MS transfer line, 280ºC; MS source, 230ºC and MS Quad 150ºC. Data acquisition and processing were performed using Agilent MassHunter Workstation Software (Agilent Technologies, Santa Clara, California, USA) which allows the qualitative and percentage area evaluation of the analysed compounds. For the structure identification/confirmation of components, the NIST library 20.L (Agilent Technologies, Santa Clara, California, USA) was used.

Antimicrobial activity evaluation

The antimicrobial activity of the *E. planum* essential oil was tested regarding *Gram-negative bacteria, Escherichia coli (ATCC 25922)* and *Gram-positive bacteria, Staphylococcus aureus (ATCC 25923)* at the Microbiology Laboratory, Faculty of Biology and Geology, Babeș-Bolyai University, Cluj-Napoca, Romania using the agar-well diffusion method [36]. Each bacterial strain was grown for 24 hours, at 37ºC, on Nutrient Agar medium [37]. Then a dilution of 0.5 McFarland turbidity standard according to EUCAST 2013 was made from each bacterial strain in sterile physiological serum [38]. From these dilutions, each Petri dish is inoculated with the help of a sterile swab spreading over the entire surface of the solid culture medium (Mueller Hinton-Oxoid).

Agar-well diffusion method. Petri dishes with Mueller Hinton Agar (M-H Agar) medium (Thermo Fisher Scientific, UK) were inoculated with each bacterial strain and left at 37ºC, for 15 min to infiltrate. Subsequently, 6 mm diameter wells were carved into the agar using a cut sterile pipette tip. The wells were then filled with sterile cotton beads, each bead being loaded with 100 µL of the *E. planum* essential oil. The plates were incubated at 37ºC, for 24 hours. The zones of inhibition were then measured, using a zone of inhibition scale [36]. All assays were performed in triplicate, under aseptic conditions and the mean value was calculated.

REFERENCES

1. R. K. Gautan; K. Roy; G. Thapa; D. Arora; S. Parashar; B. Gurung; L. C. Deb; *Indian J. Pharm. Sci.*, **2020,** *82*, 741–765.
2. M. Altamish; M. Khan; M. S. Baig; B. Pathak; V. Rani; J. Akhtar; A. A. Khan; S. Ahmad; A. Krishnan; *ACS Omega*, **2022**, *7*, 24048–24065.
3. E. P. Pérez-Muñoz; M. Antunes-Ricardo; M. Martinez-Ávila; D. Guajardo-Flores; *Front. Nutr.*, **2022**, *9*, 878306.
4. Z. Zhang; S. Li; S. Ownby; P. Wang; W. Yuan; W. Zhang; R. Scott Beasley; *Phytochemistry*, **2008**, *69*, 2070–2080.
5. T. Kartnig; J. Wolf; *Planta Med.*, **1993**, *59*, 285–285.
6. C.A. J. Erdelmeier; O. Sticher; *Planta Med.*, **1985**, *51*, 407–409.
7. M. Pinar; M. P. Galan; *J. Nat. Prod.*, **1985**, *48*, 853–854.
8. J. J. Brophy; R. J. Goldsack; L. M. Copeland; J. Palá-Paúl; *J. Essent. Oil Res.*, **2003**, *15*, 392–397.
9. J. Lam; L. P. Christensen; T. Thomasen; *Phytochemistry*, **1992**, *31*, 2881–2882.
10. S. Bouzidi; N. Benkiki; M. Hachemi; H. Haba; *Current Bioactive Compounds*, **2017**, *13*, 340–346.
11. S. H. Eslami; M. A. Ebrahimzadeh; A. H. Moghaddam; S. F. Nabavi; N. Jafari; S. M. Nabavi; *Arch. Biol. Sci.*, **2011**, *63*, 157–160.
12. S. Nusair; M. Ahmad; T. EL-Elimat; K. Al-Essa; L. Abu-Qatouseh; R. Khasawneh; *J. Res. Pharm.*, **2022**, *26*, 770–780.
13. X. Zhang; J. Chen; S. Zhou & H. Zhao; *Nutrition and Cancer*, **2022**, *74*, 2996–3006.
14. I. Tiță; G. D. Mogoșanu; M. G. Tiță; **2009**, *Farmacia*, *57*, 141–156.
15. S. Conea; A. E. Pârvu; M. A. Taulescu; L. Vlase; *Dig. J. Nanomater. Bios.,* **2015**, *10*, 693–704.
16. S. Conea; O. Vostinaru, L. Vlase; *Dig. J. Nanomater. Bios.,* **2014***, 9,* 1039–1045.
17. B. Thiem; O. Goślińska; M. Kikowska; J. Budzianowski; *Herba Polonica*, **2010**, *56*, 52–58.
18. S. Conea; L. Vlase; I. Chirilă; *Cellulose Chem. Technol.*, **2016**, *50*, 473–481.

19. A. B. Arykbayeva; G. O. Ustenova; K. O. Sharipov; U. T. Beissebayeva; I. E. Kaukhova; A. Myrzabayeva; N. G. Gemejiyeva; *Int. J. Biomater.*, **2023**, *2023*, 4702607.
20. E. M. Suleimenov; S. Machmudah; M. Sasaki; M. Goto; *Chem. Nat. Compd.*, **2010**, *46*, 826–827.
21. G. Paun; E. Neagu; V. Moroeanu, C. Albu; S. Savin; G. L. Radu; *Biomed Res. Int.*, **2019**, *2019*, 3692605.
22. E. Shabani; M. Mahmoudisourestani; M. Y. Mahen; *Iran. J. Plant Physiol.*, **2022**, *12*, 4223–4230.
23. D. Kremer; M. Z. Končić; I. Kosalec; I. J. Košir; T. Potočnik; A. Čerenak; S. Srečec; V. Dunkić; E. Vuko; *Horticulturae*, **2021**, *7*, 364.
24. M. Marcetic; S. Petrovic; M. Milenkovic; Lj. Vujisic; V. Tesevic; M. Niketic; *Chem. Nat. Comp.*, **2014**, *49*, 1140–1142.
25. A. Medbouhi; F. Benbelaïd; N. Djabou; C. Beaufay; M. Bendahou; J. Quetin-Leclercq; A. Tintaru; J. Costa; A. Muselli; *Molecules*, **2019**, *24*, 2575.
26. O. Elkiran; C. Avsar; A. Veyisoglu; E. Bagci; *J. Essent. Oil-Bear. Plants*, **2023**, *26*, 566–575.
27. E. Korbel; A. Bighelli; A. Kurowska; D. Kalemba; J. Casanova; *Nat. Prod. Commun.*, **2008**, *3*, 113–116.
28. B. Thiem; M. Kikowska; A. Kurowska; D. Kalemba; *Molecules*, **2011**, *16*, 7115–7124.
29. D. Pingret; A. S. Fabiano-Tixier; F. Chemat; *Food Anal. Methods*, **2014**, *7*, 9–12.
30. G. Chen; F. Sun; S. Wang; W. Wang; J. Dong, F. Gao; *Chin. J. Chem. Eng.*, **2021**, *36*, 38–46.
31. C. Xing; C. Qin; X. Li; F. Zhang; R. J. Linhardt; P. Sun; A. Zhang; *LWT-Food Sci. Technol.*, **2019**, *104*, 38–44.
32. A. A. Taherpour; S. Khaef; A. Yari; S. Nikeafshar; M. Fathi; S. Ghambari; *J. Anal. Sci. Technol.*, **2017**, *8*, 11.
33. M. Vinatoru; *Ultrason. Sonochem.*, **2001**, *8*, 303–313.
34. M. G. Miguel; J. Duarte; A. C. Figueiredo, J. G. Barroso, L. G. Pedro; *J. Essent. Oil Res.*, **2005**, *17*, 422–426.
35. S. A. Erdem; S. F. Nabavi; I. E. Orhan; M. Daglia; M. Izadi; S. M. Nabavi; *DARU J. Pharm. Sci.*, **2015**, *23*, 53.
36. R. Carpa; M. Drăgan-Bularda; V. Muntean; Microbiologie Generală Lucrări Practice (General Microbiology, Practical Works), Cluj University Press Publishing House, **2014**.
37. R. M. Atlas; *Handbook of Microbiological Media*, 4th ed., CRC Press, New York, **2010**.
38. R. Leclercq; R. Canton; D. F. J. Brown; C. G. Giske; P. Heisig; A. P. MacGowan; J. W. Mounton; P. Nordmann; A. C. Rodloff; G. M. Rossolini; C. J. Soussy; M. Steinbakk; T. G. Winstanley; G. Kahlmeter; *Clin. Microbiol. Infect.*, **2013**, *19*, 141–160.

STUDIA UBB CHEMIA, LXIX, 1, 2024 (p. 163-174)
(RECOMMENDED CITATION)
DOI:10.24193/subbchem.2024.1.10

DETERMINATION OF CHEMICAL COMPOSITIONS, ANTIOXIDANT, DNA CLEAVAGE AND BINDING PROPERTIES OF *VINCETOXICUM TMOLEUM* EXTRACT

Emine KILIÇKAYA SELVI[a,*], Nilgün GÜLER[a], Seher GÜVEN[b], Serdar MAKBUL[b]

ABSTRACT. In the present study, phenolic compounds, antioxidant activities, DNA cleavage and binding effects of *Vincetoxicum tmoleum* (Vt) collected from west of Anatolia (Manisa city) were investigated. Antioxidant potentials of the extracts were characterized with their total phenolic and flavonoid contents, DPPH (2,2-diphenyl-1-picrylhydrazyl), ABTS (2,2′-azino-bis (3-ethylbenzothiazoline-6-sulfonic acid), and FRAP (ferric reducing antioxidant power assay) tests. Besides, the DNA cleavage and binding features of *V. tmoleum* extract were studied using pBR322 DNA and CT-DNA, respectively. Phenolic compounds of the extract were analyzed by high performance liquid chromatography (HPLC-DAD). As a result, *V. tmoleum* methanol extract was found to have the high total phenolic and total flavonoid content and antioxidant effect. Strong positive correlations were also found between DPPH and TFC ($r = 0.995$; $p < 0.01$), and TPC ($r = 0.989$;$p < 0.01$), ABTS ($r = 0.994$;$p < 0.01$) and FRAP($r=0,995$; $p < 0.01$). Methanol extract of *V. tmoleum* had large amounts of *p*-coumaric acid, vanillic acid and catechin. While *V. tmoleum* samples showed weak DNA cleavage activity, they showed DNA binding activity at 50 µM concentration, that is, the potential to be an intercalation agent in this concentration.

Keywords: *Vincetoxicum tmoleum, antioxidant activity, DNA cleavage, HPLC-DAD*

[a] *Department of Chemistry and Chemical Processing Technologies, Mustafa Çıkrıkcıoglu Vocational School, Kayseri University, Kayseri, Türkiye*
[b] *Department of Biology, Faculty of Sciences and Arts, Recep Tayyip Erdogan University, Rize, Türkiye*
** Corresponding author: emineselvi@kayseri.edu.tr*

INTRODUCTION

Vincetoxicum Wolf belonging to the subfamily Asclepiadoideae (Apocynaceae) is represented by approximately 300 species naturally distributed in a wide region covering Far East, Africa, the Mediterranean, Anatolia, Caucasus, Russia and Europe [1], and also a few species introduced in North America [2]. The genus *Vincetoxicum* constitutes an important natural plant source for both traditional folk medicine and modern medicine [3]. Some of these herbs are known to be effective in the treatment of common diseases such as malaria, scrofula, rupture, injuries, fever, wounds and scabies [4], and the others are claimed to exhibit expectorant, diuretic, emetic [5], laxative and diaphoretic effects [6]. The literature on chemical composition of *Vincetoxicum* has verified the presence of phenolics and flavonoids [5, 7, 8], acetophenones and pregnane glycosides [9], alkaloids [10], triterpenoids [11] for the members of the genus. Furthermore, depending on the rich chemical content of the genus, many biological activities such as anticancer [12], cytotoxic [13, 14], antibacterial and antifungal [15, 16, 17], antioxidant [5, 7, 8], antidiarrheal and antispasmodic [18], antifeedant [16], antileishmanial and antimalarial [19], anti-inflammatory [20] have been reported for several *Vincetoxicum* species (e.g *V. arnottianum* (Wight) Wight, *V. hirundinaria* Medic., *V. lutea* L., *V. nigrum* (L.) Moench, *V. pumilium* Decne., *V. rossicum* (Kleopow) Barbar. *V. stocksii* Ali & Khatoon) from different countries, except Türkiye.

Türkiye, with 11 wild *Vincetoxicum* species three of which are endemics, constitutes an important natural distribution area for the genus [21]. According to the literature review, a limited number of *Vincetoxicum* species from Türkiye was investigated from a biochemical perspective. *V. canescens* (Willd.) Decne., *V. fuscatum* (Hornem.) Rchb. f. and *V. parviflorum* Decne., have recently been investigated in phytochemical aspect, and fatty acid, sterol, and tocol compositions, total phenolic, total flavonoid, amino acid, mineral, glycoside and sugar contents [22, 23], and antioxidant [23], antifeedant [22], antibacterial and antifungal activities [24, 25, 26, 27] have been reported for these taxa. Ethnobotanical studies reveal that *V. tmoleum* Boiss. has been used as a folk medicine in the treatment of scabies and fungal infections, especially in the Eastern Anatolia region [28]. This species is characterized by erect stem with crisped pubescent, campanulate, yellowish-green flowers with lanate inner surface, free and triangular corona segments, ovate pollinia, and slender ovoid fruits. The native range of this perennial herb is Türkiye to Northern Iraq and Lebanon [29, 30]. However, the widely distributed *V. tmoleum* which has the potential for medical uses has not been biochemically investigated yet.

Medicinal plants have been widely used in the treatment of diseases since ancient times for their rich secondary metabolite content such as phenolic acids, flavonoids, cinnamic acid derivatives, coumarins, tocopherols and tannins which are accepted as natural sources of antioxidants. It is known that antioxidants protect the human body against diseases caused by free oxygen derivatives [31]. Moreover, binding and cleavage of DNA, the heart of cellular transcription and translation, occurs in the cell throughout the natural process with enzymatic or oxidation processes. In addition, many anticancer drugs aim to trigger cell apoptosis by disrupting the DNA structure [32]. Therefore, revealing the interaction of plant extracts with DNA and investigating their antioxidant activity is of great importance for production of new drugs. Hence, the present research aims to determine the phytochemical components and investigate the antioxidant activities, DNA cleavage and binding effects of *Vincetoxicum tmoleum*.

RESULTS AND DISCUSSION

Main compounds in the methanolic extract of *V. tmoleum* consisted of *p*-coumaric acid, vanillic acid and catechin, respectively (Table 1, Figure 1). The amount of remaining ones was determined in the following order, chlorogenic acid, isorhamnetin, caffeic acid, rutin, ferulic acid and protocatechuic acid. Numerous studies have demonstrated that *p*-coumaric acid and vanillic acid are among the most significant phenolic compounds responsible for antioxidant activity by eliminating reactive oxygen [33, 34]. Herein, phenolic compounds of *V. tmoleum* extracts were investigated by HPLC-DAD analyses for the first time, and the obtained results are consistent with the phenolic contents identified for the other taxa of *Vincetoxicum*. In a previous study, the presence of chlorogenic acid, isoquercitrin and apigenin-7-O-glucoside was confirmed in the methanol and acetone extracts of *V. lutea* by using LC-MS methods [5]. Similarly, six substances composed of sinapic acid, ferulic acid, caffeic acid, chlorogenic acid, quercetin and kaempferol were isolated from *V. scandens* [35].

Total Phenolic Content (TPC) and Total Flavonoid Content (TFC) in the methanol extracts of *V. tmoleum* were determined spectroscopically. According to the present results, the values of TPC were 58.90±0.50 mg GAE/g ext. and 50.39±0.15 mg QE/g ext., and the amount of TFC was 41.37±0.07 mg QE/g ext (Table 2). This study is the first report on the phenolic compounds and antioxidant activity of *V. tmoleum*. The obtained data were compared with limited investigation including a few *Vincetoxicum* species.

The total phenolic and flavonoid contents of ethanol extracts of *V. canescens* subsp. *canescens* and *V. canescens* subsp. *pedunculata* seeds were recorded by Guzel et al. as 25.62 µg GAE/mg extract, 16.50 µg GAE/mg extract and 1.50 µg QE/mg extract, 1.13 µg QE/mg extract, respectively [23]. In another investigation, Šliumpaite et al. [5] reported the amount of TPC ranging from 86 to 132 mg GAE/dw in methanol and acetone extracts of *V. lutea* leaves. Slapšytė et al. [36] used gallic acid as the standard to measure the amount of TPC in *V. luteum* and *V. hirundinaria* specimens. According to that previous study, the values of TPC determined as 131.8 mg GAE/g dw for *V. luteum* and 127.4 mg GAE/g dw for *V. hirundinaria* in the acetone extracts were higher than the ones measured as 93.1 mg GAE/g dw for *V. hirundinaria* and 86.0 mg GAE/g dw for *V. luteum* in methanol extracts. Another study related to the total phenolic and total flavonoid contents of methanol, dichloromethane and ethyl acetate extracts of *V. nigrum* exposed that the methanol extract was richer in total phenolic and total flavonoids [8].

Antioxidant activity of *V. tmoleum* was determined using radical scavenging (DPPH and ABTS), reducing power (FRAP) assays, and the results of antioxidant assay are given in Table 3. The activities of DPPH, ABTS, and FRAP were 0.489±0.018 (SC_{50} mg/mL), 1.403±0.015 (SC_{50} mg/mL) and 152.23±0.35 µmol trolox/g ext, respectively. Several *Vincetoxicum* taxa have been studied for antioxidant activity. Guzel et al. [21] investigated antioxidant activity of *V. canescens* subsp. *canescens* and *V. canescens* subsp. *pedunculata* seeds. In the case of DPPH free radical scavenging assay, *V. canescens* subsp. *canescens* showed the higher antioxidant activity compared to the other subspecies [23]. In addition, HPLC-DPPH based antioxidant activity of *V. lutea* was confirmed using methanol and acetone extracts by Šliumpaite et al. [5]. The researchers indicated that acetonic extracts (with SC_{50} value of 0.13 ± 0.01 %) of *V. lutea* were stronger antioxidants compared to the methanolic extracts (with SC_{50} value of 0.21 ± 0.01 %). In another study, antioxidant activities of two endemic species from Iran, *V. pumilum* and *V. nigrum*, were evaluated using methanol extracts. According to that study, *V. pumilum* had higher antioxidant activity than *V. nigrum* [7]. Moreover, antioxidant activity of methanol, dichloromethane and ethyl acetate extracts of *V. nigrum* was studied by Nourian et al. [8], using an online HPLC-DPPH method. The highest antioxidant activity (SC_{50}, 1.44 mg/mL) was determined in methanol extract compared to the dichloromethane and ethyl acetate extracts [8].

The DNA protective effects of *Vincetoxicum tmoleum* extracts were tested using pBR322 DNA and CT-DNA. When compared to the control group in well 1, despite the same amount of DNA in the well compared to the control, a brighter line was formed in the 2th well. This indicates that there is a binding with electronic interaction between the *V. tmoleum* extract and the CT-DNA

(Figure 2). Control DNA structure in well 1, methanol extract of *V. tmoleum* in other wells with different concentrations cleaved at all concentrations, albeit slightly, samples caused cleavage from supercoiled DNA form to nicked DNA form (from Form I to II). The result is given in Figure 3.

In this study, correlation analyses among scavenging activity (DPPH), ABTS, FRAP, TPC, and TFC levels were conducted. The correlation coefficients (r) are shown in Table 4. Significant positive linear correlations (Table 4) were established between TPC and TFC ($r = 0.922$; $p < 0.01$). Strong positive correlations (Table 4) were also found between DPPH and TFC ($r = 0.999$; $p < 0.01$), TPC ($r = 0.989$; $p < 0.01$), FRAP ($r = 0.995$; $p < 0.01$), and ABTS ($r = 0.994$; $p < 0.01$).

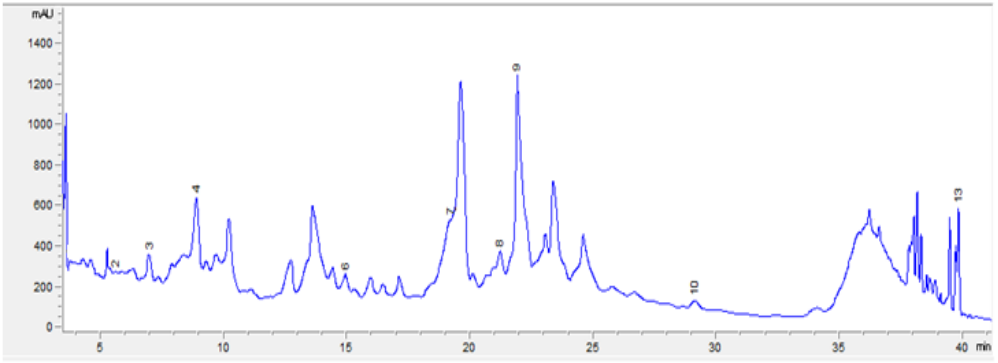

Figure 1. HPLC–DAD chromatogram of methanol extract of *V. tmoleum* at 280 nm. 2. Protocatechuic acid, 3. Catechin, 4. Chlorogenic acid, 6. Caffeic acid, 7. Vanillic acid, 8. Rutin, 9. *p*-coumaric acid, 10. Ferulic acid, 13. Isorhamnetin.

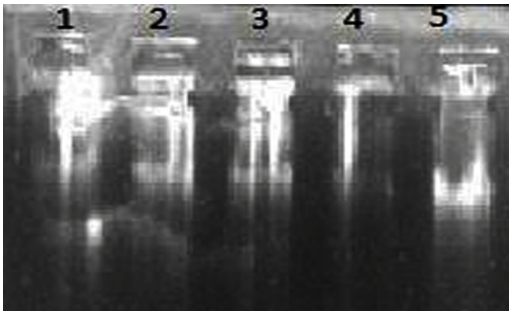

Figure 2. Agarose gel electrophoresis gel images of methanol extract of *V. tmoleum*. Ingredients of lines: Lane1: CT-DNA (3 mg/mL) in buffer (Tris HCl, pH=7), Lanes 2-5: CT-DNA (3-0.375 mg/mL) + buffer+ *V. tmoleum* (50 µM)

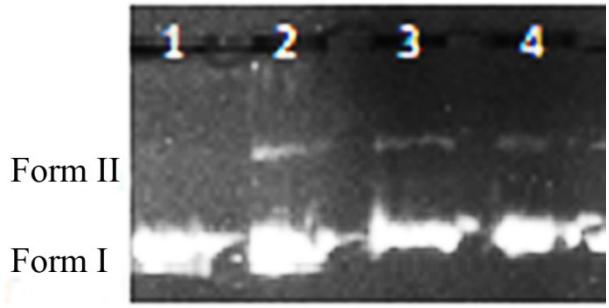

Figure 3. DNA Cleavage activity gel images of methanol extract of *V. tmoleum* Lane (1) pBR322DNA + 10 µL ddw. Lane (2) pBR 322DNA + 150µg/mL of *V. tmoleum* + ddw. Lane (3) pBR 322DNA + 100 µg/mL of *V. tmoleum* + ddw. Lane (4) pBR 322DNA + 50 µg/mL of *V. tmoleum* + ddw.

Table 1. Phenolic compounds of methanol extract of *V. tmoleum* analyzed by HPLC-DAD

Standards	RT	*V. tmoleum* mg std/g extract
Protocatechuic Acid	5.60	0.22
Catechin	6.97	4.05
Chlorogenic acid	8.88	2.89
Caffeic acid	14.94	1.75.
Vanillic acid	19.24	5.19
Rutin	21.21	1.13
p-coumaric acid	22.21	5.40
Ferulic acid	29.13	0.95
Isorhamnetin	39.83	2.28

Table 2. Total phenolic and total flavonoid contents of the extract

Extracts	Total phenolic content mg GAE/g dw	Total phenolic content mg QE/g dw	Total flavonoid content mg QE/g dw
V. tmoleum	58.90±0.50	50.39±0.15	41.37±0.07

GAE the equivalent of gallic acid (GA), QE the equivalents of quercetin (Q)

Table 3. Antioxidant activity of the methanol extract of *V. tmoleum*

Extract	DPPH, SC_{50} (mg/mL)	ABTS, SC_{50} (mg/mL)	FRAP (µmol trolox/g ext)
V. tmoleum	0.489±0.018	1.403±0.015	152.23±0.35
Gallic acid	0.002±0.000	0.008±0.000	
Quercetin	0.001±0.000	0.002±0.000	
Trolox	0.002±0.000	0.006±0.000	

Table 4. Correlation analysis between TPC, TFC, DPPH, ABTS and FRAP

r	TPC	TFC	DPPH	ABTS
TFC	0.922*			
DPPH	0.989*	0.999*		
ABTS	0.769*	0.957*	0.994*	
FRAP	0.875*	0.994*	0.995*	0.982*

r: Correlation coefficient,
*:Correlation is significant at $p < 0.01$.

CONCLUSIONS

Consequently, in this study, methanolic extract of *V. tmoleum* was investigated for the first time in terms of phenolic compounds, antioxidant activities, DNA cleavage and binding effects in order to determine the probability of medicinal usage. As in the phytochemical analysis results, the methanol extract of *V. tmoleum* was found to be rich in phenolic compounds. This finding was also supported by HPLC-DAD analysis. According to the results of HPLC-DAD analysis, the extract contained significant amount of *p*-coumaric acid and vanillic acid with well-reported biological activity potential.

Significant positive linear correlations were established between TPC and TFC ($r = 0.922$; $p < 0.01$). Strong positive correlations were also found between DPPH and TFC ($r = 0.999$; $p < 0.01$), TPC ($r = 0.989$; $p < 0.01$), FRAP ($r = 0.995$; $p < 0.01$), and ABTS ($r = 0.994$; $p < 0.01$). V*. tmoleum* extract at 50µM concentration was found suitable for evaluation as intercalating agents. The extract performed DNA separation at all concentrations.

EXPERİMENTAL SECTİON

Sample Preparation. Plant samples of *V. tmoleum* were collected from Bozdağ, Salihli-Manisa in Türkiye. The collected plant samples were identified and deposited at the Herbarium of Recep Tayyip Erdoğan University, Department of Biology (RUDB) with the voucher specimen number of S. Güven 48 & S. Makbul. All plant samples to be used in the experiments were dried at room temperature in the shade and ground with a blender (Waring Commercial, CT, USA). 5 g of dried samples were added to flask with 50 mL methanol and extracted in the ultrasonic bath (Elma Clean Box, Elma) at 40 ºC for 60 min. Extract was centrifuged for 10 min, at 5000 rpm. The resulting extracts were transferred to a new flask, and the extracts were evaporated using a rotary evaporator. Dried extracts were dissolved in methanol and stored at −18°C until analysis.

Determination of phenolic compounds by HPLC-DAD. Chromatographic analysis was performed by using an Agilent 1200 series chromatography HPLC system (Agilent Technologies, Mississauga,ON, Canada) equipped with a DAD detector. Chromatographic separation was performed on a C18 column (150 × 4.6 mm i.d., 5 µm particle, 100 A°; Agilent). Gradient elution was used for HPLC analyses using three mobile phases as: A [MeOH:water:acetic acid (10:85:5, v/v/v)], solvent B [MeOH:water:acetic acid (91:8:1, v/v/v)], and solvent C (MeOH). The gradient was as follows: the composition of solvent B was increased from 12 to 30% over 15 min, then to 42% over 3 min and held for 15 min, and finally to 100% over 5 min, while the composition of solvent C was increased to 12% over 2 min, then to 35% over 11 min and then returned to the initial conditions over 2 min and held for 5 min. The total run time was 55 min. The volume of injection was 20 µL, the flow rate was 1 mL/min and the column temperature was 30°C.

Methanol, extract of *V. tmoleum* was prepared at a concentration of 2 mg/mL. Stock solutions of the standards were prepared in MeOH at a concentration of 1 mg/mL and then diluted to different concentrations in MeOH in the range of 40–0.5 mg/mL. HPLC analysis of phenolic compounds was performed by revising the method used by Ayaz et al. [43].

Determination of total phenolic content. The total phenolic content of the methanol extract of *V. tmoleum* was analyzed with Folin-Ciocalteu's phenol reagent. Gallic acid and quercetin were used to generate a standard curve in a range from 0.0019 and 1.00 $mg.mL^{-1}$ (r^2 = 0.999) [37]. All experiments were performed in triplicates, and the absorbance of the mixture was measured at 760 nm using UV-Vis spectrophotometer (Labomed Inc.

Culver City-USA). The amount of total phenolic content was given as mg of gallic acid equivalent (GAE) per g of dry weight (dw) and quercetin equivalent (QE) per g dry weight (dw).

Determination of total flavonoid contents. The total flavonoid content was determined by the aluminum complexation method as described by [38]. In this method, 0.1 mL 10% aluminum nitrate, 0.1 mL 1 M potassium acetate, and 4.3 mL 80% ethyl alcohol was mixed with 0.5 mL plant extract. The samples were incubated for 40 min at room temperature, and the absorbance was measured at 415 nm. All analyses were performed in triplicates using spectrophotometer (Labomed Inc. Culver City-USA). Quercetin was used as the standard to generate a calibration curve, and the results were expressed as mg quercetin equivalent (QE) per g of dry weight (dw).

Free Radical Scavenging Activity Assay (DPPH). The scavenging activity of methanol extracts against the 2,2-diphenyl-1-picrylhydrazyl (DPPH) radical was determined using spectrophometric method at 517 nm [39]. Briefly, 0.75 mL of plant extracts were mixed with 0.75 mL of 0.1 mM DPPH in methanol. Radical scavenging activity was measured using gallic acid and quercetin as standards. Results presented as SC_{50} values indicate the sample of concentration required to scavenge 50% of DPPH free radicals (SC_{50}; mg sample per mL methanol).

ABTS radical scavenging assay. The radical scavenging activity of the extract against ABTS [2, 2'-azino-bis(3-ethylbenzothiazoline-6-sulfonic acid)] was spectrophometrically determined at 734 nm [40]. ABTS solution was prepared in water at a concentration of 7 mM. ABTS radical was obtained by reacting the prepared ABTS stock solution with 2.45 mM potassium persulfate and keeping the mixture in the dark at room temperature for 16-18 hours. The results were expressed as SC_{50}; (mg sample per mL).

Ferric Reducing Antioxidant Power Assay (FRAP). The antioxidant capacity of the methanol extracts was spectrophometrically determined using FRAP assay [41]. The FRAP reagent was prepared by mixing 25 mL of acetate buffer (300 mM, pH 3.6), 2.5 mL of 10 mM TPTZ solution in 40 mM HCl, and 2.5 mL of 20 mM $FeCl_3$,$6H_2O$ solutions. Trolox was used as a standard (r^2 = 0.999). Results were given as µmol trolox equivalent per gram of the extract.

DNA Cleavage experiments. An agarose gel electrophoresis was applied to examine the DNA cleavage activity of Vt samples. Supercoiled pBR322 plasmid DNA (100µg) was used without irradiation. Supercoiled pBR322 plasmid DNA was treated with different concentrations of samples

ranging from 50 to 150µM in 10 % DMSO. All samples were incubated in PCR tubes at 37°C for 2 hours. Then, the mixtures were loaded on 1% agarose gel with ethidium bromide staining in TAE buffer (Tris acetic acid-EDTA). Electrophoresis was performed at 75V for 60 minutes. The results were visualized using the BioRad Gel Doc XR system and analyzed by applying the Image Lab Version 4.0.1 Software program.

DNA Binding experiments using gel electrophoresis. The interaction of the samples with CT-DNA was studied by performing an agarose gel electrophoresis method. 50µM solutions of samples (Vt) were prepared in DMSO. Then, a series of samples containing 50µM and different concentrations of CT-DNA (0.375-3 mg/ml in ddw) were prepared, and the total volume was adjusted to a final volume of 25µl with buffer in PCR tubes. The samples were incubated at 37°C for 2 hours. Then, the mixtures were loaded with the buffer on 1% agarose gel with ethidium bromide staining in TAE. The electrophoresis was performed at 75 V for 2 hours. The results were visualized by applying the BioRad Gel Doc XR system [42].

Statistical Analysis. Results from experiments are presented as the mean ± standard deviations of three parallel measurements. The SC_{50} values were calculated from linear regression analysis (Microsoft Excel program for Windows, version 2003). Statistical analysis of the experimental results obtained was carried out in SPSS (Version 16.0, Chicago, IL) using Mann–Whitney U-test and Pearson correlation analyses. Differences of $p < 0.01$ were considered significant.

REFERENCES

1. S. Liede-Schumann; U. Meve; *Phytotaxa*, **2018**, *369*, 129–184.
2. S. E. Sheeley; D. J. Raynal; *Bull. Torrey Bot. Club*, **1996**, *123*, 148–156.
3. M. A. Zaidi; Jr. S. A. Crow; *J. Ethnopharmacol.*, **2005**, *96*, 331–334.
4. L. Q. Wang; J. H. Wang; Y. M. Shen; J. Zhou; *Chin. Chem. Lett.,* **2007**, *18*, 1235–238.
5. I. Šliumpaitė; M. Murkovic; A. Zeb; P. R. Venskutonis; *Ind. Crops Prod.,* **2013**, *45*, 74–82.
6. A. DiTommaso; F. M. Lawlor; S. J. Darbyshire; *Can. J. Plant Sci.*, **2005,** *85*, 243–263.
7. S. Noorian; A. M. Sani; A. Yazdani; *Asian J. Biol. Life Sci.*, **2015**, *4(1)*, 35–38.
8. S. Nourian; A. M. Sani; E. Golmakani; P. Feizi; K. Roghani; *Int. J. PharmTech Res.*, **2016**, *9(3)*, 150–157.
9. M. Lavault; P. Richomme; J. Bruneton; *Fitoterapia*, **1999**, *70*, 216–220.

10. M. Lavault; P. Richomme; J. Bruneton; *Pharm. Acta Helv.*, **1994**, *68*, 225–227.
11. R. Nowak; W. Kisiel; *Fitoterapia*, **2000**, *71*, 584–586.
12. U. Tanner; W. Wiegrebe; *Arch. Pharm. (Weinheim)*, **1993**, *326*, 67–72.
13. D. Staerk; J. Christensen; E. Lemmich; J. Duus; C. E. Olsen; J. W. Jaroszewski; *J. Nat. Prod.*, **2000**, *63*, 1584–1586.
14. D. Staerk; A. L. Lykkeberg; J. Christensen; B. A. Budnik; F. Abe; J. W. Jaroszewski; *J. Nat. Prod.*, **2002**, *65*, 1299–1302.
15. M. A. Zaidi; S. A. Crow; *Pak. J. Bot.*, **2012**, *44(SI)*, 395–397.
16. C. Mogg; P. Petit; N. Cappuccino; T. Durst; C. McKague; M. Foster; J. E. Yack; J. T. Arnason; M. L. Smith; *Biochem. Syst. Ecol.*, **2008**, *36*, 383–391.
17. D. M. Gibson; S. B. Krasnoff; J. Biazzo; L. Milbrath; *J. Chem. Ecol.*, **2011**, *37*, 871– 879.
18. A. J. Shah; M. A. Zaidi; H. Sajjad; H. A. H. Gilani; *Bangladesh J. Pharmacol.*, **2011**, *6*, 46–50.
19. A. Mansoor; M. A. Ibrahim; M. A. Zaidi; M. Ahmed; *Bangladesh J. Pharmacol.*, **2011**, *6*, 51–54.
20. Z. Zahra; M. R. Khan; S. A. Shah; S. Maryam; M. Majid; T. Younis; M. Sajid; *J. Ethnopharmacol.*, **2020**, *252*, 112565.
21. S. Güven; K. Coşkunçelebi; S. Makbul; *Nord. J. Bot.*, **2021**, *39(12)*, e03405.
22. S. Güzel; R. Pavela; A. İlçim; G. Kökdil; *Marmara Pharm. J.*, **2017**, *21(4)*, 872–880.
23. S. Guzel; *Chem. Nat. Compd.*, **2020**, *56(2)*, 202–206.
24. S. Güzel; R. Pavela; G. Kökdil; *International Anatolian Academic Online Journal/ Health Science*, **2015**, *3(2)*, 1–9.
25. S. Guzel; M. Ulger; G. Kokdil; *International Journal of Scientific and Technological Research*, **2018**, *4(3)*, 27–38.
26. S. Güzel; M. Ülger; G. Aslan; G. Kökdil; *Marmara Pharm. J.*, **2018**, *22(3)*, 365–373.
27. S. Güzel; M. Ülger; Y. Özay; Ö. Yumrutaş; İ. Bozgeyik; Ö. Sarıkaya; *Mersin Üniversitesi Tıp Fakültesi Lokman Hekim Tıp Tarihi ve Folklorik Tıp Dergisi*, **2019**, *9(3)*, 367–375.
28. E. Altundağ; M. Öztürk; *Procedia Soc. Behav. Sci.*, **2011**, *19*, 756–777.
29. K. Browicz; Asclepiadaceae, in Flora of Turkey and the East Aegean Islands, Vol. 6, P.H. Davis, Ed.; Edinburgh University Press, Edinburgh, UK, **1978**, pp 163-174.
30. S. Güven; S. Makbul; K. Coşkunçelebi; *Recep Tayyip Erdoğan Üniversitesi Fen ve Mühendislik Bilimleri Dergisi*, **2021**, *2 (2)*, 1–12.
31. C. Rice-Evans; N. Miller; G. Paganga; *Trends Plant Sci.*, **1997**, *2(4)*, 152–159.
32. S. Kawanishi; Y. Hiraku; *Curr. Med. Chem. Anticancer Agents*, **2004**, *4(5)*, 415–419.
33. Y. Shen; X. Song; L. Li; J. Sun; Y. Jaiswal; J. Huang; C. Liu; W. Yang; L. Williams; H. Zhang; Y. Guan; *Biomed Pharmacother,* **2019,** 111, 579-587.
34. A. Magiera; J. Kołodziejczyk-Czepas; a M.A. Olszewsk. *Molecules*, **2025**, 30(3), 467. https://doi.org/10.3390/molecules30030467.

35. N. S. Fursa; V. I. Litvinenko; L. E. Belyaeva; *Khlmiya Prirodnykh Soedinenii,* **1977**, *3*, 416.
36. G. Slapšytė; V. Dedonytė; A. Adomėnienė; J. R Lazutka; J. Kazlauskaitė; O. Ragažinskienė; P. R. Venskutonis; *Food Chem. Toxicol.*, **2019**, *134*, 110815.
37. V. L. Singleton; R. Orthofer; R. M. Lamuela Raventós; *Methods Enzymol.,* **1999**, *299,* 152-178.
38. M. Marcucci; R. Woisky; A. Salatino; *Mensagem Doce*, **1998**, *46*, 3-9.
39. P. Molyneux; *Warasan Songkhla Nakharin,* **2004**, *26,* 211–219.
40. I. F. F. Benzie; J. J. Strain; *Methods Enzymol*., 1999, *299*, 15–27.
41. Z. Lu; G. Nie; P. S. Belton; H. Tang; B. Zhao; *Neurochem. Int.*, **2006**, *48*, 263–274.
42. T. Keleş; B. Barut; A. Özel; Z. Biyiklioglu; *Dyes Pigments*, **2019**, *164*, 372.
43. F. Ayaz; E. Köngül Şafak; K. Erkan Turkmen; G. Şeker Karatoprak; H. Katırcıoğlu; N. Küçükboyacı; *J. Food Meas. Charact.* **2021,** *15*, 4267–4276.

STUDIA UBB CHEMIA, LXIX, 1, 2024 (p. 175-186)
(RECOMMENDED CITATION)
DOI:10.24193/subbchem.2024.1.11

DEVELOPMENT AND VALIDATION OF A GAS CHROMATOGRAPHY METHOD FOR QUANTITATIVE ANALYSIS OF FATTY ACIDS IN VEGETABLE OILS

Mălina FIASTRU-IRIMESCU[a,b,*], Denisa MARGINĂ[b]

ABSTRACT. The major fatty acids present in cosmetics are the unsaturated fatty acids from triglycerides, especially essential fatty acids: linoleic acid (omega-6) and α-linolenic acid (omega-3).The purpose of the study was to develop a simple and precise gas chromatography-flame ionization detection method, using an OPTIMA-WAX (macrogol 20000) capillary GC column (30m x 0.32mm x 0.25µm) with a run time of 17min, for the analysis of fatty acids composition from vegetable oils and macerated oils. The method was validated for quantifying four major fatty acids: palmitic, stearic, oleic and linoleic acids, as methyl esters. The quantification was performed by internal standardization, using the methyl ester of nonadecanoic acid as internal standard. The esterification reaction was carried out on a magnetic stirrer at a temperature of 80°C and with continuous stirring, in hermetically sealed vials.

Keywords: *fatty acid, vegetable oils, gas-chromatography, method validation*

INTRODUCTION

The benefits of natural products have been known since ancient times when our ancestors used various herbal mixtures to treat different skin diseases. Even if, at that time, they could not explain the beneficial effects, they trusted nature.

[a] *"Carol Davila" University of Medicine and Pharmacy, Faculty of Pharmacy, Biochemistry Department, 6 Traian Vuia, Bucharest, Romania*
[b] *Biotehnos SA, 3-5 Gorunului,Otopeni, Ilfov, Romania*
[*] *Corresponding author email: malina.fiastru@gmail.com*

Fatty acids play a key role in metabolism: energy substances, components necessary for all membranes and play a role in regulating the transmission of intracellular messages. They represent 30-35% of total energy consumption in several industrial countries, the most important source of fatty acids being vegetable oils, dairy products, meat products, cereals, fish fats or oils.

In the last decade, vegetable oils, such as argan oil, avocado oil, sunflower oil, broccoli oil, olive oil, have begun to be used for their emollient, moisturizing and nourishing effects. Nowadays, a very important role in the industry has been attributed to omega fatty acids, especially linoleic acid, an omega-6 acid, which is a very important element in ceramides, contributing to maintaining the structure and function of the epidermis [1-6]. They form a protective layer over the skin, reducing local inflammation. Moreover, they play a very important physiological role in the body, sustaining in the synthesis of eicosanoids or local hormones (prostaglandins, prostacyclines, thromboxanes). Therefore, deficiency of fatty acids and corresponding lipids significantly affects vascular fragility, reduces immune function and interferes with the coagulation process. Moreover, the oils are incorporated into the cell membrane and regenerate the lipid barrier [7-14]. Unsaturated fatty acids have pronounced healing effects on dermatoses, such as atopic skin inflammation and are used in creams, emulsions, ointments, hair conditioners, cosmetic masks, lipsticks, nail polishes and other personal care formulas [15-17].

In the last decade, numerous studies have been carried out regarding the fatty acid composition of vegetable oils through different chromatographic techniques: GC-MS, GC-FID, LC-MS [18, 19].

The GC-FID method is a common method for the analysis of fatty acids. Such methods are also described in the European Pharmacopoeia and United States Pharmacopoeia [20, 21].

Songul Kesen [23] describes a technique for sample preparation that involves the methylation of 0.1g of oil with 0.2mL of 2N methanolic potassium hydroxide solution and vigorously shaking. The upper phase was injected in GC.

Qiwen Young et al. [24] describe a technique for the extraction of the fatty acids from sunflower seed oil. The fatty acids were extracted with an acidification method and after the methyl esterification, the separation of the saturated fatty acid methyl ester was realized with an urea encapsulation method and the content of unsaturated fatty acid methyl ester was up to 99,67%.

The aim of this study was to develop and validate a simple method for the simultaneous determination of major fatty acids in vegetable oils.

The chromatographic method was developed on argan oil, broccoli oil, olive oil, sunflower oil, avocado oil and raspberry oil. The method was validated on sunflower oil because it is widely studied in dermatology for two main reasons: firstly, it is a cheap natural source of oil and secondly it contains lipids similar to those from the composition of the corneum layer. It contains predominantly linoleic acid, tocopherols, lecithin and carotenoids. Sunflower oil helps moisturize the skin and creates a barrier against infections [23-26].

RESULTS AND DISCUSSION

Validation results

Specificity

As can be seen in Figure 1 no interfering peaks were found at the retention times of the analytes of interest into the blank sample. The retention times of fatty acid methyl esters in the chromatogram of the test sample were confirmed by comparing with those in the standard chromatogram. All fatty acids were adequately resolved from each other.

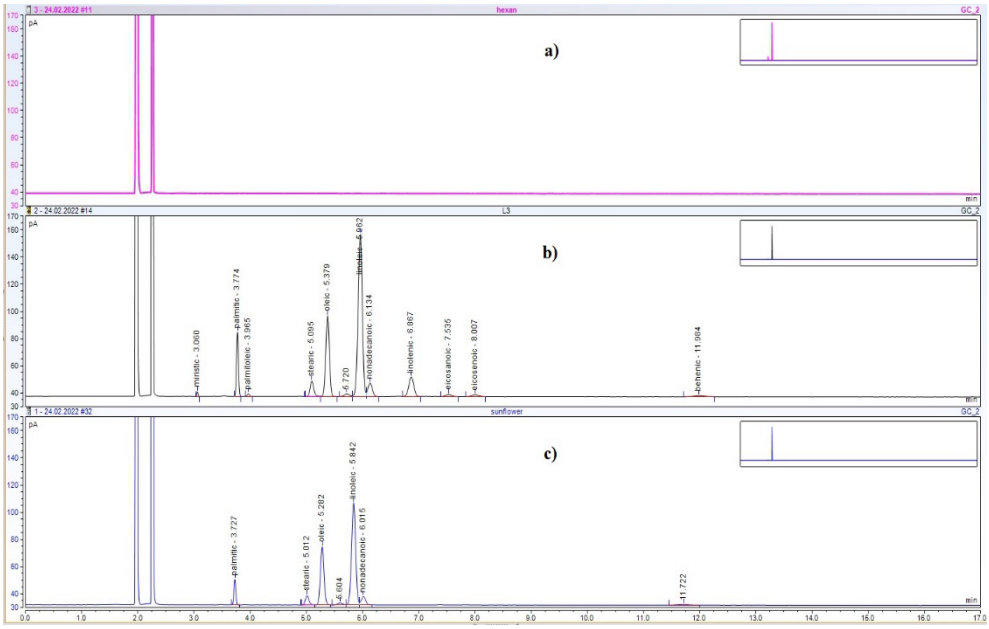

Figure 1. a) Blank (Hexane) Chromatogram, b) Standard Chromatogram and c) Sample Chromatogram

System suitability

The detailed results for the system suitability are represented in Table 1.

Table 1. System suitability

Component and chromatographic elution order	RSD %	Tailing factor	Resolution	Theoretical plates
methyl tetradecanoate (miristic, C14:0)	1.6	1.01	-	96321
methyl hexadecanoate (palmitic, C16:0)	0.7	1.00	13.96	57299
methyl palmitoleate (C16:1)	1.8	1.08	2.91	52830
methyl octadecanoate (stearic C18:0)	1.1	1.19	12.30	31289
methyl oleate (oleic C18:1)	0.8	0.97	2.42	32568
methyl linoleate (C18:2)	0.8	0.93	1.63	30046
methyl linolenate (C18:3)	0.9	1.02	4.92	26663
methyl eicosanoate (arahidic, C20:0)	1.3	0.98	3.58	21537
methyl 11 eicosenoate (C20:1)	1.4	1.01	2.20	20357
methyl docosanoate (behenic C22:0)	1.6	1.03	13.28	16248

Linearity

The linearity was assessed by plotting the ratio of the analyte peak area to the internal standard peak area versus the corresponding concentration.

ANOVA statistical analysis showed, in all cases, that there was a proportionality relationship between chromatographic response and concentration at 95% confidence level. The correlation coefficient of the regression line ranged from 0.9910 to 0.9987. The confidence interval of the intercept includes zero value. The statistical significance of the slope is checked by the Student test ($t_{calculated} > t_{critical}$), thus demonstrating the linearity of the curve. An additional element confirming the linearity of the method is the fulfilment of the condition that the experimental value of the Fisher test is greater than the critical value. Limit of detection (LOD) and limit of quantification (LOQ) were calculated based on the residual standard deviation of the calibration curve (SD) and the slope of the calibration curve (b), where LOD=3.3xSD/b and LOQ=10xSD/b [32].

The results of linearity are summarized in Table 2.

Table 2. Linearity verification by ANOVA test

Statistical characteristics of the regression	Acceptability criteria	Myristic acid	Palmitic acid	Palmitoleic acid	Stearic acid	Oleic acid	Linoleic acid	Linolenic acid	Eicosanoic acid	Eicosenoic acid	Behenic acid
Regression line equation	-	y=0.4040x +0.0662	y=0.4465x + 2.0511	y=0.4111x +0.9425	y=0.521x -0.9657	y=0.4620x +3.2940	y=0.4562x +17.0250	y=0.4624x -1.1542	y=0.4651x -0.2394	y=0.4694x +0.1605	y=0.4582x +0.9139
Correlation coefficient	>0.9900	0.9987	0.9967	0.9907	0.9922	0.9947	0.9942	0.9932	0.9947	0.9945	0.9910
Determinations, n	-	5	5	5	5	5	5	5	5	5	5
Degrees of freedom, n-2	-	3	3	3	3	3	3	3	3	3	3
Standard error of regression	-	0.2097	7.2238	0.5835	5.1310	22.0799	53.7179	8.6435	0.9890	1.0200	1.2760
Standard error of slope	-	0.0083	0.0149	0.0230	0.0267	0.0195	0.0202	0.0222	0.0195	0.0201	0.0252
Student's test $t_{n-2}(1-\alpha/2)$	$t_{calculated} > t_{critical} = 3.1824$	48.79	30.06	17.85	19.56	23.75	22.59	20.87	23.82	23.31	18.19
Confidence interval for slope (95% confidence)	does not include zero value	0.3776÷ 0.4303	0.3992 ÷ 0.4938	0.3378 ÷ 0.4844	0.4364 ÷ 0.6060	0.4001 ÷ 0.5240	0.3919 ÷ 0.5205	0.3918 ÷ 0.5329	0.4030 ÷ 0.5272	0.4053 ÷ 0.5335	0.3780 ÷ 0.5383
Standard error of intercept	-	0.2199	7.5763	0.6120	5.3814	23.1576	56.3398	9.0654	1.0373	1.070	1.3383
Confidence interval for intercept (95% confidence)	include zero value	-0.6338÷ 0.7663	-22.0601 ÷ 26.1624	-1.0052 ÷ 2.8903	-18.0918 ÷ 16.1604	-70.4039 ÷ 76.9918	-162.2731 ÷ 196.3237	-30.0043 ÷ 27.6958	-3.5405 ÷ 3.0618	-3.2440 ÷ 3.5650	-3.345 ÷ 5.1728
Fisher test (95% confidence) $F_{critical}=F_{1,n-2}(1-\alpha)$= 10.128	$F_{calculated} > F_{critical}$	2380.3	903.66	318.47	382.41	563.85	510.15	435.41	567.53	543.51	330.88
LOQ (µg/mL)		1.7129	53.3898	4.6839	32.4871	157.7140	388.5775	61.6859	7.0172	7.1709	9.1899
LOD (µg/mL)		5.1906	161.7870	14.1936	98.4459	477.9199	1177.5077	186.9269	21.2642	21.7299	27.8481

Accuracy

The average percentage recovery obtained in the range 90-110% are summarized in Table 3.

Table 3. Accuracy results

Component	The average percentage recovery %
methyl tetradecanoate (miristic, C14:0)	94.13
methyl hexadecanoate (palmitic, C16:0)	96.35
methyl palmitoleate (palmitoleic C16:1)	98.97
methyl octadecanoate (stearic C18:0)	95.62
methyl oleate (oleic C18:1)	96.98
methyl linoleate (linoleic C18:2)	96.39
methyl linolenate (linolenic C18:3)	96.51
methyl eicosanoate (arahidic, C20:0)	100.25
methyl 11 eicosenoate (C20:1)	97.11
methyl docosanoate (behenic C22:0)	95.20

These values demonstrate a good accuracy of determination of fatty acid methyl esters in sunflower oil by the proposed analytical procedure.

Precision

The relative standard deviation obtained for the results of 6 samples of sunflower oil analysis was less than 5% which is the value set for testing precision. The detailed results are represented in Table 4.

Table 4. Precision results

	Component			
	palmitic acid	**stearic acid**	**oleic acid**	**linoleic acid**
Concentration mg/100g	4.98	3.78	26.94	41.97
RSD, %	2.60	3.73	2.59	2.62
Standard error	0.0530	0.0575	0.2848	0.4496
Confidence level (95.0%)	0.14	0.15	0.73	1.16
Confidence interval	4.84-5.12	3.63-3.93	26.21-27.67	40.81-43.13

After validating the method, it can be seen that it meets all the criteria: the method is specific, linear and precise.

Table 5. Theoretical Concentration (%) of fatty acids in the studied oils from USP, EP and Technical data sheet (TDS)

Component	**Theoretical Concentration (%)**					
	Sunflower (USP29-NF24)	**Argan (TDS)**	**Avocado (TDS)**	**Olive (EP)**	**Broccoli (TDS)**	**Raspberry (TDS)**
methyl tetradecanoate (miristic, C14:0)	-	-	-	-	-	-
methyl hexadecanoate (palmitic, C16:0)	3-10	10-15	5-25	7.5-20	<5	2
methyl palmitoleate (C16:1)	-	-	1.0-12.0	0.3-3.5	-	0.2
methyl octadecanoate (stearic C18:0)	2-8	4.3-7.2	3	0.5-5	<5	1
methyl oleate (oleic C18:1)	14-24	43-50	45-75	56-85	10-20	13
methyl linoleate (C18:2)	40-74	29-37	5-20	3.5-20	10-20	59
methyl linolenate (C18:3)	-	-	3.0	1.0	5.0-10.0	24
methyl eicosanoate (arahidic, C20:0)	-	-	-	0.6	-	0.4
methyl 11 eicosenoate (C20:1)	-	-	-	0.5	5.0-10.0	-
methyl docosanoate (behenic C22:0)	-	-	-	0.2	-	-

In Table 5 we have the theoretical concentration of fatty acids in the oils examined described in USP, EP and in the technical data sheet from the oils manufacturer [20,22].

Comparing the results obtained (Table 6) with those from the literature (Table 5), it can be seen that this method can be used for the analysis of vegetable oils, being a faster and easier method.

Table 6. Concentrations of fatty acids methyl esters in the vegetable oils

Component	Concentration %					
	sunflower	**argan**	**avocado**	**olive**	**broccoli**	**raspberry**
methyl tetradecanoate (miristic, C14:0)	-	0.13	-	-	-	-
methyl hexadecanoate (palmitic, C16:0)	4.98	13.95	15.27	11.09	2.53	2.02
methyl palmitoleate (C16:1)	-	0.10	5.28	0.88	0.15	-
methyl octadecanoate (C18:0)	3.76	7.02	1.64	3.97	1.38	1.02
methyl oleate (C18:1)	26.94	50.05	54.88	78.32	15.07	11.79
methyl linoleate (C18:2)	41.97	31.47	7.85	3.29	12.13	48.82
methyl linolenate (C18:3)	-	0.08	0.56	0.41	5.57	21.57
methyl eicosanoate (arahidic, C20:0)	-	0.51	-	0.47	1.07	0.65
methyl 11 eicosenoate (C20:1)	-	0.50	0.13	0.27	11.92	0.15
methyl docosanoate (C22:0)	-	-	-	-	-	-

CONCLUSIONS

A gas chromatographic method with flame ionization detection for simultaneous analysis of the major fatty acids in vegetable oils and their quantification as methyl esters was developed and validated based on standards using an internal standard.

The method required a small amount of sample, a small volume of solvent and a short time for esterification.

This study revealed that in sunflower oil linoleic acid is in the highest concentration, followed by oleic, palmitic and stearic acids as seen in Table 6.

The highest concentration of linoleic acid is found in raspberry oil and the lowest concentration is in the olive oil.

The results of the validation tests proved that the analytical method presents a degree of linearity, accuracy, precision and specificity within the proposed limits and can be used for the determination of fatty acids in sunflower oil.

The experimental values of fatty acids from the analyzed oils are comparable to the theoretical values described in the literature.

EXPERIMENTAL SECTION

In the method development, several derivatization procedures were tested using 14% boron fluoride (BF_3) solution in methanol, 0.5M sodium hydroxide in methanol - 14% BF_3 in methanol mixture and 0.5M sodium hydroxide in methanol solution. The best results were obtained using 0.5M sodium hydroxide solution in methanol and a mixture of this and 14% BF_3 solution in methanol.

Methyl esters were identified by comparing the retention times in the test sample with those in the standard solution.

In this study, the quantification of methyl esters was carried out by the internal standard method which is more accurate and precise than the external standard method, the latter being more often used in case of a simple sample preparation. Nonadecanoic acid methyl ester, an acid that does not naturally occur in lipids, was used as internal standard; it was introduced in the derivatization step of the vegetable oil sample in the same concentration as in the standard solutions for the calibration curves.

Materials

Avocado oil, argan oil, broccoli oil, raspberry oil, olive oil obtained by cold pressing (Mayam), sunflower oil obtained by cold pressing from a local producer in the Valcea area; Fatty acid standard Mixture ME 275 (Larodan), Internal standard nonadecanoic acid methyl ester (Dr. Ehrenstorfer, purity 99.5%), Hexane (Carlo Erba, HPLC grade), Methanol (Riedel de Haen, HPLC grade), Sodium hydroxide (Lach Ner), Sodium sulphate anhydrous (Cristal R Chim), Polar stationary phase capillary column Optima-Wax 30m x 0,32mm x 0,25µm (Macherey-Nagel).

Analytical instruments

An Agilent 6890N Gas Chromatograph (Agilent Technologies) with flame ionization detection and split/splitless injector, Mettler Toledo electronic analytical balance, Parker hydrogen gas generator and Peak nitrogen gas generator were used for method development and validation.

The chromatographic conditions were established in the laboratory starting from European Pharmacopoeia Chapter 2.4.22 (Composition of fatty acids by gas chromatography) recommendations [20].

GC-FID system

The analysis was performed using an Agilent 6890N Gas Chromatograph (Agilent Technologies) with flame ionization detection and split mode for sample injection. For chromatographic separation a fused-silica capillary column (Macherey-Nagel, Optima-Wax 30m x 0,32mm x 0,25µm with macrogol 20000 as stationary phase) was used.

The gas carrier was nitrogen with a flow rate of 1.3 mL/min. The oven temperature was held at 200°C for 17minutes. The temperature of the injector was 250°C and the detector temperature was 260°C. The injection volume was 1µL, with split ratio of 50:1.

Preparation of solutions

Internal standard solution

A solution of nonadecanoic acid methyl ester with a concentration of 2000µg/mL in hexane was prepared.

Stock standard solution

A stock standard solution of fatty acid methyl esters in hexane was prepared with the concentrations shown in Table 7.

Table 7. Concentrations of fatty acids methyl esters in the standard Mixture ME 275

Component and chromatographic elution order	Composition %	Concentration mg/mL	Concentration range of linearity µg/mL
methyl tetradecanoate (miristic, C14:0)	0.50	0.08	8.01 ÷ 40.05
methyl hexadecanoate (palmitic, C16:0)	9.60	1.54	153.79 ÷ 768.96
methyl palmitoleate (C16:1)	0.50	0.08	8.01 ÷ 40.05
methyl octadecanoate (stearic C18:0)	3.80	0.61	60.88 ÷ 304.38
methyl oleate (oleic C18:1)	22.40	3.59	358.85 ÷ 1794.24
methyl linoleate (C18:2)	52.50	8.41	841.05 ÷ 4205.25
methyl linolenate (C18:3)	7.70	1.23	123.35 ÷ 616.77
methyl eicosanoate (arahidic, C20:0)	1.00	0.16	16.02 ÷ 80.10
methyl 11 eicosenoate (C20:1)	1.00	0.16	16.02 ÷ 80.10
methyl docosanoate (behenic C22:0)	1.00	0.16	16.02 ÷ 80.10

Standard calibration solutions

Five calibration standard solutions were prepared by dilution of the stock standard solution. To each solution, 500µL of internal standard was added.

Test solution

A test solution was prepared by weighing 25-30 mg oil sample into a 20mL glass vial over which 500µL of internal standard solution, 5mL hexane, 5mL methanol and 1mL 0.5M sodium hydroxide solution in methanol were added. The vial was closed and heated to 80°C with continuous shaking for 30 minutes on a magnetic stirrer. After it cooled down and the two phases were separated, 3mL were taken from the upper layer and filtered on anhydrous sodium sulfate. 1µL was injected from this solution.

Validation of the analytical method

The aim of the validation of the described method was to demonstrate that it is suitable for the quantitative analysis of fatty acids in sunflower oil. The validation characteristics used in the validation were specificity, linearity, accuracy, precision [29-32].

The linearity of the major fatty acids in sunflower oil: palmitic, oleic, stearic and linoleic was established. Linear regression analysis was carried out using the least squares method. The correlation coefficient of the calibration lines was determined; graphs of response (ratio of analyte area to internal standard area) versus each corresponding concentration of fatty acid were plotted.

The accuracy of the method was investigated by recovery tests using 3 standard solutions containing known amounts of analytes. These were analysed as unknown samples. The criterion adopted for evaluation was the percentage recovery in the range 90-110%.

The precision of the method was established by repeatability test: preparation and analysis of 6 samples. The relative standard deviation (RSD, %) of the results was determined. The criterion adopted for evaluation was RSD ≤ 5%.

Specificity refers to the ability of the analytical method to provide a different response for the analyte of interest in the presence of other compounds which may be expected in the sample matrix. It involves assigning identity to the analytes of interest under the experimental conditions of the method by obtaining positive results for the sample containing the analytes of interest when compared to the standard substances. A blank sample, a standard sample and a test sample were analyzed. In the blank sample there should be no signals interfering with those in the standard and test samples.

ACKNOWLEDGMENTS

The author Mălina Fiastru-Irimescu gratefully acknowledge Prof. Denisa Margină, for support and guidance, and Biotehnos SA for material support.

REFERENCES

1. A. Dragomirescu, *Dermatocosmetologie cu profil farmaceutic*, Brumar, **2020**, pp. 15-20
2. C. D. Marineci, C. Chiriță*, MedicHub Media,* **2018**
3. Institutul Național de Sănătate Publică, *Ghidul Controlului Produselor Cosmetice,* **2020**
4. G. Niculae, I. Lacatusu, N. Badea, R. Stan, B.S.Vasile, A. Meghea, *Photochem. Photobiol. Sci*., **2014**, 13(4), 703-16
5. A. Ispiryan, J. Viškelis, P. Viškelis, *Plants*, **2021**, 10, pp. 944
6. M. Bučar Miklavčič, F. Taous, V. Valenčič, T. Elghali, M. Podgornik, L. Strojnik, Nives Ogrinc, *Molecules*, **2020**, 25, 4080
7. Z. Charrouf, D. Guillaume, *OCL*, **2018**, 25. 2
8. G. Lizard, Y. Filali-Zegzouti, A. El Midaoui, *Int J Mol Sci*., **2017,** 28, 18(7), 1383
9. Y. Yagishita, J. W. Fahey, A. T. Dinkova-Kostova, T. Kensler*, Molecules*, **2019**, 6, 24(19), 3593
10. M. Flores, C. Vergara, F. Avila, H. Valdés*, Molecules,* **2019**, 10, 24(11), 2172
11. P. Duarte, M. Alves Chaves, C. Dellinghausen Borges, C. R. Barboza Mendonça, *Food Tehnology*, **2016**, 46(4)
12. C. Jimenez-Lopez, M. Carpena, C. Lourenço-Lopes, M.Gallardo-Gomez, J. M. Lorenzo, F. J. Barba, M.A. Prieto, J. Simal-Gandara, *Foods*, **2020**, 9(8), 1014
13. W. Chaiyana, P. Leelapornpisid, R. Phongpradist, K. Kiattisin, *Nanomat Nanotechnol*, **2016**, 6
14. M. Stoia, S. Oancea, *App. Sci. Report*., **2015,** 10(1), 45-49
15. A. Ahmad, H. Ahsan, *Biomedical Dermatology*, **2020**, 4,12
16. C. Bonnet, OCL, **2018**, 25, 5
17. A. Bialek, M. Bialek, M. Jelinska, A. Tokarz*, Int J Cosmet Sci*, **2016**, 38(4), 382-8
18. D. Kazlauskienė, G. Kasparavičienė, P. Nenortienė, M. Marksa, J. Jukilaitytė, S. Velžienė, A. Ževžikovas*, CHEMIJA*, **2021**, 32, 17-27
19. M. Toishimanov, M. Nurgaliyeva, A. Serikbayeva, Z. Suleimenova, K. Myrzabek, A.Shokan, N. Myrzabayeva, *Appl. Sci*., **2023**, 13*,* 7910
20. European Pharmacopoeia 11/2023, 0518
21. United States Pharmacopoeia 2023, USP29-NF24
22. British Pharmacopoeia, IOP Conf. Ser.: *Earth Environ. Sci*., **2021**, 680
23. S. Kesen, *J Oleo Sci*, **2019,** (9), 817-826
24. T.-K. Lin, L. Zhong, J. L. Santiago*, Int J Mol Sci*., **2018**, 19(1), 70

25. N. Ukleja-Sokolowska, E. Gawronska-Ukleja, M. Zbikowska-Gotz, Z.Bartuzi, L. Sokolowski*, Int J Immunopathol Pharmacol*., **2016,** 29(3), 498-503
26. S. Veillet, V. Tomao, F. Chemat, *Food Chem*, **2010,** 123(3), 905–911
27. J. Cayuela, K. Yousfi, M. C. Martinez, J. M. Garcia, *JAOCS*, **2014**, 91(10), 1677–1684
28. E. Fuentes, M. E. Baez, M. Bravo, C. Cid, F. Labra, *Food Anal Meth*, **2012**, 5(6), 1311–1319
29. ICH Topic Q 2 (R1) - Validation of Analytical Procedures: Text and Methodology
30. D. M. Bliesner - Validating Chromatographic Methods: A Practical Guide, Wiley-Interscience, **2006**, pp. 8-40
31. J. Ermer, J. H. McB. Miller – Method Validation in Pharmaceutical Analysis: A Guide to Best Practice, Wiley-VCH, **2002**, pp. 4-62
32. S. L. R. Ellison, V. J. Barwick, T. J. Duguid Farrant - *Practical Statistic for the Analytical Scientist*, **2009**
33. Technical data sheet (TDS) Organic Avocado Oil
34. Technical data sheet (TDS) Argan Oil Organic
35. Technical data sheet (TDS) Raspberry Seed Oil Organic
36. Technical data sheet (TDS) Broccoli Seed Oil Organic

STUDIA UBB CHEMIA, LXIX, 1, 2024 (p. 187-200)
(RECOMMENDED CITATION)
DOI:10.24193/subbchem.2024.1.12

VALORIZATION OF BIORESOURCES FOR THE PRODUCTIONOF POLYMER USING LANTHANIDE BOROHYDRIDE AS CATALYSTS

Saliha LOUGHMARI[a], Marc VISSEAUX[b], Abdelaziz EL BOUADILI[a*]

ABSTRACT. The use of natural materials derived from biomass or biodegradable polymer materials can be one of the solutions to be considered in reducing environmental pollution problems. In addition, some polymers have been shown to be biocompatible and thus beneficial in biomedical applications. Therefore, within the framework of this study, we will present the results of the application of lanthanide-borohydride systems ($Nd(BH_4)_3(THF)_3$) combined with n-butylethyl magnesium in the block copolymerization of conjugated dienes (myrcene-styrene) and a conjugated diene with a polar monomer (L-lactide) for the synthesis of bio-sourced elastomers. The analysis of copolymers resulting from the copolymerization between myrcene and styrene shows that it is possible to insert up to 9.9% of styrene. Moreover, the stereoselectivity (1,4-*trans*) of the myrcene motif has not significantly changed, even in the presence of a significant amount of styrene in the reaction medium. The presence of the copolymer wasconfirmed by the observation of a peak at 146 ppm which corresponds to the ipso carbon of styrene.

Keywords: *coordination polymerization, β-myrcene, styrene, L-lactide, biomass, elastomers.*

[a] *Laboratory of Industrial Engineering and Surface Engineering, Applied Chemistry and Environmental Sciences Team, Sultan Moulay Slimane University, FST-BM, P.B 523,23 000, Beni-Mellal, Morocco.*
[b] *Univ. Lille, CNRS, Centrale Lille, Univ. Artois, UMR 8181, UCCS, Unité de Catalyse et Chimie du Solide, F-59000, Lille, France.*
* *Corresponding author: aelbouadili@gmail.com*

INTRODUCTION

Polymeric materials today are derived from monomers obtained from petrochemicals. The current situation with petroleum resources encourages exploring alternative sources of monomers, particularly those derived from agro-resources. On one hand, terpenes and on the other hand, lactide, are among these naturally sourced molecules that should be considered for valorization in this regard Lanthanide borohydrides are advantageous for use as precatalysts in polymerization [1]. One benefit is their ability to produce well-defined compounds that can be analyzed by X-ray, leading to better control over the polymerization process. They are highly soluble and can be accurately monitored using ^{1}H NMR, enabling precise observation of the reaction. Furthermore, these borohydrides are effective pre-catalysts for polymerizing conjugated dienes [2-6], myrcene [7], and olefins [8], and can also initiate the polymerization of polar monomers like cyclic esters [9-12] and acrylates [13-16].

There is growing interest in using polymers derived from biomass as a more sustainable alternative to traditional fossil-based polymers.Biopolymers are being extensively studied as potential replacements for common commodity polymers like polyolefins. Myrcene, a dimer of isoprene, found in many plant oils [17], has shown promise as a starting material for the production of biopolymers. Visseaux and his group achieved the first stereoselective coordination polymerization of myrcene using neodymium and lanthanum borohydride-based catalysts, resulting in highly regulated polymyrcene with 1,4-*cis* and 1,4-*trans* configurations [7]. The same group carried out the copolymerization and terpolymerization of this monomer with styrene and isoprene through coordinative mechanisms [18]. This acyclic monoterpene has been also copolymerized with 1,3-butadiene in a continuous process using finely divided alkali metals as catalysts and ether as a solvent [19]. Recent research has explored copolymerizing myrcene with other comonomers, including conjugated dienes [20], and lactide [21].

Polyolefin chemistry places a lot of attention on the production of block copolymers that contain both olefins and polar monomers since these polar groups can give the hydrocarbon chains useful features like adherence and paintability. Using a single-component lanthanide initiator, the first regulated diblock copolymerization of olefins with methylmethacrylate or caprolactone was accomplished [22].

The main subject of this article concerns the study of the block copolymerization of conjugated 1, 3-dienes, namely myrcene and styrene, as well as the sequential copolymerization of myrcene with lactide. In particular,

we are investigating the use of neodymium trisborohydride ($Nd(BH_4)_3(THF)_3$) combined with n-butylethyl magnesium (BEM) as catalysts in this process.

RESULTS AND DISCUSSION

Copolymerization of myrcene-styrene

The block copolymerisation of myrcene (Myr) and styrene (Styr) using $Nd(BH_4)_3(THF)_3$ combined with (BEM) as the initiator was conducted via a two-step process:

- The first step was the polymerisation of myrcene using [$Nd(BH_4)_3$ $(THF)_3$]/[BEM], [myrcene]/[Nd] = 300, and $V_{toluene}$=1 mL for 2h at 70°C.
- The required amount of styrene was added under the same conditions after 2h with $V_{toluene}$=0,5 mL.

Copolymerization yields and copolymer composition are presented in table 1.

Table 1. Myrcene-styrene copolymerization with $Nd(BH_4)_3(THF)_3$combined to dialkyl magnesium

Entry	Time (h)	[Nd]/ [BEM]	[Styr]/ [Nd]	Yield (%)	Mn [c] (g/mol)	PDI[c]	Myr (%)[d]	Selectivity (%)[e] 1,4-trans/ 3,4
1[a]	2	1	-	84	11000	1.33	100	96.95/3.04
2[b]	2	1	1000	63	10400	1.97	93.27	96.55/ 3.44
3 [b]	2	1.5	1000	81	4400	1.72	91.1	93.86/ 6.13
4 [b]	4	1.5	1000	83	3200	1.78	92.6	87.89/12.1
5 [b]	11	1.5	1000	80	2300	1.55	90.09	84.27/15.72

[a] experimental conditions: $V_{myrcene}$ = $V_{toluene}$ = 1 mL, [Myr]/[Nd]= 300, and the Temperature =70°C.
[b] experimental conditions: $V_{myrcene}$ = $V_{styrene}$ = $V_{toluene}$ = 1 mL, [Myr]/[Nd]= 300, and the Temperature =70°C.
[c] Determined by Steric Exclusion Chromatography.
[d] Copolymer composition (myrcene content) determined by ^{1}H NMR.
[e] The selectivity 1,4-*trans*/3,4-Percentage determined by ^{1}H NMR.

We wanted to study the possibility of creating 1,4-*trans* polymyrcene-block-polystyrene diblock copolymers by adding the styrene at a later stage, after polymerizing myrcene. The block copolymerization of this conjugated dienes using $Nd(BH_4)_3(THF)_3$ and n-buthylethyl magnesium as catalysts in toluene at 70°C displayed 1,4-stereospecificity, which was observed after 2 hours of reaction (polymerization of myrcene).

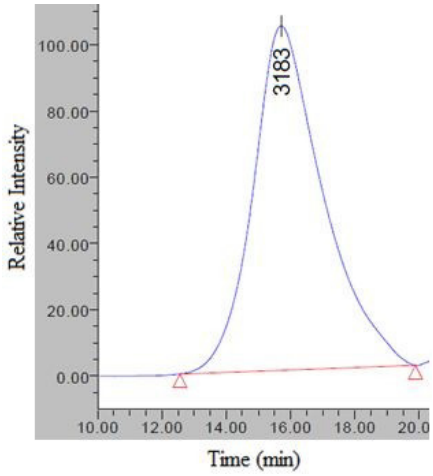

Figure 1: Chromatogram of polymyrcene-block-polystyrene copolymer (Table 1, Entry 4)

All the Steric Exclusion Chromatography (SEC) profiles show the monomodal character (Figure 1), which explains the presence of a copolymer rather than a mixture of two homopolymers, the dispersities (PDI = MW/Mn; Mn is the number-average molecular weight and MW is the weight average molecular weight) are lower than 2. In the presence of 1equiv of BEM in the reactive medium, approximately 6% of styrene can be inserted without affecting the stereoselectivity of the reaction. The microstructure of the copolymer's polymyrcene backbone displayed 84.27% to 96.55% 1,4-*trans* unit. However, when the reaction medium contains 1.5 equiv of BEM, 9% of styrene can be inserted accompanied with a gradual modification of the polymyrcene microstructure from 96.95% 1,4-*trans* to 84.27% 1,4-*trans* with an increase of the 3,4-microstructure in transfer conditions (3.4% 3,4 vs 15,72% 3,4). In addition, by varying the quantity of BEM while keeping a constant myrcene/ styrene ratio, chain transfer reactions to magnesium were observed since the molecular weights decrease as the quantity of BEM in the system increases. This modification in the polymyrcene microstructure and also the variation in the quantity of BEM were previously observed in homopolymerization of myrcene [7a].This increase in the 3,4 ratio within the polydiene is attributed to the steric hindrance induced by the presence of alkyl groups. This hindrance prevents the η^4 coordination mode of myrcene and results in the η^2 coordination mode of the monomer. A decrease in the molar mass of the polymers along with a narrow dispersity is observed, highlighting the presence of reversible transmetallation.

The microstructure of copolymer was determined by the ^{1}H NMR and the ^{13}C NMR. The ^{1}H NMR spectrum in $C_2D_2Cl_4$ (Figure 2) shows the peaks of protons corresponding to 1,4-*trans* polymyrcene in the copolymer and the peaks corresponding to styrene units in the copolymer. The signals between 1 and 1.1 ppm correspond to the methyl proton of the 1,4-double bonds of 1,4-*trans* unit of myrcene and the methylene of the styrene unit in the copolymer. The peak at 1.4 ppm corresponds to the CH_2 hydrogens of myrcene and the CH hydrogens of polystyrene, and the signal at 4.5 ppm corresponds to olefinic resonances assigned to the myrcene motif. The aromatic styrene was detected by presence of protons at 6.5 ppm.

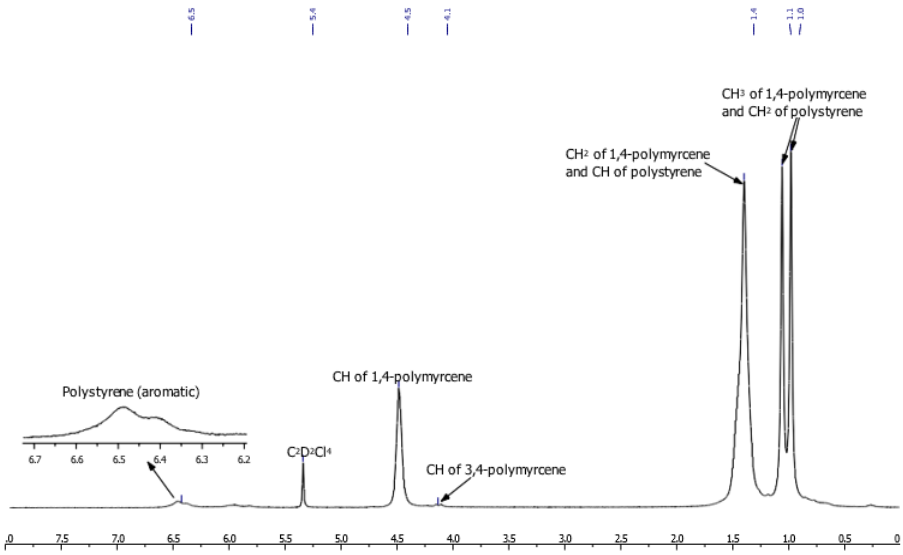

Figure 2: ^{1}H NMR (300 MHz, $C_2D_2Cl_4$) spectrum of myrcene-styrene copolymer (Table 1, Entry 4)

The ^{13}C NMR spectrum (Figure 3) displays the ten signals of poly(1,4-*trans*-myrcene) and the signals correspond to the carbons of the styrene units present in the copolymer. In the olefinic part of the spectrum, a singlet peak is detected at 146 ppm, corresponding to the phenyl ipso carbon (Cc), and chemical shifts are also observed around 140 ppm and 131.4 ppm,

corresponding to the two quaternary carbons of the myrcene unit in the copolymer (C2 and C8), as well as the signals at 128.3 ppm corresponding to aromatic signals. Around 124.8 ppm, we find the chemical shifts of the two CH groups of the myrcene unit (C3 and C7). In the aliphatic part of the spectrum, there are the two most shielded carbons correspond to the CH_3 groups of the myrcene unit (C9 at 17.70 ppm and C10 at 25.8 ppm), we have also detected the four signals corresponding to the methylene groups of the myrcene unit (C1 at 37.4 ppm, C4 at 27 ppm, C5 at 27.2 ppm and C6 at 30.5 ppm). Around 37 ppm, we identify the signal corresponding to the methylene groups of the styrene unit and at 39,9 ppm, we observe the chemical shift of the signal corresponding to the carbon of CH of styrene.

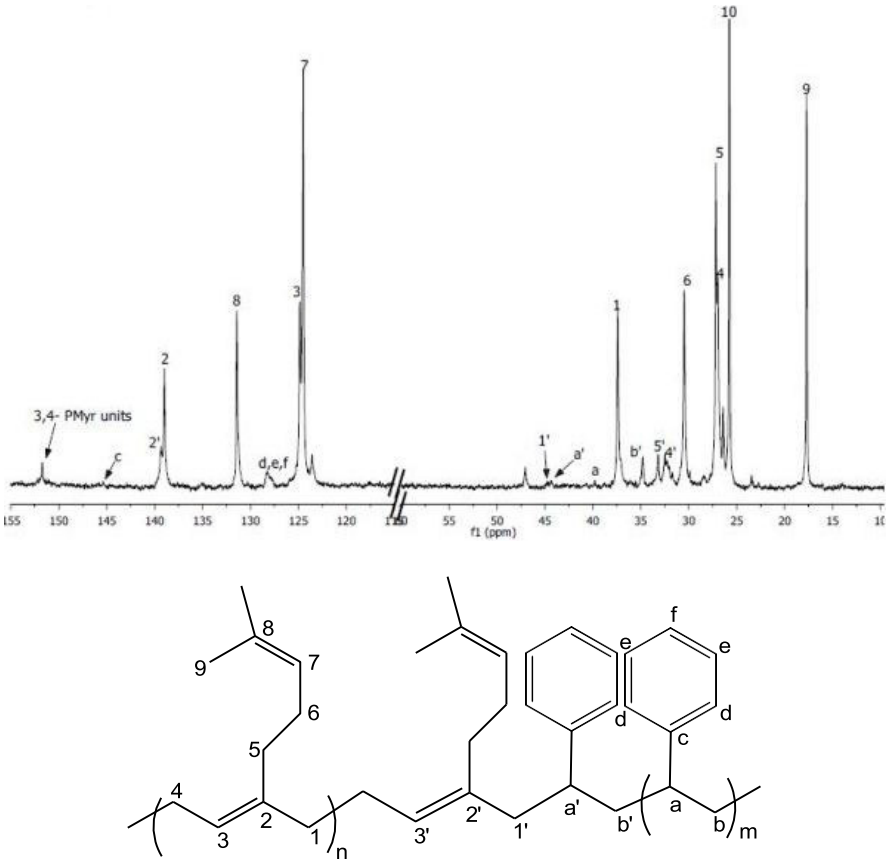

Figure 3: ^{13}C NMR (75 MHz, $CDCl_3$) spectrum of myrcene-styrene copolymer (Table 1, Entry 4) and assignments.

The ^{13}C NMR data shows the *presence of new peaks 1' and a' corresponds to the association of a* myrcene unit with a styrene. The carbon in the polymyrcene backbone show two signals each. The main signal corresponds to polymyrcene (C1) (i.e., when the unit is adjacent to two other myrcene units). The signal referred to as (carbon') (C1') is attributed to the myrcene-styrene enchainments (Figure 3).

Copolymerization of myrcene-lactide

The Table 2 provides a summary of our attempts to synthesize a block copolymer from myrcene and lactide. A diblock copolymer of polymyrcene/ polylactid was obtained by adding the two monomers sequentially. Myrcene was polymerized in toluene for 2 hours at 70°C using neodymium trisborohydride ($Nd(BH_4)_3(THF)_3$) associated with n- butylethyl magnesium (BEM) as catalysts. Once the first polymyrcene block had formed, as indicated by a rise in viscosity, a solution of L- lactide was added, and the solution was stirred for an additional 4 hours at 50°C, resulting in a visible increase in viscosity.

Table 2: Myrcene-lactide copolymerization
with lanthanide borohydrides systems

Entry[a]	[myrcene]/[Nd][f]	[lactide]/[Nd][f]	[Nd][f]/BEM	Yield (%)
1[b]	300	50	1	70
2[c]	300	100	1	88
3[d]	300	50	1	72
4[e]	300	50	1,5	78

[a] Experimental conditions for myrcene: $V_{toluene}$=1mL, T°=70°C, t=2h.
[b] After the polymerization of myrcene, we add soluble lactide in 0,5 mL of toluene.
[c] After the polymerization of myrcene, we add soluble lactide in 1 mL of toluene.
[d] After the polymerization of myrcene, we add soluble lactide in 0,5 mL of THF.
[e] After the polymerization of myrcene, we add soluble lactide in 1 mL of THF.
[f] [Nd]= $[Nd(BH_4)_3(THF)_3]$.

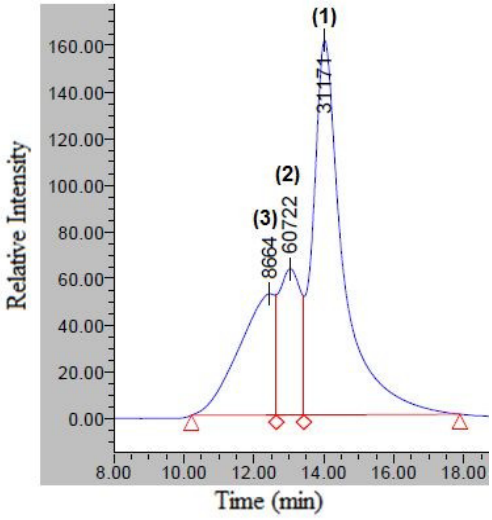

Figure 4: Chromatogram of the myrcene-lactide copolymer obtained using toluene as solvent (Table 2, Entry 1)

The initial experiments (table 2, entries 1 and 2) were conducted in toluene. After allowing the first block of myrcene to grow, lactide was added. The reaction mixture immediately solidifies. The SEC curve of the resulting polymer clearly shows the presence of three peaks with equal average molar masses of 31100, 60700, and 8700 g/mol, respectively, which may correspond to the two homopolymers and the block copolymer (see Figure 4). A sample taken before the addition of lactide showed that the mass of the first block of myrcene is approximately 31000 g/mol. Therefore, peak (1) corresponds to polymyrcene alone, likely due to the deactivation of the system at the time of adding the second monomer. Polymerization of lactide under the same conditions showed that the mass of the polylactide is significantly lower than 31100 g/mol, thus, peak (3) could be assigned to polylactide, while peak (2) could be assigned to a diblock polymyrcene-polylactide.

Additional experiments (table 2, entries 3 and 4) were performed in the presence of THF to reduce the reactivity of the system and thus achieve better reaction control. At best, bimodal SEC curves with PDI=1.75 and Mn=13500 g/mol, was obtained (Figure 5) when the reaction medium contains 1.5 equiv of BEM (table 2, entry 4).

The ^{1}H NMR spectrum of the copolymer in $CDCl_3$ (shown in Figure 6, spectrum 2) displayed signals corresponding to 1,4-*trans* polymyrcene (5 ppm (2H); 2 ppm (8H); 1.5 and 1.6 ppm (6H)) and polylactide signals (5 ppm (2H); 1.5 ppm (6H).

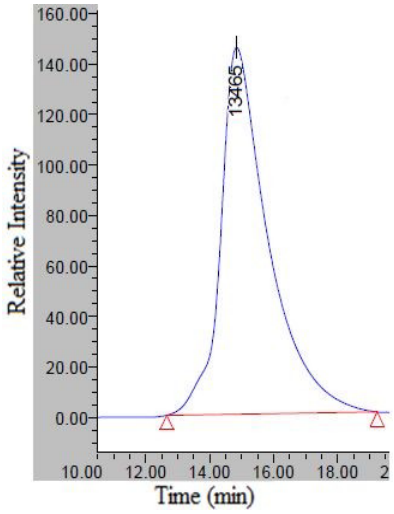

Figure 5: Chromatogram of the myrcene-lactide copolymer obtained usingTHF as solvent (Table 2, Entry 4).

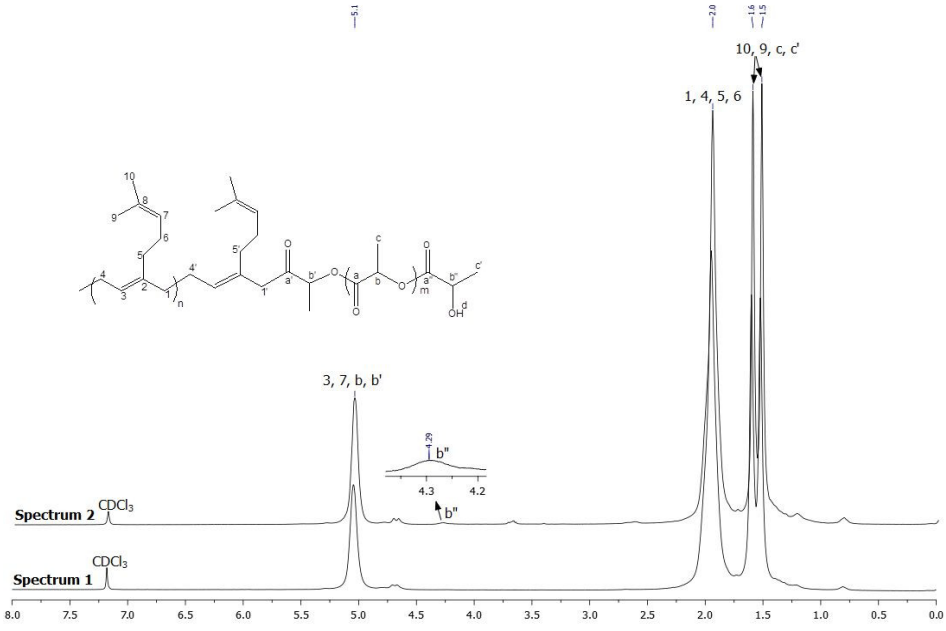

Figure 6: Spectrum 1:^{1}H NMR (300 MHz, $CDCl_3$) spectrum of homopolymyrcene; Spectrum 2: ^{1}H NMR (300 MHz, $CDCl_3$) spectrum of myrcene-lactide copolymer (Table 2, Entry 4)

The new appearing resonance signal at 4,3 ppm of copolymer was assigned to the proton of the methine linked to hydroxyl group.

The ^{13}C NMR spectrum (illustrated in Figure 7, spectrum 2) displays ten signals corresponding to the units of poly(1,4-*trans*-myrcene) as well as signals attributable to polylactide. In the aliphatic part of the spectrum, the presence of two peaks corresponding to the CH_3 groups of the myrcene motif within the copolymer are observed (C9 at 17.7 ppm and C10 at 25.8 ppm), along with a peak of the CH_3 carbon of a lactic acid unit at 16.7 ppm.

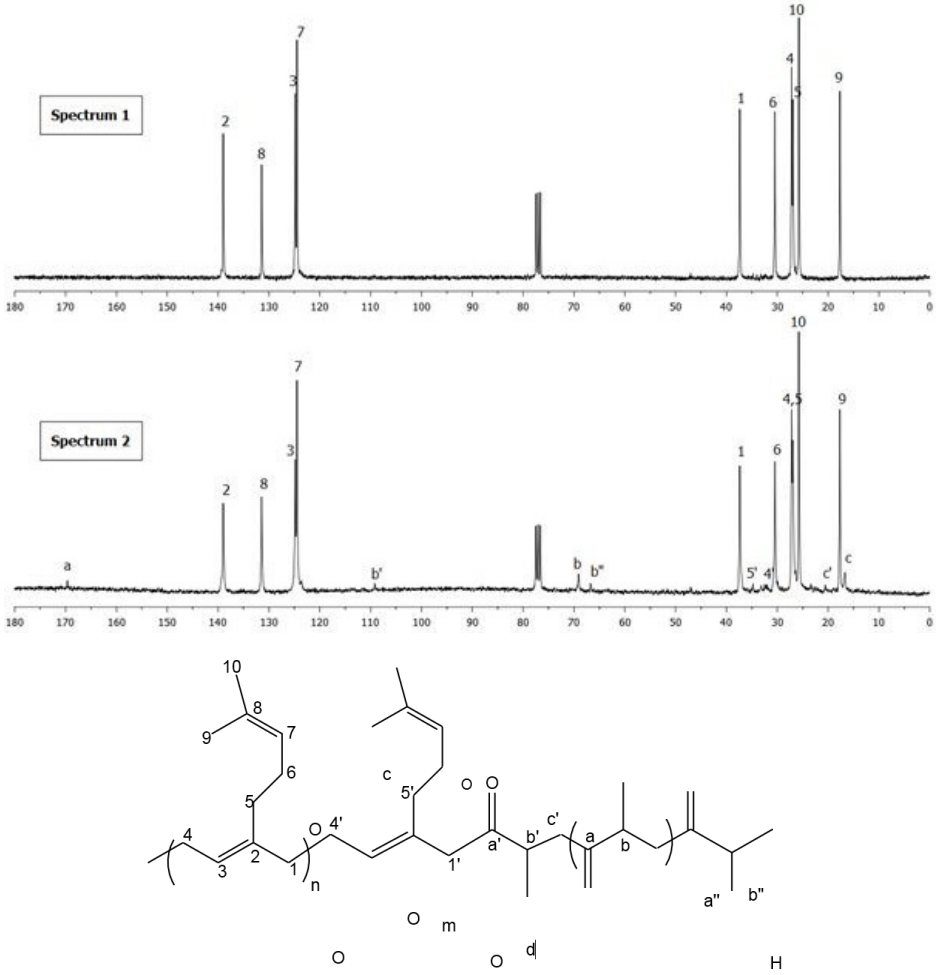

Figure 7: Spectrum 1:^{13}C NMR (75 MHz, $CDCl_3$) spectrum of homopolymyrcene; Spectrum 2: ^{13}C NMR (75 MHz, $CDCl_3$) spectrum of myrcene-lactide copolymer (Table 2, Entry 4) and assignements

Furthermore, four signals corresponding to methylene groups of the myrcene motif (C1 at 37.4 ppm, C4 at 27 ppm, C5 at 27.2 ppm, and C6 at 30.5 ppm) are detected, as well as those of the lactic acid motif around 69.2 ppm. In the olefinic part of the spectrum, the highest chemical shifts correspond to the C=O carbon of polylactide at 169.7 ppm, as well as the two quaternary carbons of the myrcene motif (C2 at 139 ppm and C8 at 131.4 ppm). Additionally, around 124.8 ppm, the signals corresponding to two CH groups of the myrcene motif (C3 and C7) are observed. The ^{13}C NMR data shows additional peaks representing the combination of a myrcene unit with a lactic acid unit. The carbon in the polymyrcene backbone shows two distinct signals. The main signal corresponds to the polymyrcene, where the unit is located next to two other myrcene units, while another signal called (carbon') is assigned to the myrcene-lactic acid linkages in the copolymer (Figure 7). In addition, the ^{13}C NMR indicates that approximately 10% of L-lactide can be incorporated into the polymer without affecting the stereo-selectivity of the reaction. The ^{1}H and ^{13}C NMR signals were assigned on the basis of thepolymyrcene-polylactide diblock [23].

The results obtained show that lanthanide borohydrides are efficient initiators for the block copolymerization of 1,4 conjugated dienes with lactide, resulting in copolymers with well-defined structures. Additionally, the presence of functionalizable terminal groups, such as the vinyl group inthe polydiene block and the hydroxy group in the polylactide block, allows for further modification of the copolymer structure. These terminal groups can be used to attach other functional groups or polymers, leading to the formation of more sophisticated structures with tailored properties.

CONCLUSION

Neodymium trisborohydride ($Nd(BH_4)_3(THF)_3$) precatalysts combined with n-butylethyl magnesium are effective catalysts for the copolymerization of myrcene with styrene. Indeed, the addition of one equivalent of n-butylethyl magnesium in the reaction medium allows the incorporation of approximately 6.7% of styrene into the copolymer, while the structure of the polymyrcene backbone in this copolymer presents about 96.55% of 1,4-*trans* units. However, by increasing the amount of n-butylethyl magnesium increases in the reaction medium up to 1.5 equivalents, it is possible to incorporate 9.9% of styrene, resulting in a modificationof the polymyrcene microstructure with an increase of the 3,4 microstructure under transfer conditions (from 3.44% to 15.72% of 3,4).

The $Nd(BH_4)_3(THF)_3$/BEM system also allows the synthesis of block copolymer of 1,4-*trans* polymyrcene/polylactide, by reducing the reactivity of the polymerization medium through the addition of a solvent such as THF. These studies provide a valuable and promising method for the synthesis of copolymers that serve as interesting precursors for bio-sourced products, thus opening new possibilities for the development of advanced materials with suitable properties.

EXPERIMENTAL SECTION

Materials

All operations were performed under dry argon using a glove box or schlenk techniques. Toluene was purified through alumina column (Mbraun SPS), stored, trap-to-trap distilled over sodium/benzophenone ketyl, then stored on molecular sieves (3A) in a glove box. β-myrcene and styrene (from Aldrich) were dried over calcium hydride, distilled once over molecular sieves, and once again just before use. Lactide was purified by recrystallization in toluene and stored under argon. n-butylethyl magnesium (BEM) (20 wt % in heptane from Texas Alkyls), was used as received. $Nd(BH_4)_3(THF)_3$ was prepared using a method described in the literature [24].

Polymerisation procedure

It is important to note that the use of a glovebox and dry argon is necessary to ensure that moisture and oxygen do not interfere with the reaction. The precatalyst, which is the initial form of the catalyst before activation, was weighted in an aluminum weighting boat inside the glove box to avoid contact with air. Then, the toluene solvent, monomers and cocatalyst were added sequentially using syringes to prevent contamination. The solution was then stirred at 70°C for a specific time to allow the polymerization reaction to occur. After completion of the reaction, the flask was opened to air, and the reaction was quenched with acidified methanol. This step stops the polymerization reaction and stabilizes the resulting polymer. The polymer was then isolated and dried under vacuum until a constant weight was achieved. The use of BHT as a stabilizing agent helps prevent degradation of the polymer during the drying process.

Polymer characterization

The ^{1}H and ^{13}C NMR spectra of polymers were recorded at 300 K, on a Bruker Avance 300 spectrometer.^{1}H experiments of polymyrcene homopolymer and myrcene-lactide copolymers were made in $CDCl_3$ while poly(myrcene-

co-styrene) copolymers were analyzed in $C_2D_2Cl_4$.The quantitative ^{13}C NMR of homopolymers and copolymers were performed in $CDCl_3$ using the zgig sequence from the Bruker library.

Size exclusion chromatography (SEC) was performed in THF as the eluent at 40 °C with a flow rate of 1 mL/min. The chromatography system used a Waters SIS HPLC-pump, a Waters 410 refractometer, and a Waters Styragel column (HR2, HR3, HR4, HR5E), which was calibrated with polystyrene standards.

REFERENCES

1. J. Jenter; N. Meyer; P. W. Roesky; S. K. H. Thiele; G. Eickerling; W. Scherer; *Chem. Eur J.,* **2010**, *16*, 5472 - 5480.
2. M. Visseaux; M. Mainil; M. Terrier; A. Mortreux; P. Roussel; T. Mathivet; M. Destarac; *Dalton Trans*., **2008**, *34*, 4558 - 4561.
3. M. Terrier; M. Visseaux; T. Chenal; A. Mortreux*, J. Polym. Sci., Part A: Polym. Chem.,* **2007**, *45*, 2400 - 2409.
4. F. Bonnet; C. D. C. Violante; P. Roussel; A. Mortreux; M. Visseaux; *Chem. Commun.,* **2009**, 3380 - 3382.
5. A. Ventura; T. Chenal; M. Bria; F. Bonnet; P. Zinck; Y. Ngono-Ravache; E. Balanzat; M. Visseaux; *European Polymer Journal*., **2013**, *49*, 4130 - 4140.
6. P. Zinck; D. Baudry; A. Loupy; *Macromol Rapid Commu.,* **2005**, *26*, 46 – 51.
7. a) S. Loughmari; A. Hafid; A. Bouazza; A. EL Bouadili; P. Zinck; M. Visseaux; *J. Polym. Sci. Part A: Polym. Chem.*, **2012**, *50*, 2898 - 2905. b) S. Georges; M. Bria; P. Zinck; M. Visseaux; *Polymer.*, **2014**, *55*, 3869 - 3878.
8. M. Visseaux; T. Chenal; P. Roussel; A. Mortreux; *J. Organomet. Chem.*, **2006**, *691*, 86 – 92.
9. S. M. Guillaume; M. Schappacher; A. Soum; *Macromolecules*, **2003**, *36*, 54 - 60.
10. I. Palard; A. Soum; S. M. Guillaume, *Macromolecules*, **2005**, *38*, 6888 - 6894.
11. N. Barros; P. Mountford; S. M. Guillaume; L. Maron; *Chem. Eur. J.*, **2008**, *14*, 5507- 5518.
12. A. C. Albertsson; I. K. Varma; *Biomacromolecules*, **2003**, *4*, 1466 - 1486.
13. F. Bonnet; A. C. Hillier; A. Collins; S. R. Duberley; P. Mountford; *Dalton Trans.*, **2005**, 421- 423.
14. D. Barbier Baudry; F. Bouyer; A. S. M. Bruno; M. *Visseaux; Appl. Organomet. Chem.,* **2006**, *20*, 24 - 31.
15. N. Barros; M. Schappacher; P. Dessuge; L. Maron; S. M. Guillaume; *Chem. Eur. J.,* **2008**, *14*, 1881-1890.
16. M. Schappacher; N. Fur; S. M. Guillaume; *Macromolecules*, **2007**, *40*, 8887–8896.
17. W. J. Runckel; L. A. Goldblatt; *Ind. Eng. Chem.*, **1946**, *38*, 749.

18. S. Georges; A. O. Touré; M. Visseaux.; P. Zinck; *Macromolecules*, **2014**, *47*, 14, 4538-4547.
19. A. H. Gleason; J. F. Nelson; US Patent 2829065; **1958**.
20. a) D. H. Lamparelli; V. Paradiso; F. D. Monica; A. Proto; S. Guerra; L. Giannini; C. Capacchione; *Macromolecules*., **2020**, *53*, 1665 -1673. b) S. Loughmari; M. Visseaux; A. Bouazza; A. Hafid; A. El Bouadili; Arkivoc., **2023,** *8*, 202312045.
21. C. Zhou; Z. Wei; X. Lei; Y. Li; *RSC. Adv.*, **2016**, *6*, 63508 – 63514.
22. G. Desurmont; T. Tokimitsu; H. Yasuda; *Macromolecules*, **2000**, *33*, 7679 – 7681.
23. a) C. Zhou; Z. Wei; C. Jin; Y. Wang; Y. Yu; X. Leng; Y. Li; Polymer., **2018**, *138*, 57- 64. b) I. Adoumaz; Valorization of bioresources for the production of polymer films using waterborne latex or nanostructuring block copolymers; University of Pauand Adour country, **2020**, Chapter 5, pp. 208 - 210.
24. Mirsaidov, U.; Shaimuradov, I. B.; Khikmatov, M.; *Russ. J. Inorg. Chem.*, **1986**, *31*, 1321-1323.

STUDIA UBB CHEMIA, LXIX, 1, 2024 (p. 201-218)
(RECOMMENDED CITATION)
DOI:10.24193/subbchem.2024.1.13

RECOVERY OF PHENOLIC COMPOUNDS FROM WILD BILBERRY, BLACKCURRANT AND BLACKBERRY POMACES BY MACERATION AND ULTRASOUND-ASSISTED EXTRACTION

Ana Maria BLEJAN[a], Violeta NOUR[b,*], Alexandru Radu CORBU[b] and Simona Mariana POPESCU[b]

ABSTRACT. Wild bilberry, blackcurrant and blackberry fruit pomaces obtained after industrial juice processing were extracted in water, 1% citric acid, 40%, 60% and 80% (v/v) aqueous ethanol using two extraction methods: maceration and ultrasound-assisted extraction. The total phenolics content (TPC), total anthocyanins content (TAC), and DPPH radical scavenging activity (RSA) were quantified in the extracts. TPC was about 2.3-3.2 times higher in ethanolic extracts as compared with the water extracts. The extracts made in 60% aqueous ethanol showed the highest values of TPC, TAC and RSA irrespective of extraction method and pomace matrix while water and 1% aqueous citric acid were very little effective in recovering anthocyanins and phenolic compounds. Bilberry pomace extracts made in 60% ethanol using maceration presented the highest TAC (585.21 mg CGE/L), TPC (3381.82 mg GAE/L) and RSA (2.05 mmol Trolox/l). The results showed that bilberry, blackcurrant and blackberry fruit pomaces can be a valuable source of bioactive compounds to be used in food supplements and functional foods.

Keywords: *fruit pomaces, extraction, total phenolics content, total anthocyanins content, DPPH radical scavenging activity, correlations*

[a] *Faculty of Food Science and Engineering, Dunărea de Jos University of Galati, Domnească Street 111, 800201 Galati, Romania*
[b] *Department of Horticulture and Food Science, University of Craiova, 13 Al Cuza Street, 200585 Craiova, Romania*
* *Corresponding author: violeta.nour@edu.ucv.ro*

INTRODUCTION

Nowadays berries are widely consumed because they represent an important source of bioactive natural compounds and antioxidants [1] with immense health benefits and medicinal properties [2]. Their production and processing into juices, jams, and jellies, have led to an increase in food waste in the form of skins, pulp, and seeds [3, 4], called by-products that also possess valuable bioactive compounds [5, 6]. Therefore, the valorization of these by-products has become of interest in the research field.

Bilberry (*Vaccinium myrtillus*), also known as the European blueberry, is a wild berry extremely rich in bioactive compounds, mainly polyphenols, with high antioxidant properties. Several potential health benefits have been associated with their consumption including amelioration of type 2 diabetes by reducing glycemia and neuroprotective properties [7, 8]. The pomace generated after bilberry processing in juices, which is mainly composed of seeds and peels, is still abundant in fibers, beneficial phenolic compounds, and other antioxidants [9, 10].

Both wild and cultivated blackcurrant (*Ribes nigrum* L.) represent a rich source of phenolics, especially phenolic acids, anthocyanins, flavonols, condensed tannins, and hydrolyzable tannins [11]. Because of their astringency, blackcurrants are mainly processed in juices, jams, jellies, and alcoholic beverages. Post-processing, a high amount of pomace is generated, which is extremely valuable due to its abundance in fiber and anthocyanins which are known to work in the prevention of cardiovascular illnesses, diabetes, and cancer [12, 13].

Blackberry (*Rubus* spp.) is a berry with increasing consumption in recent years, due to its high content of nutritional and bioactive compounds and its health benefits [14, 15]. Blackberries are consumed either fresh or processed into jam, syrups, wine, tea, and desserts. The pomace resulting from blackberry juice processing is a valuable source of fiber and antioxidants [16,17].

The bioactive substances that are preponderant in berry pomaces are phenolic compounds, fatty acids, and tocopherols [18]. The amount of bioactive compounds in the by-products of berries varies based on berry species, cultivar, genetic factors, growth season and cultivation conditions, ripening stage, and extraction methods [18, 19].

The recovery of high-valuable compounds from fruit by-products, as an alternative to the food waste problem [20-23], has become of major interest in the research field. For these compounds to be delivered in the highest amount with less degradation [24], the extraction operation plays an important role [25].

The selection of the extraction method depends on several factors such as fruit by-product matrices, physicochemical properties of the desired compound, purity of the extract, and economic value [23]. Because the wastes resulting from the processing of fruits are in the form of wet residues (pomace) with a high degree of moisture that can lead to degradation caused by different microorganisms, the preparation of the samples by dehydration and milling also plays a crucial role in the extraction process [26, 27].

For an extended period, conventional methods have been used for the extraction of bioactive compounds from fruits and pomaces [28]. The most utilized conventional methods are maceration, distillation and Soxhlet extraction [25, 26]. These conventional extraction technologies present some drawbacks like prolonged extraction time, potentially harmful solvent residue, low yields, and inferior purity of the target compounds [27, 29]. Therefore, nowadays the focus is on novel, innovative extraction technologies that have emerged as fast and efficient, safe for the environment [30], based on green chemistry principles [31].

For extraction technologies to be considered efficient and eco-friendly, they have to meet the criteria for reduced solvent consumption and energy [22], shorter operation time that can lead to less or no damage to the bioactive molecules, and high surface area of the desired compound that comes in contact with the chosen solvent [32]. Among these new technologies, pulsed electric field, ultrasound, enzyme-assisted extraction, microwave-assisted extraction, and supercritical fluid extraction [33-35] are the most commonly used for the extraction of bioactive compounds from fruits and pomaces.

Ultrasound-assisted extraction (UAE) principle works on cavitation, a phenomenon based on the ability of ultrasonic waves to produce energy dissipation by compression and rarefaction in a liquid medium, that is the extraction solvent, with the generation and subsequent collapse of vapor bubbles or cavities that transform the acoustic energy into thermal energy and cause mechanical agitation [35, 36]. This leads to the amplification of surface area contact between solid and liquid phases [37] and the rupture of plant cell structures enhancing the release and extraction of intracellular bioactive components [38].

When choosing an extraction method, several parameters must be adjusted for optimal operation, including liquid-solid ratio, extraction temperature, pH, extraction time, type and concentration of the solvent [4, 39]. Our study aimed to investigate the influence of extraction solvent (water, 1% aqueous citric acid, 40%, 60% and 80% aqueous ethanol) on conventional maceration and ultrasound-assisted recovery of bioactive phenolics from wild bilberry, blackcurrant, and blackberry pomaces. The resulting extracts were compared concerning their total phenolics content, total anthocyanins content, and DPPH radical scavenging activity.

RESULTS AND DISCUSSION

Extraction of phenolic compounds

Results on the total phenolic content of berry pomace extracts are presented in Figure 1 (a-c). In bilberry pomace extracts, the maximum and minimum TPC values were 3381.82±146.67 GAE/l (in 60% ethanol) and 981.82±38.14 mg GAE/l (in water) after maceration while 2245.45±75.56 mg GAE/l (in 60% ethanol) and 872.73±24.45 mg GAE/l (in water) after ultrasound-assisted extraction. In a previous study, Aaby et al. [40] reported a total phenolic content between 249 and 1153 mg GAE/l of extract made using hot water from the press residue obtained after industrial bilberry juice processing.

In blackcurrant pomace extracts, the total phenolic content ranged from 500.09±18.33 to 2227.27±88.56 mg of gallic acid equivalents per liter. The highest total phenolic content was found in the extracts using 60% alcohol as a solvent (2227.27±88.56 mg GAE/l), followed by those made in 40% ethanol (2036.36±96.23 mg GAE/L). Nour et al. [41] reported only 1371.1-1665.1 mg GAE/l in blackcurrant fruit extracts made in 60% ethanol and 1261.7-1646.5 mg GAE/l in those made in 40% ethanol. The increase of ethanol concentration to 80% resulted in a significantly lower extraction of phenolics from blackcurrant pomace as compared with the extraction in 60% ethanol, in agreement with the findings of Cacace and Mazza [42] who found that the content of total phenolics extracted from black currants with aqueous ethanol increased with ethanol concentration up to a maximum at about 60% and then decreased with further increase in ethanol concentration. In contrast to these results, Pompeu et al. [43] reported that 70-80% aqueous ethanol maximized the yields of total phenolics and total anthocyanins extracted from fruits of *Euterpe oleracea* (Açai palm).

In blackberry extracts, total phenolic content ranged between 754.55±28.32 and 2454.55±112.21 mg GAE/l after maceration and between 336.36±14.22 and 1827.27±77.11 mg GAE/l as a result of UAE extraction. In a study on ultrasound-assisted recovery of phenolics from blueberry pomace, Bamba et al. [44] reported a total phenolic content ranging from 5.84 to 6.31 mg GAE/g DM in water extracts obtained at a solid/liquid ratio of 1/20 at 40 °C and noticed that extraction duration significantly affected TAC, but not, TPC. In agreement with our results, Bamba et al. [44] found that TPC, TFC and TAC were about 5, 3 and 1.5 times greater in the ethanolic extracts, respectively, than in the water extracts.

The lower concentration of phenolics in water and 1% aqueous citric acid extracts as compared with the ethanolic extracts may be attributed to the nonpolar portions of the polyphenols, including aromatic rings, which limit their solubility in a highly polar solvent such as water.

The higher extraction yields of polyphenols in binary solvents of ethanol and water have been previously reported and they were related to the contribution of ethanol to increase their solubility by reducing the dielectric constant of the aqueous solvent and by increasing the diffusion of polyphenols in the solvent, and again of water to enhance their desorption from plant matrices [45]. Previous studies concluded also that water is an important co-solvent for the extraction of anthocyanins and total polyphenols from blackcurrant [1] and elderberry pomace [46].

A similar variation was found in the present study during maceration. In agreement with these findings, Ćujić et al. [47] reported also higher concentrations of TPC and TAC in chokeberry extracts made with 50% ethanol as compared to those made with water.

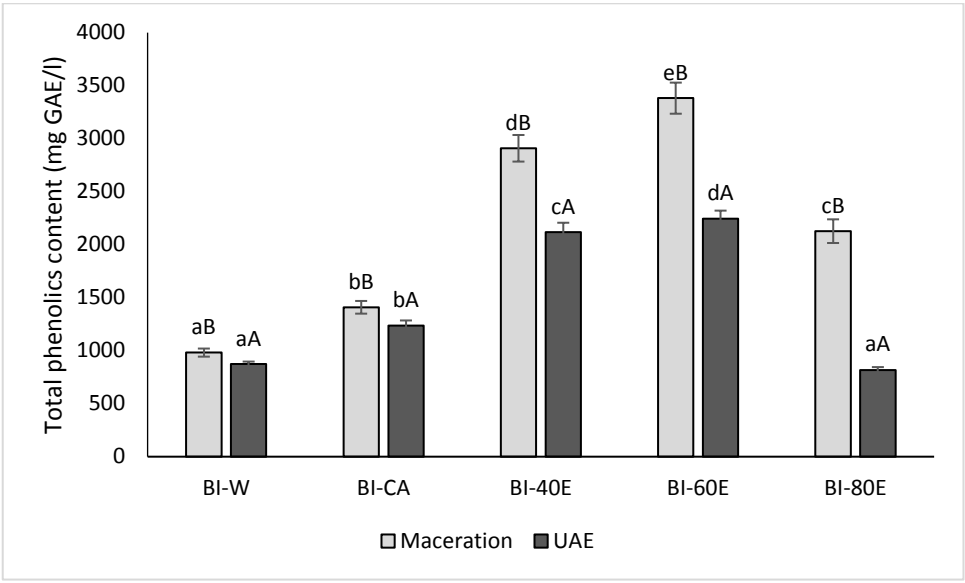

(a)

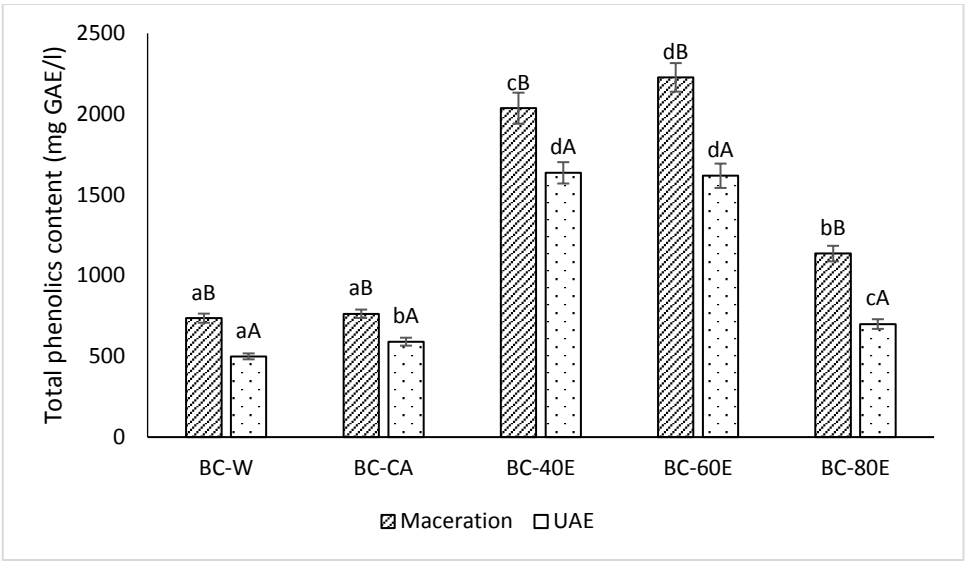

(b)

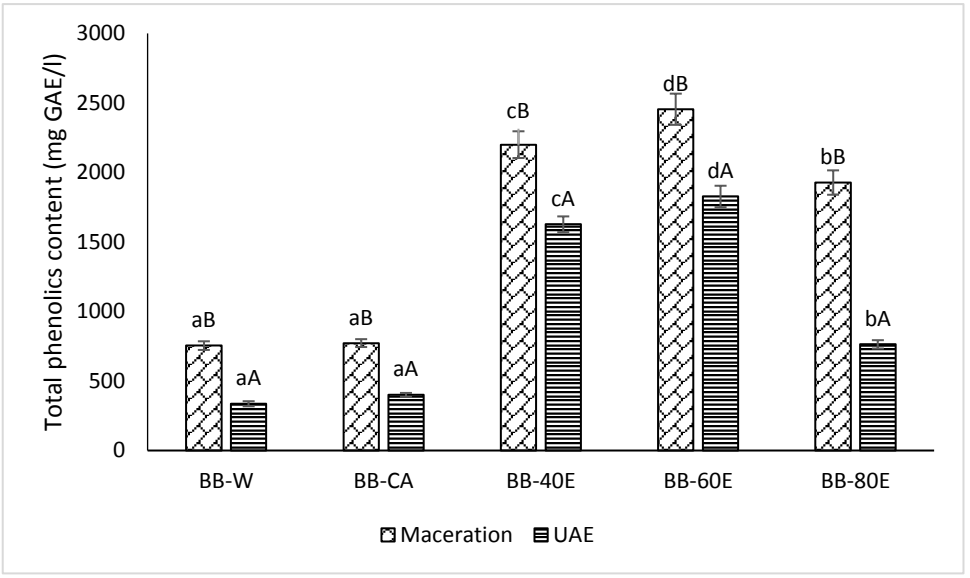

(c)

Figure 1. Effect of solvent on the total phenolic content of (a) bilberry (BI), (b) blackcurrant (BC) and (c) blackberry (BB) pomace extract made in water (W), 1% aqueous citric acid (CA), 40% aqueous ethanol (40E), 60% aqueous ethanol (60E), 80% aqueous ethanol (80E). Different uppercase letters indicate significant differences between extraction methods ($p < 0.05$) for the same solvent, while different lowercase letters are indicative of significant differences between solvents for the same extraction method ($p < 0.05$).

In the chokeberry extracts obtained through maceration, the phenolic content was about 1.5-2 times higher in ethanolic extracts as compared with the water extracts [47] while in our study the magnitude of the difference in phenolic contents between ethanolic and water extracts was about 2.5–3.2 times. Lapornik et al. [48] reported also that the phenolic content of ethanol extracts made without sonication was 2 times greater in red and black currant 70% ethanolic extracts as compared with water extract and concluded that the extraction yields vary greatly with plant material and extraction conditions.

In addition to being recognized as safe for food applications, ethanol is a suitable solvent for polyphenol extraction. However, Bamba et al. [44] found significantly higher TPC, TFC, TAC and DPPH free radical scavenging activity in the extracts made in 50% aqueous ethanol compared to 90% ethanol. They found also that increasing the concentration of ethanol from 50% to 90% resulted in significantly lower values of TPC, TAC and DPPH free radical scavenging activity than those obtained with 50% ethanol and attributed this behavior to the dehydration effect of ethanol on the plant cells which could prevent the diffusion of polyphenols from the plant material to the solvent. In blueberry leaves, Wang et al. [49] also found that phenolic extraction yield from blueberry leaves increased when raising ethanol concentration from 40% to 70%, while the further increase of ethanol concentration up to 90% decreased the extraction yield.

The addition of 1% citric acid to the water used as a solvent caused an increase in the amount of phenolic compounds extracted from all pomaces, however, the increase was not significant except for the bilberry pomace. The available literature shows that pH is an important parameter affecting the extractability of polyphenolic compounds. Moreover, the different phenolic fractions are differently affected by the pH decrease.

Maceration for 10 days proved to be more effective in extracting phenolic compounds than ultrasound-assisted extraction for 60 min for all three analyzed pomaces. Previously, Varo et al. [50] compared UAE combined with stirring versus conventional maceration on the anthocyanins and flavonol profile, as well as on the antioxidant capacity extraction from freeze-dried bilberry juice by-products using water as a green extraction solvent. They found higher total phenolic content and antioxidant activity when ultrasound was used. The highest total phenolic content was found in bilberry extracts regardless of the method or solvent used. The total phenolic content in bilberry extracts was higher than in blackberry extracts made in water and 1% citric acid, while it reversed in the extracts made in the ethanol/water mixture.

Extraction of anthocyanins

Bilberry pomace is a rich source of anthocyanins and several methods have been carried out to improve their extraction [13]. The use of 60% ethanol

as a solvent achieved the efficient recovery of anthocyanins from bilberry pomace (585.21±16.87 mg CGE/l) followed by 40% ethanol (470.45±14.44 mg CGE/l) and 80% ethanol (417.09±12.45 mg CGE/l) (Figure 2, a-c). Water and 1% aqueous citric acid were very little effective in extracting anthocyanins (31.20±0.89 and 43.64±1.22 mg CGE/l, respectively). Lapornik et al. [48] demonstrated that long extraction times in water (1-24 h) can lead to a decrease in TPC and TAC of red currant and black currant by-product extracts made without sonication and related these results to the degradation of anthocyanin compounds during the excessively long extraction. In good agreement with our results, Aaby et al. [40] reported 95 to 625 mg CGE/l of extract made in hot water from the press residue obtained after industrial bilberry juice processing. The same as for phenolic compounds, the 60% aqueous ethanol provided the best anthocyanins extraction yield from all three pomace matrices.

Ultrasound achieved higher extraction of anthocyanins from blackcurrant pomaces as compared with maceration, while for bilberry pomace maceration was more effective. Bamba et al. [44] previously concluded that an extraction time between 30 and 60 min would be a good compromise for the ultrasound-assisted extraction of anthocyanins to avoid longer processing times while Varo et al. [50] found that monomeric anthocyanin content decreased after 60 min of ultrasound-assisted extraction from bilberry juice by-products, revealing a degradation phenomenon induced by the technology.

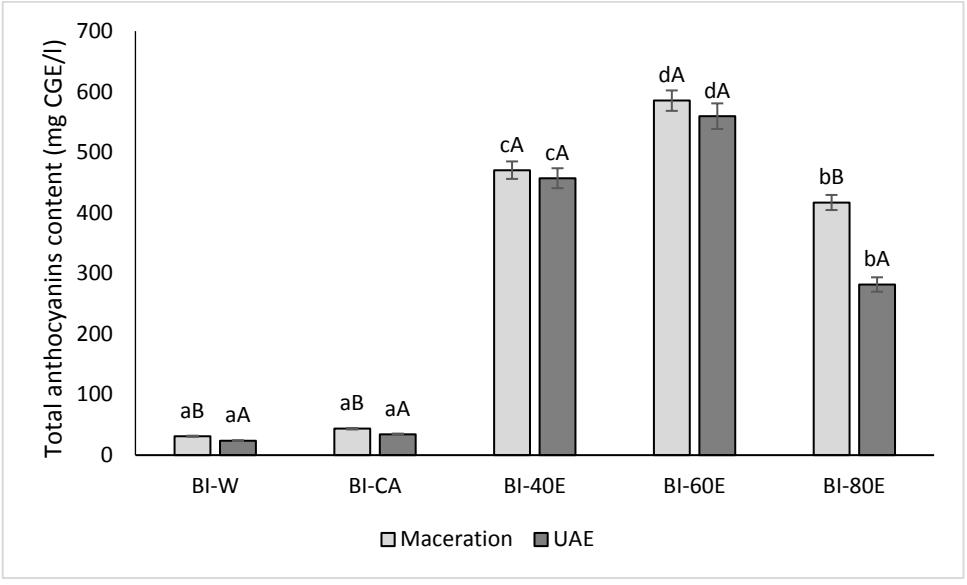

(a)

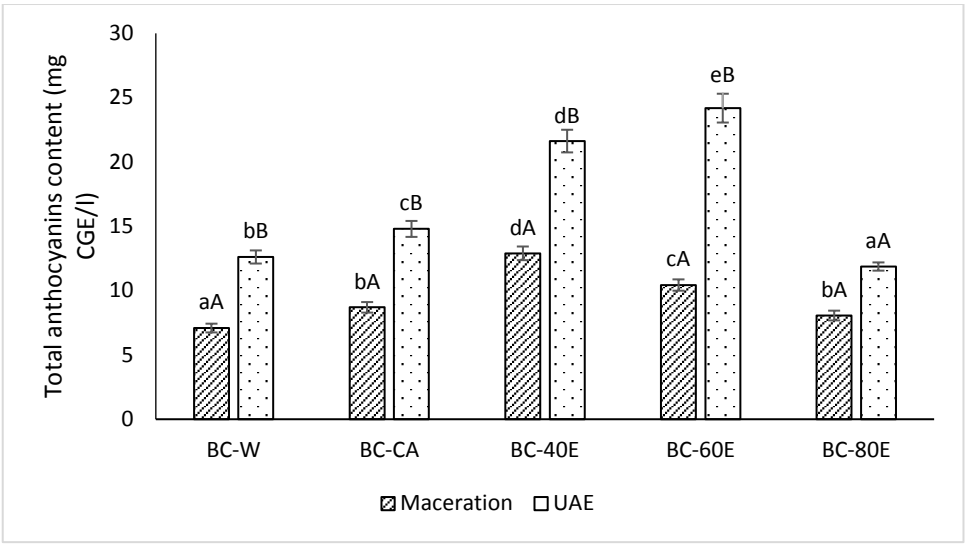

(b)

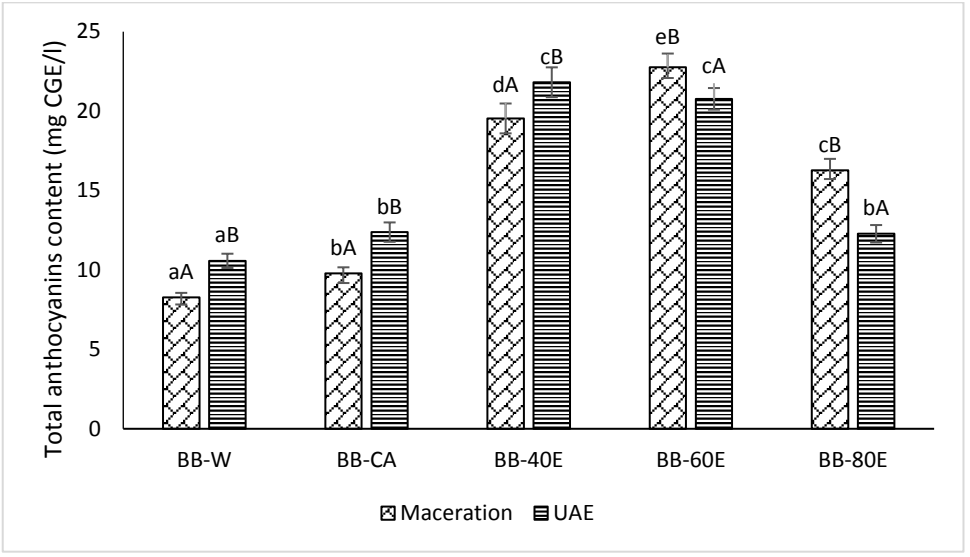

(c)

Figure 2. Effect of solvent on the total anthocyanin content of (a) bilberry (BI), (b) blackcurrant (BC) and (c) blackberry (BB) pomace extract made in water (W), 1% aqueous citric acid (CA), 40% aqueous ethanol (40E), 60% aqueous ethanol (60E), 80% aqueous ethanol (80E). Different uppercase letters indicate significant differences between extraction methods ($p < 0.05$) for the same solvent, while different lowercase letters are indicative of significant differences between solvents for the same extraction method ($p < 0.05$).

As for blackberry pomace, ultrasound was more effective than maceration when using water, 1% citric acid and 40% ethanol and less effective when using 60% and 80% ethanol as a solvent. Zafra-Rojas et al. [51] found a lower extraction yield of anthocyanins from blackberry (*Rubus fructicosus*) residues using ultrasound as compared with conventional extraction methods.

Antioxidant activity

The antioxidant capacity of bilberry, blackcurrant and blackberry extracts obtained by maceration and UAE were assessed by DPPH radical scavenging activity evaluation assay (Figure 3, a-c).

DPPH radical scavenging activity values in the extracts performed with water both in maceration and UAE were lower compared to the extracts made in polar mixtures of ethanol/water. The highest levels of radical scavenging activity were found in bilberry pomace extracts, ranging from 0.75±0.03 to 2.05±0.07 mmol Trolox/l, depending on the solvent used. As expected, the maximum radical scavenging activity of pomace extracts was achieved in 60% ethanol. Except for blackcurrant, in our study we found very strong correlations (r>0.9) between total phenolics content and radical scavenging activity of the pomaces extracts, in agreement with several previous studies on berry and berry pomaces extracts [52-54].

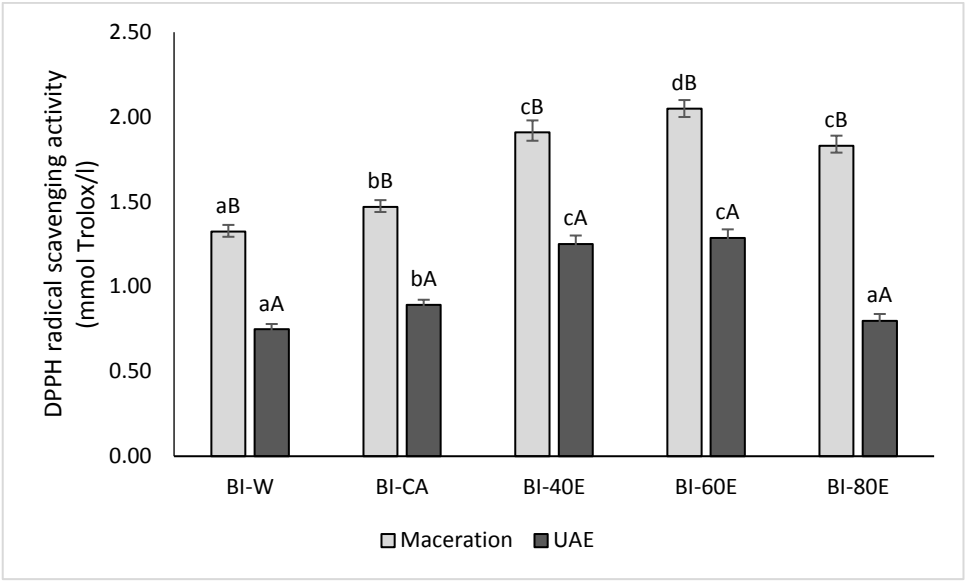

(a)

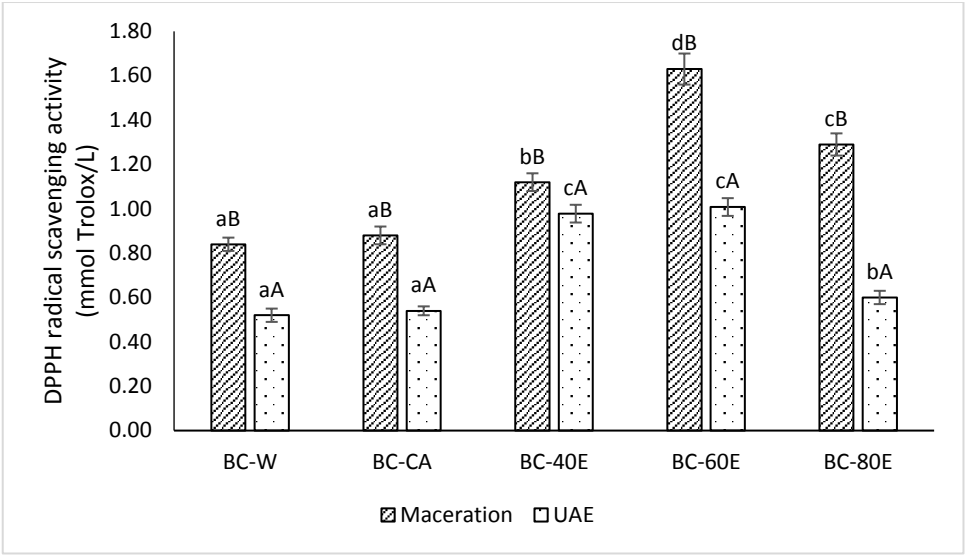

(b)

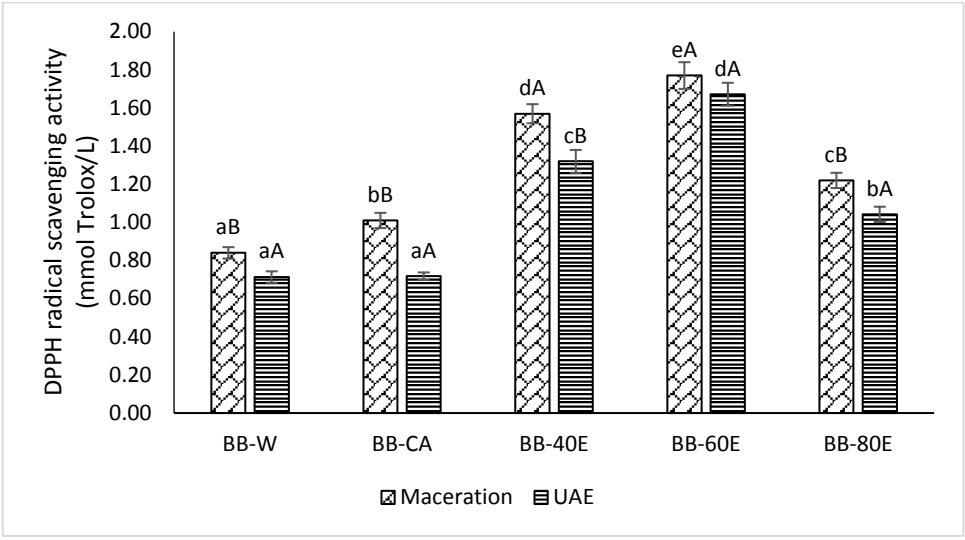

(c)

Figure 3. Effect of solvent on the DPPH radical scavenging activity of (a) bilberry (BI), (b) blackcurrant (BC) and (c) blackberry (BB) pomace extract made in water (W), 1% aqueous citric acid (CA), 40% aqueous ethanol (40E), 60% aqueous ethanol (60E), 80% aqueous ethanol (80E). Different uppercase letters indicate significant differences between extraction methods ($p < 0.05$) for the same solvent, while different lowercase letters are indicative of significant differences between solvents for the same extraction method ($p < 0.05$).

Total anthocyanin content was also highly correlated with antioxidant activity in blackcurrant UAE extracts (Table 1). Nour et al. [41] found also good correlations between antioxidant activity and the sum of anthocyanins (r=0.85) and only a moderate correlation (r=0.78) between total phenolics content and antioxidant activity of blackcurrant alcoholic extracts. However, Vulić et al. [55] found a high linear correlation between the IC50 and the content of anthocyanins (r^2=0.98) and polyphenols (r^2=0.85) of four berry (bilberry, blackberry, strawberry and raspberry) fruits pomaces, indicating the great importance of these compounds in the radical scavenging activity.

Very strong correlations were found between DPPH radical scavenging activity, total phenolic content and total anthocyanins content in blackberry extracts.

Table 1. Correlation matrix (Pearson coefficients and p values in brackets; n=45) for TAC, TPC and RSA of bilberry, blackcurrant and blackberry pomace extracts

Pomace		Maceration			UAE		
		TAC	TPC	RSA	TAC	TPC	RSA
Bilberry	TAC	1	0.9585** (0.0101)	0.9875*** (0.0017)	1	0.8178 (0.0907)	0.8714 (0.0543)
	TPC		1	0.9738** (0.0044)		1	0.9938*** (0.0006)
	RSA			1			1
Blackcurrant	TAC	1	0.8365 (0.0774)	0.3733 (0.5360)	1	0.9509** (0.0130)	0.9547** (0.0115)
	TPC		1	0.7839 (0.1165)		1	0.9981*** (0.0001)
	RSA			1			1
Blackberry	TAC	1	0.9862*** (0.0019)	0.9822*** (0.0028)	1	0.9666*** (0.0073)	0.8862** (0.0453)
	TPC		1	0.9408** (0.0171)		1	0.9731*** (0.0053)
	RSA			1			1

*** The significance level is 0.1% or less
** The significance level is 1% or less

Zafra-Rojas et al. [51] reported also a good correlation between antioxidant activity by ABTS and phenolic compounds and anthocyanins (r^2=0.824, r^2=0.893, respectively) in blackberry residues extracts, but not in

the case of DPPH. These findings have been attributed to the presence of other antioxidants such as ascorbic acid or other nonphenolic components present in berries' seed oil.

Regarding the extraction method, the results show the highest radical scavenging activity in the extracts made through maceration as compared with UAE in all three matrices and using all investigated solvents.

CONCLUSIONS

The results showed that bilberry, blackcurrant and blackberry pomaces contain considerable amounts of polyphenols and anthocyanins which deserve to be recovered and used to formulate food supplements and functional foods. The total phenolic content was about 2.3-3.2 times higher in ethanolic extracts as compared with the water extracts, showing that the presence and concentration of ethanol in the aqueous environment had significant effects on the extraction yields of these antioxidant compounds. The extracts made in 60% aqueous ethanol presented the highest values for TPC, TAC and RDA irrespective of extraction method and pomace matrix while water and 1% aqueous citric acid were very little effective in recovering anthocyanins or even phenolic compounds. Among the three pomace matrices, the highest TAC, TPC and RSA were found in bilberry pomace extracts made both using maceration and UAE. Correlation analyses revealed strong correlations between DPPH radical scavenging activity, total phenolic content and total anthocyanin content in bilberry and blackberry extracts and lower correlations in blackcurrant pomace extracts. Under the conditions of this experiment, the extracts obtained by maceration presented higher TPC values and were more antioxidant than the extracts obtained by UAE.

EXPERIMENTAL SECTION

Materials

Wild bilberries (*Vaccinium myrtillus* L.), blackcurrants (*Ribes nigrum* L.) and blackberries (*Rubus fructicosus* L.) harvested from the wild flora of Valcea county (South-West Oltenia Region, Romania) were subjected to industrial juice processing at a commercial juice manufacturer from Vaideeni (Vâlcea county, Romania). The berries were processed without enzyme treatment and samples of 5 kg fresh pomaces, consisting of peels, seeds, and residual pulp, were collected for each species. The pomaces were stored frozen (at −18 °C)

in sealed polyethylene sacks until further use. When needed, aliquots of the frozen pomaces were thawed in the air at room temperature and dried at 57°C in a convective laboratory dryer (Deca +SS Design, Profimatic, Romania). The dried pomaces were ground in a household electric grinder, sieved using a 0.5 mm screen, and stored in closed containers at 20 °C in the dark until use.

Chemicals and reagents

DPPH (2,2-diphenyl−1-picrylhydrazyl), methanol (Merck) and 6-hydroxy−2,5,7,8-tetramethylchroman-2-carboxylic acid (Trolox) purchased from Sigma-Aldrich (Steinheim, Germany) were employed for the determination of the radical scavenging activity. Folin-Ciocalteu's phenol reagent (2N, Sigma-Aldrich), gallic acid (99% purity, Sigma-Aldrich) and anhydrous sodium carbonate (Merk) were used for the determination of the total phenolic content. Hydrochloric acid, potassium chloride and sodium acetate provided by Merck (Darmstadt, Germany) were of reagent grade and used without further purification.

Preparation of the extracts

The berry pomaces (BI – bilberry, BC – blackcurrant, BB – blackberry) were subjected to conventional maceration and ultrasound-assisted extraction using five different extraction solvents: water (W), 1% (w/v) aqueous citric acid (CA), 40% (40E), 60% (60E) and 80% (v/v) (80E) aqueous ethanol. Three grams of powdered pomace were extracted with 30 ml solvent. The total time for ultrasound-assisted extraction was 60 min while conventional maceration was carried out without stirring for ten days at room temperature. Ultrasound-assisted extraction was performed in a DK 102 p Bandelin ultrasonic bath (Bandelin Electronic GmbH, Berlin, Germany). Extracts were then filtered using Whatman membrane filters 0.45 μm and stored at 4 ◦C until analysis. Each experiment was done in triplicate.

Total anthocyanin content

Total anthocyanin content was determined according to the pH differential method proposed by Lee et al. [56]. Briefly, the extracts were properly diluted in 0.025 M potassium chloride buffer at pH 1.0 and 0.04 M sodium acetate buffer at pH 4.5 insomuch that their absorbances, measured after 30 min of incubation at room temperature on a Varian Cary 50 spectrophotometer (Varian Co., USA) at 510 and 700 nm, were lower than 1000. The total anthocyanin content was calculated using the following formula:

$$\text{Total anthocyanins (mg CGE/L)} = (A \times MW \times DF \times 1{,}000)/(\varepsilon \times l)$$

where $A = (A_{510\ nm} - A_{700\ nm})pH\ 1.0 - (A_{510\ nm} - A_{700\ nm})pH\ 4.5$; MW is the molecular weight of cyanidin-3-O-glucoside (449.2 g/mol); DF is dilution factor of the samples; ε is the molar absorbtivity of cyanidin 3-*O*-glucoside [29,600 L/(mol•cm)]; l is the cuvette path length (1 cm). The results were expressed in milligrams of cyanidin-3-O-glucoside equivalents per liter of extract (mg CGE/L).

Total phenolic content

The total phenolic content of the extracts was assessed by the Folin–Ciocalteu spectrophotometric method described by Singleton et al. [57]. Briefly, an aliquot of extract (0.1 mL) diluted tenfold with distilled water was mixed with 5 mL of distilled water and 0.5 mL of Folin-Ciocalteu reagent (diluted 1:1 with distilled water). After 3 min, 1.5 mL of sodium carbonate solution (20% w/v) was added and the mixture was made up to 10 mL with distilled water. The solution was mixed thoroughly and incubated at 40 °C for 30 minutes in the dark. Further, the absorbance was measured at 765 nm using a Varian Cary 50 UV spectrophotometer (Varian Co., USA). A standard curve of gallic acid was prepared (50–250 mg/L) and the results were expressed in milligrams of gallic acid equivalents per liter of extract (mg GAE/L).

DPPH radical-scavenging activity

The pomace extracts were evaluated for their capability to scavenge the DPPH radical using the spectrophotometric method previously described by Oliveira et al. [58]. Briefly, aliquots of 50 µL extract were mixed with 3 mL of DPPH methanolic solution (0.004%). After shaking and incubation in the dark for 30 min, the absorbance of the reaction mixture was read at 517 nm with a Varian Cary 50 UV-VIS spectrophotometer (Varian Co., USA). The inhibition of the DPPH radical by the sample was calculated as follows:

$$\text{DPPH scavenging activity (\%)} = (1 - \text{absorbance of sample/absorbance of blank}) \times 100$$

Trolox was used as a standard reference and results were expressed in millimoles of Trolox per liter of extract (mmol Trolox/L).

Statistical analysis

Extraction experiments and composition analyses were carried out in triplicate and the results were expressed as mean ± standard deviation. Data were evaluated by one-way analysis of variance (ANOVA) using Statgraphics Centurion XVI software (StatPoint Technologies, Warrenton, VA). The significance

of differences was analyzed using the Multiple Range Test based on Fisher's least significant difference (LSD) procedure at $p < 0.05$. The correlation coefficients and their significance were calculated by Pearson's test.

REFERENCES

1. H. I. O. Basegmez; D. Povilaitis; V. Kitrytė; V. Kraujalienė; V. Šulniūtė; C. Alasalvar; P. R. Venskutonis; *J. Supercrit Fluids*, **2017**, *124*, 10–19
2. O. Golovinskaia; C.-K. Wang; *Molecules*, **2021**, *26*, 3904
3. N. P. Kelly; A. L. Kelly; J.A. O'Mahony; *Trends Food Sci. Technol.*, **2019**, *83*, 248–258
4. K. Kumar; S. Srivastav; V. S. Sharanagat; *Ultrason. Sonochem.*, **2021**, *70*, 105325
5. S. A. Khan; R. Aslam; H. A. Makroo; *J. Food Process Eng.*, **2019**, 42
6. N. Jiménez-Moreno; I. Esparza; F. Bimbela; L. M. Gandía; C. Ancín-Azpilicueta; *Crit. Rev. Environ. Sci. Technol.*, **2020**, *50*, 2061–2108
7. M. Alnajjar; S. K. Barik; C. Bestwick.; F. Campbell; M. Cruickshank; F. Farquharson; G. Holtrop; G. Horgan; P. Louis; K.-M. Moar; et al.; *J. Funct. Foods*, **2020**, *64*, 103597
8. D. Milenkovic; I. Krga; A. Dinel; C. Morand; S. Laye; N. Castanon; *J. Funct. Foods*, **2021**, *85*, 104609
9. G.-I. Hidalgo; M. Almajano; *Antioxidants*, **2017**, *6*, 7
10. A. M. Blejan; V. Nour; B. Păcularu–Burada; S. M. Popescu; *Int. J. Food Prop.*, **2023**, *26*, 1579–1595
11. L. Cao; Y. Park; S. Lee; D.-O. Kim; Appl. Sci., **2021**, *11*, 1863
12. N. Pap; S. Beszedes; E. Pongracz; L. Myllykoski; M. Gabor; E. Gyimes; C. Hodur; R. L. Keiski; *Food Bioprocess Technol.*, **2013**, *6*, 2666–2674
13. I. Piasecka; A. Wiktor; A. Górska; *Appl. Sci.*, **2022**, *12(3)*, 1734
14. M. Schulz; S. K. T. Seraglio; F. Della Betta; P. Nehring; A. C. Valese; H. Daguer; L. V. Gonzaga; A. C. O. Costa; R. Fett; *Food. Res. Int.*, **2019**, *122*, 627–634
15. L. Kaume; L. R. Howard; L. Devareddy; *J. Agric. Food. Chem.*, **2012**, *60(23)*, 5716–5727
16. G. O. Isopencu; A. Stoica-Guzun; C. Busuioc; M. Stroescu; I. M. Deleanu; *Carbohydr. Polym. Technol Appl.*, **2021**, *2*, 100057
17. Ž. Tarasevičienė; I. Čechovičiene; A. Paulauskienė; M. Gumbytė; A. Blinstrubienė; N. Burbulis; *Foods*, **2022**, *11(15)*, 2180
18. M. Fidelis; C. de Moura; T. Kabbas Junior; N. Pap; P. Mattila; S. Mäkinen; P. Putnik; D. Bursać Kovačević; Y. Tian; B. Yang; et al.; *Molecules*, **2019**, *24*, 3854
19. C. Govers; M. Berkel Kasikci; A. A. van der Sluis; J. J. Mes; *Nutr. Rev.*, **2018**, *76*, 29–46
20. D. A. Campos; R. Gómez-García; A. A. Vilas-Boas; A. R. Madureira; M. M. Pintado; *Molecules*, **2020**, *25*, 320
21. M. A. Chaouch; S. Benvenuti; *Foods*, **2020**, *9*, 1716
22. M. Lianza; L. Marincich; F. Antognoni; *Antioxidants*, **2022**, *11*, 2169

23. A. Patra; S. Abdullah; R. C. Pradhan; *Bioresour. Bioprocess.*, **2022**, *9*, 14
24. G. C. V. Gamage, W. S. Choo; *Heliyon*, **2023**, *9(3)*, e14426
25. Q. W. Zhang; L. G. Lin; W. C. Ye; *Chin. Med.*, **2018**, *13*
26. X. L. Ran; M. Zhang; Y. Wang; B. Adhikari; *Crit. Rev. Food.*, **2019**, *59*, 450–461
27. S. S. Nadar; P. Rao; V. K. Rathod; *Food Res. Int.*, **2018**, *108*, 309–330
28. N. A. Sagar; S. Pareek; S. Sharma; E. M. Yahia; M. G. Lobo; *Compr. Rev. Food Sci. Food Saf.*, **2018**, *17*, 512–531
29. S. J. Marathe; S. B. Jadhav; S. B. Bankar; K. K. Dubey; R.S. Singhal; *Curr. Opin. Food Sci.*, **2019**, 25, 62–72
30. F. Garavand; S. Rahaee; N. Vahedikia; S. M. Jafari; *Trends Food Sci. Technol.*, **2019**, *89*, 26–44
31. R. C. Fierascu; E. Sieniawska; A. Ortan; I. Fierascu; J. Xiao; *Front. Bioeng. Biotechnol.*, **2020**, *8*, 319
32. P. Gong; S. Wang; M. Liu; F. Chen; W. Yang; X. Chang; N. Liu; Y. Zhao; J. Wang; X. Chen; *Carbohydr. Res.*, **2020**, *494*, 108037
33. F. Garavand; S. Rahaee; N. Vahedikia; S. M. Jafari; *Trends Food Sci. Technol.*, **2019**, *89*, 26–44
34. O. Gligor; A. Mocan; C. Moldovan; M. Locatelli; G. Crisan; I. C. F. R. Ferreira; *Trends Food Sci. Technol.*, **2019**, *88*, 302–315
35. H. S. Arruda; E. K. Silva; N. M. Peixoto Araujo; G. A. Pereira; G. M. Pastore; M. R. Marostica Junior; *Molecules*, **2021**, *26*, 2632
36. J. Li; Z. Chen; H. Shi; J. Yu; G. Huang; H. Huang; *Ultrason. Sonochem.*, **2023**, *93*, 106295
37. K. Mkadmini; A. Jdey; C. Abdelly; H. Majdoub; R. Ksouri; *Food Chem.*, **2015**, *184*, 80–89
38. P. Selvakumar; V. Karthik; P. S. Kumar; P. Asaithambi; S. Kavitha; P. Sivashanmugam; *Chemosphere*, **2021**, *263*, 128071
39. X.-Q. Chen; Z.-H. Li; Z.-J. Wang; L.-L. Liu; T.-T. Sun; J.-Z. Ma; Y. Zhang; *Ind. Crops Prod.*, **2020**, *150*, 112420
40. K. Aaby; S. Grimmer; L. Holtung; *Lwt Food Sci. Technol.*, **2013**, *54*, 257–264
41. V. Nour; F. Stampar; R. Veberic; J. Jakopic; *Food Chem.*, **2013**, *141*, 961–966
42. J. E. Cacace; G. Mazza; *J. Food Sci.*, **2003**, *68*, 240–248
43. D. R. Pompeu; E. M. Silva; H. Rogez; *Bioresour. Technol.*, **2009**, *100*, 6076–6082
44. B. S. B. Bamba; J. Shi; C. C. Tranchant; S. J. Xue; C. F. Forney; L.-T. Lim; *Molecules*, **2018**, *23*, 1685
45. M. N. Safdar; T. Kausar; S. Jabbar; A. Mumtaz; K. Ahad; A. A. Saddozai; *J. Food Drug Anal.*, **2017**, *25*, 488–500
46. I. J. Seabra; M. E. M.Braga; M. T. Batista; H. C. de Sousa; *J. Supercrit. Fluids*, **2010**, *54*, 145–152
47. N. Ćujić; K. Šavikin; T. Jankovic; D. Pljevljakušić; G. Zdunić; S. Ibric; *Food Chem.* **2016**, *194*, 135–142
48. B. Lapornik; M. Prošek; G. A. Wondra; *J. Food Eng.*, **2005**, *71*, 214–222
49. T. Wang; N. Guo; S. X. Wang; P. Kou; C. J. Zhao; Y. J. Fu. *Food Bioprod. Process.*, **2018**, *108*, 69–80

50. M. A. Varo; M. Jacotet-Navarro; M. P. Serratosa; J. Mérida; A. S. Fabiano-Tixier; A. Bily; F. Chemat; *Waste Biomass Valorization*, **2019**, *10*, 1945–1955
51. Q. Y. Zafra-Rojas; N. S. Cruz-Cansino; A. Q. Lira; C. A. Gómez-Aldapa; E. Alanís-García; A. Cervantes-Elizarrarás; N. Güemes-Vera; E. Ramírez-Moreno; *Molecules*, **2016**, *21*, 950
52. G. E. Pantelidis; M. Vasilakakis; G. A. Manganaris; G. Diamantidis; *Food Chem.*, **2007**, *102*, 777–783
53. A. Konić-Ristić; K. Šavikin; G. Zdunić; T. Janković; Z. Juranic; N. Menković; I. Stanković; *Food Chem.*, **2011**, *125*, 1412–1417
54. C.-R. Metzner Ungureanu; A. I. Lupitu; C. Moisa; A. Rivis; L. O. Copolovici; M.-A. Poiana; *Sustainability*, **2020**, *12*, 5681
55. J. J. Vulić; V. T. Tumbas; S. M. Savatović; S. Djilas; G. S. Cetković; J. M. Ćanadanović-Brunet; *Acta Period. Technol.*, **2011**, *42*, 271–279
56. J. Lee; R. W. Durst; R. E. Wrolstad; *J. AOAC Int.*, **2005**, *88*, 1269-1278
57. V. L. Singleton; R. Orthofer; R. M. Lamuela-Raventos; *Methods Enzymol.*, **1999**, *299*, 152-178
58. I. Oliveira; A. Sousa; I. C. F. R. Ferreira; A. Bento; L. Estevinho; J. A. Pereira; *Food Chem. Toxicol.*, **2008**, *46*, 2326-2331

Corrigendum

Correction Note:

Article KILIÇKAYA SELVI, E., GÜLER, N., GÜVEN, S., & MAKBUL, S. (2024). Determination of Chemical Compositions, Antioxidant, DNA Cleavage and Binding Properties of Vincetoxicum Tmoleum Extract. *Studia Universitatis Babeş-Bolyai Chemia*, *69*(1), 163–174. https://doi.org/10.24193/subbchem.2024.1.10 has been corrected in the Platform (Volume 69, No. 1, 2024 | Studia Universitatis Babeş-Bolyai Chemia).
Date: Wednesday, September 10, 2025 10:40 AM
Subject: Request for Article Correction from Emine Kılıçkaya Selvi.
The changes include:
-References 34 and 43 was revised.
-Figure 1 and Table 1 was revised.
Other parts of the article were left untouched.
No changes were made that would compromise the integrity and content of the article.

Editors' Note: The article was corrected on 10.09.2025. The pdf file of the volume also includes a *Corrigendum*.